

University of Alberta

Library Release Form

Name of Author: Salina Yong

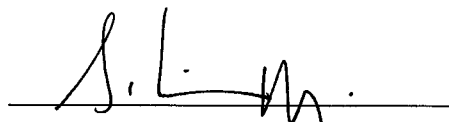
Title of Thesis: A Slide in the Harrowby Hills

Degree: Master of Science

Year this Degree Granted: 2003

Permission is hereby granted to the University of Alberta Library to reproduce single copies of this thesis and to lend or sell such copies for private, scholarly or scientific research purposes only.

The author reserves all other publication and other rights in association with the copyright in the thesis, and except as herein before provided, neither the thesis nor any substantial portion thereof may be printed or otherwise reproduced in any material form whatever without the author's prior written permission.

A handwritten signature in dark ink, appearing to read 'S. L. Yong', is written over a horizontal line.

11612 - 77 Avenue
Edmonton, Alberta
Canada T6G 0M3

April 9, 2003

Submission Date

University of Alberta

A Slide in the Harrowby Hills

by

Salina Yong

A thesis submitted to the Faculty of Graduate Studies and Research in partial fulfillment of
the requirements for the degree of Master of Science

in

Geotechnical Engineering

Department of Civil and Environmental Engineering

Edmonton, Alberta

Spring 2003

University of Alberta

Faculty of Graduate Studies and Research

The undersigned certify that they have read, and recommend to the Faculty of Graduate Studies and Research for acceptance, a thesis entitled The Harrowby Hills Slide submitted by Salina Yong in partial fulfillment of the requirements for the degree of Master of Science in Geotechnical Engineering.



C. Derek Martin



David C. Sego



Tim G. Joseph



Ben Rostron

April 4, 2003

Approval Date

To my family for their unconditional support, encouragement, and most importantly for giving me the space to pursue my interests. And most of all, to Shan, who put up with me & my ranting during these stress-filled and time-consuming years.

ABSTRACT

The Harrowby Hills are located approximately 6 km east of the Saskatchewan-Manitoba border within an 8 km section of the Canadian Pacific Railway (CPR). This section of track crosses several landslides, both relict and contemporaneous, amongst which are the two most recently active slide areas (Miles 86.8 and 86.75). Field investigations have revealed that these movements are seated in the shales of the Pierre Formation. Laboratory tests have shown the material to be a high-plasticity, inorganic clay, displaying a massive fabric with little fissility, the possibility of weak cementation, and structural complexity. Slides occurring in such materials are often of two types, deep-seated translational slump blocks moving along discrete weakened planes or shallow slides occurring within the weathered zone. Results from geotechnical site investigations and analyses (limit equilibrium and deformation) have revealed that this slope deformation is not restricted to a single mechanism, but alludes to the possibility of two.

ACKNOWLEDGEMENTS

This work would not have been possible without funding from NSERC, the support and information provided by Clifton Associates Ltd., Greg Misfeldt, Chris Bunce, Eddie Choi, Clive MacKay, and the opportunity provided by Canadian Pacific Railway to study this site. Most of all, a tremendous amount of gratitude is owed to Dr. Derek Martin, Dr. Dave Sego, and Dr. Dave Cruden for their guidance and constructive criticism, without which this thesis would have been ill-focused. They have also been a source of encouragement and enlightenment into this field of engineering, and for that I am greatly appreciative.

I would also like to thank Steve Gamble, Gerry Cyre, and Christine Hereygers for their patience and support in the lab and field, in addition to Doug Booth for helping me out with digitizing and trouble-shooting Surpac Vision, Chawki Jreige for giving me quick, on the spot tutorials in getting me started on Surpac Vision, Dr. Rob Donahue for helping me out with the mysteries of cementation, and George Braybrook for his tremendous assistance in the interpretation of the SEM photos. An enormous amount of gratitude is also owed to Andrew Corkum for helping me with FLAC in getting me started with the modelling and analysis, in addition to his review of my thesis. I am also indebted to Jaime Jimenez and Soe Moe Kyaw Win for their reviews of my thesis.

And finally, I am thankful to Andrew Corkum, Anna Ho, Tarek Abdelaziz, Jaime Jimenez, Soe Moe Kyaw Win, Santiago Paz, and Renata Wood, all of whom in one way or another contributed to and shaped the progress of this research through their support, feedback, and insightful discussions.

TABLE OF CONTENTS

ABSTRACT.....	v
ACKNOWLEDGEMENTS.....	vi
TABLE OF CONTENTS.....	vii
LIST OF TABLES	xii
LIST OF FIGURES	xiv
1 INTRODUCTION	1
1.1 Movement History.....	1
1.2 Purpose of This Research.....	5
2 SLOPE INSTABILITY IN STIFF CLAYS AND WEAK ROCKS (CLAY SHALES)	6
2.1 Properties of Clay Shales.....	6
2.1.1 Physical Properties	7
2.1.2 Mechanical Properties	9
2.1.3 Strength Properties	10
2.2 Modes of Instability.....	12
2.2.1 Typical Failure Mechanisms	13
2.2.2 Slopes in the Shales of the Pierre Formation	15
2.3 Summary.....	16
3 SITE DESCRIPTION	17
3.1 Geologic History	17
3.1.1 Mesozoic.....	18
3.1.2 Cenozoic.....	19

3.2	Geology.....	20
3.2.1	Bedrock Geology.....	21
3.2.2	Correlations of Bedrock Geology.....	22
3.2.3	Surficial Geology.....	24
3.3	Climate	24
3.4	Summary.....	24
4	FIELD INVESTIGATION.....	26
4.1	Surficial Exploration.....	26
4.1.1	Topographic Surveys	26
4.1.2	Drainage Conditions.....	26
4.2	Subsurface Exploration.....	31
4.2.1	Exploration Methods.....	31
4.2.2	Boreholes & Test Pits.....	33
4.2.3	Sampling	33
4.2.4	Instrumentation	35
4.2.5	Monitoring Of Instrumentation	37
4.3	Interpretation of Investigations: Site Characterization	41
4.3.1	Stratigraphic Profile	42
4.3.2	Groundwater Conditions.....	50
4.3.3	Slope Inclinator Interpretation.....	52
	Location of the Shear Plane	52
	Deformational Pattern.....	56
	Interpretation for Sensitivity Analysis.....	59
4.4	Field Observations from Excavation of the Second Shear Key.....	61
4.5	Summary.....	67

5	LABORATORY TESTING	69
5.1	Laboratory Tests, Procedures, and Sample Preparation	69
5.2	Results: Physical and Mechanical Properties	70
5.2.1	Specific Gravity	70
5.2.2	Grain Size Distribution	71
5.2.3	Water Contents & Consistency Limits	71
5.2.4	Chemical Test	72
5.2.5	Water Deterioration Test.....	73
5.2.6	Scanning Electron Microscope (SEM)	75
5.2.7	Consolidation Characteristics	75
5.3	Results: Shear Strength Characteristics.....	78
5.3.1	Direct Shear Tests on Intact Samples.....	78
5.3.2	Direct Shear Test on a Remoulded Sample	80
5.3.3	Consolidated-Undrained & Drained Triaxial Tests.....	82
5.4	Discussion: Material Characterization	85
5.4.1	Index Properties	87
5.4.2	Fabric.....	90
	Cementation.....	90
	Structure.....	92
5.4.3	Slaking Characteristics	94
5.4.4	Consolidation Characteristics	94
5.4.5	Stress-Strain Relationship	95
5.4.6	Volume-Change Behaviour	96
5.4.7	Strength Parameters.....	97
5.5	Summary.....	102

6	STABILITY & DEFORMATION ANALYSES	103
6.1	Limit Equilibrium Analysis.....	103
6.1.1	Shallow-Seated Failure.....	105
	Model Configuration	105
	Operational Strength	106
	Retrogressive Nature	107
	Sensitivity Analysis.....	107
6.1.2	Deep-Seated Failure.....	110
	Model Configuration	110
	Operational Strength	111
	Retrogressive Nature	113
	Sensitivity Analysis.....	115
6.1.3	Proposed Failure Mechanisms	115
6.1.4	Feasibility of the Proposed Failure Mechanisms.....	117
	Shallow-Seated Mechanism	117
	Deep-Seated Mechanism.....	119
	Alternative Mechanism.....	120
6.2	Deformation Analysis.....	120
6.2.1	Model Configuration	122
6.2.2	Slope Movement Trends.....	124
6.3	Summary	127
7	SUMMARY & CONCLUSION	131
7.1	Summary.....	131
7.2	Conclusions.....	133
7.3	Future Research Prospects	135

BIBLIOGRAPHY	136
APPENDIX A: FIELD INVESTIGATION	143
APPENDIX B: LABORATORY TESTING	173
APPENDIX C: STABILITY & DEFORMATION ANALYSES.....	198

LIST OF TABLES

Table 1-1: Approximate slope angles of the west valley wall.....	4
Table 2-1: Non-clay mineralogy of the Pierre Shale in South Dakota.....	8
Table 2-2: Clay mineralogy of the Pierre Shale in South Dakota	8
Table 3-1: Development of the Assiniboine River valley	20
Table 4-1: List of boreholes in the study area.....	34
Table 4-2: List of test pits in study area.....	35
Table 4-3: Summary of piezometer installations	40
Table 4-4: Summary of slope inclinometer installations	41
Table 4-5: Summary of piezometer monitoring.....	42
Table 4-6: Summary of slope inclinometer monitoring	43
Table 4-7: Water content and dry density ranges of the intact shale bedrock.....	45
Table 4-8: Maximum recorded displacements of the shear plane	61
Table 4-9: Maximum displacement rates of the shear plane	62
Table 5-1: Summary of ASTM standards corresponding to lab tests carried out.....	70
Table 5-2: Specific gravity values	71
Table 5-3: Summary of water contents and consistency limits	72
Table 5-4: Summary of samples analyzed in the water deterioration test and their exposure conditions.....	73
Table 5-5: Summary of initial and final consolidation sample conditions	77
Table 5-6: Summary of direct shear tests on intact samples.....	80
Table 5-7: Summary of the initial conditions of triaxial test samples	85
Table 5-8: Summary of triaxial test results	85
Table 5-9: Specific gravity, natural water contents and consistency limits of the shales of the Pierre Formation.....	90
Table 5-10: Shear strength parameters from literature.....	98

Table 6-1: Summary of stability analysis using lab-determined shear strength parameters...	107
Table 6-2: Summary of shallow-seated back-analysis	109
Table 6-3: Summary of stability analysis of deep-seated failure.....	112
Table 6-4: Summary of the operational shear strengths determined for the deep-seated failure of the lower block (groundwater conditions at surface).....	113
Table 6-5: Summary of the deep-seated back-analysis	114
Table 6-6: Summary of the material properties used in the FLAC analysis.....	123
Table 6-7: Comparison of the magnitudes of the measured and FLAC movements	126

LIST OF FIGURES

Figure 1-1: Location of study area	2
Figure 1-2: Aerial photo of the study area.....	3
Figure 1-3: Location of Miles 86.8 and 86.75 in the study site	4
Figure 1-4: Definition of terms used to describe the valley wall	4
Figure 1-5: Summary of movement and site histories from 1986 to 2002.....	5
Figure 2-1: Extent of Cretaceous shales in North America	6
Figure 2-2: Modes of sliding.....	12
Figure 2-3: Retrogressive slope failures in the Interior Plains of western Canada	13
Figure 2-4: Modes of retrogressive sliding along a discrete geological feature.....	14
Figure 3-1: Location of study area within Williston Basin and Manitoba Escarpment	17
Figure 3-2: Correlations of bedrock geology in western Canada and north-central U.S.....	22
Figure 3-3: Annual precipitation and temperature.....	25
Figure 4-1: Original topographic survey from 1986.	27
Figure 4-2: Updated topographic survey from 1995	28
Figure 4-3: Most recent topographic survey from 2000	29
Figure 4-4: Oblique view of existing slide conditions, looking south, 2001	30
Figure 4-5: Front view of existing slide conditions, looking northwest, 2001	30
Figure 4-6: Surface drainage conditions.....	32
Figure 4-7: Existing surface drainage conditions of the downslope portion.....	32
Figure 4-8: Location map of boreholes and test pits from subsurface exploration	36
Figure 4-9: Location map of all instrumentation installed from 1986 to 2001	38
Figure 4-10: Location map of active instrumentation located in 2000-2001	39
Figure 4-11: Stratigraphy of section Z3	44
Figure 4-12: Water content profile of SI 1101.....	46

Figure 4-13: Water content and dry density profiles of BH 923 and BH 834.....	47
Figure 4-14: Water content profiles of SI 1108 and SI 1109.....	49
Figure 4-15: Groundwater conditions.....	51
Figure 4-16: Location of the shear plane.....	53
Figure 4-17: Borehole log of SI 1108 compared with cumulative slope inclinometer data	54
Figure 4-18: Borehole log of SI 1101 compared with cumulative slope inclinometer data	55
Figure 4-19: Borehole log of SI 834 compared with cumulative slope inclinometer data.....	57
Figure 4-20: Borehole log of SI 1109 compared with cumulative slope inclinometer data	58
Figure 4-21: Displacement vectors of slope inclinometers within study area	60
Figure 4-22: Displacement rate vectors from slope inclinometers.....	63
Figure 4-23: Near completion of the first bench, upslope at the right.....	64
Figure 4-24: Degree of jointing in the weathered zone of the first bench.....	64
Figure 4-25: Wedge failure in the upslope wall of the second bench	65
Figure 4-26: Indication of a number of parallel continuous joints.....	66
Figure 4-27: Downslope face of the excavation wall.....	66
Figure 5-1: Grain size distribution of Block 7	72
Figure 5-2: Summary of liquid limit tests.....	73
Figure 5-3: Equilibrated state of Samples 7-A and 7-B during the water deterioration test..	74
Figure 5-4: Results from SEM photography.....	76
Figure 5-5: Results from SEM photography on the air-dried samples.....	76
Figure 5-6: Results from the Energy Dispersive X-ray Analysis	77
Figure 5-7: Pyrite nodules	77
Figure 5-8: Summary of consolidation characteristics.....	79
Figure 5-9: Summary of direct shear tests on in-situ samples.....	81
Figure 5-10: Shear surface after peak travel	82
Figure 5-11: Summary of direct shear tests on a cut surface following peak shear.....	83

Figure 5-12: Cut plane of the intact samples following the second phase	84
Figure 5-13: Summary of direct shear test on a remoulded sample	84
Figure 5-14: Remoulded sample following the shearing process.....	85
Figure 5-15: Summary of consolidated-undrained and drained triaxial tests.....	86
Figure 5-16: Typical inclination and surface features of the failure surface from the consolidated-undrained and drained triaxial tests.....	87
Figure 5-17: Comparison of grain-size distributions	88
Figure 5-18: Plasticity chart comparing lab values to others	89
Figure 5-19: Shale fabric from the dry SEM analysis	91
Figure 5-20: Possible cementation between clay platelets	92
Figure 5-21: Comparison of dry and wet SEM results.....	93
Figure 5-22: Mohr-Coulomb failure envelopes from direct shear tests.....	97
Figure 5-23: Triaxial test results in modified Mohr-Coulomb space	99
Figure 5-24: Mohr-Coulomb failure envelopes from triaxial tests	99
Figure 5-25: Triaxial test results in principal stress space	100
Figure 5-26: Undrained shear strength from lab vane and pocket penetrometers	101
Figure 6-1: Location of hypothesized shear planes.....	104
Figure 6-2: An idealized retrogressive failure.....	105
Figure 6-3: Limit equilibrium model of the shallow-seated failure.....	106
Figure 6-4: Shear strength parameters for the shallow-seated, retrogressive failure mechanism (groundwater at surface).....	108
Figure 6-5: Analysis for a retrogressive mechanism in the shallow-seated failure	109
Figure 6-6: Location of the shear surfaces and groundwater conditions used in the sensitivity analysis	110
Figure 6-7: Sensitivity analysis of the location of the shear surfaces and groundwater conditions.....	110
Figure 6-8: Sensitivity analysis of the groundwater conditions in the shallow-seated failure	111

Figure 6-9: Geometry of the possible retrogressive nature of the deep-seated slope movement	112
Figure 6-10: Shear strength parameters for the deep-seated failure of the lower block (groundwater at surface)	113
Figure 6-11: Analysis for a retrogressive failure in the deep-seated mechanism.....	114
Figure 6-12: Sensitivity analysis of the groundwater conditions of the deep-seated failure..	115
Figure 6-13: Proposed failure mechanism.....	117
Figure 6-14: Reduction in cohesion.....	118
Figure 6-15: Abandoned cliff concept	121
Figure 6-16: Configuration of the model used in the FLAC analysis	123
Figure 6-17: Location and depth of the SI data extraction from the FLAC analysis	124
Figure 6-18: Comparison of slope movements between field installations and FLAC trends	125
Figure 6-19: Slope movement trends from FLAC at different groundwater conditions.....	128
Figure 6-20: Contours of x-displacements from FLAC analysis with groundwater at surface.....	129

1 INTRODUCTION

Since the construction of the rail line along the west valley wall of the Assiniboine River valley in the late 1800's by means of sidehill cut and fill, an 8 km section of the track between Harrowby and Millwood, Manitoba (NTS 62K/11 and 62K/14) has suffered slope movements ranging from shallow-seated sloughing to severe landsliding. This section of track crosses several relict landslides and has experienced movements ranging from slow to sudden displacements. These movements have led to periodic action ranging from track maintenance (such as track lifting and re-aligning) to more frequent patrols and reductions in train speeds. Among them is the area of current interest, which is located just across the Saskatchewan-Manitoba border, near Russell, Manitoba (as indicated by the arrow in Figure 1-1). The study area (Figure 1-2), defined by mileage points Mile 86.8 and Mile 86.75 (Figure 1-3), has been the most recently unstable and was deemed the most critical in 1986, requiring frequent maintenance (lifting and aligning) and a daily patrol during the spring season (Clifton Associates Ltd., 1996).

As illustrated in Figure 1-3, these mileage segments are also coincident with an outside bend of the meandering Assiniboine River. The Assiniboine River is an underfit river consisting of numerous meanders and oxbow features (Figure 1-2). Its headwaters originate in southeastern Saskatchewan and it travels in a southeasterly direction, emptying into the Red River in Winnipeg, Manitoba.

Miles 86.8 (70 m section) and 86.75 (90 m section) are located within a broad valley of relatively gentle-sloping walls (Figure 1-2); Table 1-1 summarizes the approximate slope angles of the valley wall. The track is located approximately in the middle portion of the valley slope (Figure 1-4); the segment of slope below the track will be referred to as the downslope, while that above the track will be the upslope, and that beyond the valley wall is the upland.

These slopes have been investigated since the early 1980's, with an extensive investigation carried out in 1986 to ascertain the geology of the area, the groundwater conditions, and the current state of stability. Surface exploration included site reconnaissance and topographic surveys, while subsurface exploration involved the drilling, excavation and/or installation of boreholes, test pits, instrumentation, and monitoring. It was concluded that these landslide activities were associated with poor surface drainage and river erosion, and entailed a series of metastable, retrogressive blocks with failure seated in the high-plasticity clay shale bedrock (the Millwood Member of the Pierre Formation).

1.1 MOVEMENT HISTORY

The slide area was relatively inactive throughout the 1980's and into the mid 1990's while little change has occurred to the apparent bulge downslope of Mile 86.75, which has been visible since before the late 1970's. However, major subgrade instability occurred in 1995 following a wet spring and early summer (Figure 1-5). In 1996, cracking in the downslope portion emerged (Figure 1-5) and eventually materialized into the scarp shown in Figure 1-5 by 2000. (Clifton Associates Ltd., 1996; 1997; 2001)

Between the months of May and June in 1995, track settlements accelerated from roughly 50 mm/week in early May to nearly 350 mm/week in late June and continued into July. This section of track was found to be at the toe of an upslope slide block and just above the

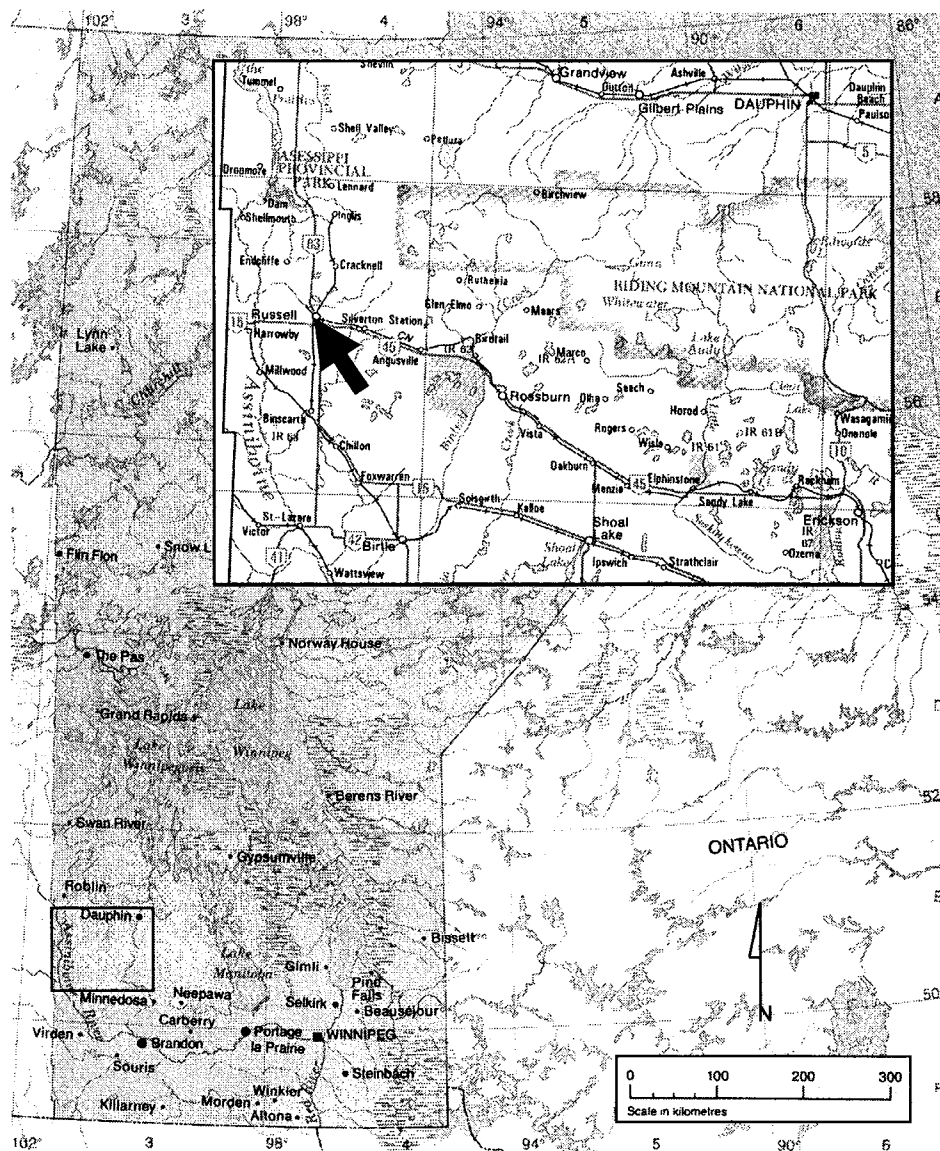


Figure 1-1: Location of study area (inset). (modified from Gage Junior Atlas of Canada, 1979; Atlas of Canada, 1981)

head scarp of a lower sliding mass. At Mile 86.8, slope movements affecting track operation involved both the upslope and downslope portions; the failure mechanism downslope of the track contributed to landsliding while in the upslope portion a shallow backslope failure (roughly 110 m in length located about 8 m above the track) caused sloughing of material into the upslope ditch. However, the mechanism at Mile 86.75 was not discernible since the backslope cut upslope of the track did not appear to be involved, but some signs of recent distress and bulging of the slope (approximately 35 m from the track) were evident in the downslope portion. (Clifton Associates Ltd., 1996)

Late in 1996, tension cracks emerged downslope of the track (most occurring within an area 35-60 m downslope of the track and some occurred within 18 m) and extended along the length of both mileage points with vertical displacements of 600 to 900 mm. Subsequent



Figure 1-2: Aerial photo of the study area, outlined by the box. Scale 1:267000. (modified from Machair Surveys, 1971)

inspection of the site revealed that these new cracks occurred along the same paths as historic ones, and most likely resulted from the prolonged wet conditions experienced during the preceding spring and summer seasons. In December 1996, 50-80 mm of vertical and horizontal movements were noted by track personnel over a length of 45 m at Mile 86.75. In October of 1999, slope inclinometers installed within the improved area showed no movements while the tension cracks shifted to the east. In 2000, reconnaissance of the site revealed substantial slope movement downslope of the track at Mile 86.75 (6 m high scarp) and to a lesser extent at 86.8 (2.5 m high scarp). (Clifton Associates Ltd., 1997; 2001)

Remedial measures taken to mitigate these movements have included: 1) the placement of rip rap along the river bank at locations of active erosion 2) improved surface drainage both upslope and downslope of the track 3) trench drains and 4) shear keys. The location, size, and shape of the Phase II shear key shown in Figure 1-5 are approximate and estimated by the writer (the second key was constructed approximately 30 m away from the first as conveyed by field personnel at the time of construction) since the construction report for this second key was not yet available at the time of this writing. (Clifton Associates Ltd., 1996; 1997; 2001)

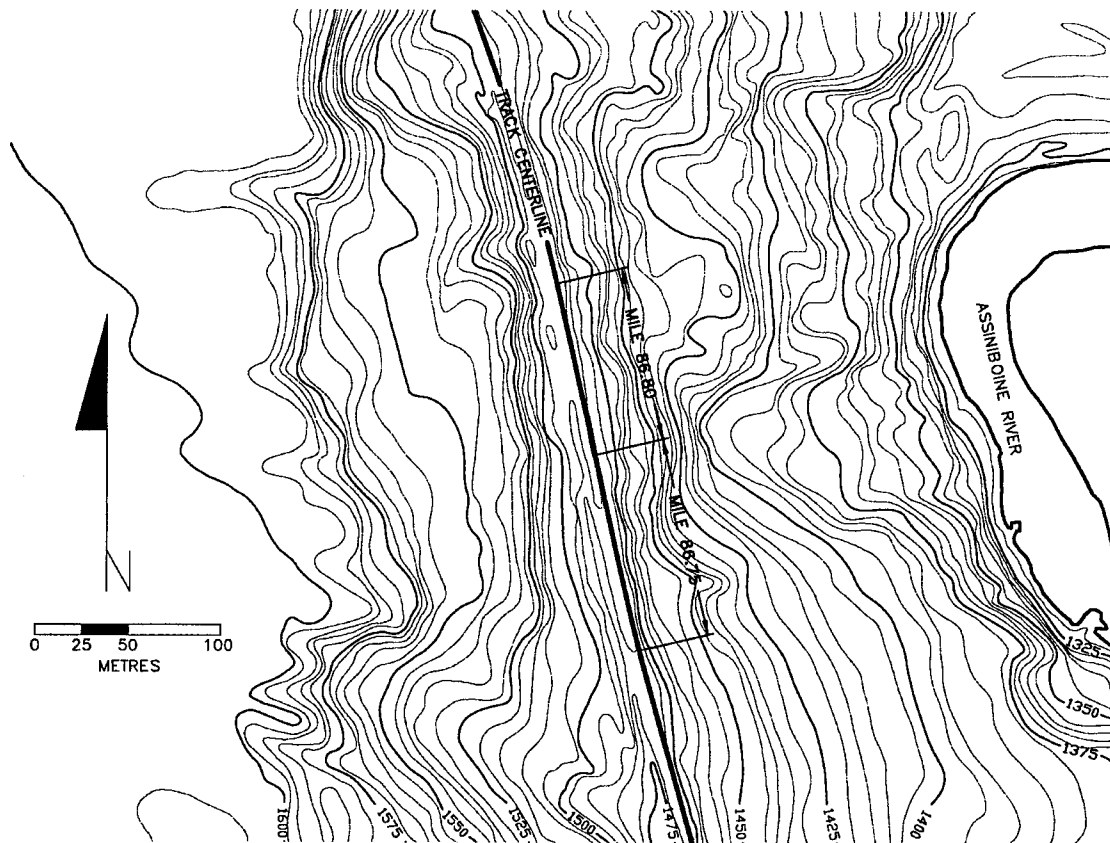


Figure 1-3: Location of Miles 86.8 and 86.75 in the study site (contours are in feet).

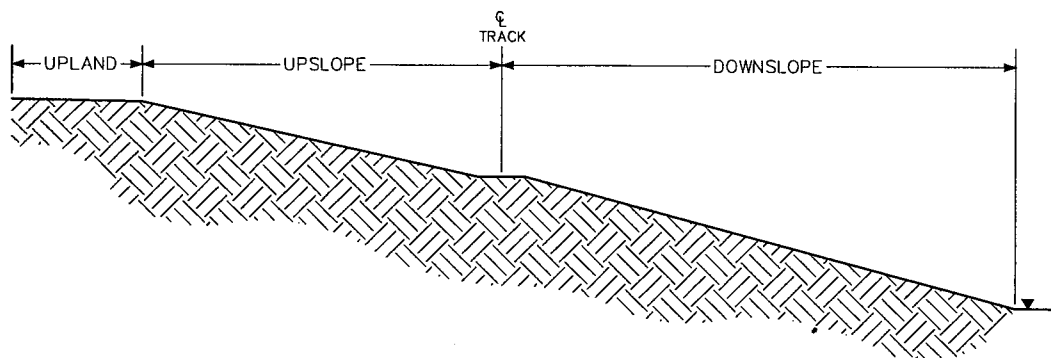


Figure 1-4: Definition of terms used to describe the valley wall.

Table 1-1: Approximate slope angles of the west valley wall.

Location	Angle (°)
Overall	13
Upland	≤ 1
Upslope	12
Downslope	14

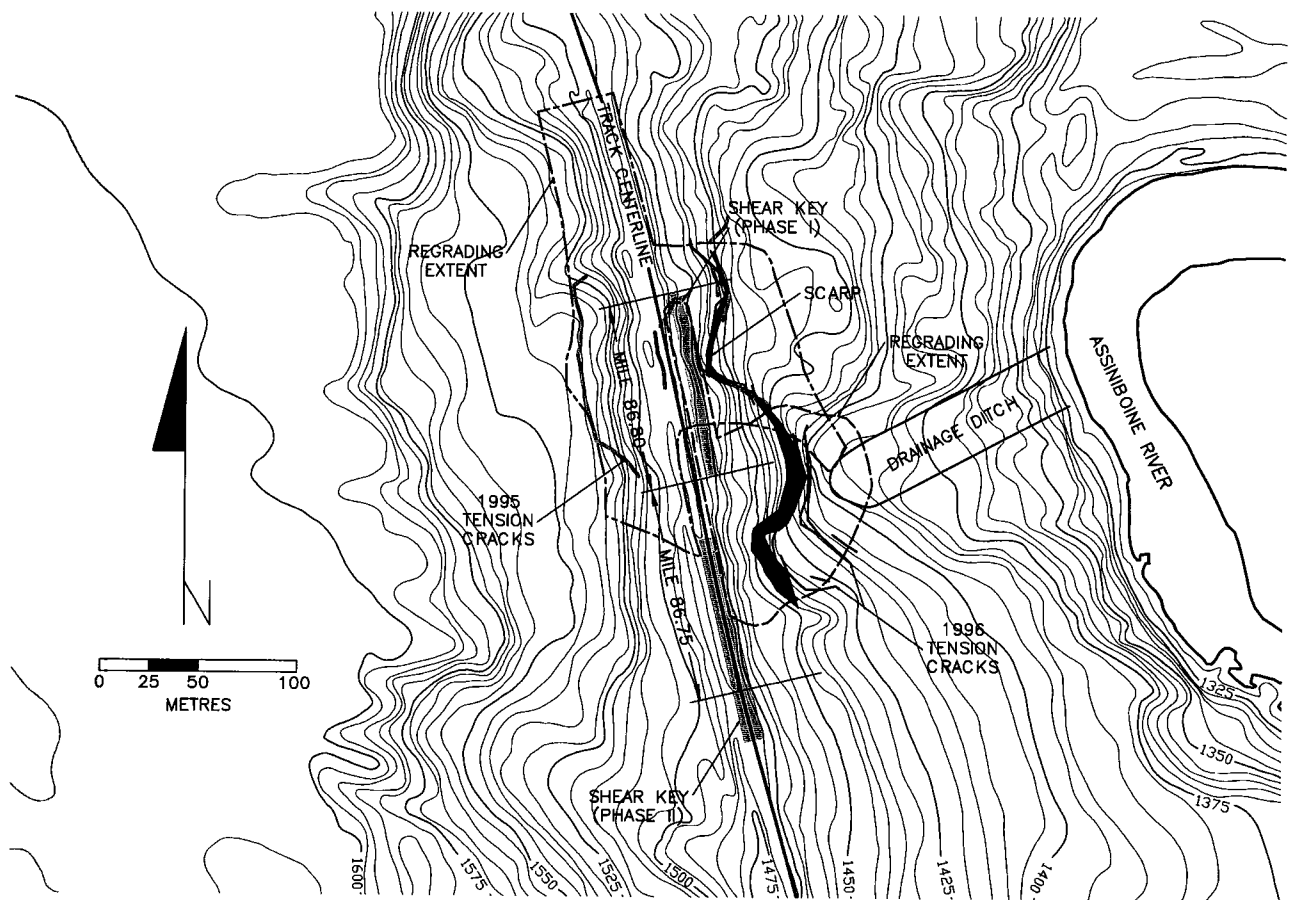


Figure 1-5: Summary of movement and site histories from 1986 to 2002 (not all movement records or remedial measures are included).

1.1 PURPOSE OF THIS RESEARCH

In order to develop mitigative measures to control landslide movements, a thorough understanding is required of the processes that drive the movements. Slope movements in weak rocks such as clay shales are particularly problematic as the triggering and failure mechanisms are complex (Terzaghi, 1936; Hardy, 1957; Peterson et al., 1960; Skempton, 1964; Scott and Brooker, 1966; Brooker and Peck, 1993). The following research will relate the physical and mechanical characteristics determined from the field investigations and laboratory testing to this specific occurrence of slope deformation found in the Assiniboine River valley in Manitoba. More explicitly the scope of this research entails:

1. The determination of the site stratigraphy and groundwater conditions.
2. The definition of the geometry of the displaced mass with significance placed on the location of its shear plane.
3. The determination of material characteristics and modelling parameters for use in stability and deformation analyses.
4. The determination of the mode of failure through stability (limit equilibrium methods via SLOPE/W) and deformation (FLAC) analyses.

2 SLOPE INSTABILITY IN STIFF CLAYS AND WEAK ROCKS (CLAY SHALES)

Clay shales are much older sedimentary deposits of silt- and clay-sized particles which have been subjected to consolidation from varying depths of overburden pressure in excess of contemporary conditions; they have been lithified through the processes of compaction and diagenesis and subsequently unloaded due to erosion. They are transitional in nature, exhibit both soil- and rock-like properties, and a tendency to exhibit strength loss with time; they are harder, more brittle, more dilatant, and often more highly discontinuous than soils, but exhibit much lower strengths, higher compressibilities, and much less brittle response than rocks (Johnston and Novello, 1993). Their presence in North America, as illustrated in Figure 2-1, encompass the extensive formations of shale bedrock that extend across the length of the continent and east from the Rocky Mountains for several hundred kilometres, covering an area once occupied by the epicontinental sea of the Late Cretaceous period (Hardy, 1957; Brooker and Peck, 1993). With continental clastics intermixed and interspersed beds of coal and pure bentonite incorporated into the formations of these materials, the water quality conditions under which they were deposited included marine, brackish, and freshwater (Morgenstern, 1977). Despite their relatively flat-lying to gentle-sloping depositional nature, their presence has become synonymous with challenging performances of foundations as well as naturally-occurring and man-made slopes. They are well-known and well-documented problematic engineering materials (Terzaghi, 1936; Hardy, 1957; Peterson et al., 1960; Skempton, 1964; Scott and Brooker, 1966; Brooker and Peck, 1993).

2.1 PROPERTIES OF CLAY SHALES

The physical characteristics of these materials have a strong influence on their mechanical behaviour, which in turn impact on strength parameters; an appreciation of these properties is thus required to understand their behaviour given a set of circumstances and within a

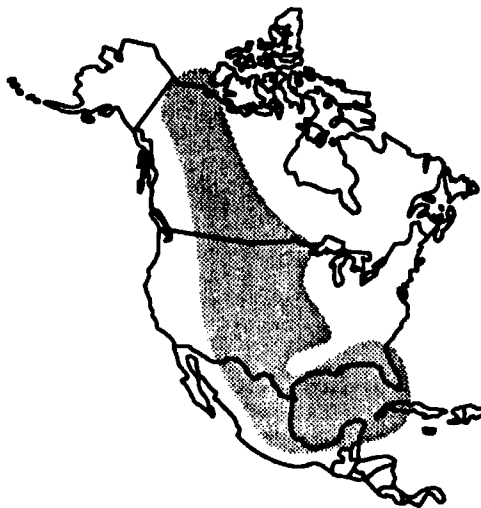


Figure 2-1: Extent of Cretaceous shales (shaded area) in North America. (modified from Brooker and Peck, 1993)

specific environment. The properties of clay shales strongly depend on the depositional history, subsequent geomorphological events, climate, and groundwater regime (Scott and Brooker, 1966). Their challenging nature is further amplified by the fact that they are much older, geologically, and hence, have suffered under more geomorphological processes which in turn have introduced complexities into their micro- and macro-structure. These materials present an unusual array of problems in engineering practice when they are encountered; identification of their presence is a crucial aspect of any project (Hardy, 1957; Pejon and Zuquette, 2002). According to Morgenstern (1977):

'The special problems that arise in the consideration of excavations and slopes in heavily overconsolidated clays [and clay shales] are associated with the selection of appropriate strength parameters, understanding the factors influencing mobilization of shear strength when failure first occurs or is renewed and diagnosing the large variety of stratigraphical situations where heavily overconsolidated clays [and clay shales] are found for clues to their likely engineering behaviour.' (p. 567)

2.1.1 PHYSICAL PROPERTIES

The Pierre Formation from South Dakota has been extensively examined and analysed by the U.S. Geological Survey in addition to many others. It has been described as a sequence of poorly indurated beds consisting of shales, claystones, siltstones, sandstones, and marls with bentonite layers and zones scattered throughout the formation (Crandell, 1958; Schaefer, 2002). Gill and Cobban were able to trace the formation from southwest of Pierre, South Dakota north into Manitoba, where they claim the Millwood Member is equivalent to the Gregory and DeGrey Members of the Pierre Formation of South Dakota (McNeil and Caldwell, 1981). In South Dakota, these facies equivalents of the Millwood Member are predominantly siliceous shale with interbedded sequences of marl, claystone, and bentonite (Crandell, 1958).

Shales of the Pierre Formation predominantly consists of clay-size particles with a secondary component of silt-size particles and minor amounts of sand; its dominant clay-size fraction mineral is the smectite group in the form of montmorillonite and/or mixed-layers of montmorillonite/smectite with illite, whereas quartz dominates the silt-size fraction (Knight, 1963; Kenney, 1967; Bruce, 1968; Fleming et al., 1970; Erskine, 1973; Nichols et al., 1985; Chevenert and Sharma, 1993; Fam and Dusseault, 1998; Schaefer and Lohnes, 2001). Tables 2-1 and 2-2 summarize and compare previous mineralogical analyses from literature. Clearly, the proportion of clay minerals is greater than that of non-clay minerals in the Pierre from South Dakota (Tables 2-1 and 2-2), and the same can be expected of the Millwood Member in Manitoba. This only amplifies the effect of the clay fraction dominance on the overall material behaviour, which according to Mitchell (1993), influences the properties of a soil '*in a manner far greater than their abundance*' (p. 18).

The quartz mineral is fairly strong and well-structured in terms of bonding and stability, and its persistence in soils is due to a variety of factors including: 1) its spiral structure resulting in an absence of cleavage planes, 2) it being an oxide, the absence of weakly bonded ions, and 3) its high hardness (Mitchell, 1993). Conversely, the smectite mineral is weakly bonded by exchangeable cations that balance structural charge deficiencies, and thus, are easily separated by the adsorption of water or other polar liquids (Mitchell, 1993). They are particularly susceptible to dilation due to their high specific surfaces which have a propensity to adsorb water during hydration; they can expand significantly thereby allowing polar molecules to penetrate between mineral layers which can lead to a substantial influence on its

Table 2-1: Non-clay mineralogy of the Pierre Shale in South Dakota.

Reference	Quartz	Cristobalite	Quartz & Cristobalite	Feldspar	Calcite	Gypsum	Dolomite	Pyrite
Knight, 1963	-	-	30%	-	-	-	-	-
Kenney, 1967	15%	-	-	5%	-	-	-	-
Fleming et. al, 1970	20-25%	25-40%	-	trace - 5%	-	-	-	trace
Erskine, 1973	13-17% (19%) ¹	trace (none) ¹	-	trace (trace) ¹	none (trace) ¹	-	-	-
Chenevert and Sharma, 1993 ²	43%	-	-	9%	trace	-	trace	trace
Schaefer and Lohnes, 2001	major (major) ³	-	-	-	-	none (trace) ³	-	-

Table 2-2: Clay mineralogy of the Pierre Shale in South Dakota.

Reference	Mixed layer Illitic Smectites or pure Smectites	Montmorillonite	Mixed layers with Montmorillonite and Montmorillonite	Illite	Mica, Hydrous Mica Illite	Kaolinite	Chlorite	Zeolite
Knight, 1963	-	40-60%	-	Small (~10-30%)	-	-	-	-
Kenney, 1967	-	-	70%	-	10%	-	-	-
Fleming et. Al, 1970	-	30-40%	-	-	trace	-	-	-
Erskine, 1973	-	58-65% (36-44%) ¹	-	-	trace (13%) ¹	trace (13-20%) ¹	-	-
Nichols et. al, 1986	60-100%	-	-	-	-	-	-	-
Chenevert and Sharma, 1993 ²	9%	-	-	20%	-	2%	2%	-
Fam and Dusseault, 1998	39-44%	-	-	44-48%	-	3-13%	2-6%	-
Schaefer and Lohnes, 2001	-	major (major) ³	-	minor (minor) ³	-	minor (minor) ³	minor (minor) ³	minor (minor) ³

¹ values are for the DeGrey Member and those in parenthesis are for the Gregory Member

² based on samples of the Pierre Formation cored in eastern Colorado: water content = 7.1% and bulk density = 2.3 Mg/m³

³ no numerical proportions were given, only descriptors used to describe their relative proportions; values are for unweathered samples and those in parenthesis are for weathered samples

overall behaviour (Mitchell, 1993). In the presence of less-restrictive reduced overburden, volume change occurs readily in materials consisting of these minerals. A significant amount of expansive clay minerals in the soil or rock mass, with an adequate supply of water, result in the mobilization of high swelling pressures in addition to a pronounced susceptibility to softening and slaking; this in turn results in the degeneration of the hard shale into a medium to high plasticity clay (Hardy, 1957; Peterson, 1958; Propescu, 1997; Pejon and Zuquette, 2002).

Despite the relatively uniform and generally massive nature of the Pierre Formation over broad areas, which appears to be devoid of structural features, bedding planes are poorly to well developed, an abundance of iron, manganese, and limestone carbonate concretions are disseminated throughout these beds, joints and blocky structures are also not uncommon, and varying degrees of fissility are evident (Crandell, 1958; Bruce, 1968; Nichols et al., 1985). Processes contemporaneous with deposition and lithification in addition to stress-relieving of these materials result in the development of joints, fissures, and fractures (Skempton, 1964, Scott and Brooker, 1966, Morgenstern, 1977, and Jaspar and Peters, 1979). This is especially apparent in the weathered zone of the shale formation and lessens in effect with depth. Joint and fracture discontinuities in the Pierre of South Dakota, with a predominant normal-to-bed orientation, resulted from local warping due to gentle folding and small displacement faults according to Crandell (1958). He postulated that a systematic pattern could only be discerned from these joints locally and not globally; thus, discontinuities in the Pierre area were attributed to random formation in response to faulting and folding stresses contemporaneous to those which produced a more definite pattern at greater depths in more competent rock. Schaefer (2002) and Nichols et al. (1985) attributed the orientation of fracturing and the development of major weak planes in the Pierre Formation to local structures and topography rather than tectonic activity such as local relict gravitational slumps. Mollard (1977) has identified two orthogonal joint systems in the shale formations of western Canada, with orientations persisting across lithologic and stratigraphic boundaries, which characterize the regional jointing over much of the plains area of Alberta, Saskatchewan, and Manitoba.

Other structural aspects which present a not uncommon occurrence in these formations are slickensides and the possibility of cementation (Knight, 1963; Nichols et al., 1985). According to Hardy (1957), slickensides may accompany the disintegration process thus introducing internally sheared surfaces. Others contribute the formation of slickensides to non-uniform consolidation, expansion during the erosional cycle, and tectonic activities (Peterson, 1958; Skempton, 1964). Cementation has often been associated with compaction and lithification, and results in increased interparticle bonding and interlocking (Clayton and Serratrice, 1997). Furthermore, bentonite beds and/or admixtures are also a common characteristic of these materials in the Interior Plains due to the volcanic activities which occurred during their deposition (Peterson, 1958; Thomson and Morgenstern, 1978). Bentonite is a highly sensitive material, which can severely weaken the rock/soil mass when found in substantial amounts and/or in continuous seams.

2.1.2 MECHANICAL PROPERTIES

Generally, these overconsolidated materials are dense, but poorly indurated with higher strengths than their normally-consolidated counterparts, and possess liquidity indices which approach zero or are negative (Terzaghi, 1936; Skempton, 1964; Scott and Brooker, 1966; Morgenstern, 1977). The mechanical properties related to these physical characteristics include: 1) anisotropy with relatively isotropic conditions parallel to bedding planes, 2) a low

coefficient of permeability of the intact material, 3) a strong tendency to weaken on weathering, and 4) a distinct brittle nature, all of which involve the presence of structural variability (i.e. discontinuities resulting from both fractures and interbeds of dissimilar materials such as bentonite seams) and the extent to which they occur.

Fracture discontinuities can cause the material to behave in a brittle, strain-weakening manner which results in a pronounced difference between the peak and residual strengths (Bjerrum, 1967; Morgenstern, 1977; Brooker and Peck, 1993; Johnston and Novello, 1993; Propescu, 1997). This condition leads to the progressive failures of slopes due to the complicated fashion with which shear strength is mobilized; failure is initiated at a single point of weakness or overstress and propagates along a plane following the mobilization of the strength of adjacent elements as the strength of the initial point is exceeded. Hence, the shear strength mobilized on the plane at any one time during the instability is non-uniform. The stress-strain relationship of the shales of the Pierre Formation is typical of overconsolidated clays in that it displays marked peak strengths at low strains, followed by strain-weakening and ultimately a much lower residual strength at larger strains (Schaefer, 2002). Knight (1963) has also noted that the large variation in the unconfined compressive strength (480 - 17430 kPa) of the shales of the Pierre encountered at the Oahe Dam site was attributed to structural weaknesses such as joint planes and slickensides. Additionally, fracture discontinuities have a pronounced effect on water migration. Despite the low coefficient of permeability exhibited by the intact material, the overall permeability of the mass is governed by the size and orientation of fractures since groundwater moves primarily through these conduits (Knight, 1963; Bruce, 1968; Erskine, 1973). Consequently, the mechanical behaviour of Pierre Formation is quite easily altered through hydration, desiccation, and changes to the chemical environment (Nichols et al., 1985).

An interesting characteristic of the shales of the Pierre is its inability to react with water, or rather slow water absorption, at its in-situ water content (Knight, 1963). Conversely, once it has been air-dried or oven-dried, it disintegrates rapidly when exposed to water; that is, swelling prior to disintegration (or slaking) (Knight, 1963). In fresh excavations, Knight (1963) described the tendency of the exposed material to rapidly deteriorate into a sticky, slippery, and plastic substance (locally known as gumbo) when hydrated and subjected to repeated wetting and drying cycles. A similar observation was also made by Bjerrum (1967) in his examination of the Little Belt Clay, which he described as a '*typical overconsolidated clay with relatively weak bonds*' (p. 15). He noted that '*an almost explosive disintegration*' (p. 17) occurred when the samples were soaked in water following air-drying due to capillary forces.

2.1.3 STRENGTH PROPERTIES

The shear failure criterion used to ascertain the shear strength parameters required for the analyses phase was the Mohr-Coulomb failure criterion:

$$\tau = c' + \sigma' \tan \phi' \quad (2-1)$$

where τ is the shear strength of the material, σ' is the effective normal stress, and the shear strength parameters are c' (the effective strength due to cohesion) and ϕ' (the effective angle of shearing resistance). The shear strength of a material is contingent on its location within the spectrum of peak (at very small displacements) to residual strengths (at much larger displacements following the formation of a fully developed shear surface).

The existence of cohesion has been long debated and will not be discussed here, but rather a short summary of the current understanding of the concept will be presented. Cohesion can be categorized into two groups: true and apparent cohesion. The former refers to the presence of tensile or shear strength despite the absence of any effective compressive stresses in the soil skeleton or on the failure plane, which can be attributed to cementation, electrostatic and electromagnetic attractions, and primary valence bonding and adhesion. Cementation results from chemical bonding of particles. Electrostatic attractions result from the edge-to-face attractions caused by the presence of negative diffuse layers adjacent to positively charged particle edges, while electromagnetic attractions result from the van der Waals (or fluctuating dipole bonds) which exist between elements of matter and cause colloidal particles to be attracted to each other. Primary valence bonds at interparticle contacts form as a result of adhesion or the “cold-welding” of clay particles in overconsolidated clays. Alternatively, apparent cohesion is independent of such interparticle bonding or cementation, and is attributed to the tensile strength of partially saturated soils due to capillary forces and/or to apparent mechanical forces resulting from the interlocking of particles. (Mitchell, 1993)

The frictional strength of a material has been attributed to particle contact in terms of sliding, rearrangement, and grain crushing (in coarse-grained materials), in addition to their resistance to volume change (i.e. dilatancy). Furthermore, Mitchell (1993) concluded that half or more of the peak strength and almost all the residual strength of a material result from the resistance to sliding of particles along contacts. The mechanism by which friction is mobilized was originally developed by Terzaghi and furthered by Bowden and Tabor, resulting in the *adhesion theory of friction* (Mitchell, 1993). The theory states that the normal load acting between two bodies in contact causes yielding at the asperities, and this yielding depends on both the solid contact area and the shear strength of such contacts. Accordingly, mobilization of friction depends on two fundamental surficial characteristics – roughness and adsorption.

Residual strength of a material is defined as the ultimate strength a material achieves as it undergoes large deformations, and its determination depends on mineralogy, gradation, bulk particle characteristics, shear rate, confining pressure, clay fraction, and the activity of this fraction (Mitchell, 1993). Typically, the value decreases with 1) increasing confinement (achieving a curved envelope at lower stresses), 2) increasing clay fraction (where the high frictional resistance of particle rolling and rearrangement from the coarse-grained fraction is reduced and owing to the fact that clay minerals have a lower sliding frictional resistance than non-clay minerals), and 3) increasing activity (Mitchell, 1993). The strength loss from peak to residual can be attributed to dilatancy, at which point water content changes are essentially complete and the fully softened or critical state strength has been passed; and orientation of the clay particles parallel to the direction of shear as deformation progresses (Skempton, 1985; Mitchell, 1993). This often results in the frequent appearance of smooth, slickensided surfaces. The extent to which particle orientation affects the residual strength is dependent on the clay fraction; strength is largely controlled by sand and silt particles when the clay fraction is less than 25%, but residual strength is almost completely dependent on the sliding friction of clay minerals when the clay fraction exceeds 50% (Skempton, 1985). In a transitory material with a clay fraction between 25% and 50%, residual strength is dependent on both the clay fraction and its mineralogy (Skempton, 1985).

2.2 MODES OF INSTABILITY

Widespread contemporary occurrences of slope movements in clay shales generally involve single, slow, and wet slides which have been reactivated in relict slope instabilities (Cruden, 1997), although first time occurrences are not uncommon as documented by Thomson and Morgenstern (1978). Rates of movement associated with such instabilities range from slow (i.e. 1.6 m/yr) to extremely slow (i.e. 16 mm/yr), with a typical rate of 100 mm/yr (Brooker and Peck, 1993; Cruden, 1997). Movements in these materials are often classified as, "slides," according to Cruden (1997), where:

'A slide is a downward movement of a rock mass occurring dominantly on surfaces of rupture or relatively thin zones of intense shear strain. Movement is usually progressive, it does not initially occur simultaneously over the whole of what eventually becomes the surface of rupture, it propagates from an area of local failure. Often the first signs of ground movement are cracks in the original ground surface along which the main scarp of the slide will form. The displaced mass may slide beyond the toe of the surface of rupture covering the original ground surface of the slope which then becomes a surface of separation.' (p. 56)

Prevention or accommodation of such reactivation encompasses the great majority of engineering problems associated with overconsolidated flat-bedded clay shales (Brooker and Peck, 1993). In general, slope instabilities which develop in overconsolidated clays and clay shales involve compound slides of the rotational and translational types (Figure 2-2). Typical characteristics of such slides include rupture surfaces with steep main scarps that tend to flatten with depth, formation of minor scarps due to internal deformation and shear along

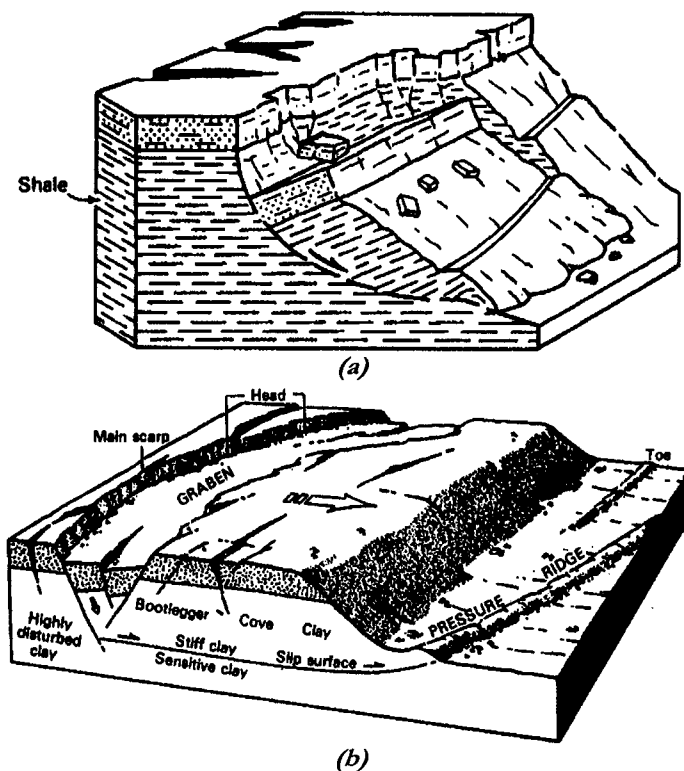


Figure 2-2: Modes of sliding: (a) rotational rock slide (b) translational earth block slide. (modified from Cruden and Varnes, 1996)

surfaces within the displaced mass as the primary curved rupture surface is formed, graben structures, and indication of a plane of weakness (such as weak material or a stratigraphic contact) which controls the location of the rupture surface. (Cruden and Varnes, 1996; Cruden, 1997)

2.2.1 TYPICAL FAILURE MECHANISMS

In the Interior Plains of Canada, slope failures in the Late Cretaceous shale bedrocks encompass massive slow-moving retrogressive failures (tens of square kilometres in area) which may extend for several kilometres along valley walls as illustrated in Figure 2-3 (Mollard, 1977). The formations with the greatest propensity for such failures, according to Mollard (1977), are the Shaftesbury, Lea Park, Judith River, Bearpaw, and Riding Mountain.

Characteristic topographic features of such movements include: 1) flattened failed-slopes (as low as 9.5° to 4°), 2) a scalloped landscape consisting of a series of coalesced arcuate slump blocks which parallel the valley, 3) graben structures near the scarp, 4) translational and rotational block movements defined by backward-tilted horst structures near the head region of the displaced mass, 5) closed depressions which may be dry or wet (e.g. ponds and swamps), 6) characteristic vegetation of trees and scrub brush when water supply is abundant compared to grass coverage in drier sections, and 7) poorly vegetated failure surfaces (Scott and Brooker, 1966; Mollard, 1977). These topographic features illustrate the compound

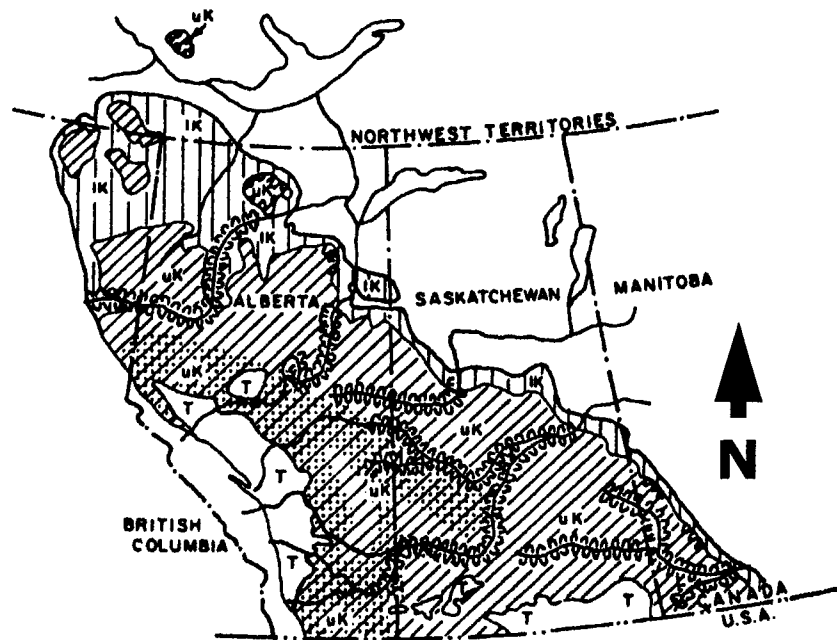


Figure 2-3: Retrogressive slope failures in the Interior Plains of western Canada. Legend: lines and bordered by U-shaped pattern are segments of major river valleys and upland plateaus along which discontinuities, massive, retrogressive landslides in bentonitic argillaceous bedrock of Late Cretaceous age have been studied from air photos and field reconnaissance; T - tertiary, non-marine sedimentary rocks, thinly covered by drift; uK with dot pattern - Upper Cretaceous, non-marine sedimentary rocks, mantled by drift; uK with diagonal lines - Upper Cretaceous, marine argillaceous sedimentary rocks, in part bentonitic, mantled by drift; IK with vertical lines - Lower Cretaceous, marine sedimentary rocks, mantled by drift. (modified from Mollard, 1977)

nature of the landslide mode, where rotation is most prevalent at the head region (evidenced by backward-tilted structures) and translational movement is well established at the toe.

Typical failure mechanisms under which mass displacement of these overconsolidated clays and clay shales occur imply a strong influence from geological factors. Most studies have inferred that the surface of rupture is of low curvature and follow bedding planes due to the nearly horizontal orientation under which deposition occurred; most failures are translational and have been attributed to structurally controlled features such as stratigraphic contacts or the presence of weakened zones (Hardy, 1957; Scott and Brooker, 1966). Laguros and Kumar (1980) have noted that the slip surface of slope failures in the Oklahoma clay shales coincided with the interface between the weathered and unweathered zone at numerous points as indicated by field sampling. The weaker materials in which movement is often seated, possess strength magnitudes lower than the rock/soil mass in which they exist, thus slope failures are very much possible in gentle-sloping terrain which contain such geological features. Typically, weakened or sheared zone materials have been associated with the presence of fractures and/or slickensides, bentonite, and montmorillonite-rich materials (Scott and Brooker, 1966; Morgenstern, 1977; Jaspar and Peter, 1979).

Figure 2-4 illustrates the geometry typical to these failure surfaces and the mechanism of retrogressive failure. Movement of the block enveloped by the planes, DE and BC (a nearly horizontal surface that is often seated in weaker material), first occurs thereby removing the support of the adjacent block defined by segments AB (a relatively flat surface with slight concavity) and BC, which in turn fails as its strength is exceeded under this new stress condition (Scott and Brooker, 1966).

Shallow-seated failures in these clay shales have also been noted by a number of authors including Hardy (1958), Skempton (1964), Bjerrum (1967), and Jaspar and Peters (1979). Hardy (1958) noted that movements were frequently confined to comparatively shallow depths with sliding coincident with the inclination of the slope. Skempton (1964) noted that common occurrences of failures in overconsolidated clay slopes were restricted to the shallow weathered zone of the material, a distance from the limit of weathering; the Jackfield landslide involved the upper 5.5 m of the weathered zone, which was estimated to be 6-8 m thick. Bjerrum (1967) noted that the majority of the slides which occurred in the upper weathered zone occurred in materials of very stiff clay or clay shales – that is, clays with strong diagenetic bonds and therefore are susceptible to progressive failure if subjected to

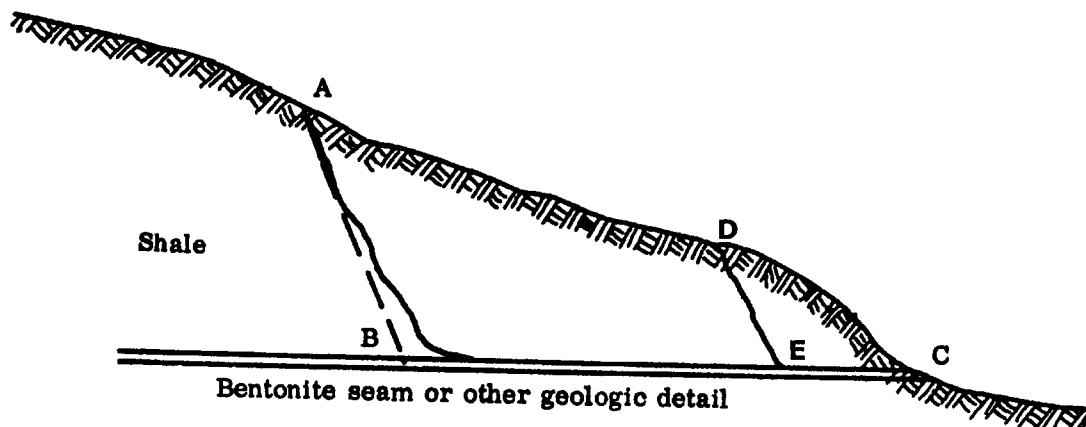


Figure 2-4: Mode of retrogressive sliding along a discrete geological feature. (modified from Scott and Brooker, 1966)

disintegration. Furthermore, he rationalized that the slip plane is often found in the lower part of the weathered zone due to the proportional manner with which the shear stresses resulting from gravitational forces and internal lateral stresses will increase with depth, despite the relatively small increase in the cohesion component of shear strength with depth.

However, Jaspar and Peter (1979) noted both shallow-seated and deep-seated failures in the highly overconsolidated clay shale encountered at the Gardiner Dam site; shallow movements occurred in the soft weathered shale, whereas deep-seated movements occurred in the hard shale below the river valley. They also commented on the lack of dissimilarity between sheared and non-sheared materials encountered at the site; shear zone material consisted of slickensided shale which contained pockets or stringers of bentonite and soft shale, whereas similar material consisting of slickensided shale and bentonite in other horizons experienced no movements.

2.2.2 SLOPES IN THE SHALES OF THE PIERRE FORMATION

The landslide modes involved in the shales of the Pierre Formation vary from slides to flows. The majority of movements have been classified as slides (or slumps) of the rotational type with some translational movement as the toe is approached (Crandell, 1952; Erksine, 1973). Although rapid-flowage phenomena such as earthflows and mudflows have also been identified in South Dakota (Crandell, 1952; Erksine, 1973), Klassen (1974) has noted their rarity in the slopes of the Assiniboine River valley despite stating that they have undoubtedly occurred since deglaciation. However, compound slides of the rotational and translational types have been identified as the dominant occurrence in the Pierre area of South Dakota by Crandell (1952), who noted that these movements usually involved masses of blocks rather than avalanches. Rotational movement tends to dominate in the presence of relatively homogeneous material, whereas planar movement persisted when the shear surface encountered a bentonite bed (Erksine, 1973).

Failures in the South Dakota region are initiated as slumps which are defined by backward-tilted head regions with a complex of smaller blocks, which comprise the horst-graben area, below prominent scarps and may continue into earthflows with an adequate water supply as the larger block breaks into smaller elements (Crandell, 1952; Erksine, 1973). In the Assiniboine River valley, two patterns of slumps have been identified by Klassen (1974): the first occurs in soft shale and the second in both shale and drift. The former are characterized by the occurrence of distinctive razor-back ridges below arcuate scarps that terminate a distance from the foot of the valley wall. The parallelism of these ridges reduces in effect as the toe of the block is approached where debris slides have merged them into irregular surfaces. The latter slump pattern is more stable and common, occurring along the straighter stretches of the valley. Ridges associated with this pattern occur parallel to the trend of the valley.

Rupture surfaces in the Pierre tend to be geologically controlled with common occurrences along a single plane either in a weak zone (e.g. bentonite seams) or along stratigraphic boundaries. At the Oahe Dam, Knight (1963) noted that problematic cut slope failures occurred in the Oacoma Facies of the DeGrey Member of the Pierre Formation; the Oacoma Facies is generally 11.3 m thick with bentonite seams, which vary in thickness from thin partings to 15 mm, spaced at roughly 0.3 m throughout. Crandell (1952) and Knight (1963) have also noted the frequent coincidence of the rupture surface with the contact of the weathered shale. Furthermore, Erskine (1973) has documented slope instabilities in the

lower 5 members of the Pierre Formation (Sharon Springs, Gregory, Crow Creek, DeGrey, and Verendrye) during his investigations of the landslides in the Fort Randall reservoir. The frequency with which closely jointed fracture zones occur adjacent to failure surfaces have also been noted by Crandell (1952), who documented a case where this zone extended 0.3-0.6 m into the surrounding mass. In addition, Knight (1963) observed that zones of weakening were evidenced by closely spaced slickensides. The importance that these discontinuities play in slope instabilities has been illustrated by Bruce (1968), who found occurrences of landslides to be controlled by the concentration of discontinuities; discontinuities are avenues of water migration thus contributing to an increase in hydraulic pressure and the progressive deterioration of the material.

2.3 SUMMARY

Identification of clay shales is a crucial aspect of any project since these materials present an unusual array of problems in engineering practice when they are encountered. Their physical and mechanical characteristics are strongly dependent on their depositional history, the subsequent geomorphological events, climate, and groundwater regime. They tend to be poorly indurated and predominantly consist of clay-size particles with a secondary component of silt-size particles and minor amounts of sand. The dominant clay-size fraction mineral is montmorillonite of the smectite group, whereas quartz dominates the silt-size fraction. Structural features which are commonly associated with the Pierre are: poorly to well developed bedding planes, an abundance of iron, manganese, and limestone carbonate concretions disseminated throughout the beds, a jointed and blocky structure, varying degrees of fissility, not uncommon occurrence of slickensides, and the possibility of cementation.

Generally, these overconsolidated materials have higher strengths than their normally-consolidated counterparts, and possess liquidity indices which approach zero or are negative, anisotropy with relatively isotropic conditions parallel to bedding planes, a low coefficient of permeability of the intact material, a strong tendency to weaken on weathering, and a distinct brittle nature. They are also predisposed to disintegration when exposed to water following a period of drying.

Typical failure mechanisms under which mass displacement of these overconsolidated clays and clay shales occur include both deep-seated sliding along a discrete plane in addition to shallow-seated sliding within the weathered zone. Rupture surfaces in the Pierre tend to be geologically controlled with common occurrences along a single plane either in a weak zone (e.g. bentonite seams) or along stratigraphic boundaries. However, shallow-seated failures in these clay shales have also been noted with movements frequently confined to comparatively shallow depths within the weathered zone and sliding coincident with the inclination of the slope.

3 SITE DESCRIPTION

The following discussion will be of a regional scale with focus on the southwestern corner of Manitoba in order to fully appreciate the extent of the geomorphologic processes and their effects within an engineering context. The study area is located near the edge of Williston Basin (Figure 3-1(a)) and southwest of the Manitoba escarpment (Figure 3-1(b)). The Williston Basin is a component of the Interior Platform or Western Canada Sedimentary Basin (also called the Western Interior Basin) of the North American craton (Stott and Aitken, 1986). The Manitoba escarpment has a total length of 675 km from its southernmost point, Pembina Mountain, in North Dakota to its northernmost point, the Pasquia Hills in Saskatchewan (McNeil and Caldwell, 1981).

3.1 GEOLOGIC HISTORY

The Pierre Formation was first named the Fort Pierre Group by Meek and Hayden in 1856 and was first subdivided by Searight in 1937 (Crandell, 1958; McNeil and Caldwell, 1981). In Manitoba, Tyrell (1890) first established the sequence of the formation into the lower Millwood Member and the upper Odanah Member in the early 1890's. Both members were named according to where exposures were first discovered; the Millwood Member was named for exposures in the Assiniboine River valley near Millwood, Manitoba, and the Odanah Member was exposed at Odanah, near Minnedosa, Manitoba (McNeil and Caldwell, 1981). In 1930, Kirk proposed new nomenclature for the Cretaceous formations in the Manitoba escarpment based on the geographic localities where characteristic exposures were found (McNeil and Caldwell, 1981). The Pierre Formation became known as the Riding Mountain Formation. However, in 1965, Gill and Cobban were able to show that of the four formal units of the Pierre established in North Dakota, 'two were applied from type localities in Manitoba' (McNeil and Caldwell, 1981 p. 32). As a result, McNeil and Caldwell (1981) proposed that use of the name "Riding Mountain" should be discontinued in favour of 'a

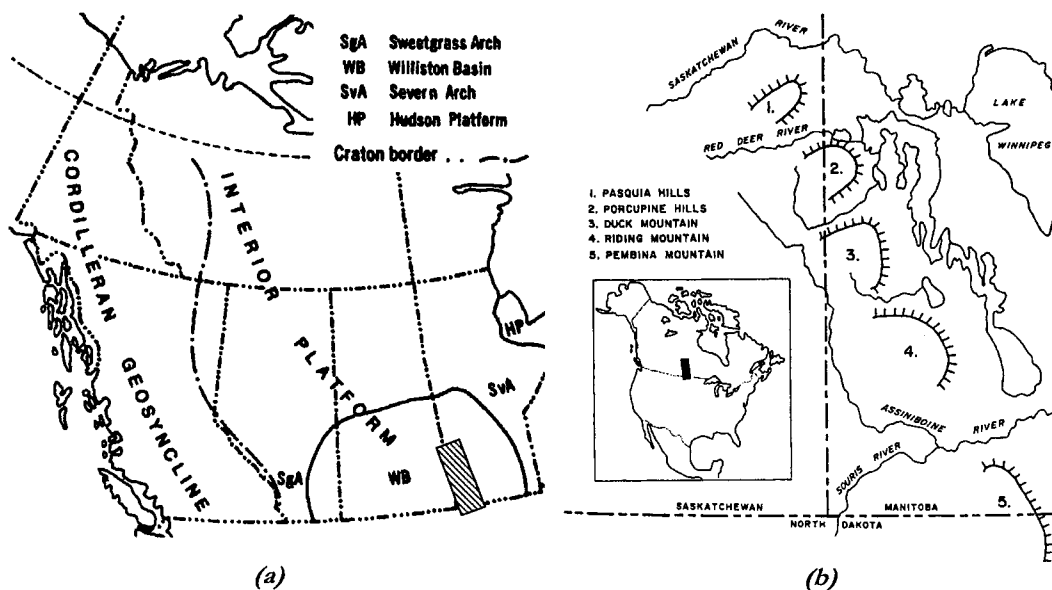


Figure 3-1: Location of study area (outlined by hatched boxes) within (a) Williston Basin (WB) and (b) Manitoba Escarpment. (modified from Douglas et al., 1970; McNeil and Caldwell, 1981)

name more in accord with the sequences developed locally and regionally' (p. 32); henceforth, the discussion below will apply the name Pierre Formation to the equivalent formation in Manitoba.

3.1.1 MESOZOIC

The Early Mesozoic Era (Triassic Period) encompassed a period of substantial erosion as indicated by the scarred Palaeozoic surface, which included numerous scarps, erosional valleys, and probably early karst development (Mineral Resources Division, 2002). During this time, the entire craton was in a state of relative stability above the seas, and this depositional lull persisted until the Middle Jurassic (Middle Mesozoic) when the craton subsided and the area became submersed. As this subsidence continued into the Late Jurassic, the oceanic circulation in the basin increased (Douglas et al., 1970). At this time, the study area was in the shallow, near-shore region of Williston Basin; this locality was further prolonged as the centre of subsidence shifted westward and its depositional character changed with the accompanying cycles of transgression and regression (Douglas et al., 1970). Extensive erosion occurred as the area emerged in the latest phases of the Jurassic and continued into the Cretaceous (Late Mesozoic) with its greatest impact appearing in the marginal regions of the basin (Douglas et al., 1970).

The Cretaceous Period in North America entailed tectonics coupled with volcanism; the intense orogenic activities of the western Cordilleran had the greatest effect on the depositional environment of the Western Interior Basin and to a milder extent, the volcanic activities centred in southwestern Montana and Idaho (Scott and Brooker, 1966; McNeil and Caldwell, 1981). Structurally, these constructive-destructive forces had little impact on the basin; secondary basins and knolls resulted from the differential depression and elevation of the basin floor (McNeil and Caldwell, 1981). However, sedimentation of the area was greatly affected by these processes due to the continuously variable interrelationship developed between the rate of subsidence and supply of sediments that resulted from inconsistent subsidence rates of the sea floor, uplift of the sedimentary source area, and influx of clastic materials (Scott and Brooker, 1966; Douglas et al., 1970). Consequently, sedimentation during this period laid down the bedrock formations now found in the Manitoba escarpment which was located at the eastern margin of the basin.

The prolonged depositional hiatus of the Jurassic was interrupted late in the Early Cretaceous as sedimentation in Manitoba resumed with a rapid southward oceanic advance over an area of relatively flat topography. This ocean from the Beaufort Sea eventually joined a slower moving northward advancing ocean from the Gulf of Mexico at the close of the Early Cretaceous – establishing the strait-like, epicontinental Western Interior seaway bordered on the west by the Cordilleran and on the east by the Canadian Shield (North and Caldwell, 1975). Within the remainder of the Cretaceous Period, this broad sea suffered two main cycles of transgression and regression: the Greenhorn and Niobrara Cyclotherms (McNeil and Caldwell, 1981). Despite the longer duration, the transgressive depositions were comparatively thinner than the regressive; thus, it appeared that the oceanic retreats involved more-rapid subsidence and heavier sedimentation (McNeil and Caldwell 1981).

It was during this depositional phase that the Manitoba escarpment was created; its surrounding environment consisted of substantial amounts of finer-grained, terrigenous, clastic sediments derived from the Cordilleran, which illustrated the extensive impact of the these orogenic activities, and small amounts from the Shield (Scott and Brooker, 1966; McNeil and Caldwell, 1981). However, the Cretaceous sedimentary sequence in Manitoba is

much thinner than the western portion of the basin since subsidence in the eastern portion was relatively more reduced; the marine waters were predominately shallow and the Cretaceous bedrock contained a higher proportion of calcareous rocks than found elsewhere within the basin (Hancock, 1975; McNeil and Caldwell, 1981). In addition to the orogenic processes of the west and general continental fluctuations, the volcanic processes of southwestern Montana and Idaho contributed various layers of volcanic ash to the sedimentary sequence – producing the bentonite layers found today (Scott and Brooker, 1966; McNeil and Caldwell, 1981). Concentrations of these bentonite layers correspond to *'times when the seas were particularly widespread or in the process of becoming more or less so'* (McNeil and Caldwell, 1981 p. 5).

At the close of the Cretaceous and into the earliest Cenozoic (recent life) times, the sea regressed towards the south as the continental interior emerged once again due to uplift of the region (Douglas et al., 1970). Considerable masses of coarser-grained, terrigenous, clastic sediments, derived from the west, were then dispersed as far east as southern Manitoba (McNeil and Brooker, 1981).

3.1.2 CENOZOIC

The orogenic processes of the Cretaceous Period continued into the Tertiary Period (Early Cenozoic Era), however either sedimentation eluded the escarpment and/or extensive denudation had occurred since these deposits were found only to occur at Turtle Mountain (located southwest of the escarpment, at the international border). In the Late Tertiary, Prest (1970) inferred the climate to be arid to semiarid with it cooling off and becoming more humid by the close of the Tertiary. In addition, Prest (1970) and Elson (1966) speculated that a dendritic system of drainage existed across the interior plains at this time carrying discharge from the Rocky Mountains to the Hudson Bay (the Assiniboine River system sits partially within this ancestral system). It was this preglacial system that introduced major entrants into the escarpment, which subsequently divided it into the contemporary series of cuestas: 1) Porcupine Hills, 2) Duck, 3) Riding, and 4) Pembina Mountains (Figure 3-1b). Events in the Quaternary (Late Cenozoic) played a significant role in defining the existing physiography of the escarpment, which included the formation of the Assiniboine River valley. The Quaternary period in Canada denoted major climatic changes from the Pleistocene (oldest epoch) to the Recent – the last ice age, consisting of four major glaciations.

Creation of the Assiniboine River valley occurred in the Pleistocene as the meltwaters from the last deglaciation carved its way through a landscape previously altered by earlier glaciations, which involved both denudation and alluviation in the establishment of ancient meltwater channels and subsequent infilling during later glaciations. The last glaciation in this region, the Wisconsin, consisted of two glacial intervals separated by an interstade, at which time the climate warmed considerably resulting in significant glacial retreat (Prest, 1970). In both cases, the escarpment was completely covered by ice sheets advancing and re-advancing from the north and northeast, and it played a major role in directing the ice flow around it to the southeast (Prest, 1970). In addition, during the last deglaciation, it also played a major role as an impoundment of the massive glacial Lake Agassiz to the east whereas to the west it was breached by the meltwater channels carrying drainage into the lake (McNeil and Caldwell, 1981). The modern Assiniboine River valley is part of this extensive system of meltwater channels that were established mainly within ancestral valleys, which were partly filled and/or re-excavated during this last glaciation (Kehew and Teller, 1994;

Klassen, 1974). Klassen (1972) defined the development of the Assiniboine River valley in the six phases summarized in Table 3-1.

Of the phases outlined in Table 3-1, the second phase was the most influential phase in the development of the modern Assiniboine River valley since a permanent depression was carved out by the large volume of floodwaters as the dammed upstream glacial lakes were released. Such catastrophic drainages resulted in the alteration of spillways to include distinctive geomorphic features such as a modern underfit stream within a deeply entrenched valley, lack of significant tributaries aside from similar spillways, consistent valley width and depth from the outlet to the inlet, and scoured regions bordering portions of the modern channel (Wolfe and Teller, 1995).

Since the last of these ice sheets melted away, valley evolution has encompassed the continued lateral erosion and deposition of alluvium by the river, as well as, valley widening and slope flattening due to slumping of the valley walls.

3.2 GEOLOGY

The geology of the study area includes a mostly sedimentary sequence overlying the stable platform of Precambrian rocks of the Canadian Shield. The Mesozoic embodied a depositional period consisting of mostly shale and sandstone, with various events of limestone, gypsum, and bentonite. Overlying these bedrock formations are the glacial deposits of the Cenozoic Era, which entail reworked material (till and stratified drift) from previously deposited strata. Most recently, deposition in the area consist of alluvium and colluvium from contemporary drainage courses and valley widening episodes.

Table 3-1: *Development of the Assiniboine River valley (after Klassen, 1972).*

Phase	Description
1	The Assiniboine River valley was formed as a major spillway and meltwater channel into glacial Lake Agassiz following a northerly ice retreat. Between Shellmouth and Brandon, it was a continuous, broad, shallow channel draining the Duck Mountain upland.
2	The valley was excavated to a depth 15-30 m above the modern valley bottom and it continued to drain Duck Mountain as well as Porcupine Hills and glacial Lake Assiniboine (which was catastrophically ⁴ drained by the end of this phase).
3	The continued northward ice retreat increased flow into the valley from newly formed glacial lakes (including Melfort).
4	The retreating ice front stood well in the northeast while the valley between Kamshack, Saskatchewan and Brandon, Manitoba reached its maximum glacial depth due to a marked drop in Lake Agassiz. Upstream of Brandon, major slumping occurred along the valley.
5	The ice sheet in western Ontario re-advanced and retreated resulting in fluctuations of Lake Agassiz while a subsequent re-advance resulted in the deposition of the majority of the alluvium in the Assiniboine valley.
6	Lateral erosion of the Assiniboine valley resulted in the deposition of 3- 6 m of fill upstream of Brandon and the formation of abandoned meanders and other related landforms now found along most of the valley bottom.

⁴ Kehew and Teller (1994) and Wolfe and Teller (1995)

Deposition in the Mesozoic involved a system of sandstone and shale units. Prior to the deposition of the Cretaceous bedrock in the Mesozoic, undifferentiated sedimentation occurred in the Jurassic. These entailed sandstone and shale deposited in shallow waters, shale with minor occurrences of sandstone corresponding to a deepening basin, interbedded shale and sandstone deposited during transgression-regression cycles, and shale and siltstone derived from the west in Late Jurassic times (Douglas et al., 1970). The depositional episode of the Cretaceous involved approximately 600 m of sediments laid down in the area encompassing and surrounding the Manitoba Escarpment, and corresponded to the two cycles of marine sedimentation, the Greenhorn and Niobrara Cyclotherms (McNeil and Caldwell, 1981). Continental and marginal-marine sands, silts, and clays constitute the sediments at the beginning and end of this depositional episode, while marine shales of differing lithology dominate the intervening sediments, which represent the majority of the Cretaceous sequence (McNeil and Caldwell, 1981). The Early Cretaceous, characterized by non-marine and marine sandstone and arenaceous shale, is separated from the Late Cretaceous, characterized by considerable thicknesses of marine shale, by a definite boundary that occurs at the base of a bed of fish scale sand deposits (Kirk, 1929; Douglas et al., 1970). The Cretaceous formations, in order from oldest to youngest, found in Manitoba are: Swan River, Ashville, Favel, Morden Shale, Niobrara, Pierre, and Boissevain formations.

Lithology of the Pierre Formation in Manitoba is separated into five members (from oldest to youngest): 1) Gammon Ferruginous, 2) Pembina, 3) Millwood, 4) Odanah, and 5) an Unnamed Member. The Gammon Ferruginous is a dark grey, chunky shale with abundant reddish-brown or ferruginous concretions or thin concretionary beds, while the overlying Pembina Member consists of a lower, greyish-black, noncalcareous, carbonaceous shale with the distinctive occurrence of yellowish-grey-weathering bentonite beds and an upper, dusky yellowish brown shale that passes through a contact zone into the Millwood. The Millwood is a soft, uniform, noncalcareous, silty clay shale, whereas the Odanah (locally known as "slate") is a pale grey, hard, siliceous shale, composed of fine-grained, siliceous particles or flakes, and interbedded with thin olive-grey, soft shale. The overlying Unnamed Member has been described as a dark grey, soft shale and yellowish grey silts. (McNeil and Caldwell, 1981)

Landsliding activity in the study area has been found to occur exclusively in the Millwood Member of the Pierre Formation (Clifton Associates Ltd., 1986). Site investigation indicates that till and/or stratified drift directly rests on the top of the Millwood Member, indicating the absence of the Boissevain and the upper members of the Pierre, the Odanah and Unnamed members.

3.2.1 BEDROCK GEOLOGY

The Millwood Member is an olive-grey, soft, uniform, silty, clay shale with selenite crystals, numerous calcareous concretions, a considerable number of ironstone nodules occurring in bands, and numerous bentonite beds occurring within or close to the top contact with the Odanah Member (Tyrell, 1892; Ries and Keele, 1912; Wallace, 1925; Kirk, 1929; McNeil and Caldwell, 1981; Stott and Aitken, 1993). It thins towards the southeast and changes from 150 m of silty clay shale at the Saskatchewan-Manitoba border to a 15 m sequence of interbedded noncalcareous and calcareous shales and thin marls at the international border (Tyrell, 1892; Ries and Keele, 1912; Wallace, 1925; Kirk, 1929; McNeil and Caldwell, 1981; Stott and Aitken, 1993). According to Stott and Aitken (1993), *'the base of Millwood indicates conditions of open-marine sedimentation and near-peak transgression.'* Spherical and ellipsoidal concretions are abundant in the area surrounding Millwood and Harrowby. According to

Kirk (1929), a characteristic feature of the Millwood Member is the presence of a certain amount of fine sand dispersed throughout the member. In dry conditions, the shale is hard, showing laminations, but not strikingly fissile; it tends to break into equi-dimensional particles. In water, the shale slakes easily, turning into a very tenacious, plastic clay; clay from its disintegration almost always covers exposed surfaces (the surface becomes hard and mud-cracked when the clay dries). In addition, the plasticity of the material triggers slides when the slope steepens. A distinctive topographic feature and corresponding soil characteristic emerges in the presence of the Millwood Member; rounded hills tend to develop with very little to no vegetation on its sides and weathered fragments of ironstone are scattered around these landforms while the adjacent ground becomes hard and mud-cracked in dry conditions (Kirk, 1929).

3.2.2 CORRELATIONS OF BEDROCK GEOLOGY

Due to the second-hand nature of the majority of the information provided and used in this study, it was important to develop correlations of this material with similar materials that have been well/better established. Aforementioned, the Pierre Formation in Manitoba is also known locally as the Riding Mountain Formation and its presence and character is also known in southern Saskatchewan (Dr. Rob Donahue, pers. com. 2002). According to Wickenden (1945), correlations with the Riding Mountain include the formations extending from Lea Park to Bearpaw found in the northern part of the Albertan plains and western Saskatchewan, and the formations extending from the Milk River to Bearpaw found in the southern Albertan plains. Douglas et al. (1970) draw equivalency from most of the Milk River Formation, as well as the Pakowki, Foremost, Oldman, and Bearpaw formations. Figure 3-2 (Figure 4J.7 from Stott and Aitken, 1993) correlate the Pierre of North Dakota with the Riding Mountain of Manitoba and with the Lea Park, Judith River, and Bearpaw of southern Saskatchewan and with the Claggett (Pakowki), Judith River (Oldman, Foremost,

ERA PERIOD	EPOCH	SOUTHERN ALBERTA		NORTHEASTERN MONTANA		SOUTHERN SASKATCHEWAN		NORTHWESTERN NORTH DAKOTA		SOUTHWESTERN MANITOBA		CENTRAL ALBERTA		CENTRAL FOOTHILLS	
		GLACIAL DRIFT		GLACIAL DRIFT		GLACIAL DRIFT		GLACIAL DRIFT		GLACIAL DRIFT		GLACIAL DRIFT		GLACIAL DRIFT	
QUATERNARY	PLEISTOCENE														
	PLIOCENE					EMPIRE									
	MIOCENE			FLAXVILLE		WOOD MOUNTAIN						HARD HILLS			
	OLIGOCENE					CYPRESS HILLS		WHITE RIVER							
	Eocene					SWIFT CURRENT CREEK		GOLDEN VALLEY							
TERTIARY	PALEOCENE	PORCUPINE HILLS		SENTINEL BUTTE				SENTINEL BUTTE							
				TONQUE RIVER		RAVENSCRAIG		TONQUE RIVER				PASKAPOO		PASKAPOO	
				LEBO				LUDLOW							
		WILLOW CREEK		TULLOCK				CANNONBALL		TURTLE MOUNTAIN					
MESOZOIC CRETACEOUS				HELL CREEK		FRENCHMAN		HELL CREEK							
		BATTLE (ROSEHILLS)		COLOMATE		BATTLE		COLOMATE							
		WHITESAND				WHITEMUD									
		ST. MARY RIVER		FOX HILLS		EASTEND		FOX HILLS							
		BLOOD RESERVE								BOISEVAIN					
		BEARPAW		BEARPAW		BEARPAW									
		JUDITH RIVER (BELLY RIVER)		JUDITH RIVER		JUDITH RIVER						JUDITH RIVER / BELLY RIVER			
		CLAGGETT (PAKOWKI)		CLAGGETT		LEA PARK						LEA PARK		WAPIABI	
								PIERRE OR PIERRE SHALE*		RIDING MOUNTAIN					

Figure 3-2: Correlations of bedrock geology in western Canada and north-central U.S. (modified from Stott and Aitken 1993). *In this thesis, Pierre Formation and Pierre Shale are used synonymously.

and Belly River), Bearpaw, and Blood Reserve of southern Alberta. It is evident from this figure and Figure 4J.15 from Stott and Aitken (1993) that only the upper Pierre or Riding Mountain Formation corresponds to the Bearpaw Formation. According to the *Lexicon of Canadian Stratigraphy* (1990), the Millwood Member correlates with the lower unnamed, Outlook and lower Broderick Members of the Bearpaw Formation.

In Manitoba, the Pierre Formation has been separated into five lithologic units with the Millwood Member occurring in the middle, whereas the Riding Mountain Formation is synonymous with only the Millwood and Odanah Members (McNeil and Caldwell 1981). More specifically, the lower 13 m of the Millwood Member appears to correlate with the Lea Park Formation of western Saskatchewan and eastern Alberta, while the upper portion correlates with the uppermost Lea Park, Judith River, and the lowermost Bearpaw Formations of western Saskatchewan. These correlations were drawn based on the biostratigraphy of formally established foraminiferal zonal schemes; the lower portion of the member was established via the *Glomospira corona* Zone and the upper portion via the *Eoepionidella linki* Zone (McNeil and Caldwell 1981). South of the international border, McNeil and Caldwell (1981) found that the Millwood Member of the Pierre Formation correlated with the Gregory and DeGrey members of the Pierre Formation found in the Dakotas; the primary difference between the Pierre found north of the border and that south of the border is that the northern counterpart tended to be less calcareous. In terms of equivalency based on foraminifera, McNeil and Caldwell (1981) traced the *Glomospira corona* Zone of the Lower Millwood Member southward into the Gregory Member of North Dakota. Stott and Aitken (1993) also place equivalency of the Millwood Member with that of the Gregory and DeGrey Members of the Pierre Formation of South Dakota. According to Scott and Brooker (1966), the Bearpaw Formation is most likely correlative with the upper part of the Riding Mountain Formation, the Odanah Member.

The Lea Park Formation is a marine shale sequence that is glauconitic and noncalcareous with ferruginous concretions in the lower part while bentonitic in its upper part (Stott and Aitken, 1993). Tweedie (1976) describes the Belly River Formation (Judith River equivalent) as a sequence of interbedded sandstone, siltstone and shale, and thin coal seams that consists of an interfingering succession of marine shales and deltaic sands. In southern and central Alberta and southwestern Saskatchewan, these alternating nonmarine sandstones were assigned to the Judith River while the marine shales were allocated to the Lea Park (Stott and Aitken, 1993). The Bearpaw Formation appears to be a sequence deposited in shallower marine waters; the lower portion consists of alternating sandstone and shale units with foraminiferal fauna evidence of shallow marine origin (Stott and Aitken, 1993). In addition, Stott and Aitken (1993) describe the formation as a sequence of six silty clay units alternating with five silty sand units as found in the South Saskatchewan River valley.

In South Dakota, the Gregory (the older member) and DeGrey Members of the Pierre Formation are the equivalents to the Millwood Member of the Manitoba sequence. Crandell (1958) describes the type section of the Gregory as consisting of approximately 3 m of shale and marl underlying about 8 m of grey shale and noncalcareous claystone while the DeGrey Member is predominantly light-olive grey shale and claystone. The DeGrey can be separated into two facies – a siliceous shale facies at the bottom and a shale and bentonite facies. The siliceous facies is well consolidated, tending to ‘clink or ring when pieces are struck together’ (p. 13) and contains carbonates of iron and manganese (Crandell, 1958). Overlying this, is the succession of interbedded claystone and shale with layers of bentonite that comprise the shale and bentonite facies; the shale and claystone are also well consolidated and the bentonite beds are very well defined and can be traced for some distance (Crandell, 1958).

Crandell (1958) also mentions the frequent occurrence of concretions consisting of iron manganese carbonate and large spherical masses of limestone.

3.2.3 SURFICIAL GEOLOGY

The surficial geology of southwestern Manitoba includes till, stratified drift, alluvium, and colluvium resulting from glaciation, deglaciation, and contemporary erosional processes of the Cenozoic era (Klassen, 1969; 1972; 1974). With the exception of re-entrant areas where the surficial cover consists of stratified drift from glacial lakes, most of the region is covered in till. In the Assiniboine River valley, the continuing process of lateral erosion of the river has further evolved its walls and floor, and the thickness of alluvium and colluvium are ever-changing.

Klassen (1969) places the till coverage to be approximately 30-60 m thick, whereas it is about 110-140 m thick in buried valleys. Regarding its constituents and origin, he has found that,

'the tills of successive glaciations are similar in composition and consist primarily of material derived from local marine shale bedrock mixed with erratic material derived from carbonate, igneous and metamorphic rocks northeast of the Manitoba escarpment.' (p. 2)

On average the tills found in the region have a definite pebble fabric trending approximately east-west and are composed of 30-50% sand and 40-70% silt and clay with a carbonate content of 20-30% (Klassen, 1969).

3.3 CLIMATE

The climate of Manitoba is of a continental type where temperatures vary enormously; it is characterized by warm, sunny summers (average of 25°C in July and August) and cold, bright winters (average of -24°C in January). In the summer months, more than half of the annual precipitation falls in the form of brief heavy showers. In the winter months, southern Manitoba receives 110 to 114 cm of annual snowfall with its heaviest concentration in the Duck and Riding Mountains (160 cm). (Websites of Travel Manitoba, 2002; OCanada.ca, 2002; Manitoba Trade & Investment Corporation, 2002)

A summary of the climate data for the study area is illustrated in Figure 3-3. The mean annual minimum temperature is 5.5°C, its maximum is 18.4°C, and the mean annual total precipitation is about 530 mm. The data was obtained from a weather station located approximately 15 km southeast of the site at Binscarth, Manitoba (Clifton Associates Ltd. Report File, 2001).

3.4 SUMMARY

The Cretaceous Period in North America entailed tectonics coupled with volcanism. In the Western Interior Basin, the intense orogenic activities of the western Cordilleran had the greatest impact on the depositional environment while the volcanic activities centred in southwestern Montana and Idaho had a milder impact. Sedimentation during this period laid down the bedrock formations now found in the Manitoba escarpment (where the study area is located), located at the eastern margin of the basin. Creation of the Assiniboine River valley occurred in the Pleistocene epoch of the Quaternary period as meltwaters from the

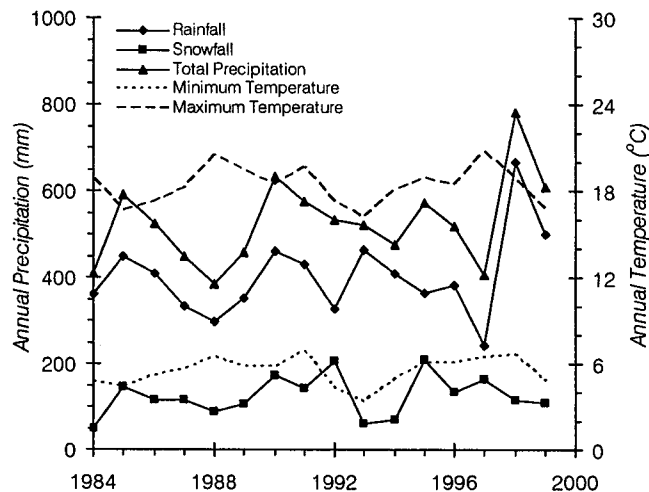


Figure 3-3: Annual precipitation and temperature.

last deglaciation carved its way through a landscape previously altered by earlier glaciations. The modern Assiniboine River valley is part of an extensive system of meltwater channels that were established mainly within ancestral valleys, which were partly filled and/or re-excavated during the last glaciation. Subsequent to the glacial period, valley evolution has encompassed the continued lateral erosion and deposition of alluvium by the river, as well as, valley widening and slope flattening due to slumping of the oversteepened valley walls.

The bedrock geology of the study area includes a mostly sedimentary sequence overlying the stable platform of Precambrian rocks. Overlying these bedrock formations are glacial deposits, which entail reworked material from previously deposited strata. Most recently, deposition in the area consisted of alluvium and colluvium from contemporary drainage courses and valley widening episodes. The bedrock stratum, the Millwood Member of the Pierre Formation, is an olive-grey, soft, uniform, silty, noncalcareous clay shale with selenite crystals, numerous calcareous concretions, a considerable number of ironstone nodules occurring in bands, and numerous bentonite beds occurring within or close to the top contact with the overlying Odanah Member. The Millwood Member thins towards the southeast and changes from 150 m of silty clay shale at the Saskatchewan-Manitoba border to a 15 m sequence of interbedded noncalcareous and calcareous shales and thin marls at the Canada-United States border. A characteristic feature of the Millwood Member is the presence of a certain amount of fine sand dispersed throughout the member. In dry conditions, the shale is hard, showing laminations, but not strikingly fissile and tends to break into equi-dimensional particles. In water, the shale slakes easily, turning into a very tenacious, plastic clay. This disintegrated form of the shale most often covers exposed surfaces, which become hard and mud-cracked when dried. In addition, the plasticity of the material triggers slides when the slope steepens.

Correlations of the Millwood Member of the Pierre Formation (locally, the Riding Mountain Formation) include: the Lea Park, Judith River, and the Bearpaw Formations in the Canadian prairies, and the Gregory and DeGrey Members of the Pierre Formation in the Dakotas. More specifically, the lower 13 m of the Millwood Member correlate with the Lea Park Formation of western Saskatchewan and eastern Alberta, while the upper portion correlates with the uppermost Lea Park, Judith River, and the lowermost Bearpaw Formations (the lower Unnamed, Outlook and lower Broderick Members) of western Saskatchewan.

4 FIELD INVESTIGATION

The field investigation of the 8 km stretch of rail line from Harrowby to Millwood, Manitoba began in 1986 with an extensive surface and subsurface examination of the entire site. Subsequent investigations fine-tuned the conclusions from this original investigation and were carried out in 1995, 2000-01, and 2002. Surface exploration included general site reconnaissance and topographic surveys, while subsurface exploration involved boreholes, test pits, instrumentation, and monitoring.

4.1 SURFICIAL EXPLORATION

Site reconnaissance of the surface in the original investigation of 1986-87 entailed ascertaining topographic features in addition to surface drainage conditions. Subsequent explorations focused on updating the original investigation where necessary; topographic surveys of the newly scarred portions of the site were carried out and combined with the original and previous surveys.

4.1.1 TOPOGRAPHIC SURVEYS

The first topographic survey of the study site was carried out in 1986 (Figure 4-1), and involved a large area covering the stretch of rail line from Mile 84.3 to 88.6. An updated topographic survey of the study area was conducted in 1995 following a major subgrade instability in the same year (Figure 4-2), and another survey was undertaken in 2000 to define details of the most recent instability (Figure 4-3). As a visual aid and enhancement of the site topography, interpolated surfaces (Digital Terrain Models or DTM's) of these surveys were produced with the aid of Surpac Vision and included in each of the above figures. The existing (2000-01) slide scarp is also superimposed on the 1986 and 1995 topographic maps in the above figures to illustrate the stage of its development at these times.

Both the surface topography of the valley wall and site visits revealed a gentle-sloping yet hummocky nature, consistent with landslide-scarred terrain. Vegetation of the slope (Figure 4-4 and Figure 4-5) consisted of trees in the upslope portion while the treed sections of the downslope portion surrounded the grassed area of the instability. The height of the existing scarp (Figure 4-5) increased from 2.5 m in the north at Mile 86.8 to 6 m in the south at Mile 86.75. (Clifton Associates Ltd., 2001). The toe of the slide was not visible, but appeared to surface in the Assiniboine River as indicated by an apparent bulge adjacent to the river (Figure 4-4).

4.1.2 DRAINAGE CONDITIONS

Numerous surface drainage courses and ponded areas were mapped between Mile 84.1 and Mile 89.2 in 1988 (Clifton Associates Ltd., 1988).

'The source of each drainage course was located and flagged down to track level and then followed to its outfall location, [while the condition of ponded areas ranged from] water in animal tracks to permanent marshes with heavy vegetation and open water up to 1m deep...[and] some ponded areas were up to 4000 m² in area.' (p. 24)

Within the study area, six drainage courses (DC15 to DC20) and four ponded areas (hatched areas) were identified, as shown below in Figure 4-6.

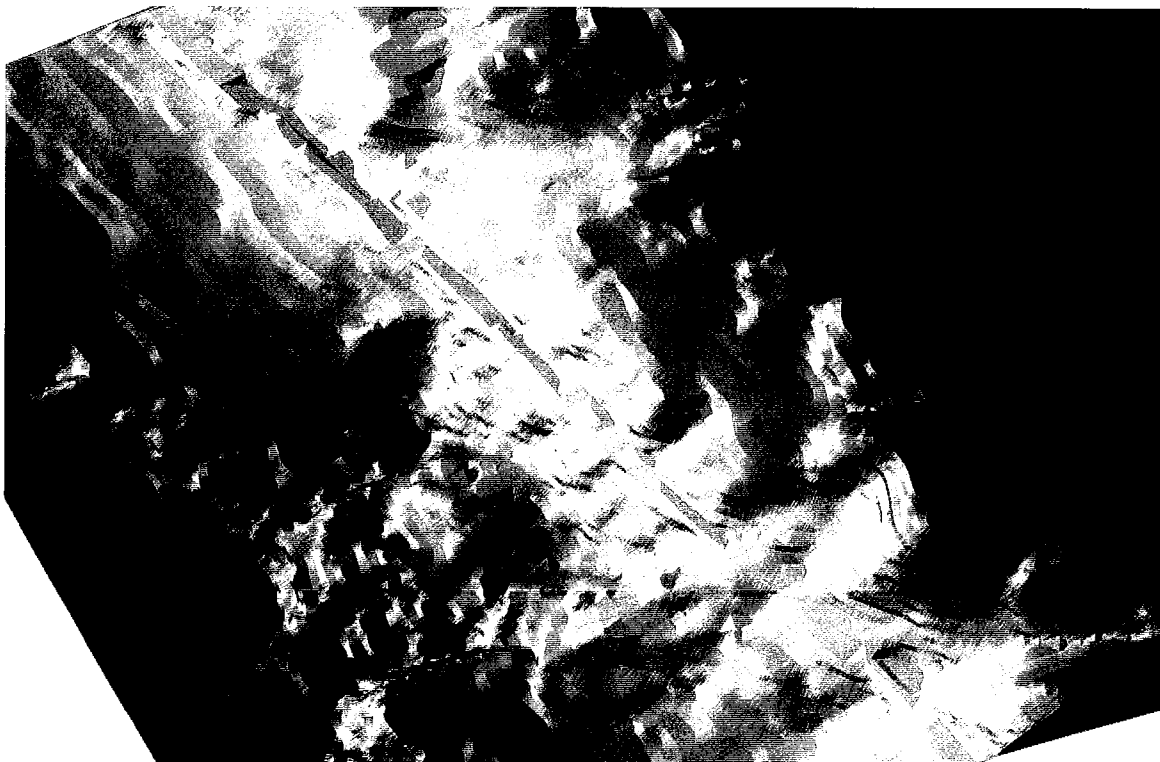
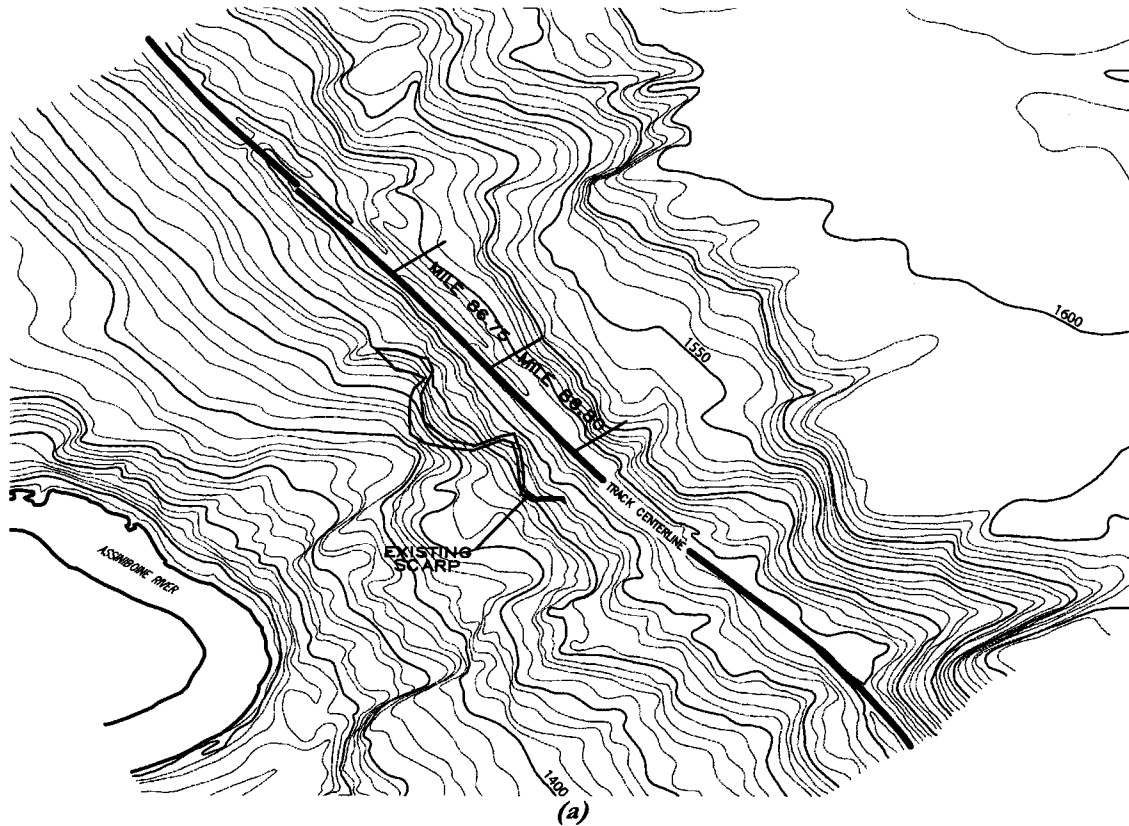
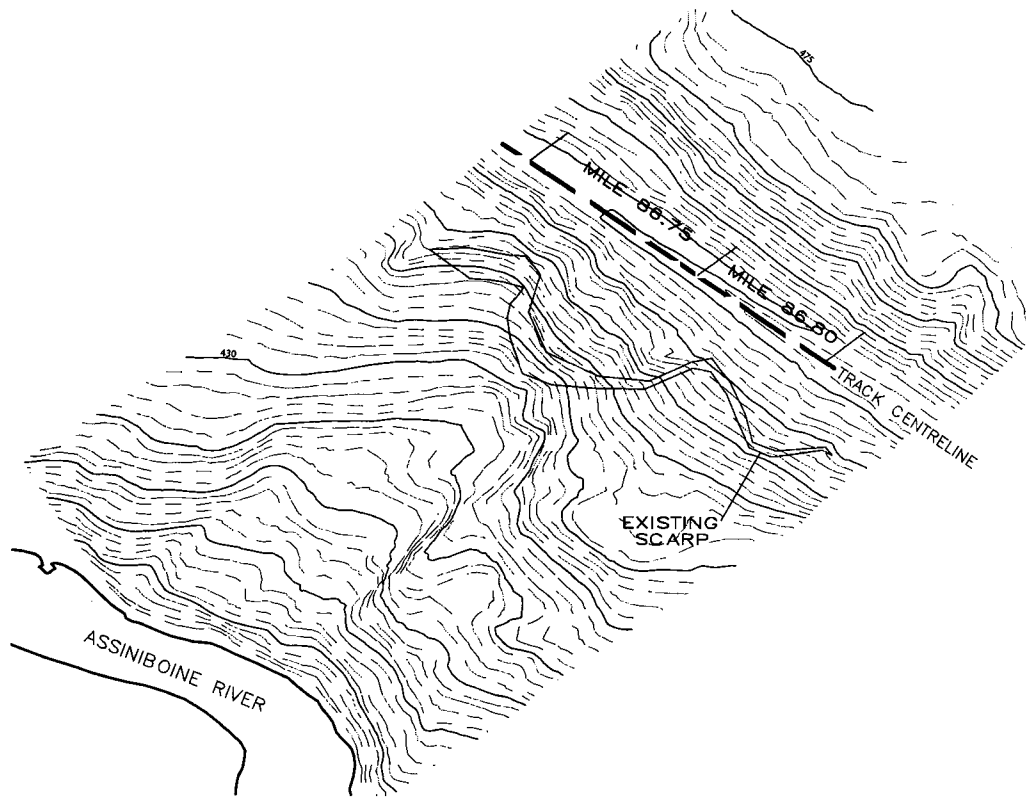
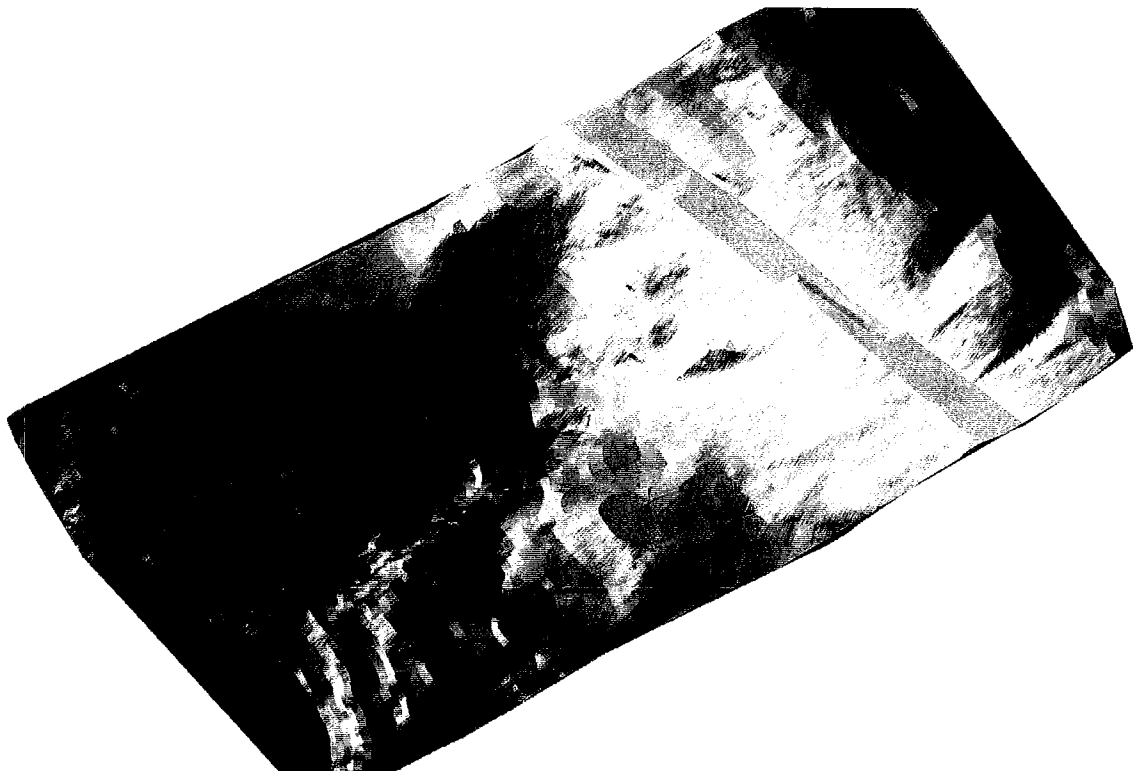


Figure 4-1: Original topographic survey from 1986 (Clifton Associates Ltd., 1986): (a) contour lines at 1-foot intervals (b) interpolated surface (DTM).



(a)



(b)

Figure 4-2: Updated topographic survey from 1995 (Clifton Associates Ltd., 1996): (a) contour lines at 1-m intervals (b) interpolated surface (DTM).

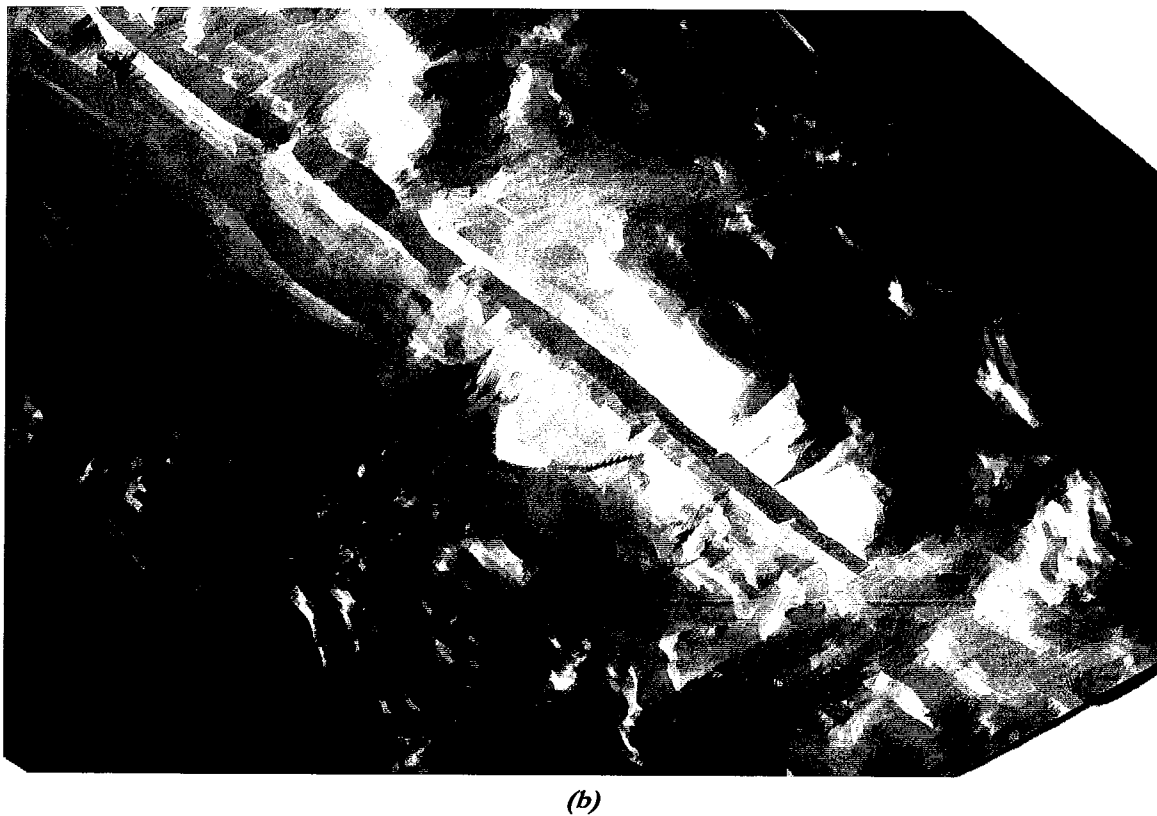
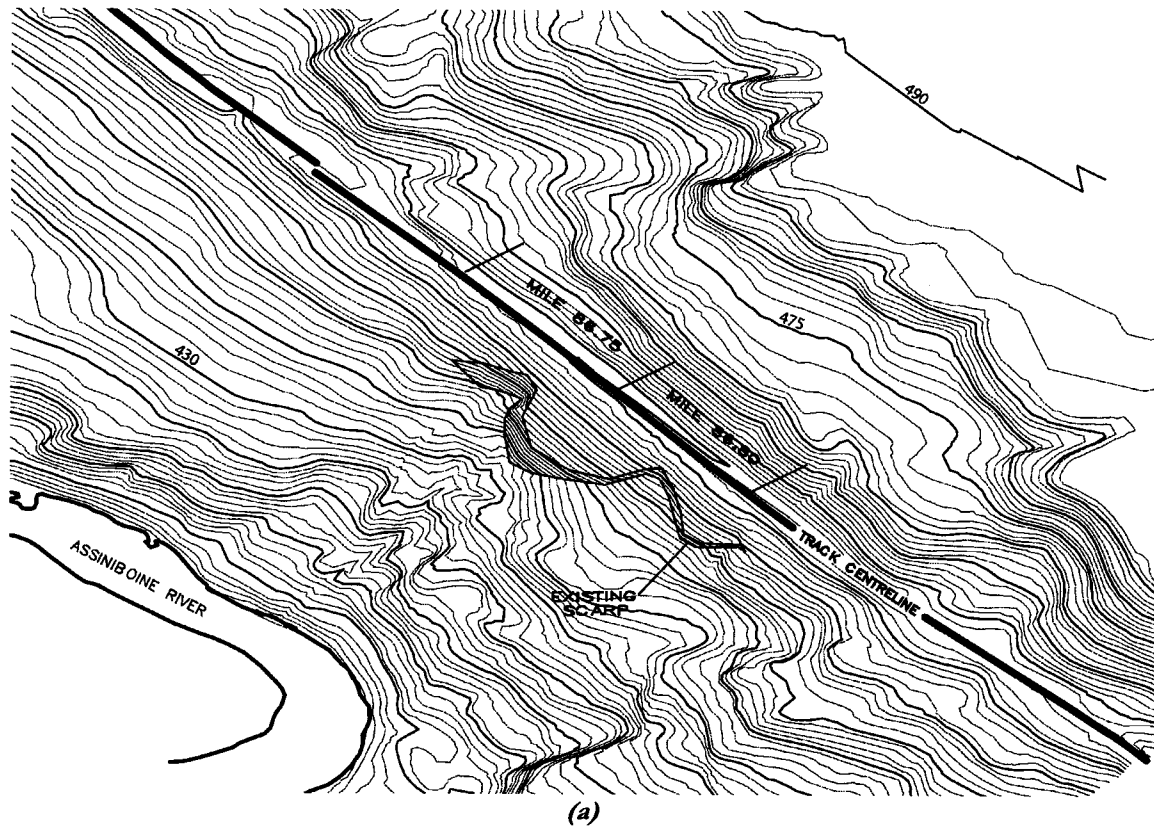


Figure 4-3: Most recent topographic survey from 2000 (Clifton Associates Ltd., 2001): (a) contour lines at 1-m intervals (b) interpolated surface (DTM).

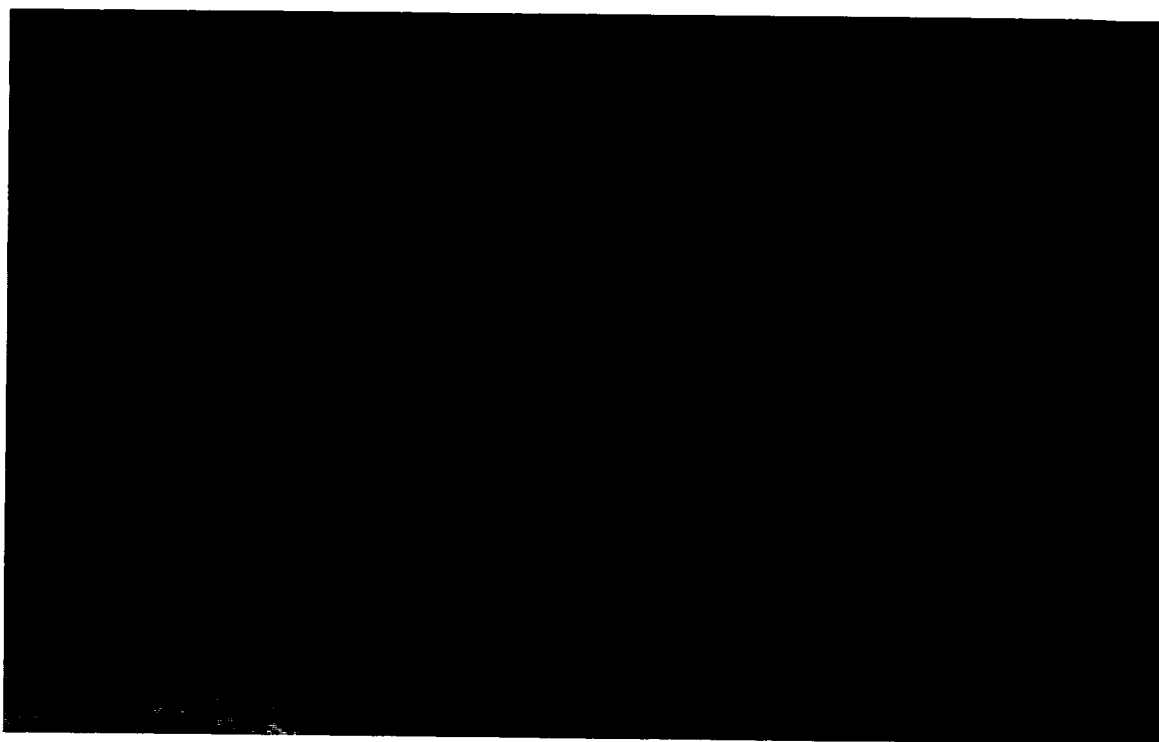


Figure 4-4: Oblique view of existing slide conditions, looking south, 2001 (courtesy of Clifton Associates Ltd.).

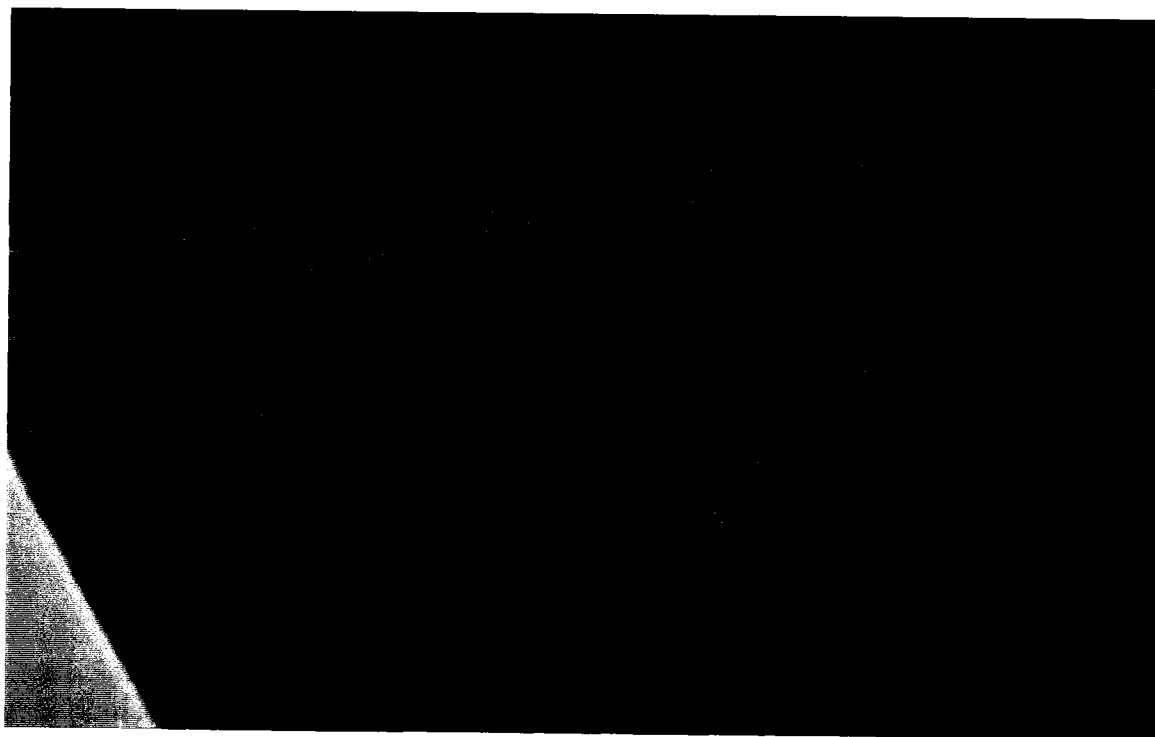


Figure 4-5: Front view of existing slide conditions, looking northwest, 2001 (courtesy of Clifton Associates Ltd.).

In addition to surface runoff and precipitation, the sources of these drainage courses and ponded areas included drainage from a gravel stratum that intersected the slope surface along with sand and gravel layers found in the till sheets in the upland (Clifton Associates Ltd., 1988). Furthermore, the Clifton Associates Ltd., 1986 mentioned the occurrence of a permanent year-round spring at an old gravity water station located above the track at Mile 86.6 (Figure 4-6) that was once used for steam engines, and most severely affected DC15. At the time the report was written, the outlet had already been destroyed and it was speculated that *'surface discharge [was] no longer carried across the track and [was] undoubtedly saturating the existing fill materials' (p. 8)*. Up to 2 L/s of groundwater flow has been recorded at this spring in the past (Clifton Associates Ltd., 1988). Another spring above DC18 was also located in the Clifton Associates Ltd. (1988). Allegedly, both springs supply part of the groundwater affecting the downslope instability of the study area. According to Clifton Associates Ltd. (1988), the ponding at DC15 and DC18 was speculated to be due to *'ponding [that] normally occurs at the toe of a steep slope where the lower slump block has rotated and created a closed depression' (p. 24)*. Moreover, the report has identified that the major ponded areas were those feeding DC15, DC16, and DC18.

In 1995, site reconnaissance of the Mile 86.8 site revealed the presence of both groundwater seepage and ponded water along the base of the backslope and in the upslope drainage ditch (Clifton Associates Ltd., 1996). The 2001 and 2002 site visits revealed that DC16 and DC17 were generally shallow in the downslope portion and indicated a high groundwater table in the lower downslope portion (Figure 4-7), whereas substantial ponded areas were neither apparent upslope nor downslope of the track.

4.2 SUBSURFACE EXPLORATION

Subsurface exploration entailed drilling boreholes and excavating test pits in order to determine geology, stratigraphy, groundwater conditions, possible shear planes and for the installation of instrumentation. The majority of site geology and stratigraphy were determined in the first investigation in 1986-87 (Clifton Associates Ltd., 1986) while subsequent investigations fine-tuned this model. Most of the boreholes were instrumented with either piezometers or slope inclinometers. However, due to the frequency of construction and/or landsliding activities in the last 16 years, some of these holes have been damaged.

4.2.1 EXPLORATION METHODS

Boreholes were drilled using either rotary or auger techniques during the first two investigations in 1986 (Phase I conducted from March 11 to 24 and Phase II from June 17 to 25) and 1987 (June 22 to July 17). The deeper holes entailed rotary drilling via a truck-mounted Failing 1250 drill, whereas the shallower holes were augered with a truck-mounted Brat 22 drill rig equipped with a continuous flight solid stem auger. Geophysical logs were obtained at each rotary hole while only in selected auger holes. The geophysical logs captured spontaneous potential, resistivity, resistance, caliper, natural gamma, gamma-gamma, and neutron readings of each rotary hole. In the auger holes, spontaneous potential, resistivity, and resistance were not run due to the lack of the necessary fluid conditions in these dry holes. Test pits were also excavated in the 1987 investigation via either an O&K RH6 Backhoe or Caterpillar 215B Backhoe, both track-mounted. (Clifton Associates Ltd., 1986; 1988)

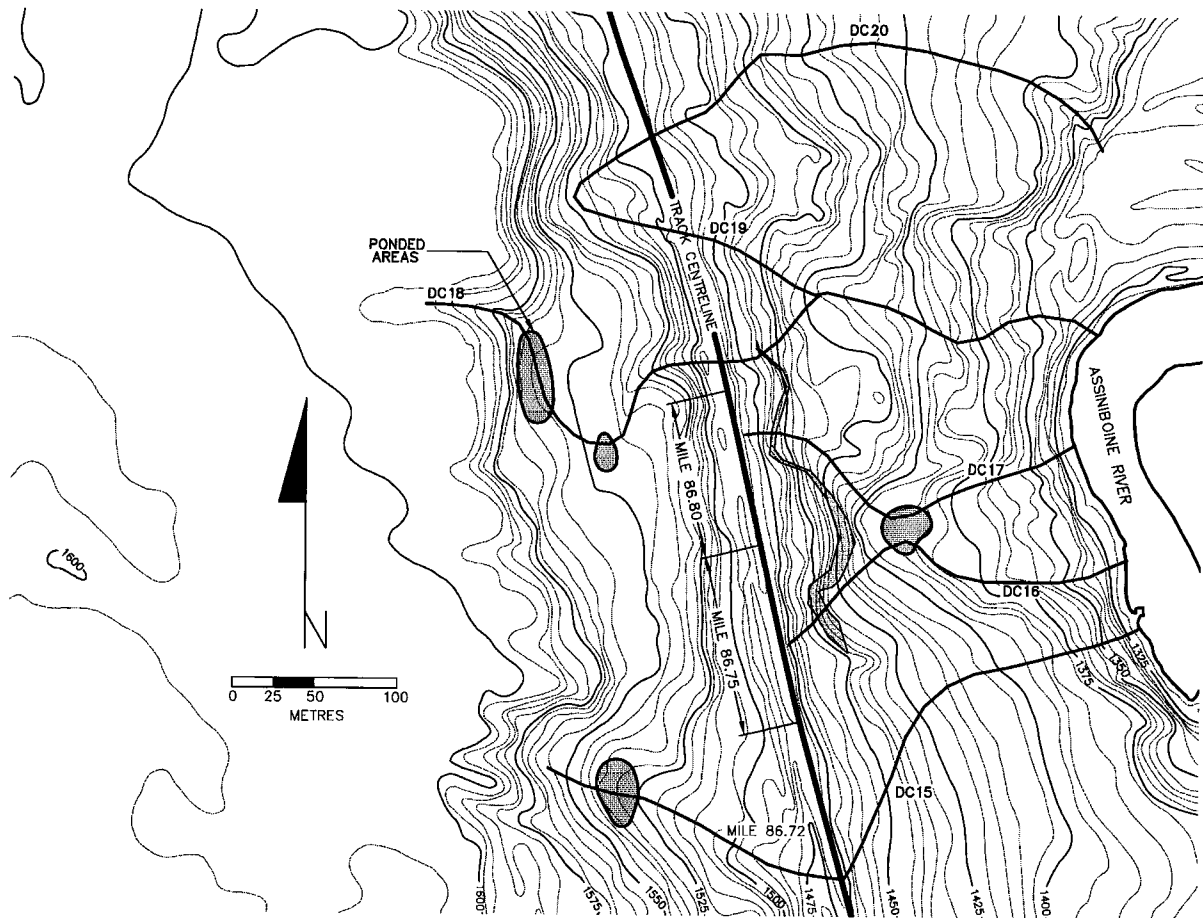
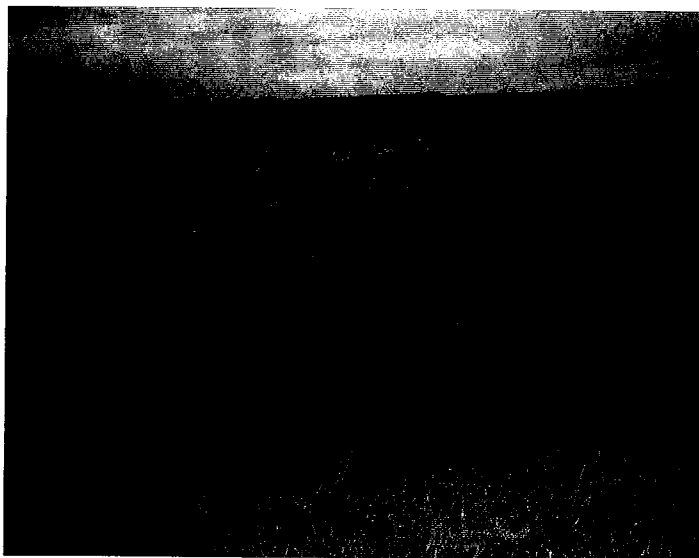
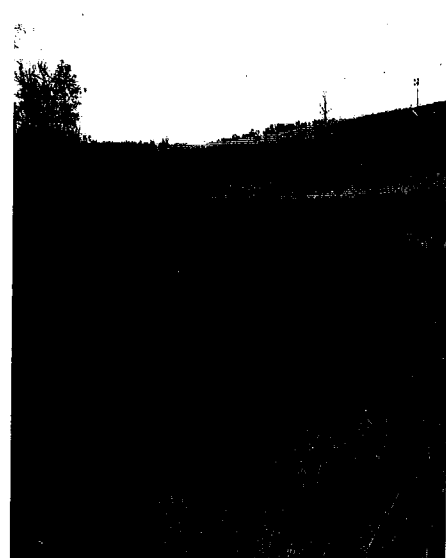


Figure 4-6: Surface drainage conditions, contours are in feet (Clifton Associates Ltd., 1986).



(a)



(b)

Figure 4-7: Existing surface drainage conditions of the downslope portion: (a) downslope view of DC16 and DC17 (b) upslope view of DC17 (2002 site visit).

The 1995 investigation, carried out from September 19 to 20, involved only test pits which were excavated with a track-mounted John Deere Backhoe (Clifton Associates Ltd., 1996). An additional eight boreholes were drilled from that time to the investigation of 2000-2001, however, no information detailing their excavation was found. The field investigation of 2000-2001 started on November 29, 2000 and was completed on January 25, 2001. This investigation involved the excavation of additional boreholes drilled using a Nodwell-mounted Mobile-S61 drill equipped with a solid stem auger that had continuous coring capabilities; the exception was BH 1101, which was drilled with a Brat 22, solid stem auger (Clifton Associates Ltd., 2001).

4.2.2 BOREHOLES & TEST PITS

The study area has been probed by a total of 41 boreholes (including those abandoned) as listed in Table 4-1. Of these, three (BH 505, 704 in 1986 and BH 923 in 1987) were rotary holes with a maximum depth of 100.2m (BH 505) and a minimum depth of 35 m (BH 704). The remaining holes were augered to a maximum depth of 60.5m (SI 1108) and a minimum depth of 4.6m (BH 1108). As illustrated by the gaps below, complete sets of field observations were not available for all boreholes. The only information found on BH 505 was a geophysical log and this was likewise with BH 704, but the “summary of sampling and laboratory test data” was also found for BH 704. All installation, exploration, and test data information was missing for Boreholes BH 901-903 and 1001-1005. In addition, three boreholes were reported in Clifton Associates Ltd., 1986 at BH 505; two were instrumented and one was abandoned. It is unknown why one was abandoned and which hole the geophysical log was carried out in. BH 304 was abandoned due to severe sloughing at a depth of 2 m, according to the borehole log. Likewise, BH 1108A was also abandoned due to the hole “squeezing” closed at a depth of 1.5 m and it was subsequently backfilled with cuttings.

In addition to these boreholes, 23 test pits (Table 4-2) were also excavated to aid in the investigation. The first 10 (TP 6-13, 30-31) were approximately 5 m long, 1 m wide and 2.5 to 6 m deep (Clifton Associates Ltd., 1988). TP 7 was left open for a few days in order to observe the seepage rate and groundwater level while the remaining pits were backfilled immediately. The dimensions of the last 13 pits (TP 1-8B) were unknown, but ranged in depths from 5 to 7.7 m. Locations of all boreholes and test pits relevant to the study area are shown below in Figure 4-8.

4.2.3 SAMPLING

Samples were retrieved during each investigation and examined with a variety of laboratory tests in order to establish material and strength characteristics of the different stratum encountered. Various methods were employed in the extraction of both representative disturbed and undisturbed samples. The 1986 investigation obtained washed cuttings at approximately 0.75 m intervals in the deep rotary holes and thin-walled Shelby tube samples at roughly 1.5 m intervals in the auger holes (Clifton Associates Ltd., 1986). The 1987 investigation recovered continuously cored samples in the rotary holes (core was extracted with a 3 m Christiansen Core Barrel in BH 923), thin-walled Shelby tube samples at selected intervals in auger holes, and disturbed samples from selected test pits (Clifton Associates Ltd., 1988). In the 1995 investigation, representative disturbed and large block samples were obtained (Clifton Associates Ltd., 1996). Similarly, the 2000-2001 investigation recovered representative disturbed and core samples (Clifton Associates Ltd., 1996).

Table 4-1: List of boreholes in the study area (see Figure 4-8 for borehole location).

	Borehole	Clifton Associates Ltd. Report	Installation Date	Drilling Method	Slope Location	Depth (m)
1	BH 207	R573	86MAR14-15	auger	upslope	24.99
2	BH 301		86MAR11	auger	upslope	19.05
3	BH 302		86MAR12	auger	upslope	37.49
4	BH 303		86MAR13	auger	upslope	29.87
5	BH 304		86MAR13	auger	upslope	18.29
6	BH 304A		86MAR14	auger	upslope	30.11
7						100.20
8	BH 505		-	rotary	upland	. ⁵
9						. ⁵
10	BH 704		86JUN25	rotary	upslope	35.00
11	BH 812		86JUN17	auger	downslope	39.62
12	BH 814		86JUN17	auger	downslope	24.69
13	BH 815		86JUN11	auger	upslope	18.29
14	BH 816		86JUN11	auger	upland	12.19
15	BH 817		86JUN12	auger	upland	18.29
16	BH 834		86JUN11	auger	downslope	21.34
17	BH 834A		86JUN11	auger	downslope	7.01
18	BH 912	R677	87JUN17	auger	upslope	9.10
19	BH 914		87JUN18	auger	downslope	7.60
20	BH 915		87JUN18	auger	downslope	7.60
21	BH 916		87JUN18	auger	downslope	6.10
22	BH 917		87JUN18	auger	downslope	6.10
23	BH 918		87JUN18	auger	downslope	10.70
24	BH 919		87JUN18	auger	downslope	6.10
25	BH 923		87JUN16	rotary	upslope	60.00
26	SI 901 ⁶	no installation information	96DEC03	-	downslope	18.60
27	SI 902 ⁶		96DEC03	-	downslope	17.40
28	SI 903 ⁶		96DEC03	-	downslope	23.50
29	SI 1001 ⁶		97APR12	-	upslope	60.70
30	SI 1002 ⁶		97APR12	-	downslope	60.70
31	BH 1003 ⁷		-	-	downslope	-
32	BH 1004 ⁷		-	-	downslope	-
33	BH 1005 ⁷		-	-	downslope	-
34	BH 1101	S884.2	01JAN08	auger	downslope	7.60
35	SI 1101		00NOV29	auger	downslope	60.40
36	BH 1108		01JAN04	auger	downslope	4.60
37	BH 1108A		01JAN17	auger	downslope	9.10
38	SI 1108		01JAN10	auger	downslope	60.50
39	BH 1109		01JAN04	auger	downslope	13.70
40	SI 1109		01JAN18	auger	downslope	57.30
41	BH 1110		01JAN06	auger	downslope	7.60

⁵ one was abandoned and no information was found on a second/third hole

⁶ installation date and depth based on slope inclinometer data

⁷ assumed to have occurred at the same time as SI 1001 and SI 1002

Table 4-2: List of test pits in study area (see Figure 4-8 for test pit location).

Test Pit	Clifton Associates Ltd. Report	Installation Date	Slope Location	Depth (m)
1 TP 6	R677	87JUN22	upslope	3.0
2 TP 7		87JUN22	upslope	3.5
3 TP 8		87JUN22	upslope	2.5
4 TP 9		-	upslope	3.0
5 TP 10		87JUN23	upslope	3.0
6 TP 11		87JUN23	upslope	5.0
7 TP 12		87JUN23	upslope	4.0
8 TP 13		87JUN23	upslope	4.0
9 TP 30		87JUN26	upslope	6.0
10 TP 31		87JUN26	upslope	6.0
11 TP 1	S884	95SEP19	upslope	6.9
12 TP 2		95SEP19	upslope	6.0
13 TP 3		95SEP19	upslope	5.8
14 TP 4		95SEP19	upslope	5.0
15 TP 5A		95SEP19	downslope	7.0
16 TP 5B		95SEP19	downslope	6.3
17 TP 5C		95SEP20	downslope	6.0
18 TP 6A		95SEP20	downslope	6.3
19 TP 6B		95SEP20	downslope	6.1
20 TP 7A		95SEP20	downslope	6.4
21 TP 7B		95SEP20	downslope	7.0
22 TP 8A		95SEP20	downslope	7.2
23 TP 8B		95SEP20	downslope	7.7

For the work in this thesis, 10 block samples were retrieved during the 2002 site visit. An opportunity arose to confirm previous lab results when the last phase of the 1995 remediation recommendation (installation of the second shear key at Mile 86.75) was under construction. However, due to the small window allotted for the decommissioning of the track for this installation, these samples were extracted from the excavation spoil pile in order to prevent any unnecessary burden and delay to the contractors and client. As a result, the depth from which each block was obtained was unknown except that they were all assumed to be from the “intact shale” stratum (i.e. the unweathered bedrock). Needless to say, the condition of these blocks was not ideally undisturbed, but rather representatively disturbed according to Hvorslev’s (1962) definition:

‘Representative samples contain all the mineral constituents of the stratum from which they are taken and have not been contaminated by material from other stratum or by chemical changes, but the soil structure is seriously disturbed and the water content may be changed.’ (p. 8)

4.2.4 INSTRUMENTATION

Two types of instrumentation have been installed in these investigations: piezometers to monitor groundwater conditions and slope inclinometers to monitor lateral movement of the slope. Of the 41 boreholes used in this investigation, 44 have been instrumented with either

piezometer(s) or slope inclinometers. A total of 33 piezometers and 11 slope inclinometers have been installed from 1986 to 2001. Unfortunately, information is missing on boreholes BH 1003-1005; hence, it is unknown whether they were instrumented with piezometers. Figure 4-9 illustrates the spatial relationship of these points of information in the study area, whereas active instrumentation located in the 2001 Clifton Associates Ltd. Reports File S884.2 is shown in Figure 4-10.

All piezometers installed in the study area (Table 4-3) are of the standpipe type, which entailed a PVC pipe casing with a screened tip at the bottom. A sand pack, with lengths ranging from 1.22 m in P 914A to 13.1 m in P 812A, surrounded the tip and bentonite plugs were employed either above (deeper installations) or both above and below (shallow and intermediate installations) to isolate the sand pack. Piezometers P 207A & B to P 304 & 304A entailed a 38 mm ID casing with a 50 mm ID No. 10 x 914 mm PVC Rice screen in a 150 mm diameter borehole while piezometers 505A & B to P 834 employed a 40 mm ID casing with a 50 mm ID No. 10 PVC Rice screen in a 125 mm diameter borehole. The sand pack for these piezometers was composed of 10-20 silica sand and the bentonite seals were 300 mm in thickness (Clifton Associates Ltd., 1986). Piezometers P 912 to 919 involved a 38 mm ID casing with a 38 mm ID No. 10 PVC Rice screen in a 150 mm diameter borehole and 12-20 silica sand packs. Piezometers 1101 to 1110 entailed 25 mm ID casing with a 25 mm ID Schedule 40 PVC screen, "frac" sand packs, and 1.6 m to 2.4 m thick bentonite plugs.

Table 4-4 summarizes the slope inclinometers installed within the study area. The oldest slope inclinometers consisted of standard plastic casings, backfilled with 10-20 silica sand and cuttings; the casing of SI 302 was 85 mm OD in a 150 mm diameter borehole and SI consisted of 95 mm OD casing in a 125 mm diameter borehole. In SI 923, the casing was 85 mm in diameter, the borehole was 160 mm in diameter, and 12-20 silica sand was used. No installation information on slope inclinometers SI 901-903, 1001, and 1002 was found. Slope inclinometers SI 1101, 1108, and 1109 consisted of 50 mm diameter casing with a cement bentonite grout.

By convention, the A-axis is normally installed with its positive direction in the direction of movement (i.e. parallel to the slope cross-section); hence, the B-axis records lateral movement of the slope. However, it appeared that the direction of movement (i.e. A-axis direction) for these installations was consistently in the negative direction with the exception of SI 1101, which was in the opposite direction. Thus, the data vectors from SI 1101 have been turned 180° to be consistent with the direction of movement of the other slope inclinometers.

4.2.5 MONITORING OF INSTRUMENTATION

Due to the continual addition of instrumentation to the study area and previous construction activities, monitoring data have been irregular and sporadic. Groundwater levels in piezometers installed in 1986 (P 207A & B to P 834A) were initially observed and monitored weekly during the months of April and May, 1986 while a monthly monitoring program was put into place following this period. The initial groundwater conditions were observed at the end of the field investigation in the piezometers installed in 1987 (P 912 to P 919). Likewise, this was the procedure followed for those installed in the 2000-2001 investigation (P 1101 to P 1110). At various times of monitoring, some piezometers were either frozen or could not be located (with the high likelihood of their decommissioning during previous construction

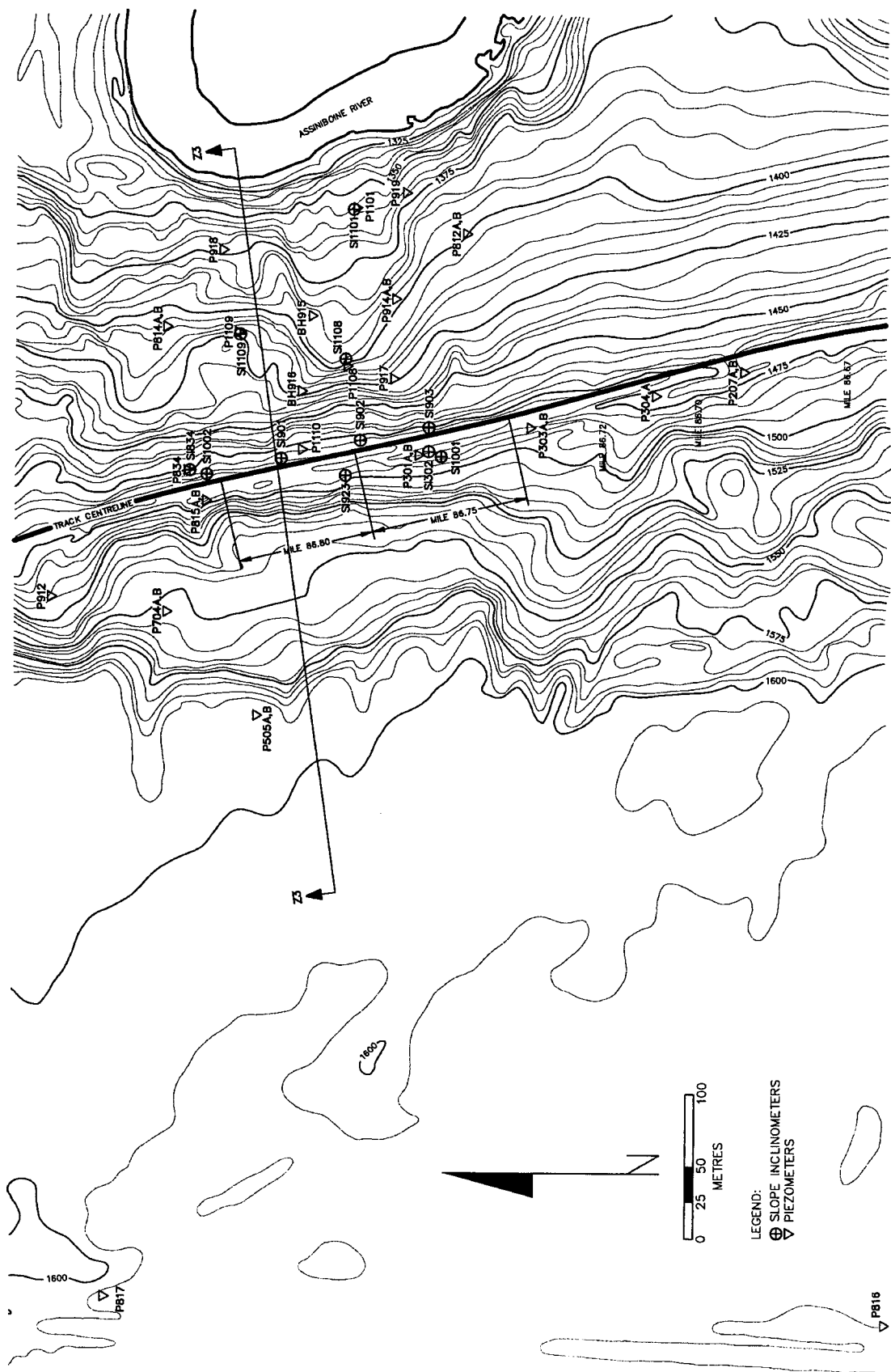


Figure 4-9: Location map of all instrumentation installed from 1986 to 2001 (contours in feet).

Table 4-3: Summary of piezometer installations.

Borehole	Instrumentation Number	Quantity	Installation Date	Tip Depth (m)	Sand Pack Thickness (m)	Stratum Isolated
BH 207	P 207A	2 nested	86MAR15	12.19	1.70	unoxidized shale & till
	P 207B			3.54	2.63	till & sand
BH 301	P 301A	2 nested	86MAR11	19.05	2.01	unoxidized shale
	P 301B			5.49	2.11	unoxidized & oxidized shale
BH 303	P 303A	2 nested	86MAR13	29.87	2.59	unoxidized shale
	P 303B			4.57	3.75	unoxidized & oxidized shale
BH 304A	P 304	2 nested	86MAR14	4.02	3.35	till & oxidized shale
	P 304A			30.11	2.01	unoxidized shale
BH 505	P 505A	2 in 2 boreholes	86MAR21	25.06	5.67	unoxidized shale
	P 505B			9.14	4.87	till & unoxidized shale
BH 704	P 704A	2 nested	86JUN25	27.13	6.40	unoxidized shale
	P 704B			9.14	3.04	till & oxidized shale
BH 812	P 812A	2 nested	86JUN17	39.62	13.10	unoxidized shale
	P 812B			5.03	2.90	oxidized shale
BH 814	P 814A	2 nested	86JUN17	24.38	1.52	unoxidized shale
	P 814B			4.88	1.98	oxidized shale
BH 815	P 815A	2 nested	86JUN11	17.22	4.42	unoxidized shale
	P 815B			6.86	4.60	unoxidized & oxidized shale
BH 816	P 816	1	86JUN12	6.10	3.36	oxidized till & sand
BH 817	P 817	1	86JUN12	14.00	12.17	till, sand & gravel
BH 834A	P 834	1	86JUN11	7.01	5.03	unoxidized & oxidized shale
BH 912	P 912	1	87JUN18	6.10	1.38	oxidized shale
BH 914	P 914A	2 (nested)	87JUN18	7.62	1.22	oxidized shale
	P 914B			2.74	1.52	oxidized till, gravel & oxidized shale
BH 915	P 915	1	87JUN18	7.62	1.83	oxidized till
BH 916	P 916	1	87JUN18	5.79	1.83	oxidized till & unoxidized shale
BH 917	P 917	1	87JUN18	3.66	1.53	oxidized till & unoxidized shale
BH 918	P 918	1	87JUN18	4.57	1.83	unoxidized & oxidized till
BH 919	P 919	1	87JUN18	6.10	1.53	unoxidized till & shale
BH 1101	P 1101	1	01JAN08	7.00	1.60	clay & oxidized till
BH 1108	P 1108	1	01JAN04	4.55	1.30	unoxidized shale
BH 1109	P 1109	1	01JAN04	5.50	2.45	oxidized till & clay
BH 1110	P 1110	1	01JAN06	7.00	1.80	unoxidized & oxidized till

Table 4-4: Summary of slope inclinometer installations.

Boreholes	Instrumentation Number	Installation Date	Depth (m)
BH 302	SI 302	86FEB12 ⁸	37.49
BH 834	SI 834	86JUN11	21.03
BH 923	SI 923	86JUL15	60.16
SI 901 ⁹	SI 901	96DEC03	18.60
SI 902 ⁹	SI 902	96DEC03	17.40
SI 903 ⁹	SI 903	96DEC03	23.50
SI 1001 ⁹	SI 1001	97APR12	60.70
SI 1002 ⁹	SI 1002	97APR12	60.70
SI 1101	SI 1101	00NOV29	58.20
SI 1108	SI 1108	01JAN10	60.00
SI 1109	SI 1109	01JAN18	57.60

activities). Table 4-5 summarizes the information available for the monitoring of these piezometers.

Slope inclinometers were monitored in accordance with those dates summarized in Table 4-6. The frequency of slope inclinometer monitoring in comparison with piezometers has been relatively higher. Despite this, some inclinometers have large gaps (in terms of years) between readings while others have a small number of readings before their destruction due to construction activities or having been sheared off due to slope movement. Slope inclinometer readings were taken at approximately 0.6 m intervals.

Of the 29 piezometers and 3 slope inclinometers previously installed, the 1995 investigation could only locate two piezometers (P 812 and P 917) and one slope inclinometer (SI 834). The 2000-2001 investigation could only locate one of the previously installed piezometers (P 919) and five of the more recently installed slope inclinometers (SI 901-903 and 1001-1002). In addition, SI 1108 could not be monitored during the monitoring dates indicated in Table 4-6 due to ice blockage in the casing while SI 1101 had sheared off sometime between February 22, 2001 and March, 2001 (Clifton Associates Ltd., 2001).

4.3 INTERPRETATION OF INVESTIGATIONS: SITE CHARACTERIZATION

This section encompasses the processing of available field investigation information in order to deduce a model to be used in the following stability and deformation analyses. However, the second-hand (i.e. already -interpreted) or incomplete nature of the information made this a challenge.

⁸ this is mostly an error since the borehole was installed on March 12, 1986 and the investigation was carried out between March 11 and 24, 1986

⁹ installation date and depth based on slope inclinometer data

Table 4-5: Summary of piezometer monitoring.

Piezometer	Initial Reading	Monitoring Dates	Reading Interval (days)	Piezometer	Initial Reading	Monitoring Dates	Reading Interval (days)
P 207A P 207B	86MAR23	86APR21	29	P 505A P 505B	86APR06	86APR20	14
		86APR28	7			86APR28	8
		86MAY10	12			86MAY11	13
		86JUN06	27			86MAY24	13
		86JUL22	46			86JUN13	20
P 301A P 301B	86MAR23	86APR20	28	P 704A P 704B	86JUL02	86JUL23	21
		86APR28	8				
		86MAY10	12				
		86MAY25	15				
		86JUN06	12				
P 303A P 303B	86MAR23	86JUL23	47	P 812A P 812B	86JUL02	86JUL23	21
P 304 P 304A	86MAR23	86APR21	29	P 814A P 814B	86JUL02	86JUL23	21
		86APR28	7				
		86MAY10	12				
		86MAY25	15				
		86JUN06	12				
P 1101	01JAN25	86JUL23	47	P 815A P 815B	86JUL02	86JUL23	21
P 1108	01JAN25	86APR20	28	P 816 P 817	86JUL02	86JUL23	21
		86APR28	8				
		86MAY10	12				
		86MAY25	15				
		86JUN06	12				
P 1110	01JAN25	86JUL23	47	P 834	86JUL02	86JUL23	21
P 1109	01JAN25	86APR20	28	P 912 P 914A P 914B	-	01MAR20	-
		86APR28	8				
		86MAY10	12				
		86MAY25	15				
		86JUN06	12				
P 1110	01JAN25	86JUL23	47	P 915 P 916 P 917 P 918	-	01MAR20	-
P 1109	01JAN25	86JUL23	47	P 919	-	01MAR20	-
P 1110	01JAN25	86APR20	28	P 1109	01JAN25	01FEB25	31
		86APR28	8			01MAR20	23
		86MAY10	12				
		86MAY25	15				
		86JUN06	12				
P 1110	01JAN25	86JUL23	47	P 1110	01JAN25	01FEB25	31
						01MAR20	23

4.3.1 STRATIGRAPHIC PROFILE

Determination of the stratigraphic profile was one of the biggest challenges in the interpretation of the field investigation due to the heavy reliance on the borehole logs. This was further amplified by the long period over which the investigations have occurred – 16 years. Over this period, borehole and test pit logging have been carried out by a total of eight different people and within at least three topographic stages of valley slope development. Topographically, the model has been based on the 1986 contours since that investigation was the most complete in terms of the size of the area investigated and laboratory testing carried out. Boreholes and test pits used in the following interpretation are shown in Figure 4-9. From this figure, the scattered and yet concentrated nature of the field investigation can be established; the upland and upslope portions are sparsely investigated while the majority of the investigations have been concentrated in the downslope portion. Table 4-1 and 4-2 summarizes the boreholes and test pits used and their location relative to the track centreline. Only three boreholes were used in establishing the upland conditions while the upslope conditions were determined by 10 boreholes and 14 test pits, and the downslope conditions were deduced from 18 boreholes and nine test pits. The location of section, Z3, was selected based on maintaining as small a projected distance from boreholes

Table 4-6: Summary of slope inclinometer monitoring.

Slope Inclinometer	Initial Reading	Monitoring Dates	Reading Interval (days)	Slope Inclinometer	Initial Reading	Monitoring Dates	Reading Interval (days)
SI 302	86APR07	86JUL22 88MAR22	106 609	SI 903	96DEC03	97JAN06	34
SI 834	86JUL23	88MAR22 95SEP21	608 2739			97MAR24	77
SI 923	87JUL17	87NOV 88MAR22	107-136 113-142			97MAY22	59
SI 901	96DEC03	97JAN06	34			97OCT23	154
		97MAR24	77			99OCT20	727
		97MAY22	59			00OCT20	356
		97OCT23	154			01FEB23	136
		99OCT20	727			01APR25	61
		00OCT20	356			01JUL03	69
		01FEB23	136	SI 1001	97APR12	97MAY22	40
		01APR25	61			97OCT23	154
		01JUL05	71			99OCT20	727
SI 902	96DEC03	97JAN06	34			00OCT20	356
		97MAR24	77			01FEB23	136
		97MAY22	59			01APR25	61
		97OCT23	154			01JUL03	69
		99OCT20	727	SI 1002	97APR12	97MAY22	40
		00OCT20	356			97OCT23	154
		01FEB23	136			99OCT20	727
		01APR25	61			00OCT20	356
		01JUL05	71			01FEB23	136
				SI 1101	01JAN10	01FEB22	43
						01MAR19	60
						01APR26	38
				SI 1108	01JAN18	01FEB22	28
						01MAR19	25
						01APR26	38
				SI 1109	01JAN25	01FEB22	28
						01MAR19	25
						01APR26	38

and test pits as possible and its spatial relationship to the existing scarp in addition to the encroaching meander of the Assiniboine River.

Due to the inconsistency of stratigraphic interpretations from the logging of boreholes and test pits in the last 16 years, the interpreted stratigraphic profile in Figure 4-11 was not solely dependent on these logs, but also on the water content and dry density profiles corresponding to these logs. In addition, the number of strata was reduced to three (till, intermix of till and clay shale, and intact clay shale bedrock) owing to the difficulty in differentiating the weathered zone from the disturbed zone in the clay shale stratum from the exclusive use of these logs.

The till consisted of an olive brown, sandy or silty clay matrix that was predominantly calcareous and oxidized. In the upland, the till was stained with iron and manganese and contained layers of wet sand and/or gravel. Glauber salts and a fissured structure were observed in the downslope portion, in addition to the similar presence of iron and manganese staining.

The term “intermix” encompassed not only the disturbed region consisting of intermixed material from the two strata (i.e. colluvium consisting of till and shale), but also the underlying disturbed and weathered zone of the shale bedrock. Generally, the intermix was highly disturbed and consisted of olive grey to dark greyish brown, calcareous to

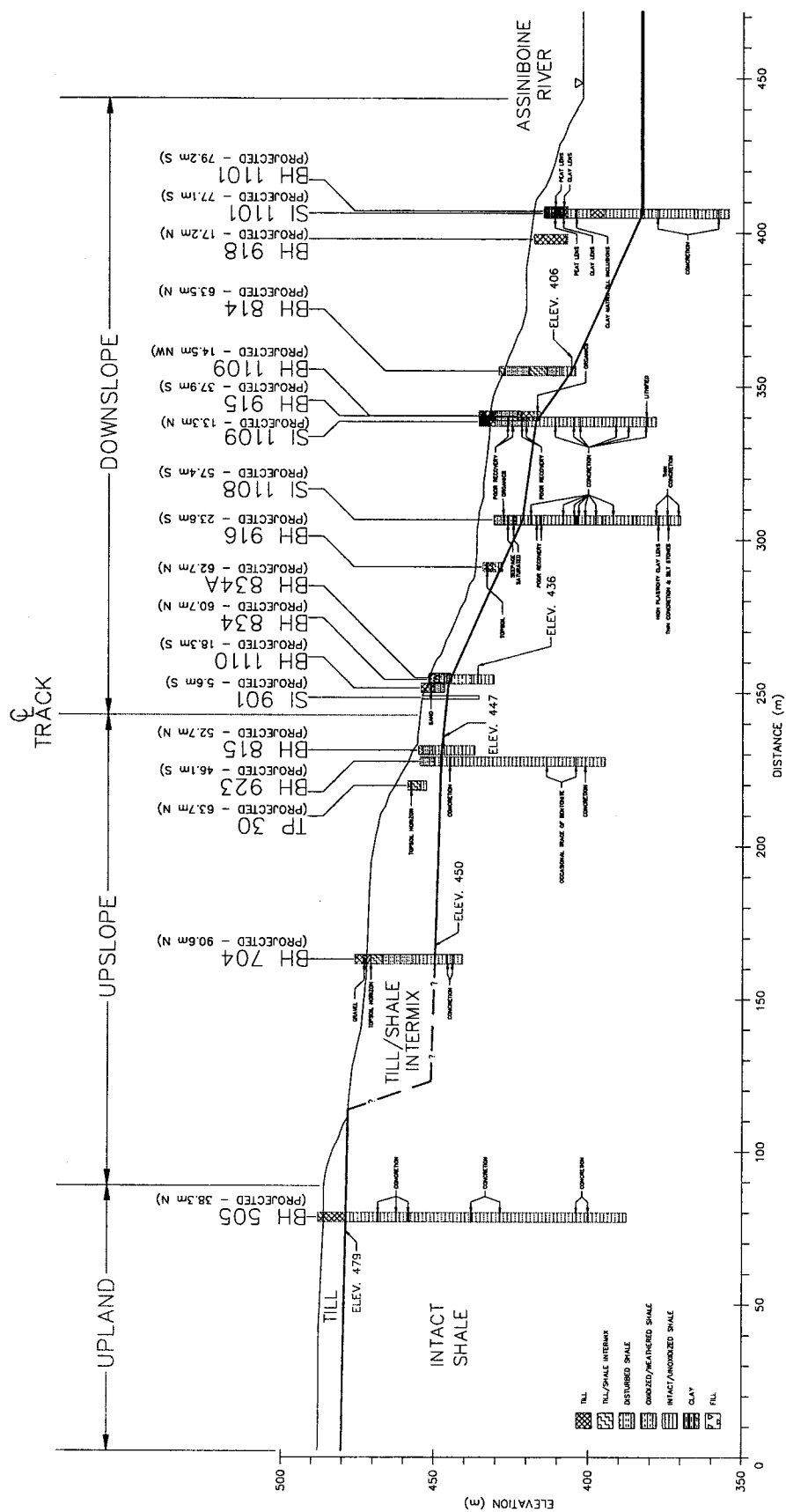


Figure 4-11: Stratigraphy of section Z3 with enlarged figure (Figure A-21) in Appendix A. (See Figure 4-8 for location of section)

noncalcareous, brecciated, jointed, silty clay shale and sandy clay matrix till. The disturbed shale stratum contained shear zones and ranged in colour from dark olive grey to very dark grey, and was noncalcareous, highly weathered, oxidized, brecciated, jointed and blocky, and ironed stained. In most holes, the weathered zone appeared to occur as “oxidized” shale (with a consistent water content profile above 20%) whereas “unoxidized” corresponded to a water content profile very near 20% (Table 4-7). However, as the lower portion of the slope was approached, the water content profile was not consistently near 20% in the presence of the “unoxidized” shale (as indicated by SI 1101 in Figure 4-12).

The intact shale (unweathered bedrock) was very dark grey in colour, unoxidized, silty, and highly plastic with an overall blocky and jointed structure. In addition, it was described as noncalcareous with the exception of SI 1101. Figure 4-11 clearly shows an occasional trace of bentonite logged in BH 923 and the numerous concretion zones commonly found in the stratum: seven in BH 505 (with thicknesses of up to 0.7 m), two in BH 704, two in BH 923, 11 in SI 1108 (with thicknesses of up to 0.9 m), six in SI 1109, and two in SI 1101. Other structural elements logged in the intact shale included three fracture zones in SI 1108, three jointed zones in SI 1109, one jointed zone in SI 1101, and slickensides in both the unweathered and weathered zones of the shale in SI 1101 (Figure 4-12). Despite the presence of these structural features in the intact shale, there was no evidence of their horizontal continuity.

Upland conditions of section Z3 were established by the relatively shallow investigations of BH 816 (12.2 m) and BH 817 (18.3 m), located near the access road, and the deeper investigation of BH 505 (100.2 m), located near the crest of the valley wall. Only two strata were identified in the upland, till and the intact shale bedrock. Till was evident as the uppermost stratum in all holes with thicknesses varying from about 8 m to almost 15 m near the road and 9 m at the crest of the valley wall. As expected, the clay shale bedrock (“intact shale” in Figure 4-11) was found to lie directly beneath at elevations ranging from 475 m (BH 817) to 485 m (BH 816). These elevations to the bedrock were interpreted by Clifton Associates Ltd. (1986). Bedrock in BH 505 was identified at an elevation of 479 m, while the ground elevation was established by back-calculating from this elevation with the assumption that it corresponded to the top of the clay shale stratum reported by the geophysical log (borehole logging for BH 505 was missing). This was not an unreasonable assumption owing to its locality in the upland portion and therefore, most likely outside any zones of past disturbances. The till layer was assumed to cover the bedrock shale in a rather horizontal orientation according to the depositional history of the area; thus, the interface between the till and the shale was located at the interpreted bedrock elevation provided in BH 505 and extended at a slope parallel to the upland until it intersected the slope surface.

Table 4-7: Water content and dry density ranges of the intact shale bedrock.

Slope Location	Borehole Identification	Water Content Range (%)	Average Water Content (%)	Dry Density Range (kg/m ³)	Dry Density Average (kg/m ³)
Upslope	BH 923	18.2-22.3	19.6	1758-1836	1789.6
	BH 834	18.3-21.2	20.2	1752	1752
Downslope	SI 1108	18.4-26	20.8	-	-
	SI 1109	16-24.6	21.2	-	-
	SI 1101	15.8-31.2	22.3	-	-

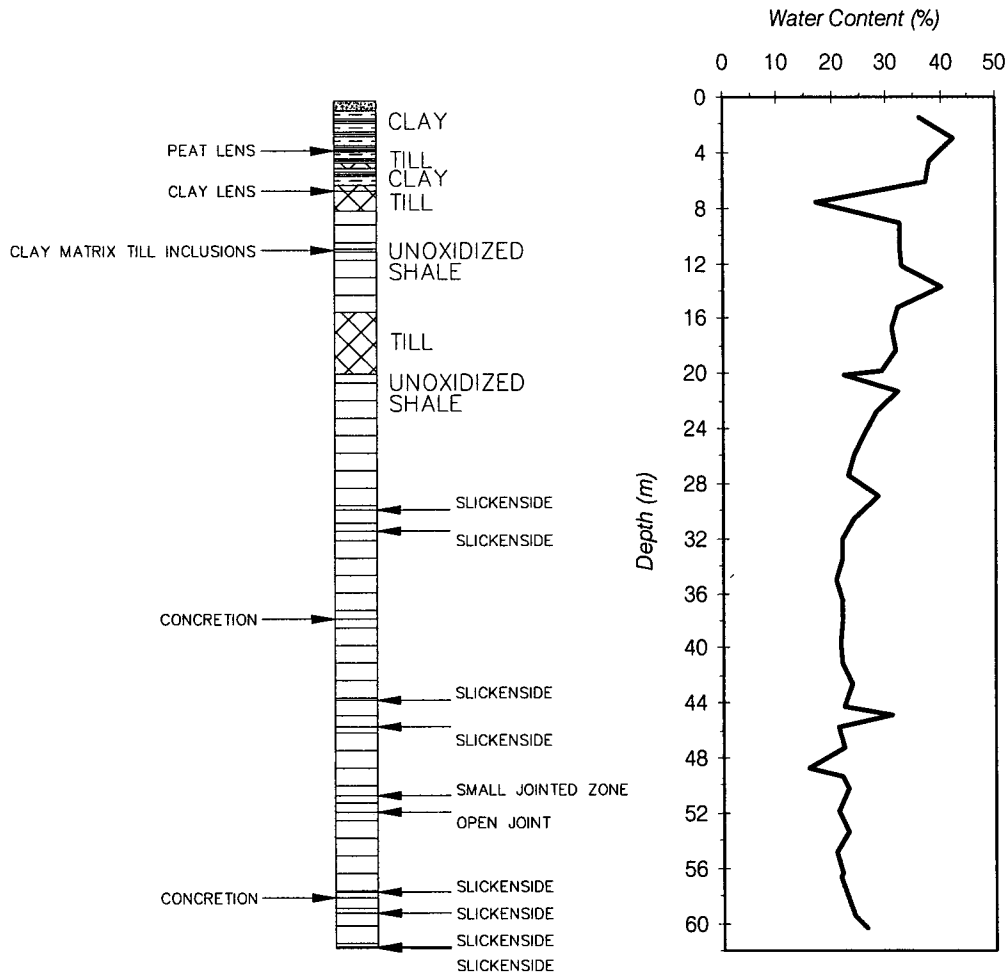


Figure 4-12: Water content profile of SI 1101.

The mid-upslope condition (Figure 4-11) was determined from BH 704, while TP 30, BH 923, and BH 815 were used to establish the near-track portion of the upslope. Again, only two strata were identified, intermix and the intact shale bedrock. Till, directly overlying the clay shale stratum, was also found at the top of BH 704 with a thickness of 8.8 m. The clay shale stratum was weathered with shear zones and disturbed regions in the top 17.2 m, and was underlain by intact shale at an elevation of 450 m (this was the only hole in the study area which reported the occurrence of an “intact shale” stratum that was differentiated from the “clay shale” stratum). In the upslope and near the track, the occurrence of any till layer was absent. Instead, the clay shale stratum was directly overlain by either topsoil or fill. In TP 30, the bottom of the weathered/oxidized shale, as evidenced by iron and manganese staining (Crandell, 1958; Schaefer and Lohnes, 2001), and disturbed shale zone was reached at a depth of 4.2 m when the shale became unoxidized and hard. No interpreted intact shale elevation was observed in BH 923 and no mention of it was made in the borehole log. In this case, both the water content and dry density profiles (Figure 4-13) were used in determining its location. The water content at elevation 448.9 m was consistently near 20%; below this elevation, the water contents ranged from a low of 18.2% to a high of 22.3% (average of 20%), while those above this point ranged from 22.2% to 31.5% (average of

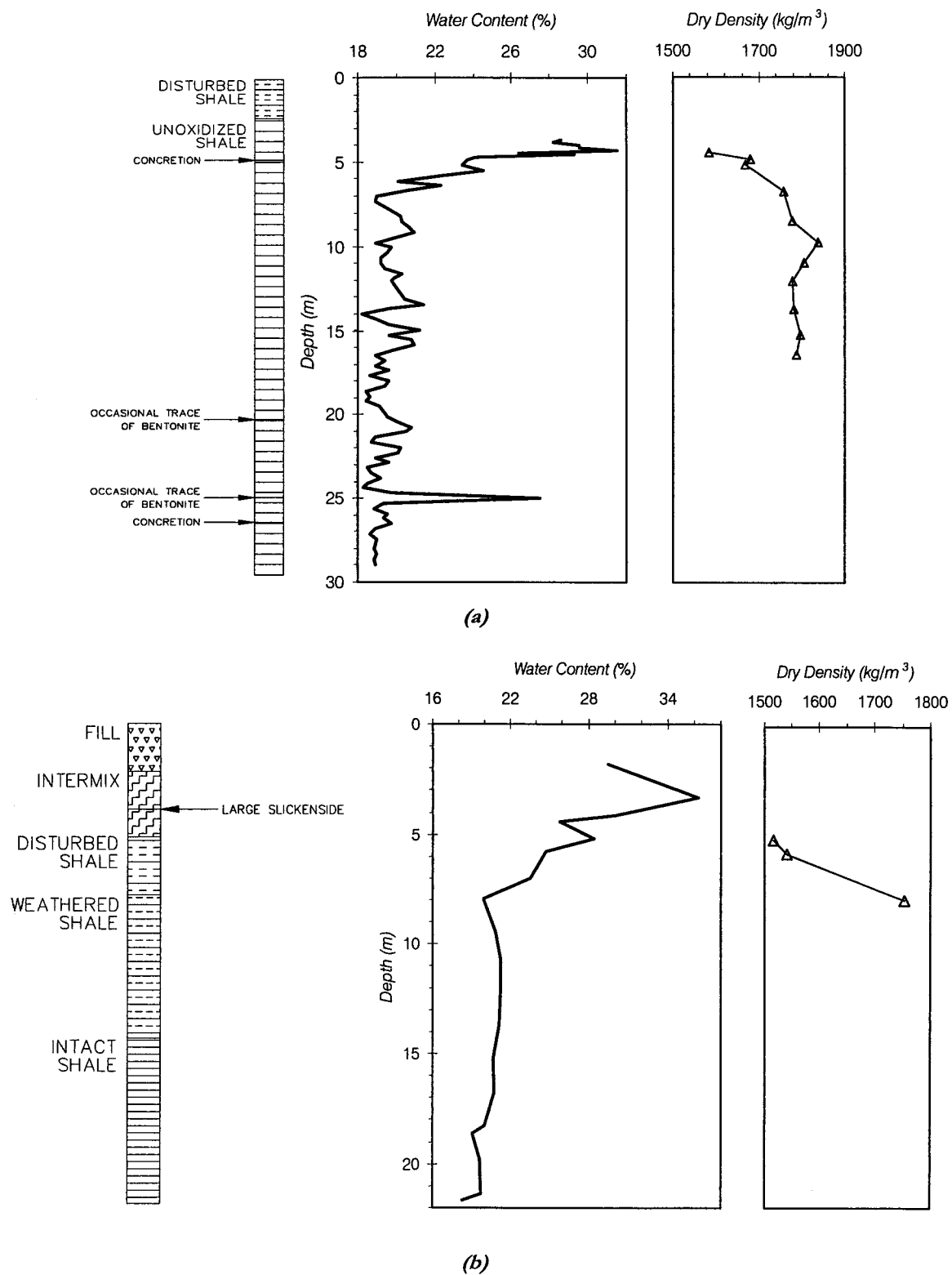


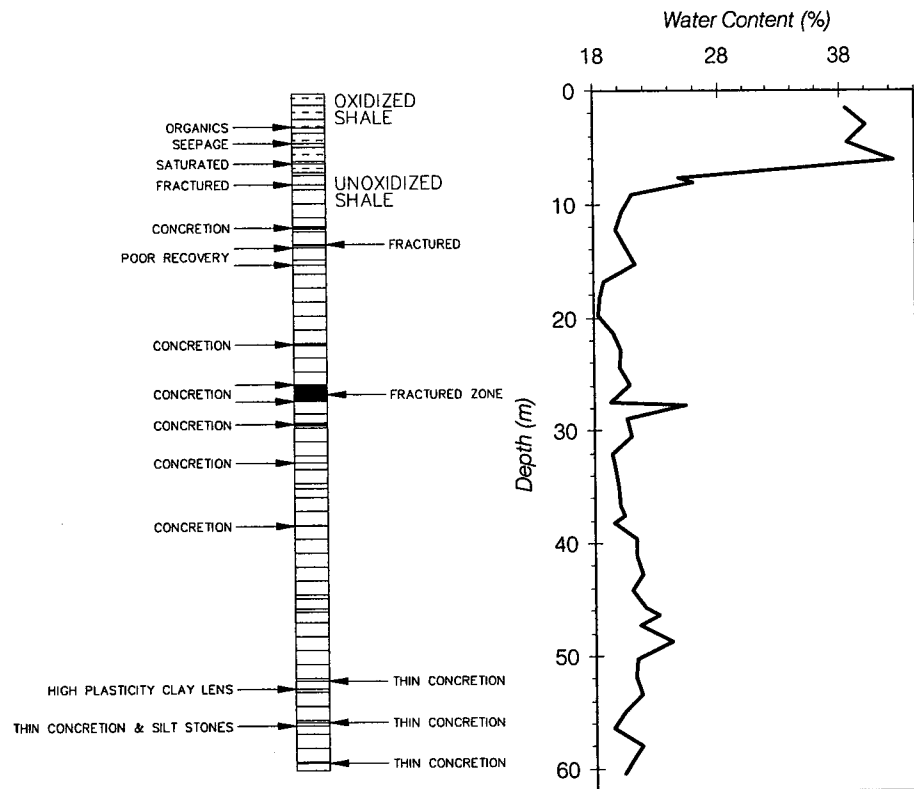
Figure 4-13: Water content and dry density profiles of (a) BH 923 and (b) BH 834.

27%). The dry density averaged 1640 kg/m³ above elevation 448.9 m, while those below averaged 1790 kg/m³. However, an interpreted intact shale elevation was observed in BH 815 at an elevation of 447 m; the weathered and disturbed zone was roughly 8.4 m thick. Owing to the close proximity of these two boreholes on the projected section and the similarity of their projected distances (46.1 m to BH 923 and 52.7 m to BH 815), the intact shale stratum was placed at an elevation of 448 m between these two holes.

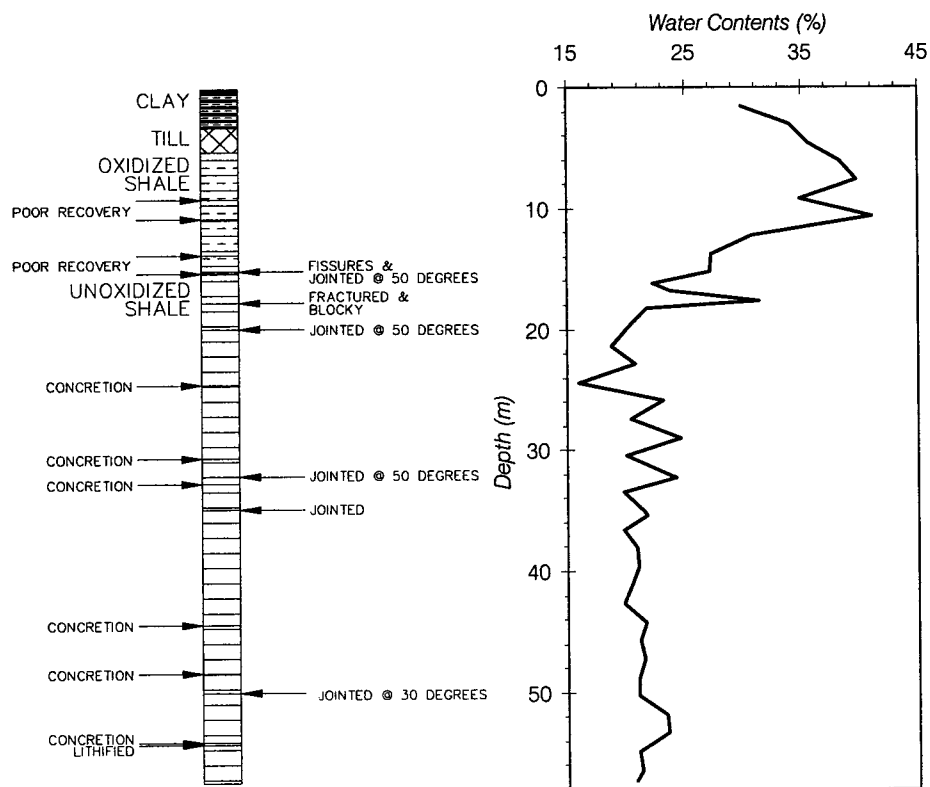
In section Z3, interpretation of the downslope portion of the valley wall was based on information provided by the 13 boreholes shown in Figure 4-11; the near track conditions by BH 901, 1110, 834 and 834A, the mid-downslope by BH 916, SI 1108, 1109, BH 915, 1109, and 814, and the lower portion by BH 918, SI 1101, and BH 1101. Again no borehole log was found on BH 901; therefore it was not used in the following stratigraphic profile interpretation. The number of strata identified here was also two, the intermix and intact shale bedrock.

Near the track, the uppermost till layer was only observed in BH 1110 at a thickness of 4.1 m, whereas the other holes logged 2.1-3.4 m of fill at the top overlying 2.4-2.9 m of disturbed material composed of intermixed till and clay shale. No intact shale was observed in BH 834A (with an end of borehole elevation at 444.9 m), which was consistent with its water content (ranging from 23.7-24.2% and averaging 24%) and dry density (1620 kg/m³). In BH 1110, intact shale did not appear until near the bottom of the hole (elevation 447 m) where a single water content of 19.8% was recorded. Therefore, the weathered or oxidized shale zone ranged in thickness from 2.3 m in BH 1110 (water contents ranging from 27.1-33.6% and averaging 30%) to 11.2 m in BH 834 (water contents ranging from 23.5-28.4% and averaging 26%, with an average dry density of 1530 kg/m³) and perhaps even thicker in BH 834A. The intact shale stratum was interpreted at an elevation of 436 m in BH 834. However, both water contents and dry density data (Figure 4-13) seem to suggest its occurrence at a higher elevation of 446.1 m (water contents ranged from 18.3-21.2% and averaged 20%, while the average dry density was 1750 kg/m³). Due to the closer proximity of BH 1110 to section Z3, (projected distance of 18.3 m compared to 60.7 m of BH 834), the final interpretation of the intact shale was located at an elevation of 445.6 m between these two holes.

In the mid-downslope region, the uppermost layer observed in almost all boreholes (BH 916, SI 1109, BH 915, and BH 1109) was till. BH 915 was exclusively till with a thickness of 7.6 m, whereas roughly 52.5 m away, it was only 3.5 m thick in BH 916. In SI 1109, it was overlain by clay and underlain by clay shale, while it alternated between layers of the same clay stratum in BH 1109 with thicknesses averaging 0.9 m. SI 1108 had no till logged, while a 7.9 m thick stratum of clay shale was logged between the intermix strata with thicknesses ranging from 1.8 m to 5.5 m in BH 814. This alternation of layers and the lack of continuity between the till layers of surrounding holes suggested that this region was disturbed. The thickness of the weathered/oxidized clay shale zone ranged from 8.2 m in BH 814 to 13.1 m in SI 1109. Intact shale was not observed in the clay shale stratum in BH 916, BH 915, and BH 1109, which was also confirmed by water content data; the single water content of BH 916 at the bottom of the borehole (6.1 m) was 22.4% while the average water content of BH 1109 was 33%. The only interpreted intact shale elevation provided was at 406 m in BH 814, whereas the water content profile was used for both SI 1108 and SI 1109 in locating the top of the intact shale bedrock within the clay shale stratum. In SI 1108, the water content (Figure 4-14) ranged from 24.8-42.3% (averaging 37%) above an elevation of 421.9 m, while it ranged from 18.4-26% (averaging 21%) below this elevation. The water content profile did not decrease to 20% until below an elevation of 417.5 m in SI 1109 (Figure 4-14); a range



(a)



(b)

Figure 4-14: Water content profiles of (a) SI 1108 and (b) SI 1109.

of 22.3-41.1% (averaging 32%) was recorded above this elevation and a range of 16-24.6% (averaging 21%) was recorded below it.

The greatest uncertainty lay in the interpretation of the lower slope due to the limited information available (with respect to the number of boreholes and the information their logs provided). The borehole log of BH 918 (projected distance of 17.2 m) consisted of solely till to a depth of 10.7m. Both SI 1101 and BH 1101 contained till (ranging from 0.4 m to 1.8 m in thickness) alternating with clay strata (ranging from 1.2 m to 3.7 m in thickness). BH 1101 was only advanced to a depth of 7.6 m and its lowest stratum was till. However, SI 1101 was advanced to a depth of 60.4 m and the last till layer in BH 1101 was found to have been underlain by clay shale (7.2 m thick) in SI 1101, which was in turn underlain by another till layer (4.4 m thick) and clay shale was then encountered to the terminus of SI 1101. The difficulty in the interpretation of the intact shale bedrock in SI 1101 lay in the use of a greater varying water content profile (Figure 4-12), which ranged from 15.8-31.2% and averaged 22%. The intact shale was located at an elevation of approximately 383 m, at a point where the water contents seemed to have stabilized near 20%. Accordingly, the weathered zone of the clay shale for this hole was approximately 12.6 m thick and contained unoxidized shale.

4.3.2 GROUNDWATER CONDITIONS

Figure 4-15 summarizes the maximum and minimum groundwater level elevations recorded in each piezometer. It was particularly difficult to establish the groundwater table due to the substantial gap in data in the middle portion of the slope. Both BH 916 and BH 1108 have piezometers installed, but readings for the set of piezometers installed in the 1987 investigation could not be found and BH 1108 was frozen during periods of monitoring. Similarly, groundwater level information is missing for BH 915 and BH 918. However, in both cases, other boreholes (BH 1109 near BH 915 and BH 1101 near BH 918) were located within their projected proximity.

Initially, it was thought that the difficulty in establishing the groundwater conditions extended beyond the lack of information to the quality of information available (i.e. due to a combination of the soil type being monitored and the type of piezometers used). Most piezometers were installed in the clay shale stratum and all piezometers were of the standpipe type. In the succeeding section on laboratory testing, the clay shale stratum has a reported coefficient of permeability ranging from 3.3×10^{-10} m/s to 6.5×10^{-12} m/s (depending on the applied normal stress), rendering it relatively impermeable. The major limitations with this kind of piezometer are inherent to its design, where according to Dunnicliff (1988),

'A major limitation is their slow response [hydrodynamic time lag] to changes in piezometric head, because a significant volume of water must flow out of or into the soil or rock mass to register a change in head. ... A second major limitation is caused by the existence of the standpipe...the standpipe is subject to damage by construction equipment.' (p. 120)

In order to counter an inevitably slow response in a relatively impermeable material, the completion zone (sand pack surrounding the filter) must be of an adequate surface area in order for equalization of pore water pressure to occur. This would require a completion zone of an incredibly small volume in order to accommodate the low permeability. Hence, monitoring results from such piezometers are not reliable when used in this kind of material. As a result and based on surface seepage observations, the groundwater level was assumed at ground surface.

However, the 2002 site visit revealed extensive jointing in the weathered shale bedrock with its possible extension into the unweathered (intact) shale, albeit to a lesser degree. This was alluded to by the high heads measured in the deeper piezometers which only isolated what was presumed to be the intact shale stratum (Table 4-3). The sand packs of piezometers P301A, 303A, 304A, 505A, 704A, and 814A isolated unoxidized shale (logs indicated unoxidized clay shale and tip depths ranged from 17.2-30.1m), and the measured heads ranged from 2.1-30.7 m. Installation information on P304A indicated that the tip was located at a depth of 29.9 m, however monitoring records showed a measured head of 30.7m; thus, it was uncertain whether the installation information or the monitoring record was in error. It appeared that even these deep piezometric measurements indicated a high groundwater level, thereby implying that the degree of jointing in the intact shale may be sufficient to allow substantial groundwater movement within the stratum. Hence, the initial assumption that the groundwater level was at surface appeared to be plausible (but possibly conservative), which was further substantiated by the number of ponded areas, the shallow nature of the surface drainage courses, and the fact that major movements have been associated with abnormally wet climatic conditions.

Despite this uncertainty, a generalized profile of the groundwater table was developed from the piezometers shown in Figure 4-15 for use in sensitivity analyses. The upland condition was ascertained by P 505B, which indicated the groundwater level to be approximately 7 m below surface. The upslope condition was established by P 704A & B and P 815B at a depth of roughly 3.5 m. The downslope condition was determined from P 814B, P 834, P 1101, P 1109, and P 1110 at a depth of about 1.5 m. From the maps of surface drainage and topography, it appeared that DC17 intersected the surface as indicated in Figure 4-15. At this point, the profile was brought to the surface. The overall profile has been interpreted to follow the surface topography as indicated in Figure 4-15.

4.3.3 SLOPE INCLINOMETER INTERPRETATION

Data from the inclinometers were reduced to yield information for establishing the deformational pattern of the slope movements and locating possible shear surfaces within the movement mass.

LOCATION OF THE SHEAR PLANE. Interpretation of the shear plane in section Z3 shown below in Figure 4-16 was based on a combination of borehole logs and slope inclinometer data. Due to the well dispersed nature of slope inclinometer installations (Figure 4-9) and the patchy history since their installation, the shear plane was interpreted by projecting not only the closest inclinometers, but also those that “filled in the gaps” of information along the length of the slope. Slope inclinometer installations have clearly been concentrated in the downslope portion due its vulnerability to past instabilities. Consequently, the upper portion of the upslope condition was determined by the borehole and test pit logs of BH 704 and TP 30. The condition near the track was established by SI 923, SI 901, and SI 834, while the condition for the downslope portion was determined by SI 1108, SI 1109, and SI 1101. It should be noted that the occurrences of “fractured” and “slickensided” zones in the borehole logs did not consistently correspond with movement zones in the slope inclinometer data (Figures 4-17 and 4-18), nor was it apparent that there was any indication of continuity of such zones between boreholes. As a result, only the obvious movement zones recorded by the inclinometers were used in interpreting the shear plane(s) below.

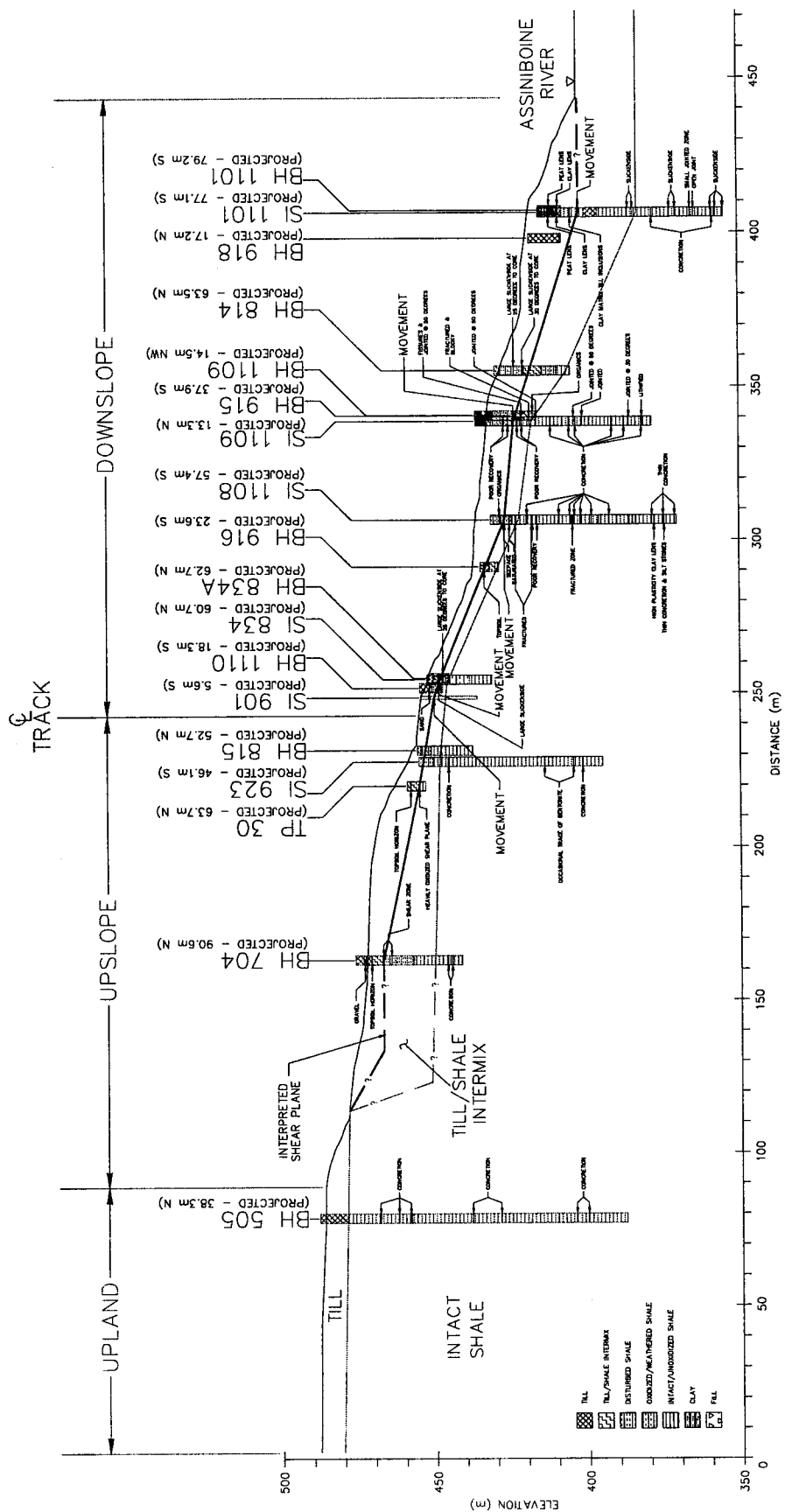


Figure 4-16: Location of the shear plane with enlarged figure (Figure A-23) in Appendix A.

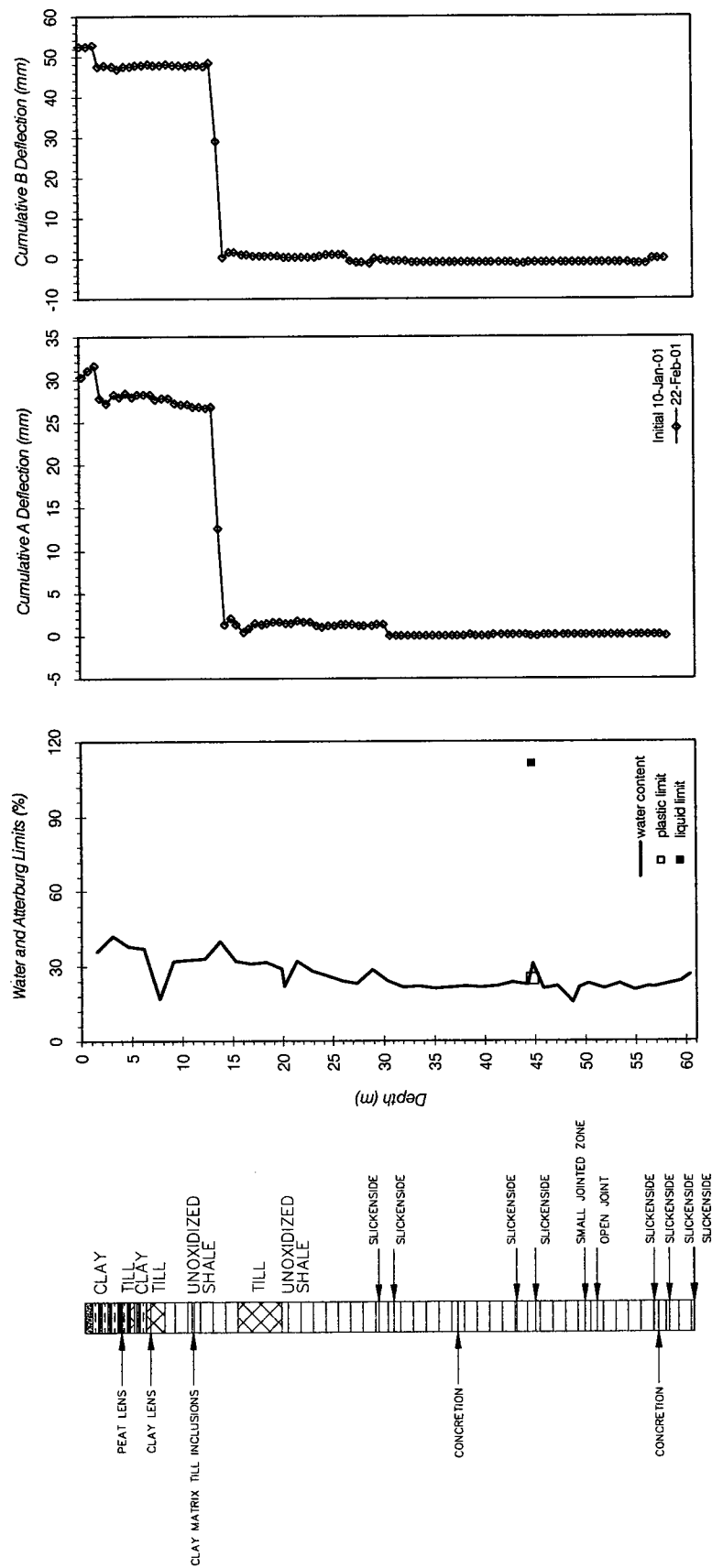


Figure 4-18: Borehole log of SI 1101 compared with cumulative slope inclinometer data.

Two distinct types of slope movements were indicated from the analysis of the slope inclinometer data. The first was associated with gradual downslope movement with displacement most prevalent at the ground surface and decreasing with depth. This pattern of movement was observed in SI 302, SI 902, SI 923, and SI 1001 as shown in Figures A-1, A-8, A-13, A-14 in Appendix A. The rather wavy nature of the data from SI 302 and SI 1001 seemed to be indicative of problematic installation where the grout may not have set the casing properly in place (i.e. completely vertical). The second type of movement involved a characteristic offset, which is associated with movement along a discrete shear zone. Movements of this type were observed in SI 834, SI 901, SI 903, SI 1002, SI 1101, SI 1108, and SI 1109 and are shown in Figures A-5, A-7, A-9, A-15, A-16, A-17, A-19 in Appendix A. The stratum associated with these discrete movements (SI 1108, 1109, and 1101) was the clay shale, with the exception of SI 834 (movement occurred in the till/shale intermix). In SI 834, the depth of movement was 4-5.2 m, which was near the base of the highly disturbed till/shale intermix stratum but below where the water content profile spiked (Figure 4-19) and a large slickenside logged at a depth of 3.8 m. In SI 1108 (Figure 4-17), movement occurred at a depth of 4.6-5.8 m in the clay shale stratum, which was below a seepage zone (4.4 m depth) but above where the water content profile kinked (from near 40% to near 20%). In SI 1109, the depth of movement was 11.9-13.1 m in the clay shale stratum, just below a spike in the water content profile (Figure 4-20) and with zones of poor recovery logged above and below this location. In SI 1101, movement occurred at a depth of 13.1-14.3 m near the base of the clay shale stratum (Figure 4-18), corresponding to a spike in the water content profile. The following interpretation of the shear plane incorporates both of these deformational modes.

Location of the shear plane was based on the interpretation of both the incremental and cumulative displacement plots from inclinometer monitoring profiles when the cumulative displacement plots did not clearly identify a “kink” in the casing (i.e. SI 901 and SI 902). Readings near track level and in the upper portion of the downslope indicated movement at a shallow depth ranging from 3.9-5.3 m with the exception of SI 923. It was unclear if any shear plane in SI 923 was realistic or valid due to the linear slant of the casing above this point and the small differential movement in the A-axis (Figure A-13 in Appendix A) between the two monitoring periods (0.13 mm). Similarly, the other inclinometers located above the track (i.e. SI 302 and SI 1001) gave inconclusive results with respect to any indication of a shear plane; both inclinometers indicated movement only in the top portion of their installation, but without any obvious kinking in the casing.

The shallow nature of the slip plane continued into the mid-downslope portion as indicated by SI 1108 with the depth to the shear plane at 4.6-5.8 m, whereas a much deeper shear plane ranging from depths of 11.9-14.3 m was indicated in the lower downslope by SI 1109 and SI 1101. This analysis appeared to indicate a relatively shallow failure which followed the slope of the valley wall for the most part but deepened as the river was approached. Upon closer inspection, a nearly horizontal line (at a slope of 1.4% or 0.8°) could be traced from SI 1101 at the elevation which recorded movement (Elev. 401.8) near the river through the jointed zones in SI 1109 (Elev. 401.1 to 403.8) through the fractured zone in SI 1108 (Elev. 404.2) and finally, through the trace of bentonite observed in SI 923 (Elev. 404.4). Hence, the following analyses will consider both possibilities of a shallow and deep movement zone.

DEFORMATIONAL PATTERN. The directions, magnitudes, and rates of movements were determined from the data recorded in the moving mass represented by the material above the inferred shear plane. Two types of calculations were involved in defining these quantities: an average value representing all the data within the movement zone and the

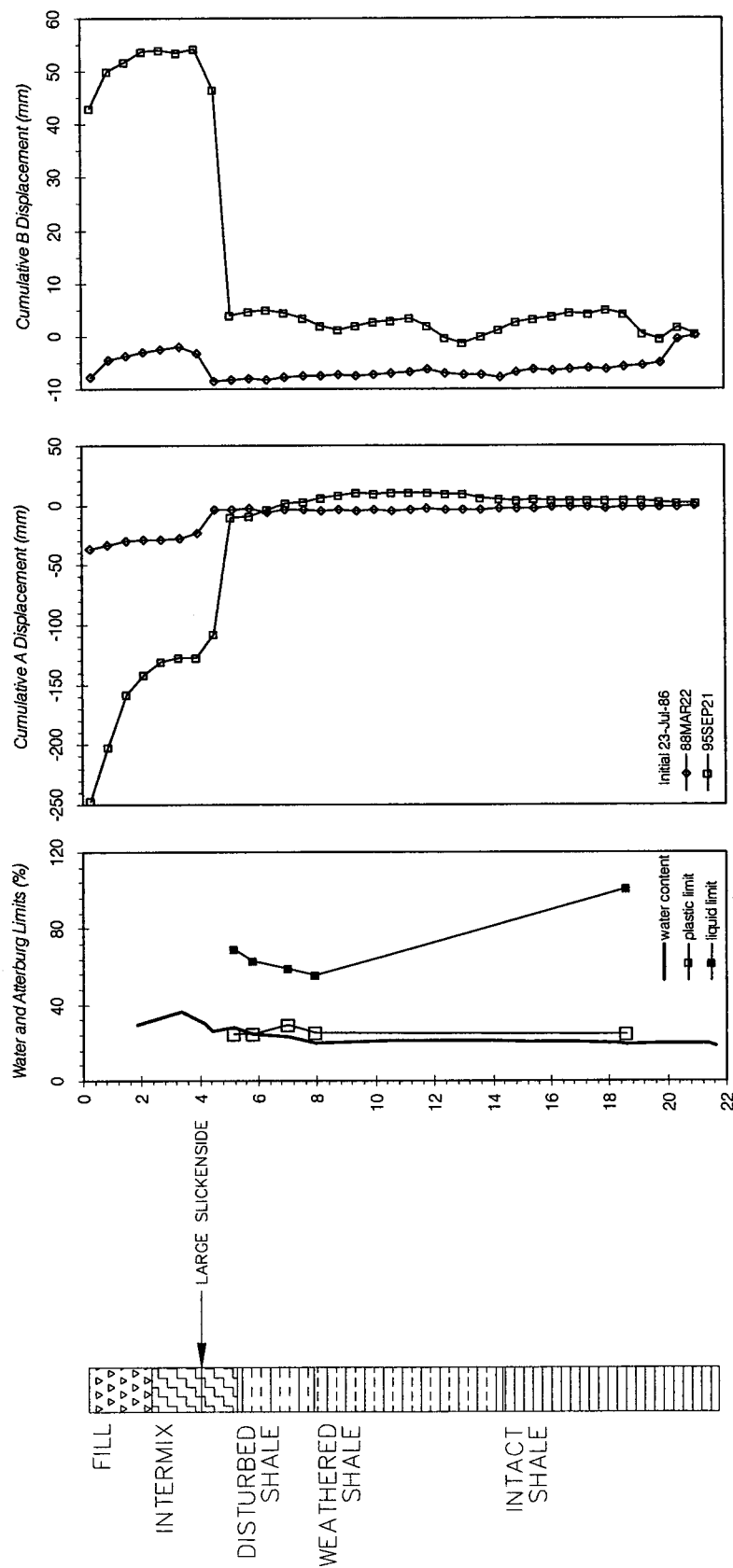


Figure 4-19: Borehole log of SI 834 compared with cumulative slope inclinometer data.

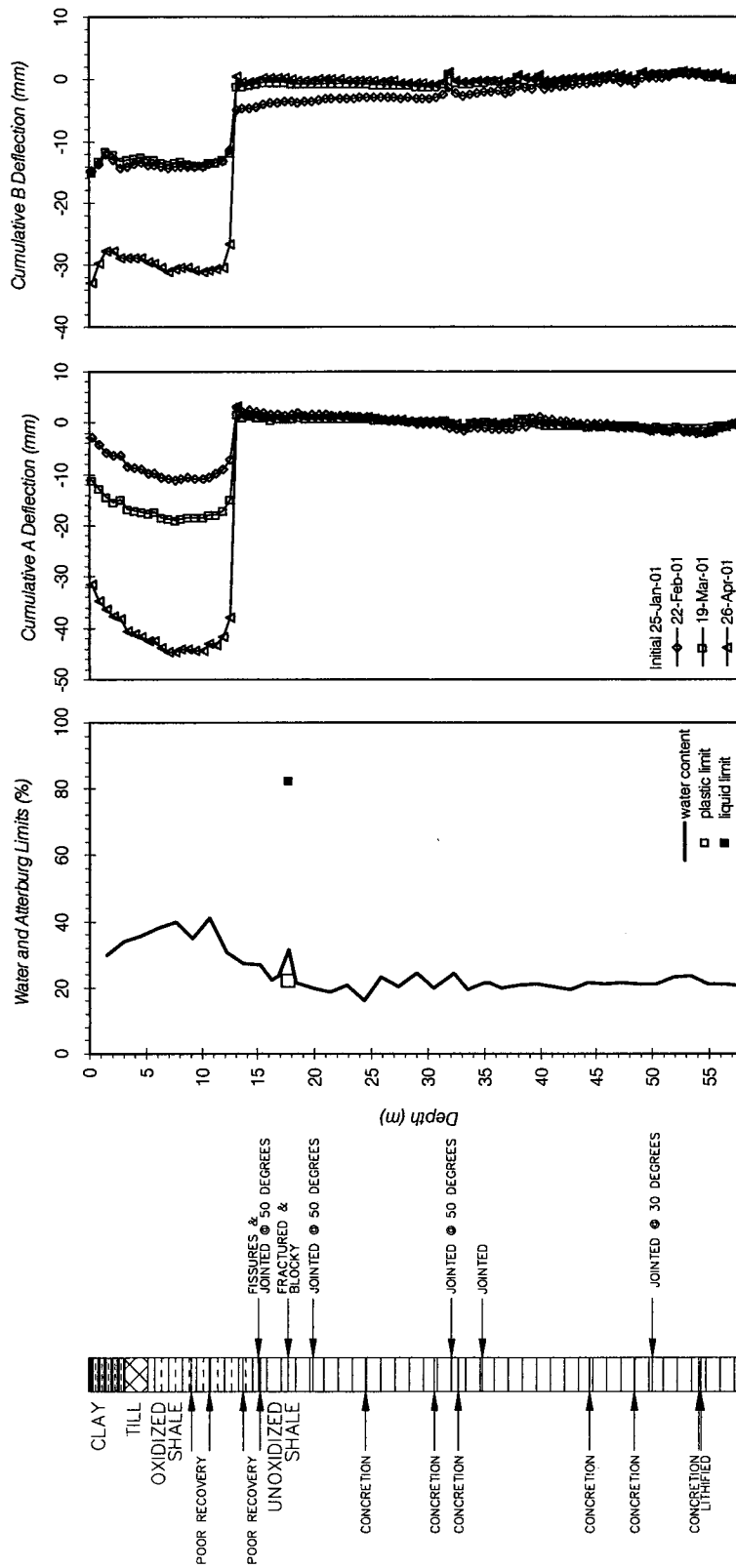


Figure 4-20: Borehole log of SI 1109 compared with cumulative slope inclinometer data.

value recorded near the shear plane. Both values represented the maximum accumulated measurements recorded since installation, the time intervals over which this amount occurred are included in the following tabulated values.

The directions and average magnitudes of the slope movements within the moving mass are indicated in Figure 4-21, while Table 4-8 summarizes the maximum displacements recorded near the suspected shear planes. Inclinator SI 302 was not included in Figure 4-21 due to its extremely wavy nature, its close proximity to SI 1001 (9.3 m), and the longer monitoring period of SI 1001. The smallest movements near the shear plane were recorded by slope inclinometers SI 901, SI 902, and SI 923 ranging from 3.5-4.5 mm, whereas the largest movements were recorded in SI 1108 and SI 834, ranging from 138.7-139.7 mm respectively. The majority of displacement vectors pointed in a northeasterly direction (SI 834, 901, 902, 903, 923, 1002, and 1108). However, both SI 1101 and 1109 pointed in the southeasterly direction. The dashed vector of SI 1101 in Figure 4-21 illustrates the direction of movement according to the slope inclinometer data; however, since this was inconsistent with the direction of movement of the other inclinometers, it was rotated 180° as indicated by the solid vector.

The displacement rates of the movements recorded near the shear plane are summarized in Table 4-9, while those for the movement zone are tabulated and illustrated in Figure 4-22. These values were calculated from the displacements over the temporal interval that they occurred (the intervals are indicated in the appropriate columns in Table 4-9). An attempt was made to separate displacement data into the four seasons in order to evaluate seasonal variation; however, due to the irregular monitoring intervals, this was deemed unfeasible. Additionally, the average rates calculated did not necessarily involve surficial rates because the surface often moved at a rate significantly different than those near the shear plane (SI 834, SI 901, and SI 1108-1109). The normalized total rate was carried out according to the accumulated monitoring interval as shown.

Both incremental and normalized accumulated displacement rates are greatest in the downslope portion (SI 1101 and SI 1108-1109) and least at track level. The performances of these most recent inclinometers (SI 1101 and SI 1108-1109) are also consistent with the existing slope conditions (i.e. topography). SI 1109 has the slowest rate in terms of incremental and normalized total displacements and the least amount of total displacement, which is consistent with expectations of its performance due to the possible stabilizing presence of the first shear key (built in 1996). SI 1108 has both the maximum total displacement and incremental rate, consistent with behaviour due to its close proximity with the scarp where movements are expected to be relatively large and occur quickly over a short term. SI 1101 is closest to the river and has the maximum normalized total displacement rate, which may be indicative of active river erosion of this lower mass. At track level, the total normalized displacement rates also appear to be consistent with the existing slope conditions; the largest values were recorded by the inclinometers closest to the scarp (SI 901 and SI 903), the smallest values were recorded by those closest to the first shear key (SI 834 and SI 1002), and the intermediate value was recorded by that just outside the first shear key, but farthest away from the scarp (SI 902).

INTERPRETATION FOR SENSITIVITY ANALYSIS. With respect to the sensitivity analysis in Chapter 6, the shear zone was dropped approximately 2.6 m in the upslope and lower downslope portion, while it was dropped 1 m in the upper downslope region. A second, but lower shear zone was indicated by the borehole log of BH 704 at roughly 2.6 m below the interpreted failure plane. However, this drop could not be accommodated due to

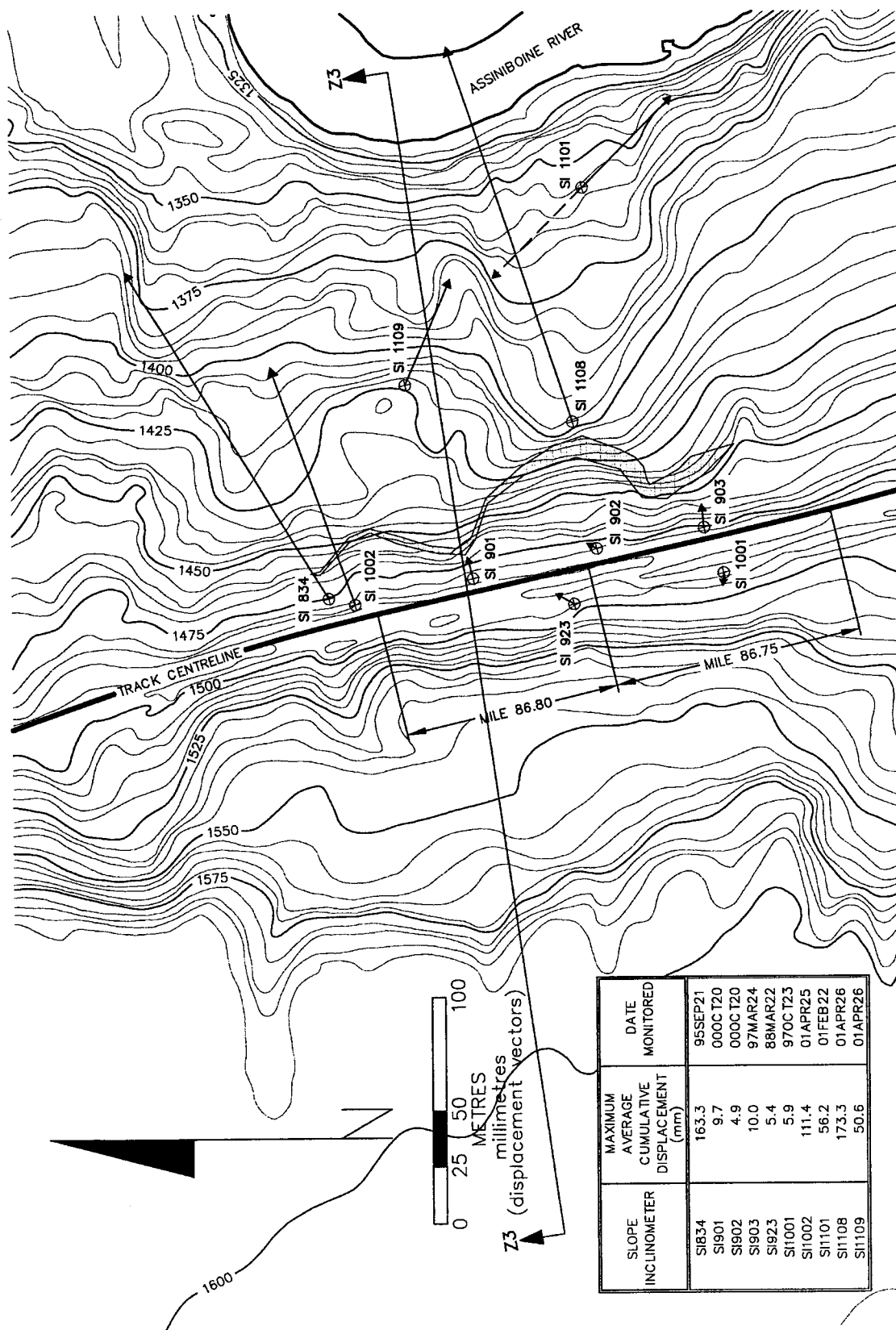


Figure 4-21: Displacement vectors of slope inclinometers within study area (contours are in feet).

Table 4-8: Maximum recorded displacements of the shear plane.

Slope Inclinometer	Date Recorded	Date Interval (days)	Shear Plane Elevation (m)	A-axis Displacement (mm)	B-axis Displacement (mm)	Total Displacement (mm)
SI 302	-	-	n/a	-	-	-
SI 834	95SEP21	3347	448.3-447.1	-127.6	54.4	138.7
SI 923	88MAR22	249	422.3-421.5	-0.7	3.4	3.5
SI 901 ¹⁰	01APR25	1604	(4.6-5.2)	-5.0	1.6	5.3
SI 902 ¹⁰	00OCT20	1417	(4.6-5.2)	-3.3	3.8	5.0
SI 903 ¹⁰	97MAR24	111	(4.0-4.6)	-8.2	-1.2	8.3
SI 1001 ¹⁰	-	-	n/a	-	-	-
SI 1002 ¹⁰	01APR25	1474	(4.6-5.2)	-95.8	3.8	95.9
SI 1101	01FEB22	43	401.9-400.7	26.8	48.6	55.5
SI 1108	01APR26	98	426.4-425.2	-139.2	12.0	139.7
SI 1109	01APR26	91	423.3-422.7	-37.9	-26.5	46.3

the significantly thinner layer of intermix stratum in the upper downslope portion; hence it was only dropped by 1 m in this portion of the slope.

4.4 FIELD OBSERVATIONS FROM EXCAVATION OF THE SECOND SHEAR KEY

The last site visit to the study area was made during the excavation for the second shear key in late May, 2002. It was a two-day trip with the objective of extracting samples from the shale bedrock. On arrival, progress of the excavation was into its third day with the first bench of the key near completion while excavation for the second bench was just beginning (Figure 4-23). Based on verbal communication with the foreman, excavation for the second bench reached a depth of at least 12 m from ground surface on the north end. Completion of the excavation phase was reached during the second day of the trip and construction of the key was well under way with a substantial depth of the sandy material placed and compacted. The depth of excavation on the south end exceeded that of the north end according to one of the project managers on site. The actual dimensions of the key are not known at this time since the construction report was not yet available during the writing of this thesis.

The trip afforded a few key observations to be made, which alluded to the possibility that the shale may possess some atypical characteristics (with respect to its engineering behaviour). Excavation to the intact bedrock revealed that the weathered zone of the bedrock was highly jointed (Figure 4-24) with its colour grading from brown at its uppermost surface to dark grey as the intact, unweathered bedrock was approached. Orthogonal joints sets were also clearly evident as an occurrence of a wedge failure on the north end was observed by the author (Figure 4-25). The failure occurred in the upslope wall of the second bench a short period following its initial excavation. Figure 4-25 (b) further illustrated the jointed nature of

¹⁰ the ground elevation of these installations were unknown since no installation information was available, values in paranthesis are depths from the ground surface

Table 4-9: Maximum displacement rates of the shear plane.

Slope Inclinometer	Incremental Displacement Rate				Cumulative Displacement Rate			
	Date Interval ¹¹ (days)	A-axis Rate (mm/yr)	B-axis Rate (mm/yr)	Total Rate (mm/yr)	Date Interval ¹¹ (days)	Interval (yr)	Total Rate (mm/yr)	Normalized Total Rate (mm/yr)
SI 302 ¹²	106 (86APR07 86JUL22)	0.7	0.7	1.0	715 (86APR07 88MAR22)	2.0	1.0	0.5
SI 834	2739 (88MAR22 95SEP21)	-17	7.2	18.5	3347 (86JUL23 95SEP21)	9.2	15.1	1.6
SI 923 ¹³	249 (87JUL17 88MAR22)	-1.0	5.0	5.1	249 (87JUL17 88MAR22)	0.7	5.1	7.5
SI 901	71 (01APR25 01JUL05)	-3.3	-45.1	45.2	1675 (96DEC03 01JUL05)	4.6	0.1	0.03
SI 902	34 (96DEC03 97JAN06)	18.6	-2.5	18.8	1604 (96DEC03 01APR25)	4.4	0.8	0.2
SI 903	34 (96DEC03 97JAN06)	-31.4	53.0	61.6	1604 (96DEC03 01APR25)	4.4	0.9	0.2
SI 1001 ¹²	61 (01FEB23 01APR25)	31.4	45.4	55.2	10216 (97APR12 01APR25)	4.0	1.9	0.5
SI 1002	61 (01FEB23 01APR25)	-70.1	7.5	70.5	921 (97APR12 99OCT20)	4.0	23.7	5.9
SI 1101	4414 (01JAN10 01 FEB22)	227.3	412.3	470.8	4414 (01JAN10 01FEB22)	0.1	470.8	3996.3
SI 1108	2588 (01MAR19 01APR26)	-895.1	50.4	896.6	3012 (01JAN18 01APR26)	0.3	520.3	1937.9
SI 1109	2588 (01MAR19 01APR26)	-219.7	-141.4	261.3	455 (01JAN25 01APR26)	0.2	185.5	744.0

¹¹ values in paranthesis are the corresponding dates

¹² rates are based on surficial movement from initial reading to last recorded reading for incremental and cumulative displacement

¹³ cumulative displacement used for incremental rate since data does not indicate what day in November, 1987 monitoring occurred

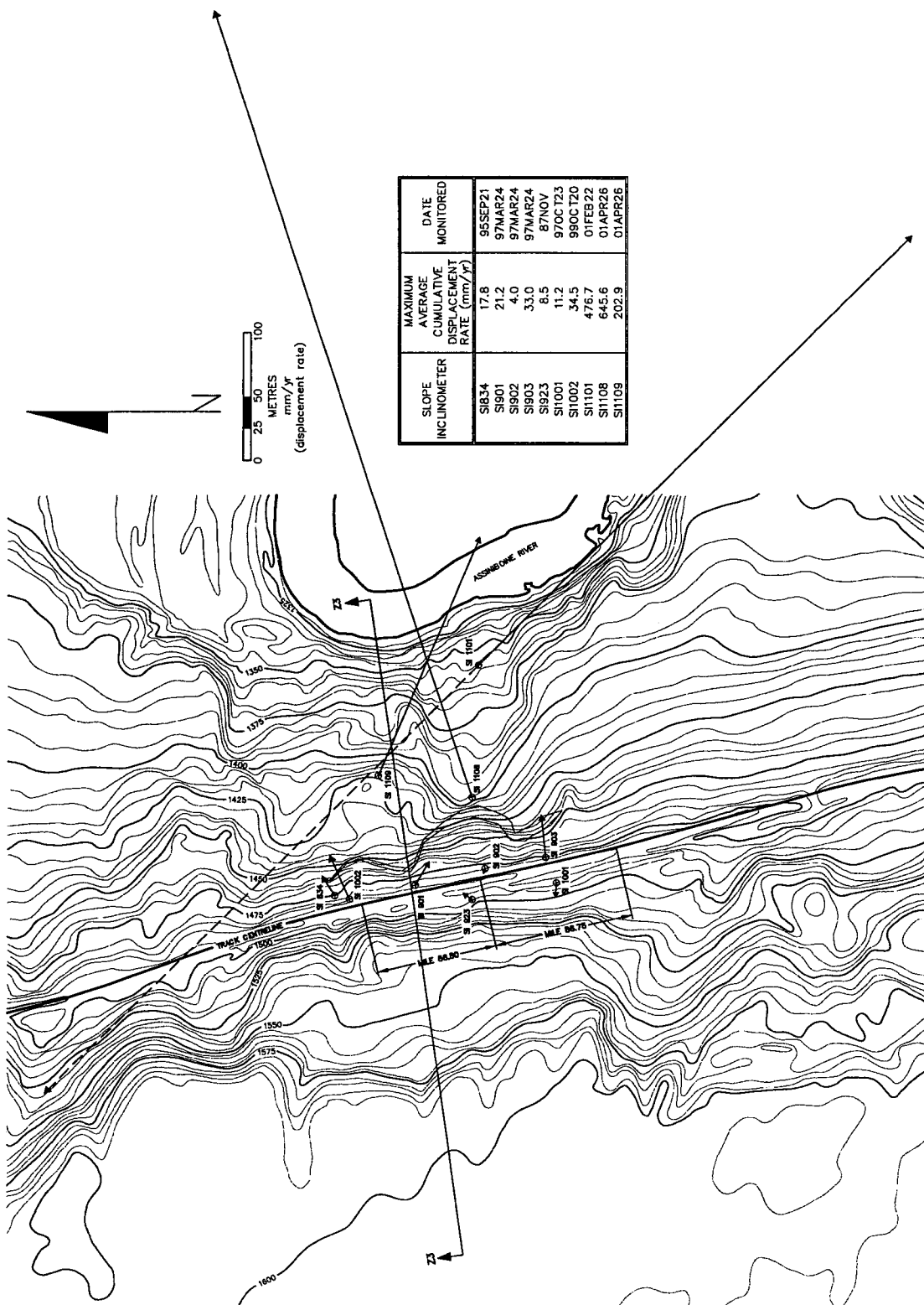


Figure 4-22: Displacement rate vectors from slope inclinometers (contours are in feet).



Figure 4-23: Near completion of the first bench, looking south with the upslope at the right (2002 site visit).



Figure 4-24: Degree of jointing in the weathered zone in the upslope wall of the first bench (2002 site visit).

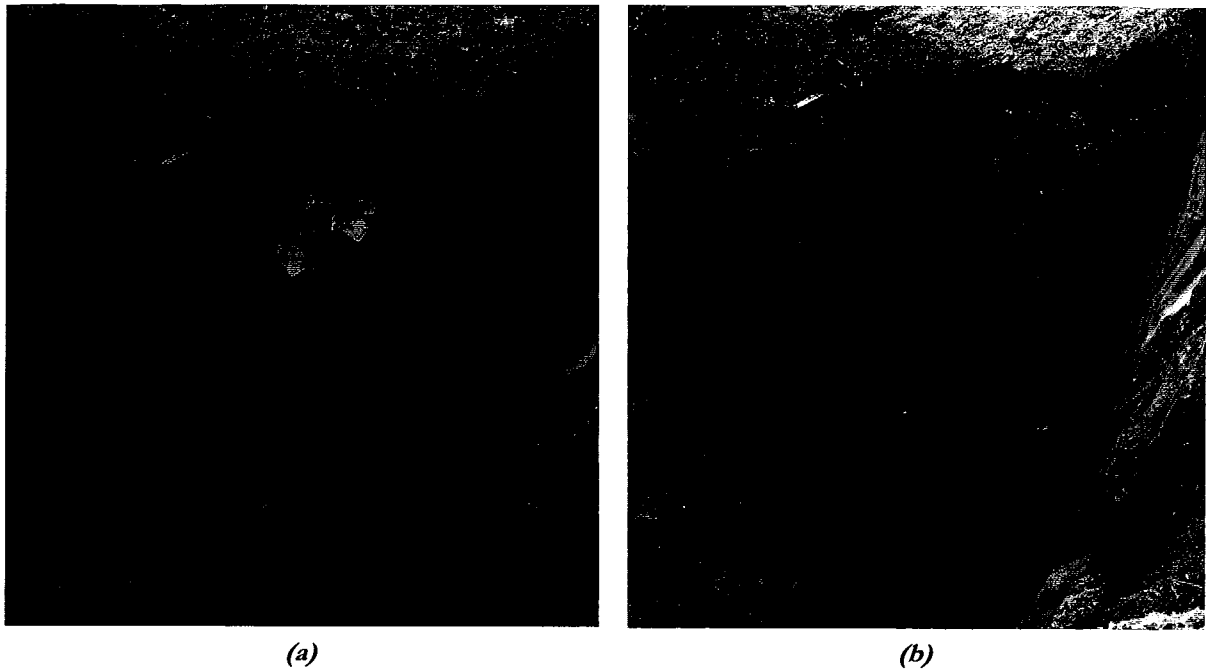


Figure 4-25: *Wedge failure in the upslope wall of the second bench (a) before (b) after (2002 site visit).*

the weathered bedrock as the failed wedge consisted of blocks of various sizes. Several parallel, diagonal continuous joints can also be seen in the upslope face of the excavation wall in Figure 4-26. In addition, iron staining was also evident on several joint faces in the weathered zone (Figure 4-24 and 4-26).

Communication with field personnel revealed that no shear zone was readily identifiable during the excavation except for its possible location along an iron-stained plane which appeared to extend almost the entire length of the excavation (Figure 4-23). This plane was well above the weathered-unweathered bedrock contact as evidenced by the characteristic brown colouration of the weathered shale below it. Due to the oxidized state of the plane, it was speculated that significant quantities of groundwater most likely moved along this zone. However, for the duration of the trip, no groundwater seepage into the excavation occurred (confirmed by field personnel), and to the knowledge of the author, the excavation was not plagued by any interference from groundwater seepage for the duration of the open excavation. As illustrated by its absence in Figure 4-27, this iron stained plane did not appear to follow the slope of the ground surface, but appeared to be horizontal and perhaps previously projected through the slope surface. Unfortunately, because no shear zone was identified, only intact, unweathered shale bedrock samples were extracted and tested in the laboratory to determine peak and residual strengths to be used in subsequent stability and deformation analyses.

Another observation of interest was the rather steep, nearly vertical inclination of the walls excavated into the shale bedrock, which was maintained throughout the duration of the trip without the assistance of any external support. The only indications of instability were the small, local orthogonal wedge failures evidenced by the rubble piles along the base.

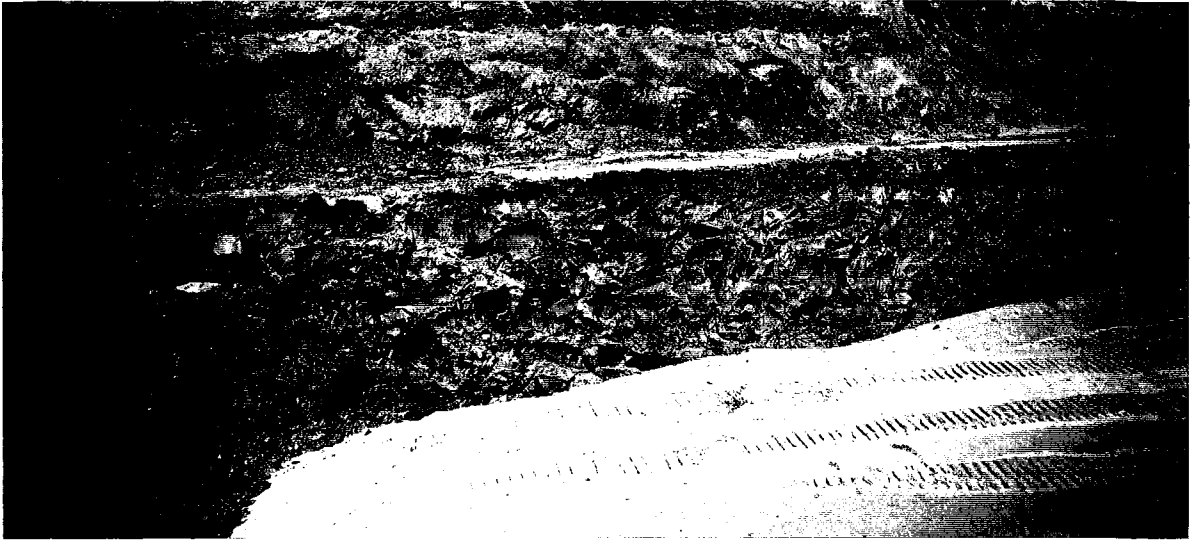
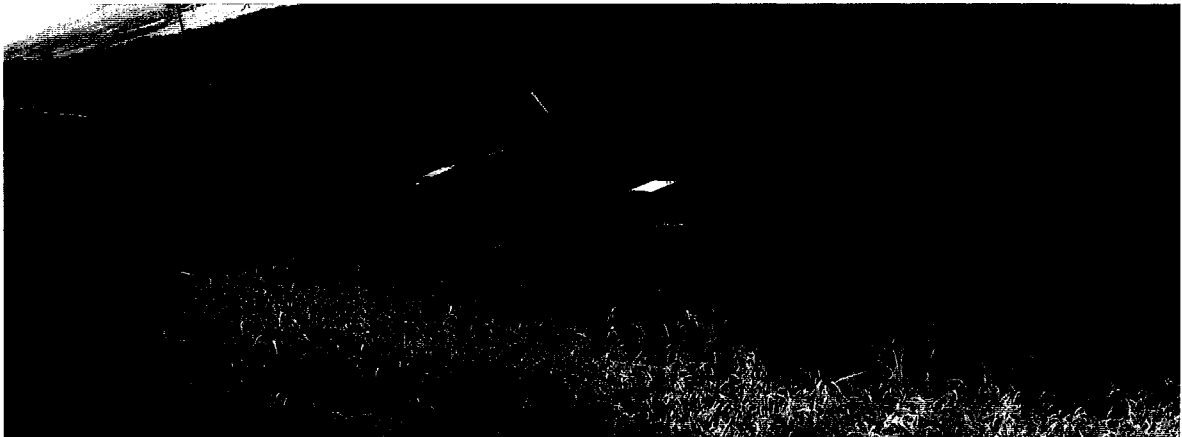


Figure 4-26: Indication of a number of parallel continuous joints (2002 site visit).



(a)



(b)

Figure 4-27: Downslope face of the excavation wall (a) north end (b) south end (2002 site visit).

4.5 SUMMARY

The field investigation of the study area has been examined from both the surface and subsurface. Surficially, the area has been topographically surveyed on three different occasions since the field investigation began in 1986. The most complete record was obtained in the 1986 survey, while the subsequent surveys of 1995 and 2000 focused on the areas of instability; both upslope and downslope areas of Miles 86.8 and 86.75 were surveyed in 1995, whereas only the downslope portion was surveyed in 2000. Tension cracks of the 1995 instability were also mapped in the 1995 survey and again following the 1996 installation of the first shear key at Mile 86.8; they were found to coincide remarkably well with the existing scarp. The overall nature of the valley wall appeared to be rather gentle sloping and hummocky due to past landsliding activities. In addition to the topographic surveys, surface drainage of the area was also investigated and mapped in 1987. Immediately affecting the study area were six drainage courses and four ponded areas, whose sources included not only precipitation and surface runoff, but also drainage from the layers of sand and gravel found at surface and in the blanketing till sheet and two springs located above the track.

The subsurface was explored by a combination of boreholes and test pits excavated within the entire slope and the upland plateau. A total of 41 boreholes and 23 test pits have been drilled and excavated by means of auger or rotary methods (boreholes) and backhoes (test pits). Borehole exploration ranged from a minimum depth of 4.6-100.2 m with five in the upland, 11 in the upslope, and 25 in the downslope. Test pits have been excavated with depths ranging from 2.5-7.7 m, and 14 were located in the upslope while nine were in the downslope. Sampling was also carried out in both boreholes and test pits via grab samples, washed cuttings, Shelby tube, and continuous coring. In addition, block sampling was also carried out in 2002 for the work in this thesis. Almost all boreholes were instrumented with either piezometers or slope inclinometers in order to monitor the groundwater conditions and lateral movement of the slope respectively. On the whole, 33 piezometers and 11 slope inclinometers were installed from 1986 to 2001. However, monitoring has been somewhat sporadic and irregular.

Interpretation of these field investigations have been shadowed by the second-hand and sometimes incomplete nature of the information used. The interpreted stratigraphy was carried out based on interpreted bedrock elevations provided by the consultant, borehole logging, and the use of water content and dry density profiles. Only three strata were identified: till, intermix of till and shale, and clay shale bedrock. The water contents for the intact shale appeared to linger around 20% while the dry densities were in excess of 1700 kg/m³. In general, the intact shale appeared to follow the slope topography in a quasi stepwise fashion.

Groundwater conditions were simplified to ground surface due to the limited monitoring records available and based on site reconnaissance that indicated a high groundwater table; high groundwater levels were indicated by the number of ponded areas, the shallow nature of the surface drainage courses, and the fact that major movements have been associated with abnormally wet climatic conditions. However, a generalized depth to groundwater was deduced from the monitoring results of these piezometers for use in a sensitivity analysis in Chapter 6. Groundwater levels from these records appeared to be at 3.5 m depth in the upslope portion and at 1.5 m in the downslope.

Location of the shear plane was based on both borehole logging in the sparsely instrumented upper upslope and slope inclinometer data of the relatively well-instrumented near-track and

downslope portions. Generally, the shear plane was found to follow the surface topography for the majority of the slope with the exception of the region closest to the Assiniboine River. This indicated relatively shallow failures within most of the slope with a somewhat deeper-seated failure at the bottom of the slope. The stratum most commonly associated with the measured movement zones was clay shale. Movements recorded near and/or at the shear plane indicated maximum movement of 139.7 mm at a corresponding rate of 520.3 mm/yr (the interval over which this rate was calculated was 98 days), both recorded in SI 1108.

The last site visit was made during the excavation of the second shear key in late May, 2002. This opportunity enabled a few key observations to be made. The weathered zone of the shale bedrock was rather blocky and jointed with evidence of orthogonal joint sets and perhaps indicated regional jointing due to a number of parallel, continuous joints apparent in the upslope excavation wall. A shear plane was not clearly identified by the field personnel, but it was speculated to coincide with a horizontal iron-stained plane located within the weathered zone of the bedrock. This plane did not appear to follow the slope of the ground surface, but it may have previously projected through the ground surface in a nearly horizontal manner. No seepage was observed from this plane, although it has undoubtedly occurred in the past. The excavation was dry and the walls were maintained at rather steep inclinations without any external support for the duration of the two-day trip.

5 LABORATORY TESTING

The field investigations have revealed that the slope movements measured at Miles 86.8 and 86.75 have mostly occurred in the clay shale stratum located within the till/shale intermix stratum of the interpreted stratigraphy (Chapter 4). However, at least one occurrence of movement has involved the till (SI 834). The till along the length of the valley wall has been logged as one in which the coarser fraction (i.e. silt or sand) exists within a clay matrix. In addition, the occurrence of till along the valley wall appears to be in blocks and not as a continuous blanketing layer, thereby implying its existence within what appears to be a blanket of colluvium consisting of both till and clay shale. Thus, it appears that the material which has been consistently involved in the slope instabilities is the clay shale stratum. Ten block samples of the intact shale bedrock obtained in the late spring of 2002 were tested in the laboratory for the determination of physical, mechanical, and strength characteristics. Each block was approximately 250 mm³ in size with shapes ranging from semi-cubical to rectangular. Only two blocks were needed for the extraction of test samples (Block 6 and Block 7). Both blocks were retrieved from the spoil pile on May 2, 2002 and were possibly close to an oxidized joint set due to iron staining on one surface. Results were then compared with those obtained by the consultant and selected sources of literature that have examined shales of the Pierre Formation and similar material from equivalent formations.

5.1 LABORATORY TESTS, PROCEDURES, AND SAMPLE PREPARATION

The types of tests which characterized the intact shale physically and mechanically included grain size distribution, water content, consistency limits, specific gravity, consolidation characteristics, and stress-strain relationships whereas shear strength parameters for use in the subsequent limit equilibrium and deformation analyses were determined from shear strength tests. All lab tests were conventional and standard, and their testing and corresponding sample preparation procedures will be referenced to the appropriate ASTM standard (Table 5-1).

Two additional tests were also carried out as part of a preliminary examination into the peculiar non-disaggregation behaviour of the material when it was placed in water. At the onset of lab testing, a small piece was taken from Block 6 and submersed in water. It remained intact in terms of retaining its shape and cohesion with minor “flaking” (of loosened parts) only occurring on the surfaces, and remained in this state even after all the water had evaporated while its colour changed from dark grey to light steel grey. Cementation was hypothesized as an explanation of this abnormality. As a result, its presence was tested by exposure to weak and pure solutions of hydrochloric acid, and exposure to water left in an uncontrolled environment (i.e. at the author’s desk) for an extended period of time. In the following sections, the former falls under chemical tests while the latter will be referred to as the water deterioration test. The scanning electron microscope (SEM) was also employed in this investigation and the observations and interpretations of the images are included below.

Exposures to the different solutions of hydrochloric acid were carried out on samples of Block 6, while the water deterioration test was carried out on samples of Block 7. Fresh (i.e. in-situ) samples taken from each block were used in both cases with the addition of an exposed (i.e. air dried) sample from Block 7. For the chemical tests, the solutions of

Table 5-1: Summary of ASTM standards corresponding to lab tests carried out.

<i>Lab Tests</i>	<i>ASTM Standard</i>
Specific Gravity	D 854 - 00
Index Properties:	
1. Grain Size Distribution:	
a) Sieve Analysis (cohesive soil)	D 421 - 85 (sample preparation) D 422 - 63 (procedures)
b) Hydrometer	same as above
2. Water Content	D 2216 - 98
3. Consistency Limits:	
a) Plastic Limit	D 4318 - 00
b) Liquid Limit	same as above
Consolidation	D 2435 - 96
Shear Strength:	
1. Direct Shear	D 3080 - 98
2. Triaxial	D 4767 - 95

hydrochloric acid were added directly onto the surface of two separate samples and observations on how the shale reacted to the acid were made. In the water deterioration test, three samples were examined: a fresh sample completely submersed in tap water, an exposed sample also completely submersed in tap water, and a fresh sample with only the bottom portion in direct contact with water. These samples were left in such states until the water evaporated from all containers. The only change made to any of these samples was the addition of water to the fresh sample that was partially exposed to water due to the more rapid rate of evaporation from its shallow dish.

5.2 RESULTS: PHYSICAL AND MECHANICAL PROPERTIES

This section covers the results attained from the specific gravity, grain size distribution, water content, consistency limits, and consolidation oedometer tests in addition to the observations made during the chemical and water deterioration tests and two different SEM sessions.

5.2.1 SPECIFIC GRAVITY

The specific gravity of both blocks were determined from the results of three simultaneous water pycnometer tests, one set carried out for each block. Due to the concurrent nature of testing, three different pycnometers and correspondingly, three different vacuum tubes were used for each test set. The final values (Table 5-2) were obtained by averaging the two computed values from each set of tests that were not more than 2% apart (Bowles, 1992). This condition was also within the ASTM guidelines, which required that no two results range more than 0.08 from each other with respect to laboratory reproducibility (i.e. equipment error) and 0.03 with respect to laboratory repeatability (i.e. operator error). However, only laboratory reproducibility was applicable in this case due to the differing vacuum tubes and pycnometers used.

Table 5-2: Specific gravity values

Block	Specific Gravity	Value Proportionality	Range in Values
6	2.73 (2.73 – 2.73) ¹⁴	0.00%	0.00
7	2.80 (2.81 – 2.78) ¹⁴	0.96%	0.03

5.2.2 GRAIN SIZE DISTRIBUTION

Again three samples from each of the two blocks were tested in order to obtain the grain size distribution of the shale. From visual inspection of Block 6, which was rather uniform in appearance and fine-grained, it was decided that only the hydrometer method would be necessary. However, the distribution obtained from the hydrometer method yielded only a maximum of 51% finer than the largest measured particle size of 59 μm (Figure B-1 in Appendix B). Therefore, approximately half of the curve was unaccounted for. As a result, following the hydrometer tests of the all three samples from Block 7, a wet sieve analysis was performed in order to capture the top half of the curve. However, these resulted in gap-graded curves with clay-size particles consisting of less than 35% of the total mass (Figure B-2 in Appendix B), which was unexpected of a material with a dominance in clay-sizes (according to literature). Cementation was initially thought to be the cause of this since the samples were left for only a minimum 16-hour period in the dispersing agent; this may not have been an adequate soaking period for cementation bonds to be completely broken. In addition, it was also suggested that the non-disaggregation behaviour of the material when exposed to water in its natural water content may have affected the disaggregation process of the dispersing agent. Thus, further testing was carried out. Another three samples from Block 7 were first air-dried (water contents ranging from 3.4-3.7%) and then soaked in the dispersing agent for a minimum period of four days prior to carrying out grain-size analyses. The results are shown in Figure 5-1.

5.2.3 WATER CONTENTS & CONSISTENCY LIMITS

Water contents were determined for each sample carved or extracted from both blocks for use in the series of laboratory tests. In Block 6, eight samples were carved or obtained for direct shear tests, one for consolidation test, three for hydrometer tests, and three for specific gravity tests. In Block 7, five samples were carved for triaxial tests, one for consolidation, three for hydrometer tests, three for specific gravity tests, and two for the water deterioration test. Below, Table 5-3 summarizes the water contents obtained from these samples.

The consistency limits tested for in both blocks were the liquid and plastic limits (Atterberg limits), from which the plasticity and liquidity indices were calculated. Two trials were carried out in both blocks at different times to confirm earlier results; the equipment used differed from trial to trial. Liquid limit results are shown in Figure 5-2 and tabulated in Table 5-3. Despite the use of the multipoint method in the liquid limit tests, a good spread in the data (Figure 5-2) was not always achieved due to the sensitivity of the mixture to the relative

¹⁴ values in brackets represented the results of the two tests which were averaged to give the above specific gravity

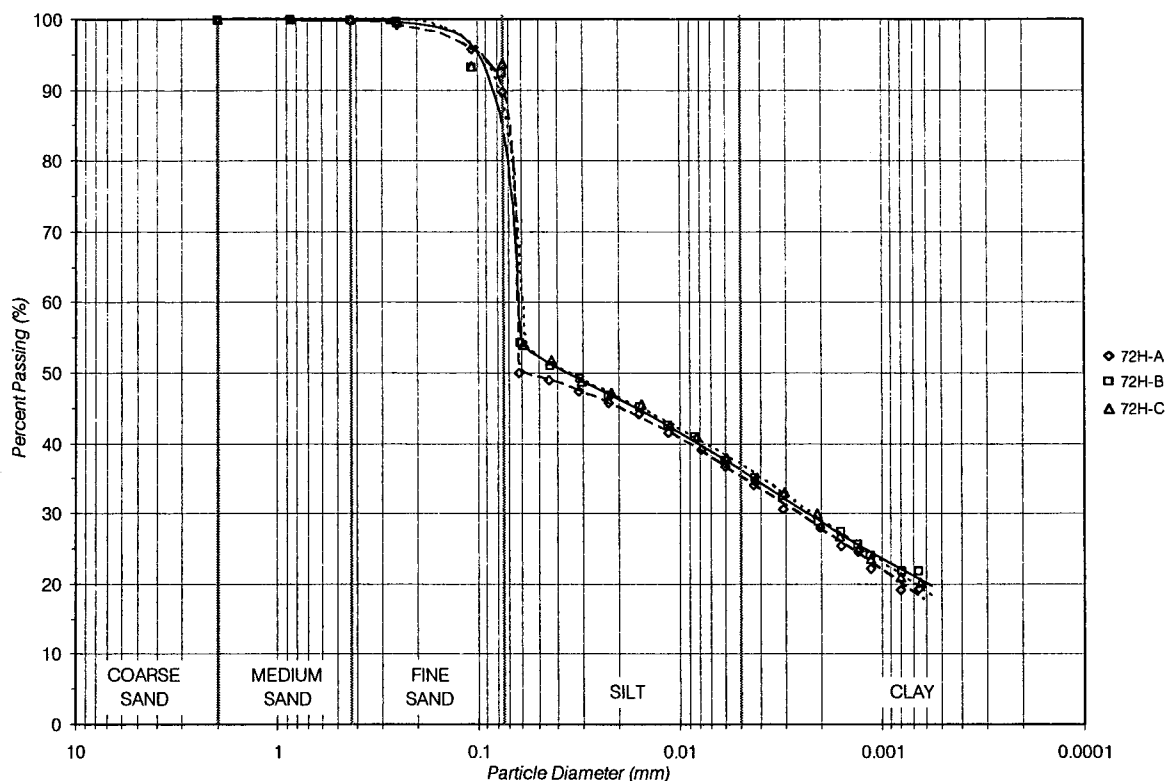


Figure 5-1: Grain size distribution of Block 7.

Table 5-3: Summary of water contents and consistency limits.

Block	Average Water Content (%)	Liquid Limit: Trial 1 (%)	Liquid Limit: Trial 2 (%)	Average Liquid Limit (%)	Plastic Limit Trial 1 (%)	Plastic Limit Trial 2 (%)	Average Plastic Limit (%)	Average Plasticity Index (%)
6	21.1	55.0	57.8	56.4	27.9	27.3	27.6	28.8
7	20.3	63.0	59.7	61.3	25.7	26.1	25.9	35.4

humidity of the laboratory. The results summarized in Table 5-3 are in accordance with the precision set out in the ASTM guidelines for acceptability of test results with respect to laboratory reproducibility; for a CH (so classified in the following section on “Discussion: Material Characterization”) material, the acceptable range between results are 4% for the liquid limit, 6% for the plastic limit, and 7% for the plasticity index.

5.2.4 CHEMICAL TEST

This test involved the exposure of two solutions of hydrochloric acid to fresh (in-situ) samples of Block 6 in order to ascertain the possibility of carbonate-based cementation in the shale. The first attempt involved exposure to a very weak solution in the form of vinegar, which yielded a negative result with respect to any visible surficial reaction (i.e. bubbling). For ease of deduction, the next attempt involved exposure to its pure form (100% solution). This also yielded a negative result. Consequently, additional trials with differing concentrations were deemed unnecessary.

5.2.5 WATER DETERIORATION TEST

The behaviour of three samples from Block 7 exposed to tap water in an uncontrolled environment (with respect to the relative humidity) was observed in this test. Table 5-4 summarizes the state of each sample, the exposure conditions, and the initial water contents. Samples 7-A and 7-C were taken from the remainder of Block 7, which was kept in bags sealed in its original container, after samples had been extracted for consolidation and shear strength tests. Sample 7-B was taken from a bag of shavings from carving one of the triaxial test specimens, which had been left sitting in the author's office for a period of time (the exact time is unknown, but it had been at least three months since the last triaxial test was disassembled when this test was initiated).

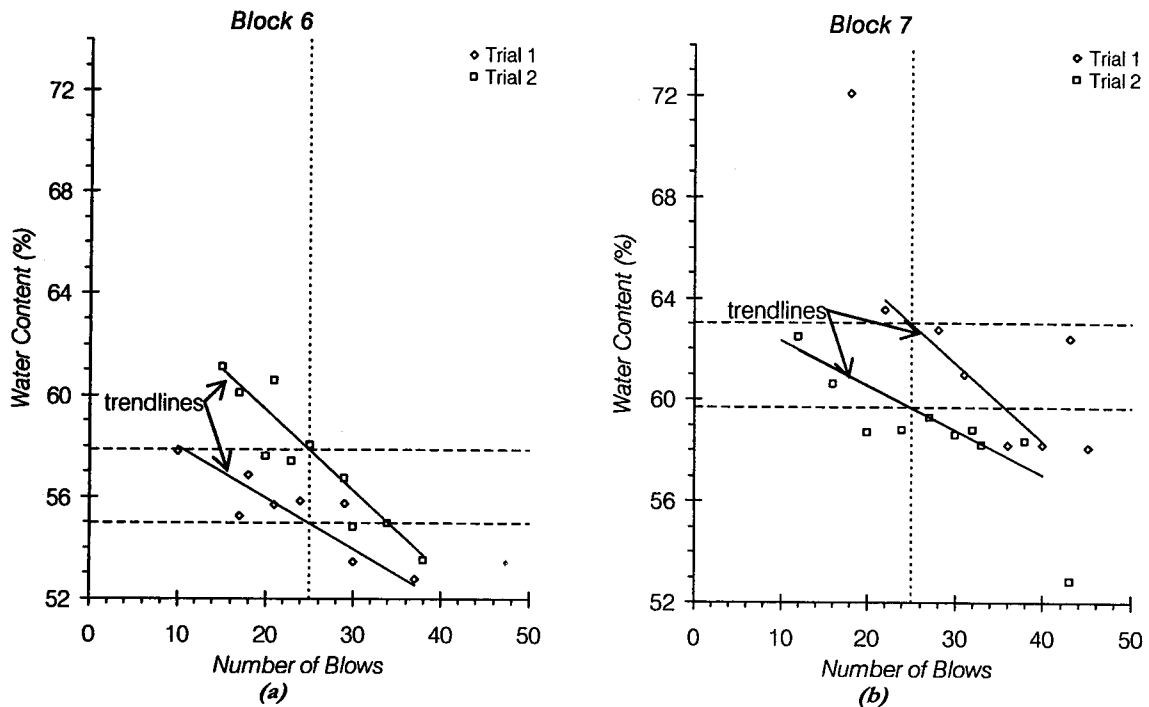


Figure 5-2: Summary of liquid limit tests.

Table 5-4: Summary of samples analyzed in the water deterioration test and their exposure conditions.

Sample	Material Conditions	Exposure Conditions	Initial Water Content (%)
7-A	in-situ (fresh)	fully submerged in tap water	21.5
7-B	air-dried (exposed)	fully submerged in tap water	13.0
7-C	in-situ (fresh)	partially submerged in tap water	20.9

The purpose of this test was to observe the possible disintegration of the shale samples when exposed to tap water for a period of time, and the results are presented in Figure B-3 in Appendix B. When tap water was added to Sample 7-A, loosened surficial flakes became dislodged. Some of this may have been due to the initial force of the water hitting the surface, but this flaking continued even after the sample was completely submerged and no noticeable turbulence was present in the beaker. However, the flaking stopped within seconds of the water settling down, and the water remained relatively clear to the end of the test period (approximately 17-20 days). In comparison, once the tap water was added to Sample 7-B, it became murky as the specimen began to break apart as shown in Figure B-3 (b). This murky condition continued until some time prior to the eleventh hour of the test, when it became as clear as that in Sample 7-A. Collapse of the overall shape of Sample 7-B appeared to have stopped by the 15 minute mark, but disintegration of the exposed surfaces continued until the 50 minute mark. Although unseen in the photos, tiny air bubbles ascended to the surface from the specimen throughout the disintegration process; this did not occur in Sample 7-A. After this time, there were no noticeable changes to Sample 7-B. Unlike previously undocumented tests, the entire air-dried sample (Sample 7-B) did not completely disintegrate, but retained its original shape to a certain degree and the degree of bubbling from air escaping the sample was also markedly less in this documented test. Equilibrated states of Samples 7-A and 7-B are illustrated in Figure 5-3. The disintegrated pieces of the exposed Sample 7-B were flake-like and angular (Figure 5-3). Sample 7-C appeared relatively intact and unchanged throughout the entire test period.

Following a prolonged period of drying (after all the water had evaporated from the containers), a deposit could be seen covering portions of the surface area of these specimens. A white to light brown-grey residue was noted on the inside surface of the beaker holding Sample 7-B corresponding to the top of the water level at different stages of evaporation. In addition, white, rod-like crystals appeared on the top surface of the sample after all the water had evaporated. A white to light grey-ish crust also appeared at the topmost point of Sample 7-C. Similarly, but to a lesser degree, this occurrence was also noted in Sample 7-A, but the crust was uniform in colour and light grey. However, no chemical analysis was undertaken of these deposits since this was beyond the scope of this research.



Figure 5-3: Equilibrated state of Samples 7-A (a) and 7-B (b) during the water deterioration test.

5.2.6 SCANNING ELECTRON MICROSCOPE (SEM)

Samples of the Millwood Member from Block 6 were observed under scanning electron microscopes in order to examine the possibility of cementation. Two sessions of SEM photography were carried out using different machines; because the first session required air dried samples, a second session was needed to examine an in-situ sample and assess the possible differences in structure between the dry and wet states (Figure 5-4¹⁵). Samples in the first session were coated with gold (approximately 100 Å thick) in order to enhance its conductive response to the subsequent bombardment of electrons, and both bedding orientations (i.e. cross and parallel) were examined (Figure 5-5). However, it was rather difficult to distinguish which, if any, orientation was examined in the second session due to the relatively poor results obtained (i.e. it was difficult to differentiate between the constituents of the material) as shown in Figure 5-4 (b). The obvious distinction between silt and/or sand grains from the stacks of clay platelets was nearly impossible in this second session, whereas it was clearly distinguishable in the air-dried samples of the first session shown in Figure 5-4 (a).

In addition, a semi-quantitative Energy Dispersive X-ray analysis was carried out on the samples examined in the first SEM session to determine the elemental composition of the shale (Figure 5-6). The gold (Au) shown in Figure 5-6 is due to the coating used on the samples while the other elements registered are indicative of the composition of the Millwood member, which included calcium (Ca), titanium (Ti), iron (Fe), magnesium (Mg), aluminum (Al), silica (Si), and potassium (K). The largest component was silica, followed by aluminum and then approximately equal proportions of the remaining elements. The entire spectrum of elements was produced in this analysis. However, those that registered a presence transmitted different amounts of x-ray energy; hence, some elements appeared more than once along the x-axis. In addition, pyrite nodules, as suspected by the presence of sulphur in combination with iron from the Energy Dispersive X-ray analysis, and voids left by such loosened nodules were evident in the parallel bedding sample (Figure 5-7).

5.2.7 CONSOLIDATION CHARACTERISTICS

One-dimensional consolidation characteristics were determined by testing in a standard oedometer apparatus. Two samples were tested, one from each block. However, only complete results for Block 6 will be presented due to an error of the data logging equipment during the last load increment (800 kPa) of Block 7. During this last increment, the data logging channels were reset and the channel monitoring vertical displacements was not among the default channels; data for the last loading stage was incomplete and data for all subsequent unloading stages were not recorded. Each sample was loaded at standard load increments and unloaded in the reverse order. The initial and final conditions of the test specimens are summarized in Table 5-5 while results from each loading stage are summarized in Table B-1 (Appendix B).

The coefficient of consolidation was determined by the square-root-time method for Sample 6-2 due to the rather irregularly shaped log-time curves that resulted for most of the load increments (Figures B-4 to B-11 in Appendix B). Conversely, the log-time method was used for Sample 7-1 due to its easier interpretation from an S-shaped curve rather than attempting

¹⁵ The figures from both SEM sessions shown are not to the same magnification owing to the fact that different machines were used; therefore the same magnification could not be achieved without extensive effort. In addition, photos showing the general landscape of the fabric were not available at the same scale. However, the primary purpose of this comparison was to demonstrate the inability of the wet SEM session to capture the different constituents of the fabric in a clearly distinguishable manner.

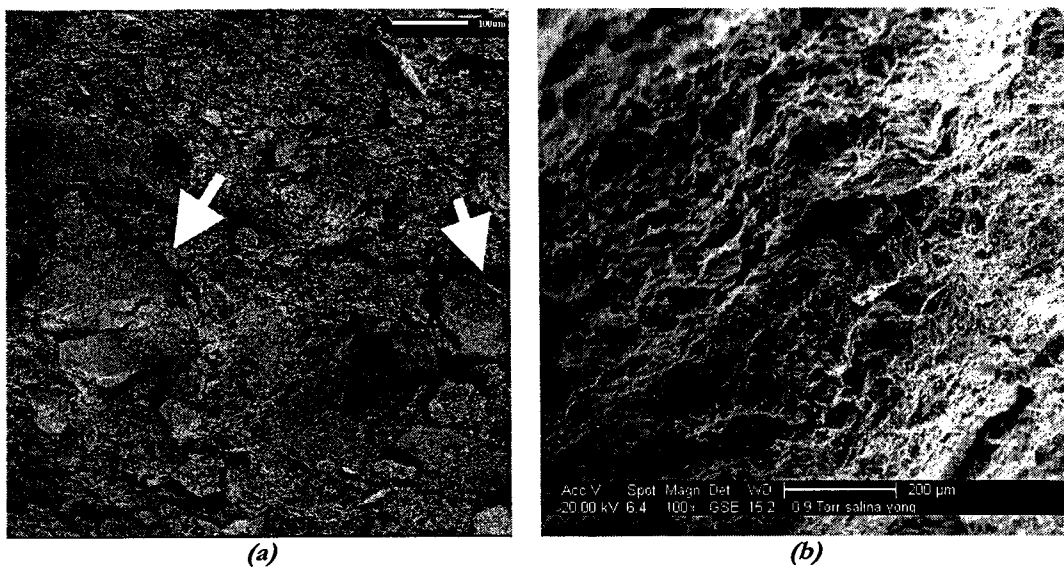


Figure 5-4: Results from SEM photography: (a) air-dried and coated in gold, arrows indicate silt- and sand- size particles (b) in-situ and uncoated.

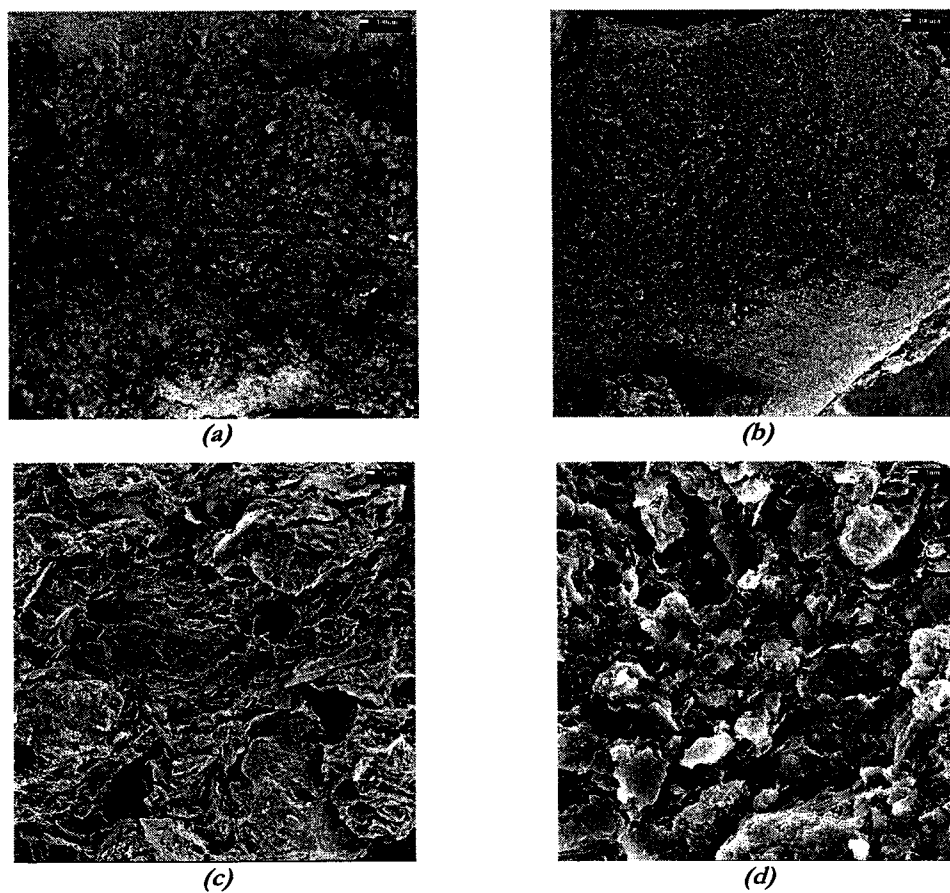


Figure 5-5: Results from SEM photography on the air-dried samples: (a) cross bedding at 20× magnification (b) parallel bedding at 20× magnification (c) cross bedding at 2000× magnification (d) parallel bedding at 2000× magnification.

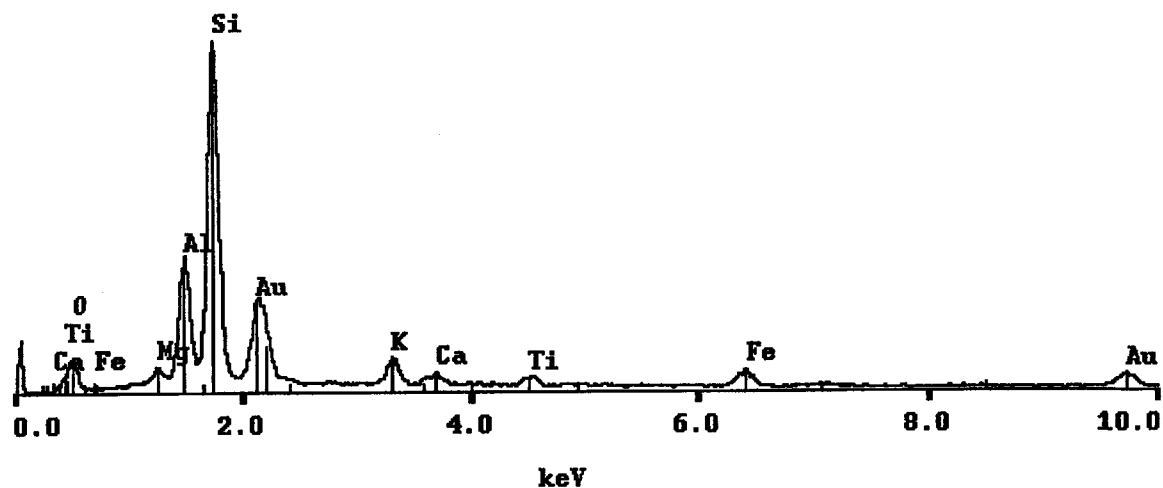


Figure 5-6: Results from the Energy Dispersive X-ray Analysis: y-axis represents the number of counts (i.e. number of x-rays) whereas the x-axis represents the number of electron volts (i.e. the energy of the x-ray).

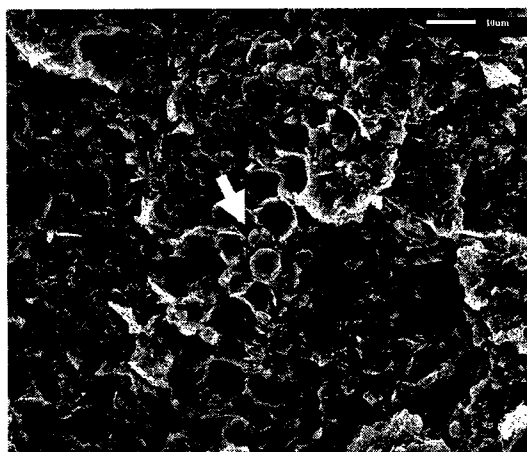


Figure 5-7: Pyrite nodules.

Table 5-5: Summary of initial and final consolidation sample conditions.

Sample	Height (mm)	Water Content (%)	Bulk Density (kg/m ³)	Dry Density (kg/m ³)	Degree of Saturation (%)	Void Ratio
6-2:						
initial conditions	18.9	22.4	2046.2	1672.3	96.7	0.63
final conditions	18.6	23.5	2100.6	1700.8	106.2 ¹⁶	0.60
7-1:						
initial conditions	19.0	20.5	2079.0	1725.3	92.4	0.62
final conditions	-	21.4	-	-	-	-

¹⁶ the degree of saturation so calculated often results in values greater than 100% (Head, 1982)

to distinguish the straight portion of the square-root-time curve necessary for interpretation. During the first loading stage of Sample 7-1 at approximately 25 kPa, the specimen height decreased initially as expected, but began to reverse in direction about an hour after loading commenced and continued in this direction until roughly 14 hours later when vertical displacement appeared to have ceased (Figure B-19 in Appendix B). However, this increase in height did not exceed the original sample height. The consolidation characteristics have been summarized according to the coefficients of volume compressibility, consolidation, and permeability in Figure 5-8. It must be remembered that these coefficients are inherently related to the load and the direction that was applied, and do not define global nor isotropic behavioural characteristics of the material under any other condition.

5.3 RESULTS: SHEAR STRENGTH CHARACTERISTICS

The shear strength characteristics necessary for the following limit equilibrium and deformation analyses were determined via the direct shear and triaxial tests. In-situ samples of Block 6 were used in the direct shear tests, while in-situ samples of Block 7 were used in the triaxial tests. In addition, a single remoulded sample of Block 6 was tested during the direct shear phase. All tests were allowed to deform through as much of the full spectrum of strength as possible (i.e. from peak to residual).

5.3.1 DIRECT SHEAR TESTS ON INTACT SAMPLES

The objective of this test was to determine both the peak and residual shear strength parameters of the material. This was carried out in two phases: the first phase ("peak" travel) involved shearing the intact sample a minimum of 9 mm to capture both peak and post-peak strengths from one direction of travel, while the second phase ("residual" travel) encompassed re-shearing of the sample following the introduction of a wire-cut shear plane to capture the residual strength of the cut surface. In total, five circular samples (with average diameters of 64 mm and heights of 19 mm) from Block 6 were extracted and tested at loads ranging from 100-500 kPa at 100 kPa increments in a standard direct shear apparatus (Table 5-6).

In the first phase, each sample was allowed to consolidate under their respective loads until primary consolidation was complete (a minimum period of 24 hours) prior to the shearing process. From these consolidation plots, the coefficient of consolidation was determined via both the log-time and square-root-time methods, which in turn were used to calculate the time to reach peak shear strength (time to failure) according to the formulation developed by Gibson and Henkel (1954). The longer duration of the two was used in combination with an estimated displacement to peak strength of 1-2 mm to ascertain a displacement rate slow enough to ensure drained conditions (i.e. no development of excess pore pressures during shearing). In addition, the displacement rate was reduced by a minimum factor of two due to the large variation between the rates calculated from the two methods. The square-root-time method consistently yielded the higher rate (ranging from a minimum of 1.1 times to a maximum of 3 times) at an average of 2 times faster than the log-time method. Results from the direct shear tests on these intact samples for peak and residual values are summarized in Table 5-6 and are illustrated below in Figure 5-9.

Sample 6-7 did not have a shear plane introduced following the peak travel as one of the halves was preserved (i.e. coated with varnish) in order to illustrate the angular and undulating nature of the sheared surface following this initial travel (Figure 5-10). A note of

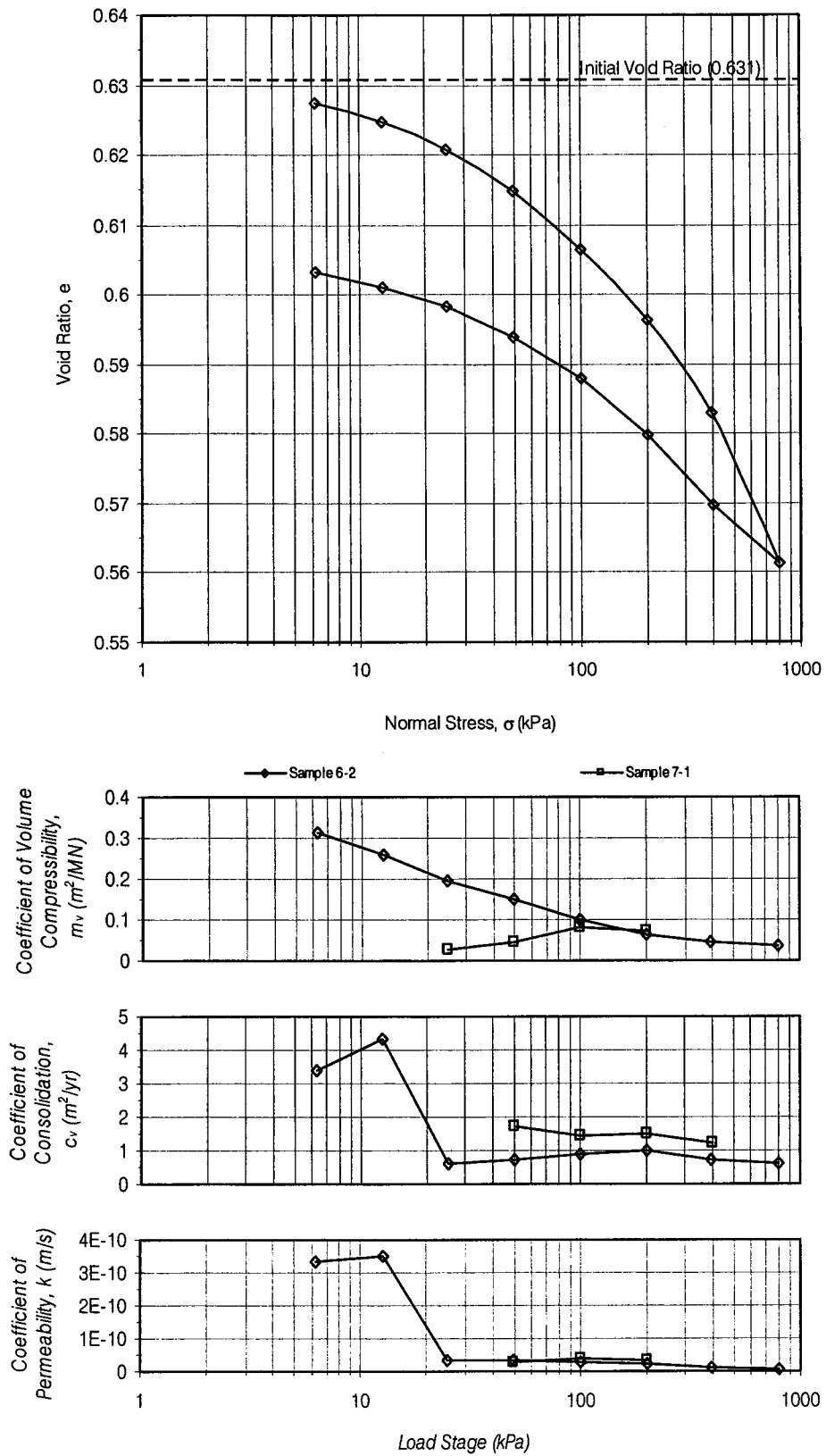


Figure 5-8: Summary of consolidation characteristics.

Table 5-6: Summary of direct shear tests on intact samples.

Sample	Normal Load (kPa)	Displacement Rate (mm/min)	Intact Sample		Cut Surface	
			Peak Shear Stress (kPa)	Displacement at Peak (mm)	Residual Shear Stress (kPa)	Residual Shear Stress (kPa)
6-7	100	0.0350	215.7	1.07	63.9	-
6-6	200	0.0050	282.9	0.79	118.6	89.4
6-5	300	0.0089	369.3	1.45	196.0	77.7
6-8	400	0.0089	284.5	1.39	174.4	131.1
6-9	500	0.0015	475.4	1.42	173.7	149.8

interest on Sample 6-7 was the distinct separation of the original intact sample into two halves following only one direction of travel (i.e. without any cut) when the shear box was disassembled. No additional force was required to separate these two halves as they simply lay on top of each other.

In the second phase, a plane was cut in each sample following the first travel and sheared again; results are tabulated in Table 5-6 and are illustrated below in Figure 5-11. However, since the sample was cut without removal from the apparatus, this introduced surface was neither smooth nor straight. An attempt was made to smooth this surface by cycling the sample back and forth four times following the cut prior to the re-shearing of Sample 6-6. However, due to the amount of material lost from this cut surface during the process, this practice was discontinued in the remaining samples. Head (1982) noted the inevitable loss of fine material during the course of cycling as a disadvantage since it is the fine fraction that exhibits a significant influence on the residual strength of the material. Moreover, this cycling did not appear to improve the smoothness of the shear plane by a substantial amount. Hence, some of the residual travel plots peaked near the same horizontal displacement as their respective peak travel plots (Figure 5-11). A typical cut plane from the second phase is illustrated below in Figure 5-12.

Water contents of the disturbed and undisturbed zones were also taken following disassembly of the shear box. The average water content of the disturbed zones was approximately 36.6% and that of the undisturbed zones was 24.3%.

5.3.2 DIRECT SHEAR TEST ON A REMOULDED SAMPLE

In addition to the direct shear tests on the intact, in-situ shale, a single direct shear test was also carried out on a remoulded sample to examine the influence of structure on its shear strength characteristics. The remoulding process involved mixing broken-up pieces of fresh shale and distilled water into a slurry, which was then placed into a mould and consolidated at 200 kPa (at three load increments in 2-3 days). Similarly, the same direct shear testing procedure as above was followed with the elimination of the second phase. Again the displacement rate (0.004 mm/min.) was reduced by a minimum factor of two (in this case, by 2.5 times) due to the variation between the square-root-time and log-time methods; the former was 1.3 times faster than the latter. The peak shear stress reached was 143 kPa, as shown in Figure 5-13.

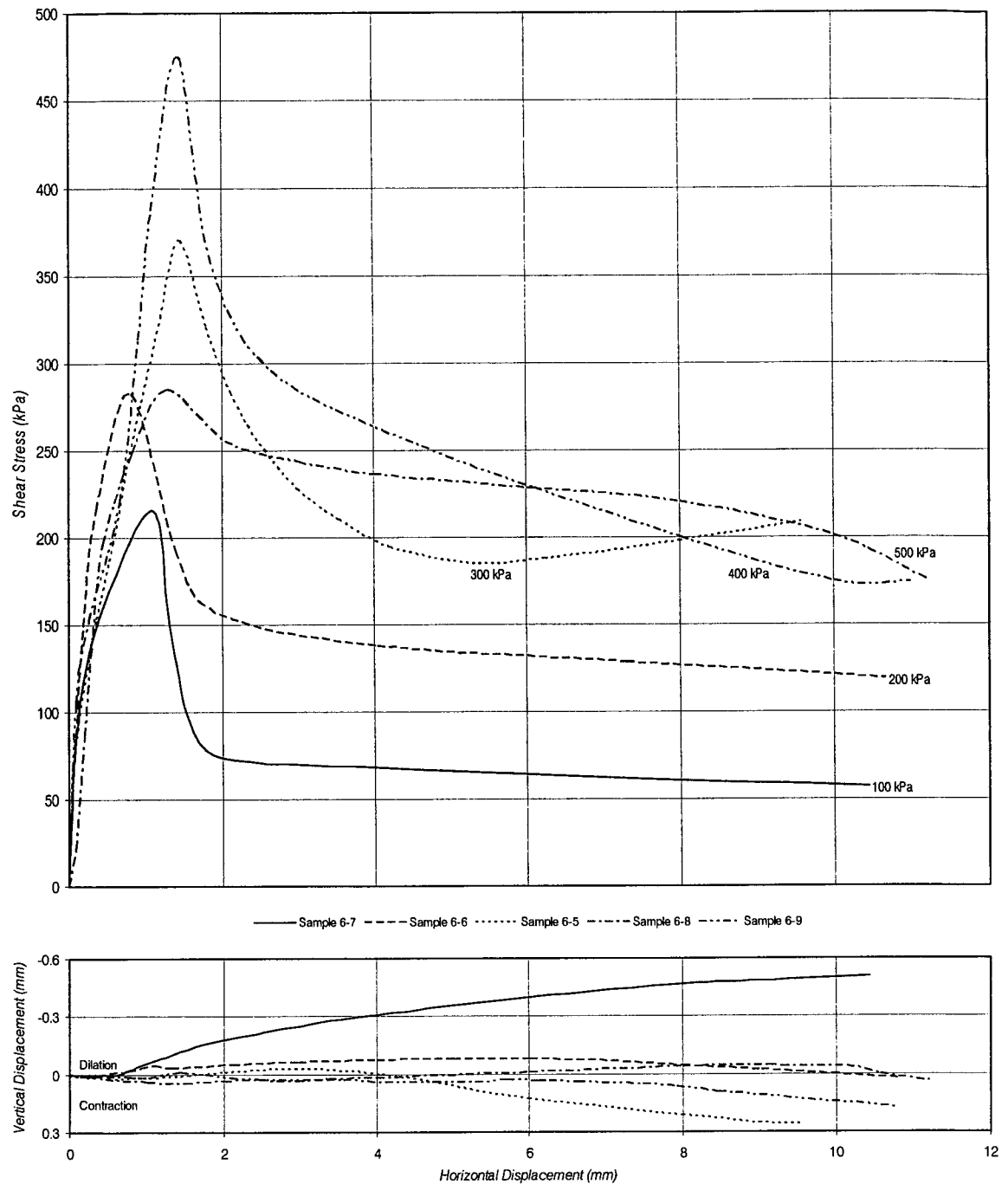


Figure 5-9: Summary of direct shear tests on in-situ samples (peak travel).

Unlike the intact samples, there was no distinct separation between the two halves following shearing (Figure 5-14) and they had to be manually separated from each other in order to take water contents. Due to this rather awkward situation, water content of the sheared zone (59%) was taken prior to separation at both ends where the shearing process exposed the imposed shear plane. However, this water content sample was like watered-down slurry

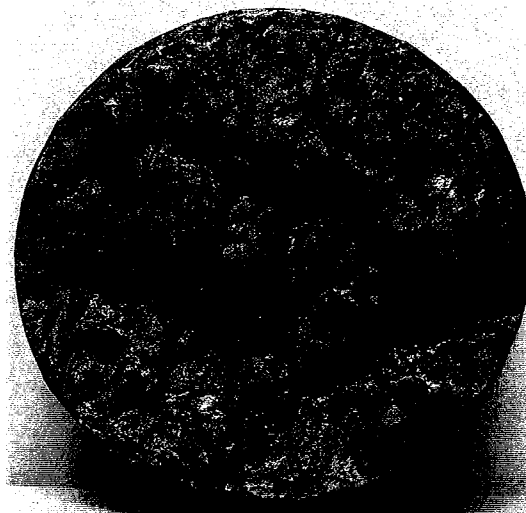


Figure 5-10: Shear surface after peak travel (Sample 6-7).

and no doubt contained a lot of excess water from the apparatus itself. A water content was also taken of what was thought to be the shear zone from one of the halves and the remaining portion of the two halves. Little variation was found in these last calculated contents; they ranged from 33-35% and averaged 34%.

1.1.1 CONSOLIDATED-UNDRAINED & DRAINED TRIAXIAL TESTS

A series of consolidated-undrained triaxial tests were also carried out under low confining pressures to investigate the effects of stress-relief. With the unit weight of this shale estimated at 20 kN/m³ (Table 5-7), the confining pressures tested ranged from 100-500 kPa (corresponding to depths of approximately 5-25 m). Four samples (averaging 50 mm in diameter and 99 mm in height, with an average height to diameter ratio of 2) were extracted from Block 7, and their in-situ properties and characteristics are summarized below in Table 5-7.

As indicated by Table 5-7, none of these samples were completely saturated. Saturation of each sample was undertaken in the first phase of each test via the use of back-pressure; samples were left for an average period of three days (minimum of two days and maximum of five days). Once the samples were saturated, the respective confining pressure was induced in preparation for isotropic consolidation and each sample was left overnight in an undrained condition to allow pore pressures to stabilize. Following this, consolidation was carried out, and the time to failure was calculated from the resulting coefficient of consolidation. Unlike the direct shear, the time to failure was only calculated from the square-root-time method according to the correlations developed by Bishop and Henkel in 1962 (Head, 1986). These were then combined with the estimated strain at peak (failure) of 1-5% for brittle soils (as indicated by the distinctive shape of the stress versus displacement curves in the direct shear tests) in order to calculate the required displacement rate. Subsequently, shearing of the samples was carried out under undrained conditions with measurement of pore pressures and stopped a short period after the peak deviatoric stress was reached. Results of each test are tabulated below in Table 5-8 and illustrated in Figure 5-15.

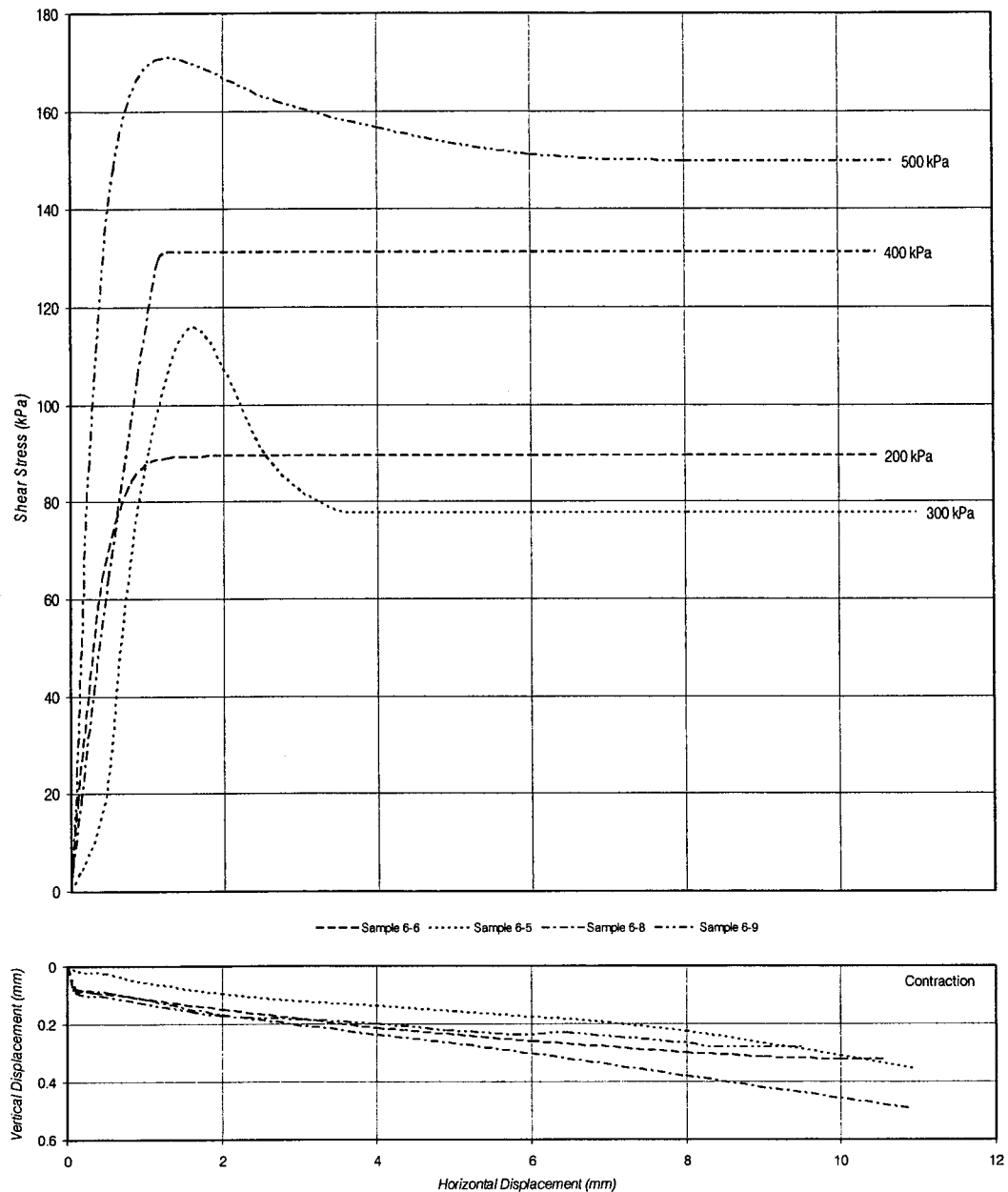


Figure 5-11: Summary of direct shear tests on a cut surface following peak shear (residual travel).

As indicated in Figure 5-15, not all samples were tested in an undrained condition. During the shearing phase of Sample 7-3, the back-pressure valve was mistakenly left open for the entirety of the compression phase, thus imposing drained conditions. Similarly, Sample 7-2 was compressed under drained condition despite having closed all appropriate valves. It was most likely that either the valve leaked or the valve had a loosened handle which when turned would not necessarily close. These errors would most severely incur adverse effects to the displacement rate, since the calculated time to failure would be roughly 7.8 times longer for a drained test (Head, 1986). However, the displacement for Sample 7-2 was within the range calculated for drained conditions, conversely the rate determined for Sample

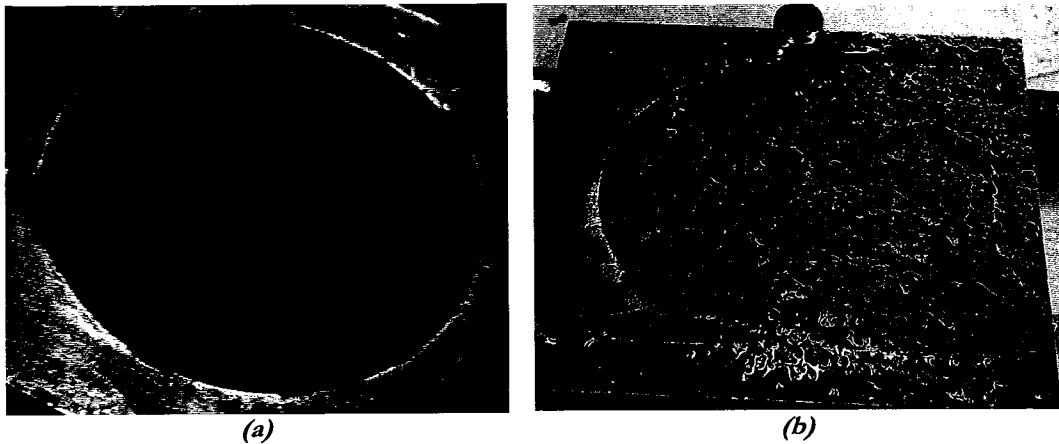


Figure 5-12: Cut plane of the intact samples following the second phase: (a) top half (b) bottom half.

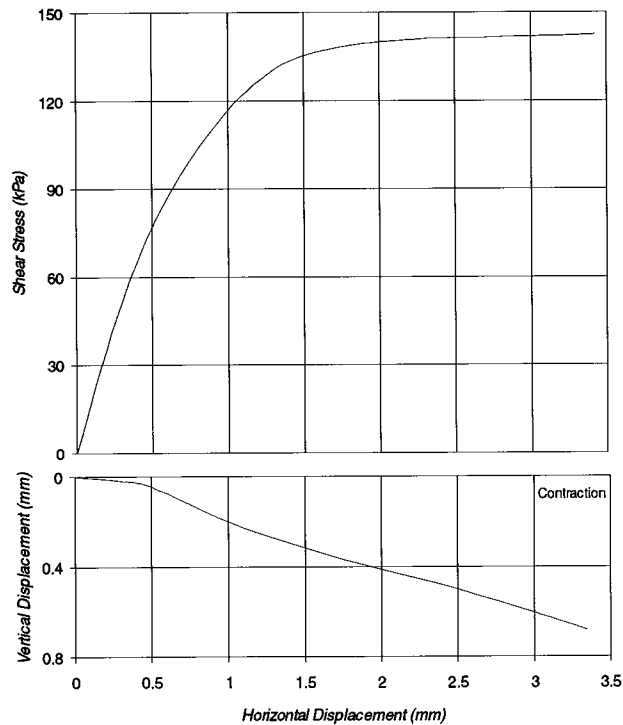


Figure 5-13: Summary of direct shear test on a remoulded sample.

7-3 was not. The estimated strain at failure for the rate used in Sample 7-2 was 3.6%, which was lower than the actual failure 4.3% strain. The estimated strain for the rate used in Sample 7-3 was 7.8%, which was higher than the actual failure at 2.7% strain. In spite of this and because pore pressure measurements were made throughout the compression phase, any affects caused by the displacement rate could be accounted for. In addition, the vertical LVDT for Sample 7-2 did not work and it was not apparent until the end of the test; the strain rate was used to determine vertical displacements.

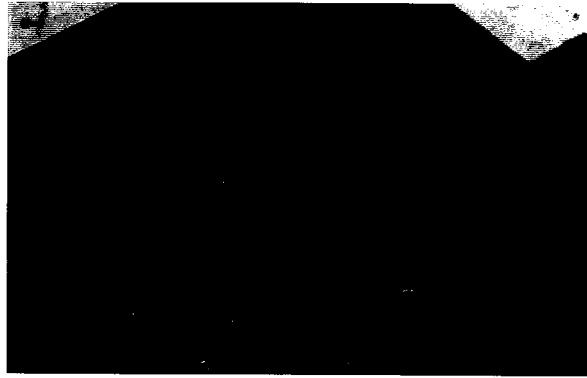


Figure 5-14: Remoulded sample following the shearing process.

Table 5-7: Summary of the initial conditions of triaxial test samples.

Sample	Water Content (%)	Bulk Density (kg/m^3)	Bulk Unit Weight, γ_b (kN/m^3)	Dry Density (kg/m^3)	Dry Unit Weight, γ_d (kN/m^3)	Initial Void Ratio	Initial Degree of Saturation (%)
7-2	20.1	2071.5	20.3	1725.2	16.9	0.62	90.5
7-3	19.9	2080.7	20.4	1735.0	17.0	0.61	91.1
7-4	20.2	2075.8	20.4	1726.3	16.9	0.62	91.4
7-5	20.1	2077.0	20.4	1730.1	17.0	0.62	91.1

Table 5-8: Summary of triaxial test results.

Sample	Confining Pressure (kPa)	Displacement Rate (mm/min.)	Failure		
			Deviatoric Stress, $\Delta\sigma_{1f}$ (kPa)	Axial Strain, ϵ_f (%)	Pore Pressure, u_f (kPa)
7-4	98.3	0.0300	592.4	3.8	73.0
7-3	198.6	0.0060	1452.2	2.7	-0.02
7-2	285.2	0.0008	1322.5	4.3	-2.6
7-5	502.8	0.0008	1095.1	2.5	337.9

All the triaxial specimens sheared along a distinct plane, which travelled the length of the entire sample (Figure 5-16). However, the primary shear plane was neither smooth nor straight (Figure 5-16), consisting of small divets and mounds. In addition, the surfaces of the shear planes were not shiny, but consisted of striations which suggested and were consistent with the direction of shear. With the exception of Sample 7-5, shearing of all the samples involved secondary planes (such as Sample 7-2 and 7-4 in Figure 5-16), which often intersected the primary shear plane at some angle.

1.2 DISCUSSION: MATERIAL CHARACTERIZATION

The following discussion will focus on the interpretation of the laboratory results and observations of the physical and mechanical characteristics of samples taken from Blocks 6

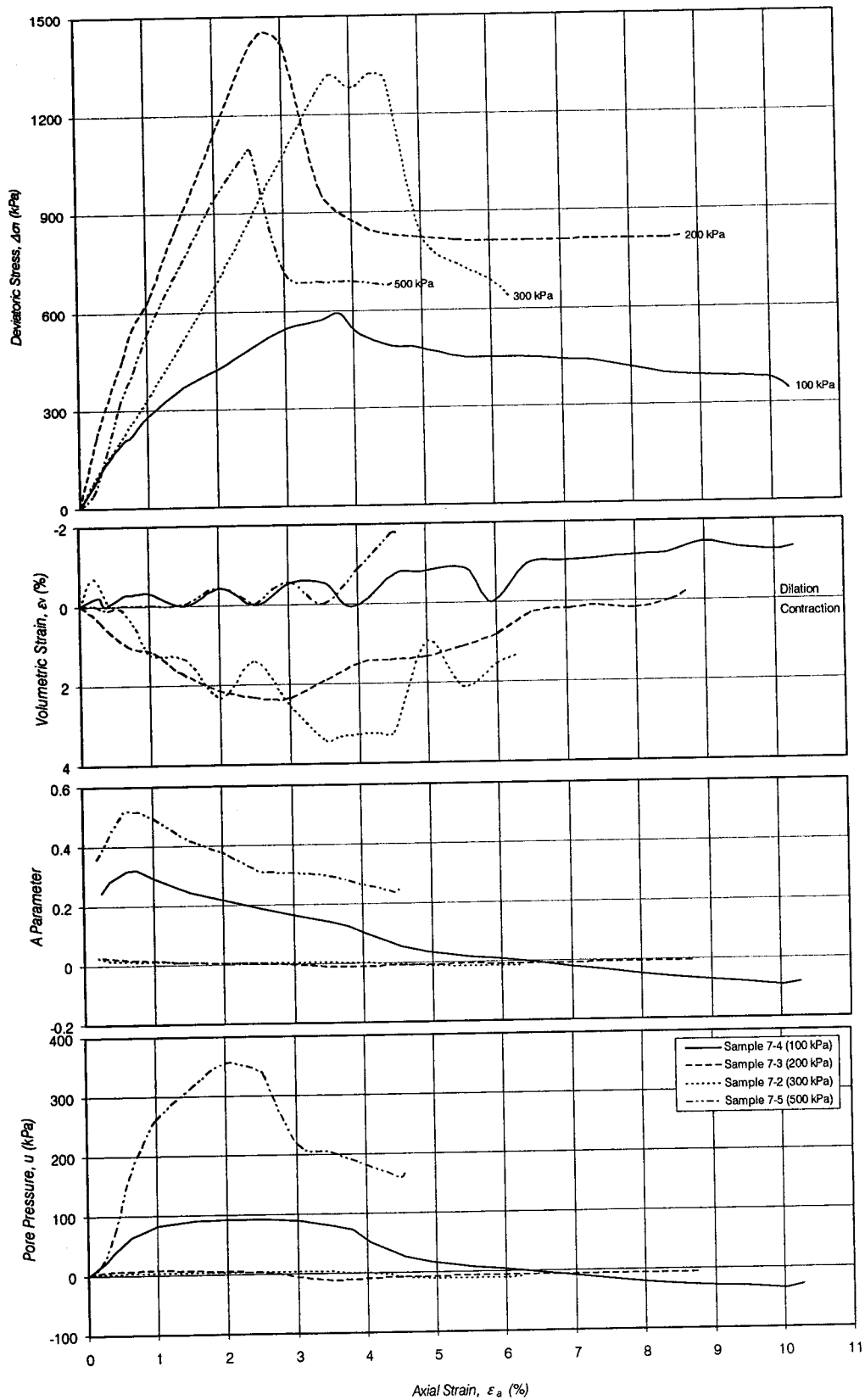


Figure 5-15: Summary of consolidated-undrained and drained triaxial tests.

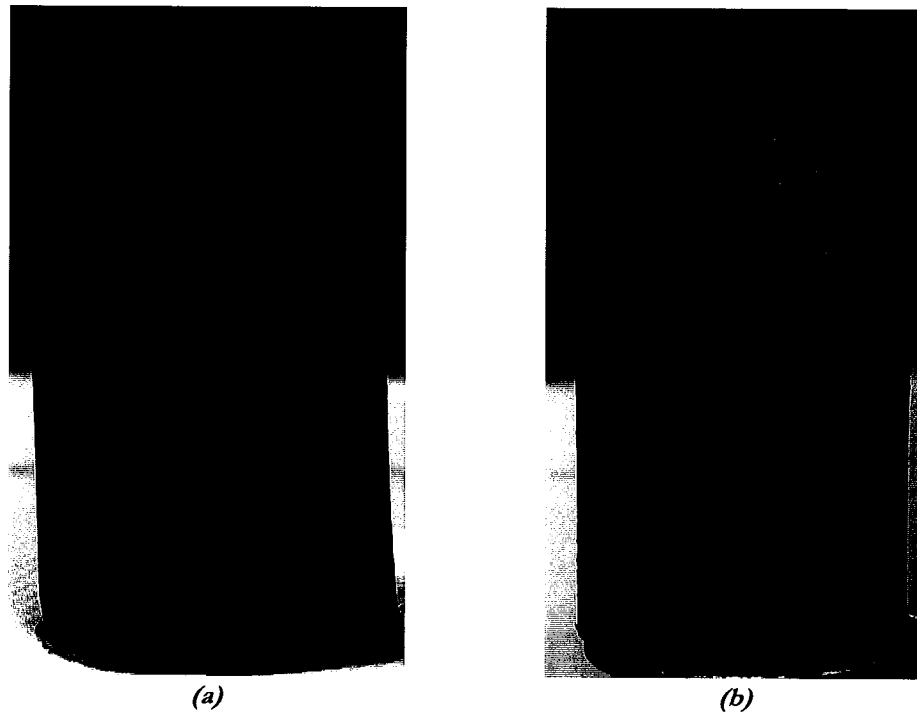


Figure 5-16: Typical inclination and surface features of the failure surface from the consolidated-undrained and drained triaxial tests: (a) inclination and secondary failure surfaces of Sample 7-2 (b) failure surface of Sample 7-3.

and 7 in order to develop a behavioural framework for this material specific to slope instability. The resistance of this material to slope movements at a given geometry and the extent to which they occur will depend on these characteristics, which in turn depend on the depositional and geomorphological history.

1.1.1 INDEX PROPERTIES

The grain-size distribution of the shale suggested that it was predominately fine-grained with its main constituents comprising of silt-size (56-57%) and clay-size (34-36%) materials (6-10% sand-size particles made up the remaining portion). The second round of testing of Block 7 also displayed a decidedly gap-graded nature as indicated by the sharp and steep curvature between particle diameters of 0.075 and 0.060 mm (Figure 5-1). The discrepancies between the lab results and those obtained by the consultant are illustrated in Figure 5-17 (a); lab results indicated a gap-graded material dominant in silt-size particles whereas the consultant indicated a better to well graded material with a dominance in clay-size particles. A similar observation was made by Kenney (1967) on test results from Cucaracha, Bearpaw, and Pierre clay shales, where the clay fraction determined was too small for a soil predominantly composed of clay minerals and with cation exchange capacities consistent with these minerals. In addition, Figure 5-17 (b) includes the grain-size distribution of five members of Pierre Shale from South Dakota as compiled by Erskine (1973). These distributions also show higher clay contents; on average, the sand content ranged from 1-8%, silt ranged from 25-34% and clay ranged from 58-74%. Since these final samples were air-dried to a water content of less than 4% and left to soak in the dispersing agent for a period of four days, it is unknown why the results did not vary significantly from those of the previous lab tests (Figure B-2 in Appendix B).

proportions of the different grain sizes and not the expected mechanical behaviour. Hence, the remaining tests will deduce which of these dominant fractions govern the engineering behaviour.

The plasticity of Blocks 6 and 7 was also compared with the values obtained by the consultants as well as those obtained by Schaefer and Lohnes (2001) from samples of Pierre Shale obtained near Pierre, South Dakota as illustrated in Figure 5-18 and Table 5-9. Additionally, the plasticity of the tested specimens are also compared to similar materials as illustrated in Figure 5-18. Based on the grain-size distribution and plasticity of the samples tested, this shale was considered a CH material (i.e. an inorganic, high-plasticity clay) according to the USCS (Unified Soil Classification System). In addition, the range in specific gravities obtained from both blocks were consistent with that of inorganic clay (specific gravity ranging from 2.7-2.8) and the possible presence of mica or iron as indicated by specific gravities ranging from 2.75-3.00 (Bowles, 1992). These values are, however, higher than those obtained by Schaefer and Lohnes (2001) but only slightly higher than that obtained by Knight (1963) from the Oahe Dam project also located near Pierre, South Dakota (Table 5-9). Consequently, it appears that the clay fraction does in fact exhibit dominance over the silt fraction despite its lower proportion in the samples of the Millwood Member tested here.

The liquidity indices of the samples tested ranged from -0.1 to -0.8, which indicated a heavily overconsolidated soil. Materials which exhibit liquidity indices near or exceeding 0.5 are considered normally consolidated, lightly overconsolidated soils have indices approaching zero, while those that exhibit negative liquidity indices are heavily overconsolidated (Scott and Brooker, 1966). Indices of samples from Block 6 ranged from -0.1 to -0.3 and averaged -0.2, while samples from Block 7 averaged -0.6 with a minimum of -0.2 and a maximum of -0.8. Hence, it appears that Block 7 may have been located at a lower elevation than Block 6.

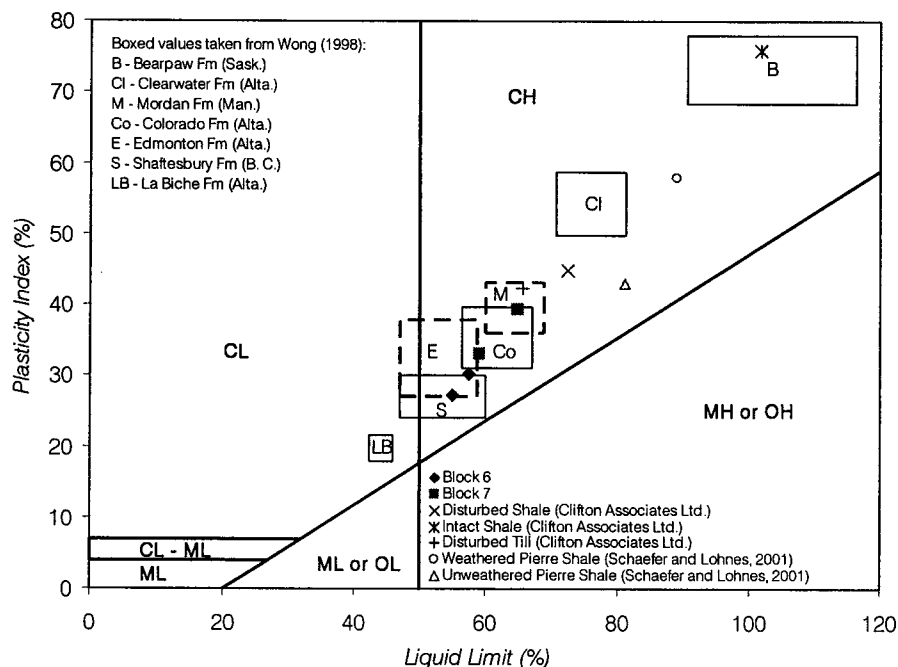


Figure 5-18: Plasticity chart comparing lab values to others.

Table 5-9: Specific gravity, natural water contents and consistency limits of the shales of the Pierre Formation.

Sample Source	Specific Gravity	Natural Water Content (%)	Liquid Limit (%)	Plastic Limit (%)	Plasticity Index (%)
Block 6	2.73	21.1	56.4	27.6	28.8
Block 7	2.80	20.3	61.3	25.9	35.4
Disturbed Shale ¹⁷	2.53	29.3	72.4	27.6	44.8
Intact Shale ¹⁷	2.65	20.5	101.8	26.0	75.8
Weathered Pierre Shale ¹⁸	2.70	32.5	89	31.0	58.0
Unweathered Pierre Shale ¹⁸	2.73	28.2	81	38.0	43.0
Pierre Shale bedrock ¹⁹	2.80	25.0	-	-	-

5.4.2 FABRIC

Examination of the material fabric or structure was required to explain its non-disaggregation when placed in water at in-situ water contents and due to the discrepancy in the grain size analysis. Cementation was initially hypothesized as the cause of these abnormalities since it was not an uncommon occurrence in the Pierre Shale (Schafer, 2002; Crandell, 1958). Schafer (2002) has described Pierre Shale in South Dakota as a weakly cemented compaction shale, while Crandell (1958) has noted the presence of iron and manganese carbonates in the DeGrey member (equivalent to the Millwood member in Manitoba) of the Pierre Shale in South Dakota. However, the null results from exposure to hydrochloric acid suggested that no carbonates were present in the samples tested. As a result, carbonate-based cementation was ruled out. However, this did not necessarily discount cementation all together, but expanded the search to cementation of other types. Consequently, the SEM was employed to examine the shale fabric in search of this evidence.

CEMENTATION. Plausible substantiation of cementation was found during the dry SEM session and was most apparent in the cross-bedding view as illustrated in Figures 5-19 (a) to (d). The cementation was represented by apparent texture, as indicated by the “lumps” in Figure 5-19 (a), which covered the clay platelet surfaces. Some of this texture was undoubtedly due to the gold coating, however this coating acted like a blanket thereby preserving the original surface topography as indicated in Figure 5-19 (a) where this texture was roughly 100 nm in thickness compared to the thickness of 100 Å for the gold coating. It was suggested that this texture appeared to be a fine particulate of an amorphous nature due to it lacking a definite shape. Additional evidence of physical bonding was indicated by the occurrence of several “bridges” between platelets as denoted by the arrows in Figures 5-19 (b) and (c). Other details supporting the hypothesis of cementation included the apparent fusing of platelets together (circled area) as shown in Figure 5-19 (c) and the reappearance of the nearly horizontal platelet after disappearing behind some substance in Figure 5-19 (d).

It was postulated (from the greater detail of this bridging shown in Figure 5-20) that the origin of this cementation might be organic in the form of sugars or bacterial mucilage developed from the decomposition of ancient animal and/or plant life during the diagenesis of the deposition into the present shale formation. The biological processes of plant and

¹⁷ Clifton Associates Ltd., 1986

¹⁸ Schaefer and Lohnes, 2001

¹⁹ Knight, 1963

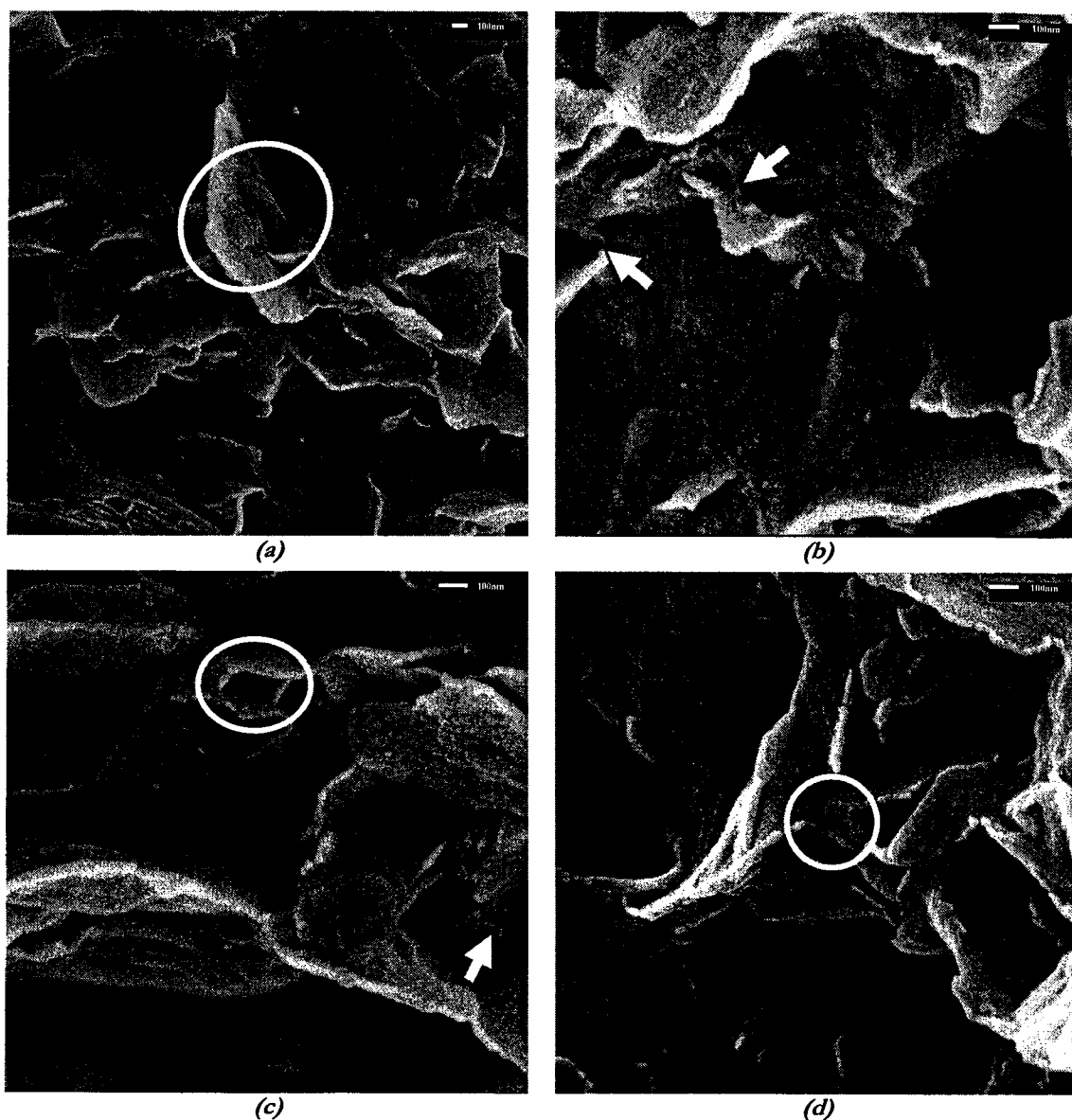


Figure 5-19: *Shale fabric from the dry SEM analysis, illustrating the possibility of cementation.*

animal interaction with their surroundings occur from the onset of sedimentation, such as bioturbation (burrowing of the sea or lake bed by animals) which leads to progressive densification and to possible post-depositional cementation as some animals will employ body secretions in the stabilization of these tunnels, as well as organic decay which aid in the bonding of sediments (Clayton and Serratrice, 1997). Clayton and Serratrice (1997) also mention that possible sources for cementation in early diagenetic processes include biogenic material that may be deposited either in shallow or deep (still, low-energy environments) marine conditions thereby resulting in immediate particle to particle contact which also gives rise to a superficial porosity that can withstand large vertical stresses, in addition to the conversion of chemically unstable sediments soon after deposition. Clayton and Serratrice (1997) summarize the possible sources of cementation as follows: dissolution of small supersoluble particles and re-precipitation of calcium carbonate, precipitation of iron

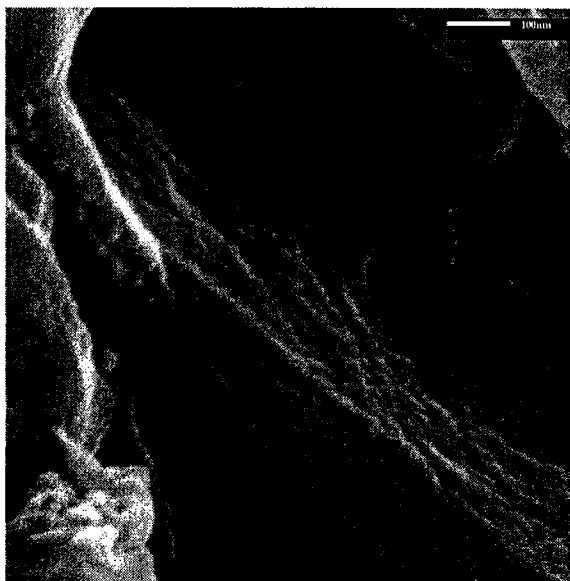


Figure 5-20: Possible cementation between clay platelets.

hydroxides or dissolved aluminum, deposition of organic material, recrystallization during alteration, and changes in the adsorbed water and face and edge charges on clay particles.

Other sources of inorganic cementation include sulphates, oxides, silica, and alumina. Sulphates are most prevalent in semi-arid and arid climates with gypsum (selenite) as the most common form, while oxides are commonly found in regions affected by volcanic ash and in the tropics where aluminum, silicon, and iron oxides and hydroxides are commonly found (Mitchell, 1993). Both circumstances are consistent with the historical and climatic conditions of Manitoba, where volcanic activities of the western orogenies have contributed to the depositional history of the area and the climatic conditions of the region can be considered semi-arid (selenite crystals have been identified in borehole logs). In addition, precipitations of silicates are also a viable source of cementation, such as the case with cristobalite. The occurrence of cristobalite in soils, a precipitation product of silica, may result from organic processes since it is found in many grasses, leaves of deciduous trees, and it is precipitated in lakes by diatoms and siliceous sponges as well as in oceans by diatoms, sponges, and radiolaria (Langmuir, 1997). Cristobalite has been identified in the Pierre Formation by others in Chapter 2 (Table 2-1). However, without proper chemical, mineralogical, and biological analyses, these speculations are just hypotheses and have yet to be proven.

STRUCTURE. The overall fabric of the samples seemed to indicate a rather flocculated, cardhouse structure with no identifiable pattern in particle orientation in either the cross-bedding or parallel-to-bedding orientations; however, the bulk of the particles were consistent with their bedding orientations (i.e. more edges than faces were seen in the cross-bedding view and vice versa in the parallel to bedding sample) as illustrated in Figures 5-21 (a) and (b). Particle to particle spacing varied extensively and disconnected pore spaces may be a possibility due to the unpatterned cardhouse structure seen in these photos. These clay particles appeared as equidimensional flakes with a large range of sizes as shown in Figure 5-21 (b). The macro fabric of the samples appeared to suggest that it was indeed a clay matrix in which the coarser silt and sand fractions existed; thus, the behaviour of this material would be expected to be governed by its clay fraction.

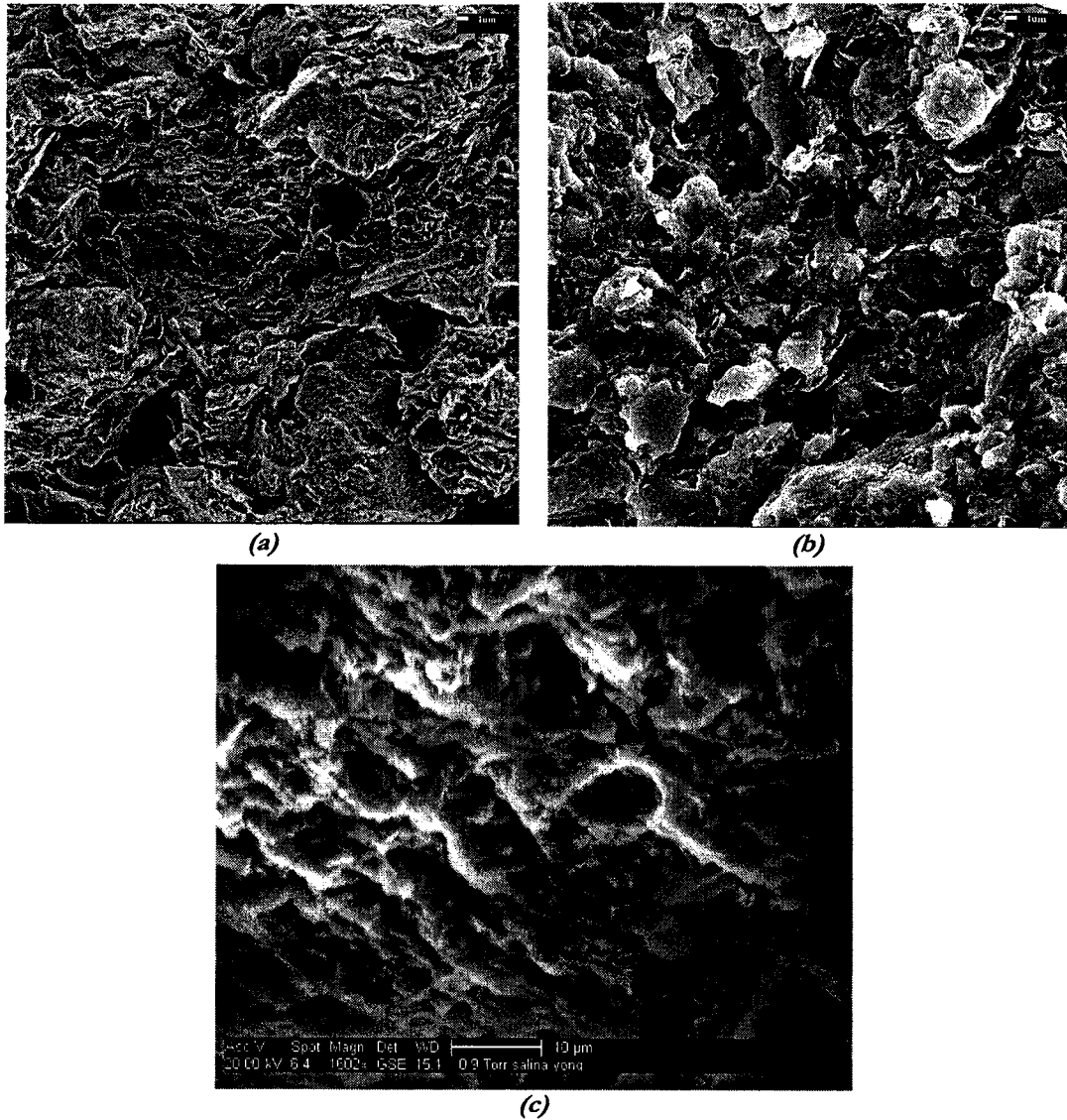


Figure 5-21: Comparison of dry and wet SEM results (a) dry SEM at cross-bedding, 2000X magnification (b) dry SEM at parallel-bedding, 2000X magnification (c) wet SEM, bedding orientation unknown, 1602X magnification.

Comparison of the dry and wet SEM analyses, illustrated the interaction between the in-situ interstitial water and the granular fabric of the sample. The clarity of the fabric of the dry SEM sample could not be attained by the wet SEM due to a combination of the adverse effects of the in-situ water (i.e. its interference with individual particles thus preventing distinguishable differentiation between the individual grains) and differing equipment features (such as aperture size and vacuum arrangement). Figure 5-21 shows three photos taken at approximately the same scale for the dry and wet SEM analyses, (a) and (b) are from the dry SEM while (c) is from the wet SEM. Clearly, the lattice structure of the granular fabric is apparent in the dry SEM photos, but it is not so in the wet SEM photo.

5.4.3 SLAKING CHARACTERISTICS

The abnormal non-disintegration behaviour of the shale when exposed to water at its in-situ water content but disintegrating following a period drying has been noted by Fleming et al. (1970), who recorded similar occurrences in the samples (of the clay shales in the upper Missouri Basin which included the Colorado Group, Claggett Formation, Bearpaw Formation, Fort Union Group, and Pierre Formation) they tested for slaking behaviour, where samples at in-situ water contents appeared unaffected when exposed to water while those that had been air-dried slaked completely in one cycle. In addition, Nakano (1970), Morgenstern and Eigenbrod (1974), and Botts (1986) have all made the same observation with other mudstones or shales.

Observations from the test indicated a surface slaking mode since disaggregation of the exposed sample was primarily surficial and analogous to numerous tiny brittle slope failures (almost like mini debris flows) as the sample crumbled into tiny flakes and chips and settled at the bottom of the beaker. Botts, in his 1986 thesis, termed this process, “drying-induced” slaking. The mechanism by which this occurred could be any of three: dispersion, swelling, or air entrapment (Mitchell, 1993). Pejon and Zuquette (2002) have indicated that samples of mudrock when air-dried to their in-situ water content following a wetting cycle tended to swell less and slower than samples air-dried to constant weight. They have contributed this to the phenomenon of “air breakage,” which promotes swelling and breakdown of the material due to the air pressure developed by internal pores when moisture returns via capillarity of the outer pores.

In light of this, the hypothesis of cementation was brought into question, but it was ultimately not discounted, since the possible sources of cementation postulated earlier (for example, from sulphatic and biological sources) are considered to be weak forms and may very well be adversely affected when the material is dried. Fleming et al. (1970) did find evidence of cementation (carbonate-based with degrees ranging from slight to high), but concluded that it was too weak to prevent breakdown from a drier state since complete deterioration of the specimens in water occurred after one cycle of slaking.

The mystery in this test may not have been the process by which the deterioration occurred, but the process by which the fresh sample in its in-situ water content remained intact and inert to the exposure of water for a prolonged period (i.e. until all the water evaporated out of the beaker, which occurred somewhere between 18-20 days). The search should focus on locating the characteristic which is present in the in-situ state, but absent and/or altered in the dried state that may in turn affect the overall strength and stability of the material. This test has significant implications on the process of weathering, and in turn valley formation. However, this topic is beyond the scope of this thesis and additional investigation into such work will be proposed in the last chapter in a discussion on the recommendations for future research.

5.4.4 CONSOLIDATION CHARACTERISTICS

It can be seen from Figure 5-8 that the consolidation of Sample 6-2 did not reach the normally consolidated stage (overall void ratio change of 0.07), and the same can be speculated about Sample 7-1 since the same maximum load was incurred on both samples. However, the results did provide some insights on the vertical hydraulic conductivity of the material, albeit a load-dependent value since its determination is calculated from the coefficient of consolidation (Head, 1982). The hydraulic conductivities ranged from 3×10^{-10} m/s (vertical load of 6.25 kPa) to 7×10^{-12} m/s (vertical load of 800 kPa) for Sample 6-2 and

3×10^{-11} m/s (vertical load of 50 kPa) to 4×10^{-11} m/s (vertical load of 200 kPa) for Sample 7-1. These values were within the range of hydraulic conductivities (10^{-9} to 10^{-14} m/s) determined from consolidation tests carried out by Neuzil (1986; 1993; 1994; 1995), who has extensively researched the hydraulic properties of Pierre Shale in South Dakota. However, these values are of intact specimens and are most likely not representative of the soil/rock mass, which in all likelihood is governed by the permeability of the fractures within the joint system. However, no mapping of joint sets was carried out at this site and only “intact” samples were retrieved; the properties of the joint system in the Millwood Member at the study site are unknown at present.

Other results from consolidation tests performed on the shales of the Pierre included the work by Fleming et al. (1970) in their study of clay shales in the upper Missouri Basin. The overconsolidation ratio they determined for the Pierre Formation ranged from approximately 13 to 68, while swelling pressures ranged from roughly 330 to 1300 kPa. However, the overconsolidation ratio determined for the study area was much smaller than these reported values. An indication of the overconsolidation ratio (OCR) for the samples tested in this study was obtained from the values of the A pore pressure parameter at failure (A_f) from both undrained triaxial tests. The OCR of Sample 7-4 was estimated at 3 (A_f of 0.1), while Sample 7-5 indicated an OCR of approximately 2.2 (A_f of 0.3).

5.4.5 STRESS-STRAIN RELATIONSHIP

An early indication of the stress-strain behaviour of the Millwood Member was seen in the direct shear tests as the shear stress dropped dramatically after reaching a peak value. This strain-weakening behaviour is characteristic of a brittle material and was also seen in all the triaxial test samples. Materials which exhibit such behaviour have a tendency for progressive failure since peak strength would not be reached simultaneously at every point along a failure surface; some points will have displaced to a greater extent than the peak strain, while others will have yet to reach the peak strain (Wu, 1996). In addition, variability in the stress-strain relationships of the samples tested was also noted implying complexity in the mechanical behaviour of this material, which also has significant implications on the possibility of progressive failure (Chandler, 1984a).

The material in triaxial Sample 7-4 was somewhat ductile at the lowest confining pressure of 100 kPa as indicated by its non-linear nature in the pre-peak portion and its relatively small peak (Figure 5-9). This ductility was possibly due to a blocky or nuggety fabric which resulted in structural readjustments from collapse of the intact material into discontinuities that remained open during this low pressure, but closed under higher pressures. At higher confining pressures (200-500 kPa), the remaining triaxial samples displayed distinctly brittle behaviour. Sample 7-5 (confining pressure of 500 kPa) also displayed non-linear behaviour in the pre-peak with seating at the initial portion of the curve. Sample 7-2 (confining pressure of 300 kPa) may have also experienced seating for a longer period of time at the beginning of the compression stage as the curve became linear only in the latter portion of the pre-peak.

In addition, Sample 7-2 exhibited an interesting double deviatoric peak as illustrated in Figure 5-15. If the straight portions on either side of the double peaks were extended, a deviatoric peak strength of nearly 1600 kPa corresponding to an axial strain of approximately 4.25% could be extrapolated. This peculiar “by-passing” behaviour of the peak deviatoric strength was also noted by Hsu and Nelson (2002) in their drained triaxial testing of Eagle Ford Shale, and attributed to small, nonexistent fissures resulting from strain localization

during failure and strength reduction down to a pre-split condition. Similar occurrences of this by-passed behaviour was also discussed by Chandler (1984a) and attributed to the '*apparent presence of incipient fissures.*' Materials which exhibit this behaviour are inherently brittle and thus susceptible to progressive failure.

The Young's moduli were determined from the linear portion of each stress-strain curve with the exception of Sample 7-4 which was determined from the initial portion of the curve since this was where linearity was most prominently exhibited. The values ranged from a low of 32 MPa (Sample 7-2) to a high of 73 MPa (Sample 7-5). These values appeared to be low compared to Nichols et al. (1986), who indicated modulus values ranging from 260 to 4520 MPa for Pierre Shale tested in South Dakota.

5.4.6 VOLUME-CHANGE BEHAVIOUR

All direct shear tests were carried out under drained conditions and indicated a general trend of contraction prior to dilation followed by contractive behaviour with the exception of the lowest normal load (Sample 6-7 at 100 kPa) as indicated in Figure 5-9. Sample 6-7 experienced no contraction initially and only exhibited dilation in the post-peak. Sample 6-6 contracted prior to peak and dilated for almost the entirety of the remaining portion of travel with contraction occurring near the end. In addition, a bump in the dilative portion of the Sample 6-6 was noted close to peak. Sample 6-9 exhibited maximum dilative behaviour very near its peak, whereas the highest point of dilation in Sample 6-5 occurred almost 1.5 mm subsequent to peak. Conversely, the initial contractive behaviour of Sample 6-9 extended to just beyond 5 mm of travel (peak occurred at 1.4 mm), with its peak dilation occurring near the end of travel. At the end of travel, only the vertical displacements of Samples 6-7 and 6-5 appeared to slow down, whereas the rate of vertical displacements of the remaining samples appeared to continue in a quasi-linear fashion. The vertical displacements of these tests appeared to correlate little with the location at which peak shear strength occurred, but more with the normal load imposed. It was found that dilation was prohibited with increasing normal load. A similar observation was made by Georgiannou et al. (1993) on direct shear tests carried out on the hard clays of the Woolrich and Reading Beds and London Clay.

In the drained triaxial compression tests (Samples 7-3 and 7-2), the samples contracted to a maximum value that correlated with the peak deviator stress (Figure 5-15). At the peak deviator stress, dilation occurred and continued in this fashion until the end of the test. Sample 7-2 also experienced minor dilation (0.7%) initially prior to contraction.

In the undrained triaxial compression tests (Samples 7-4 and 7-5), no volume change was allowed, but its general behaviour was approximated by the pore pressures measured. Both samples incurred maximum pore pressure change increase prior to peak deviator stress (Figure 5-15). Heavily overconsolidated clay tends to dilate, but due to an undrained condition, no water can be drawn in, thus negative pore pressures and A-values result (Craig, 1995). This was attested to by Sample 7-4 (average A value of -0.03 and ranged from -0.1 to 0.3) as indicated by the drop in pore pressure post peak into negative values. However, this was not the case with Sample 7-5 since the both the pore pressures and average A-value remained in the positive region. A-values greater than unity result from structural collapse due to increasing major principal stress, which induce high pore pressures (Craig, 1995). However, this did not appear to be the case in Sample 7-5 (average A value of 0.4 and ranged from -17 to 12), where these high values do not correspond to high pore pressures, but instead appeared to represent the high differential between a small deviatoric pressure

change and its corresponding pore pressure change (Figure 5-15). Despite the drainage conditions, the undrained tests also registered small volume changes, which indicated only dilative behaviour, thus confirming the expected dilative response suggested by the A values.

5.4.7 STRENGTH PARAMETERS

Both peak cohesion and friction parameters were obtained from the direct shear and triaxial tests, whereas only the residual parameters were obtained from the direct shear tests carried out on the pre-cut surface. Indications of the peak-residual differential were also approximated from individual stages in both tests.

From the direct shear tests, the failure envelopes for both the peak and residual conditions in Figure 5-22 were ascertained by discounting one anomalous test value from each data set. The peak strength so determined had a cohesion intercept of 184.7 kPa and a friction angle of 28.7° with individual peak stresses occurring at horizontal displacements ranging from 0.8-1.4 mm. The residual strength had a cohesion intercept of zero and a friction angle of 16.7° . Both envelopes were similar to the values obtained by the consultant; friction angles varied by 22-28% with Block 6 resulting in a lower value, while the cohesion varied from as little as 6% again with the lower value from Block 6. The higher residual friction angle from Block 6 was attributed to the uneven and rough shear surfaces attained despite having been

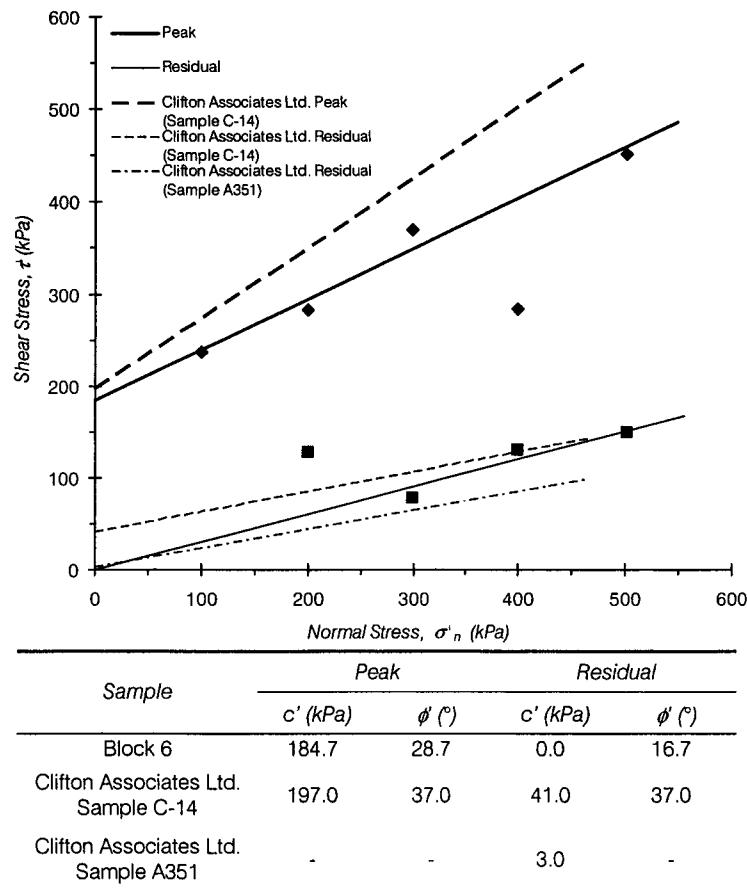


Figure 5-22: Mohr-Coulomb failure envelopes from direct shear tests.

wire-cut, which was attested to by the peaks in the stress-displacement curves from the residual travel of Samples 6-5 and 6-9. These shear strength values were consistent with those reported in the literature (Table 5-10) with values for peak ranging from 14-160 kPa for cohesion and friction angles of 23-41° in similar materials (Belly River and Lea Park formations), while those reported for the residual condition ranged from cohesion values of 0-25 kPa and friction angles of 4-12° for Pierre Shale and 8-28° for similar materials (Belly River and Lea Park formations).

The peak shear strength properties determined from the triaxial tests (effective cohesion of 139.3 kPa and an effective friction angle of 36.1°, with peak deviator stresses occurring at axial strains ranging from 2.5-4.3%) varied by 20-25% from the direct shear tests. Despite the two differing drainage conditions in this phase, the trendline fit of the effective stress results from all the samples in the modified Mohr-Coulomb or $q - p'$ (where $q = \frac{1}{2}(\sigma_1 - \sigma_3)$ and $p' = \frac{1}{2}(\sigma'_1 + \sigma'_3)$) space was not difficult nor complicated as illustrated in Figure 5-23. The equivalent Mohr-Coulomb shear strength parameters were then calculated from these modified values. This was the preferred method of determining the strength parameters from the triaxial tests due to the non-linear nature of the envelope at low normal stresses from plotting the Mohr circles and their close proximity to each other (Figure 5-24). The

Table 5-10: Shear strength parameters from literature (direct shear tests).

Material	Reference	Peak		Residual	
		c (kPa)	ϕ (°)	c' (kPa)	ϕ' (°)
weathered Pierre Shale (South Dakota)	Knight, 1963	-	-	24.9	11.9
Pierre Shale (U.S.A.)	Kenney, 1967	-	-	-	5.7
Pierre Shale (Missouri Basin)	Fleming et al., 1970	-	-	0.0	4.0 - 11.6
weathered Pierre Shale with distilled water (South Dakota)	Schaefer and Lohnes, 2001	-	-	18.2	5.6
weathered Pierre Shale with interstitial water (South Dakota)		-	-	23.9	5.9
weathered silty clay shale of the Belly River Formation (Alberta)	Tweedie, 1976	159.9	23.0	0.0	10.0
unweathered silty clay shale of the Belly River Formation (Alberta)		68.5	41.0	0.0	16 - 19
in-situ clay shale of the Lea Park Formation (Saskatchewan)	Krahn et al., 1979	-	-	0.0	13.0 - 28.0
remoulded clay shale of the Lea Park Formation (Saskatchewan)		-	-	0.0	8.0
intact bedrock clay of the Lea Park Formation (Saskatchewan)	Misfeldt et al., 1991	14.0	27.0	-	-

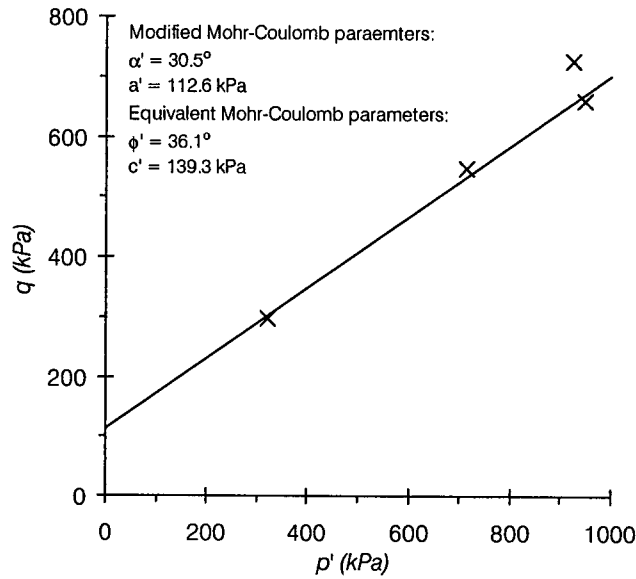


Figure 5-23: Triaxial test results in modified Mohr-Coulomb space.

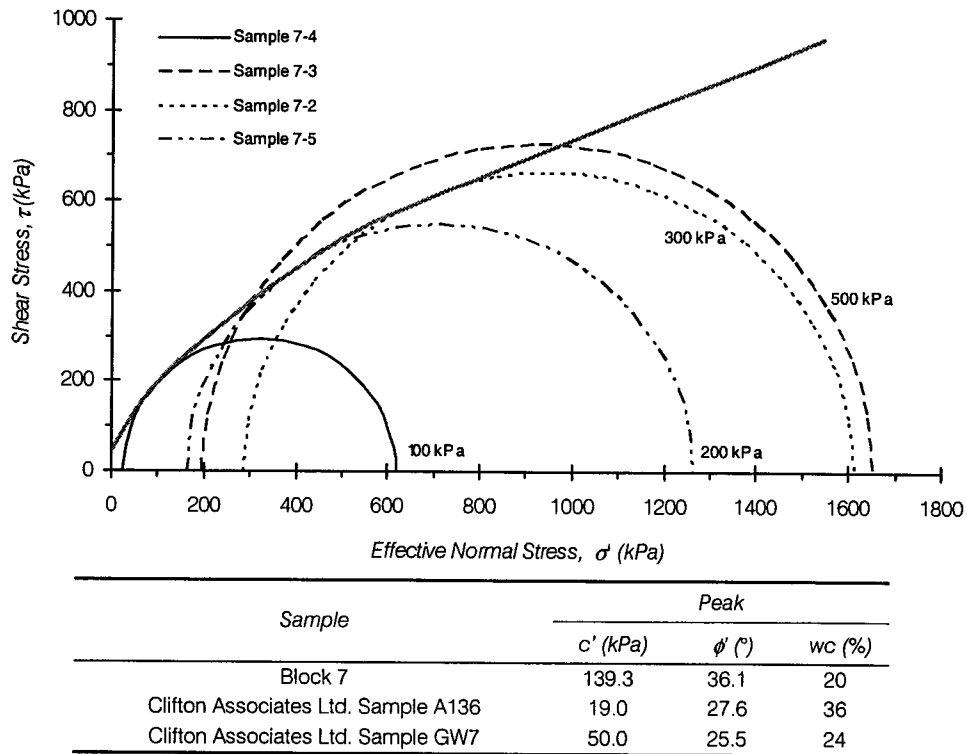


Figure 5-24: Mohr-Coulomb failure envelopes from triaxial tests.

peculiar enveloping of the Mohr circle for Sample 7-2 by Sample 7-3 shown in Figure 5-24 was attributed to the procedural error of imposing drained conditions under an undrained displacement rate; the faster rate did not allow for pore pressure equalization of the sample

and therefore resulting in lower pore pressure readings. Consequently, this data point was removed from the trendline fit in the modified Mohr-Coulomb plot. Relative to the results reported by the consultant (Figure 5-24), the largest variation occurred in determining the cohesion, while the friction angle varied much less (23-30%).

The residual strength obtained from each direct shear test sample was at least 27 and at most 50% of the peak value. As expected, the values of residual shear stress obtained from the peak travel were higher than those obtained from the residual travel by 14-58%. Therefore, the maximum reduction in strength from the peak to residual, according to the residual travel in the direct shear tests, ranged from 54 to 79% and averaged 68%. However, the triaxial tests (Samples 7-3 and 7-5) indicated a smaller reduction from peak to residual, which ranged from 38% to 44%. Furthermore, the remoulded sample tested under direct shear conditions illustrated a strength loss of 50%. Thus, the residual properties of this material would play a significant role in its strength and corresponding deformation behaviour. In addition, the lone test on the remoulded sample suggested that roughly half of the material strength could be attributed to its in-situ structure. Also, several drained tests appeared to indicate that residual strength had yet to be reached by the end of travel or testing period since volume change had not levelled off (Samples 6-6, 6-8, 6-9, and 7-2).

The uniaxial compressive strength of the material, as extrapolated from the Mohr-Coulomb envelope plotted in principal stress ($\sigma'_1 - \sigma'_3$) space, was approximated at 571 kPa (Figure 5-25). This appears to be within the lower spectrum of values obtained by Fleming et al in 1970 and Scully in 1973 (Botts, 1986), which ranged from 0-17 MPa. Correspondingly, the estimated undrained strength was 285-286 kPa, which compared well with those values determined from the lab vane and pocket penetrometer plotted below in Figure 5-26. With the exception of the till, all materials exceeded either one or both of the methods employed. The disturbed and/or weathered shale indicated a strength about 11% lower than the intact shale, while the high strength of the intermix could be indicative of the high shale content which may exist as substantial-sized intact blocks throughout the matrix rather than well integrated within the matrix.

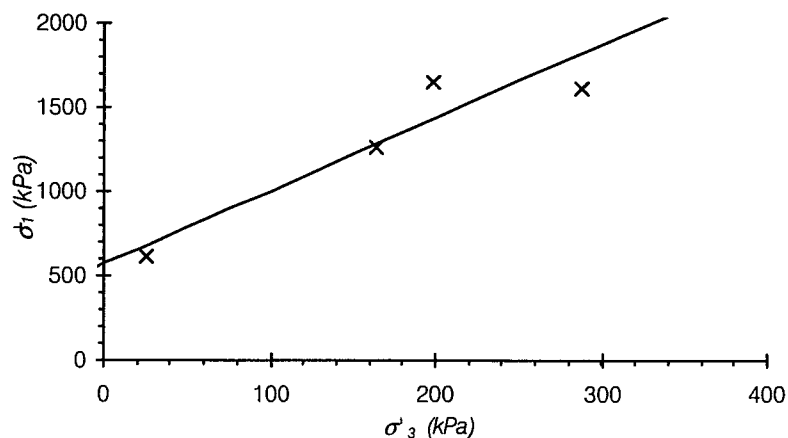
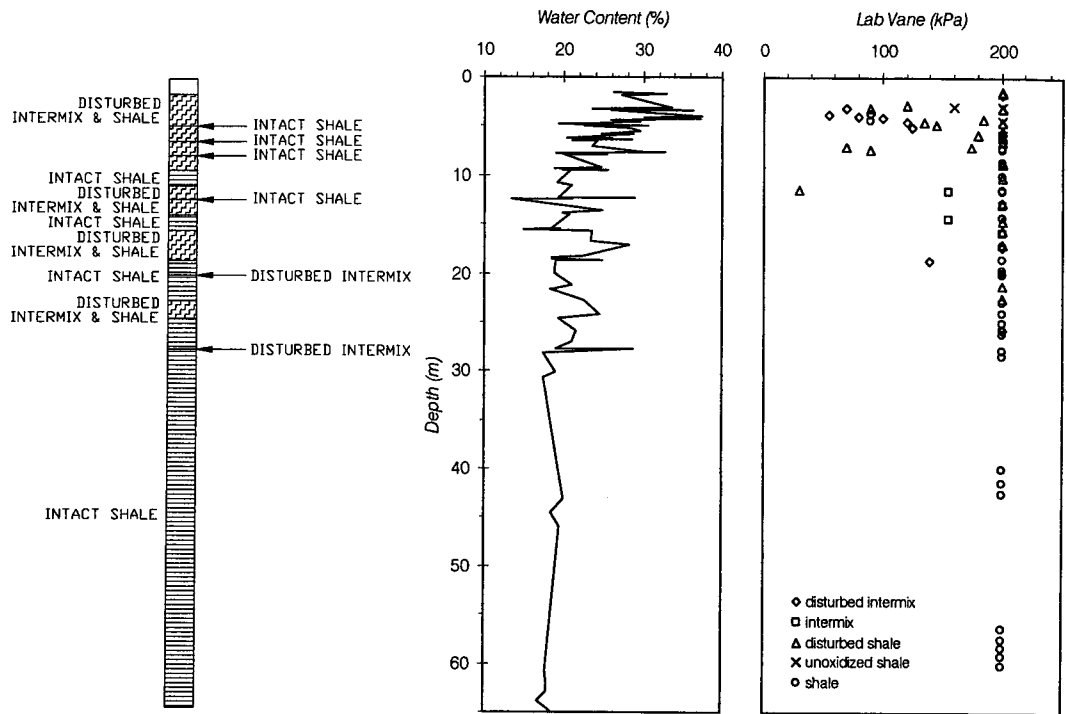
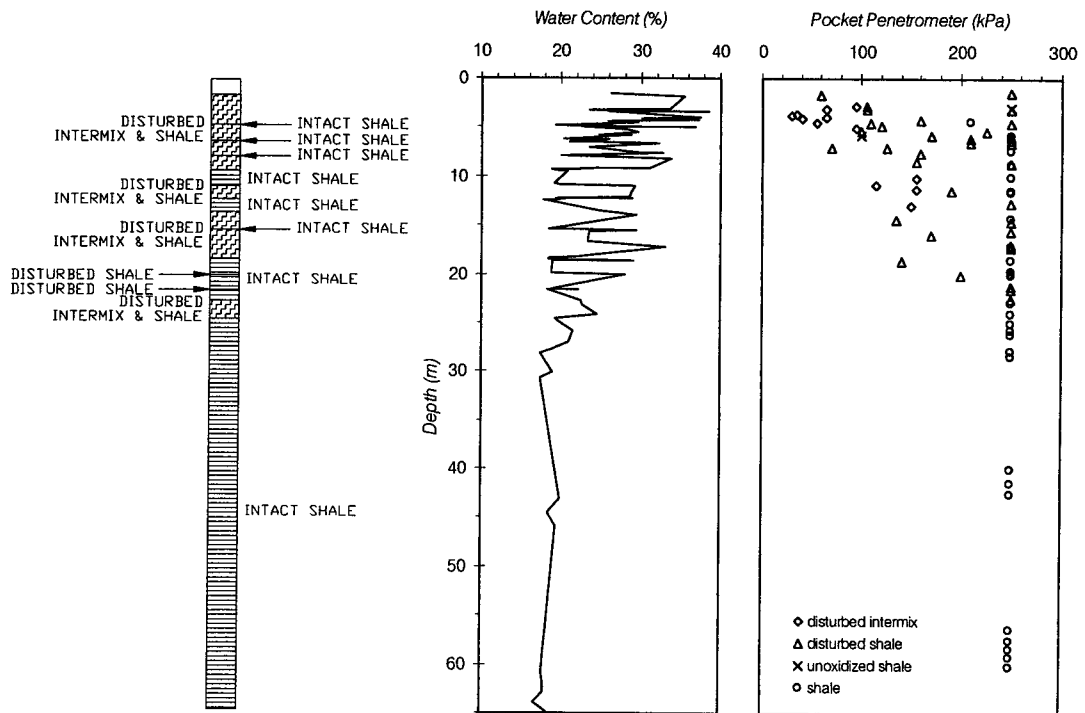


Figure 5-25: Triaxial test results in principal stress space.



(a)



(b)

Figure 5-26: Undrained shear strength from (a) lab vane and (b) pocket penetrometers (Clifton Associates Ltd. Report File R573 and R677). The values plotted at 200 kPa and 250 kPa represent values which reached the limit of the lab vane and pocket penetrometer respectively, and most likely exceeds these limits.

5.5 SUMMARY

The grain-size distribution of the material tested suggested a primary dominance in silt-sizes with a secondary proportion of clay sizes. However, further testing suggested that it was inorganic clay of high plasticity with a massive fabric displaying no fissility and consisting of a clay matrix in which the coarser fractions existed. This is consistent with the range of hydraulic conductivities determined from consolidation tests ranging from 3.3×10^{-10} m/s (vertical load of 6.25 kPa) to 6.5×10^{-12} m/s (vertical load of 800 kPa). These characteristics are consistent with a medium in which the clay fraction dominates the engineering behaviour. In addition, the possibility of cementation in the material tested appeared to be very likely. However, despite its persistence in water at its natural water content, it slaked completely after one cycle of air-drying; hence, the form of cementation appeared to be a weak one.

Variability was also exhibited by the test samples of the Millwood Member as evidenced by the range of stress-strain curves (i.e. brittle, ductile, and by-passed behaviour), which is indicative of the complexity of the soil/rock mass structure. Samples tested under direct shear and consolidated-drained and consolidated-undrained triaxial conditions indicated a brittle material with an elastic modulus ranging from 32 to 73.2 MPa. Peak strengths from the direct shear tests indicated a cohesion intercept of 184.7 kPa and a friction angle of 28.7° , while the triaxial tests indicated an effective cohesion of 139.3 kPa and a friction angle of 36.1° . According to the direct shear tests, the residual strength of the material had a cohesion of zero and an angle of friction of 16.7° . The reduction in strength from peak to residual appeared to be significant, ranging from 38% to 79%. Results from a remoulded sample tested under direct shear conditions, indicated a loss in strength of roughly 50% from peak to residual due to the destruction of its in-situ structure. Under the low confining pressures of both the direct and triaxial tests, the material exhibited typical overconsolidated behaviour, resulting in brittle stress-strain curves, well-defined failure planes, and a degree of dilatancy (Johnston and Novello, 1993).

6 STABILITY & DEFORMATION ANALYSES

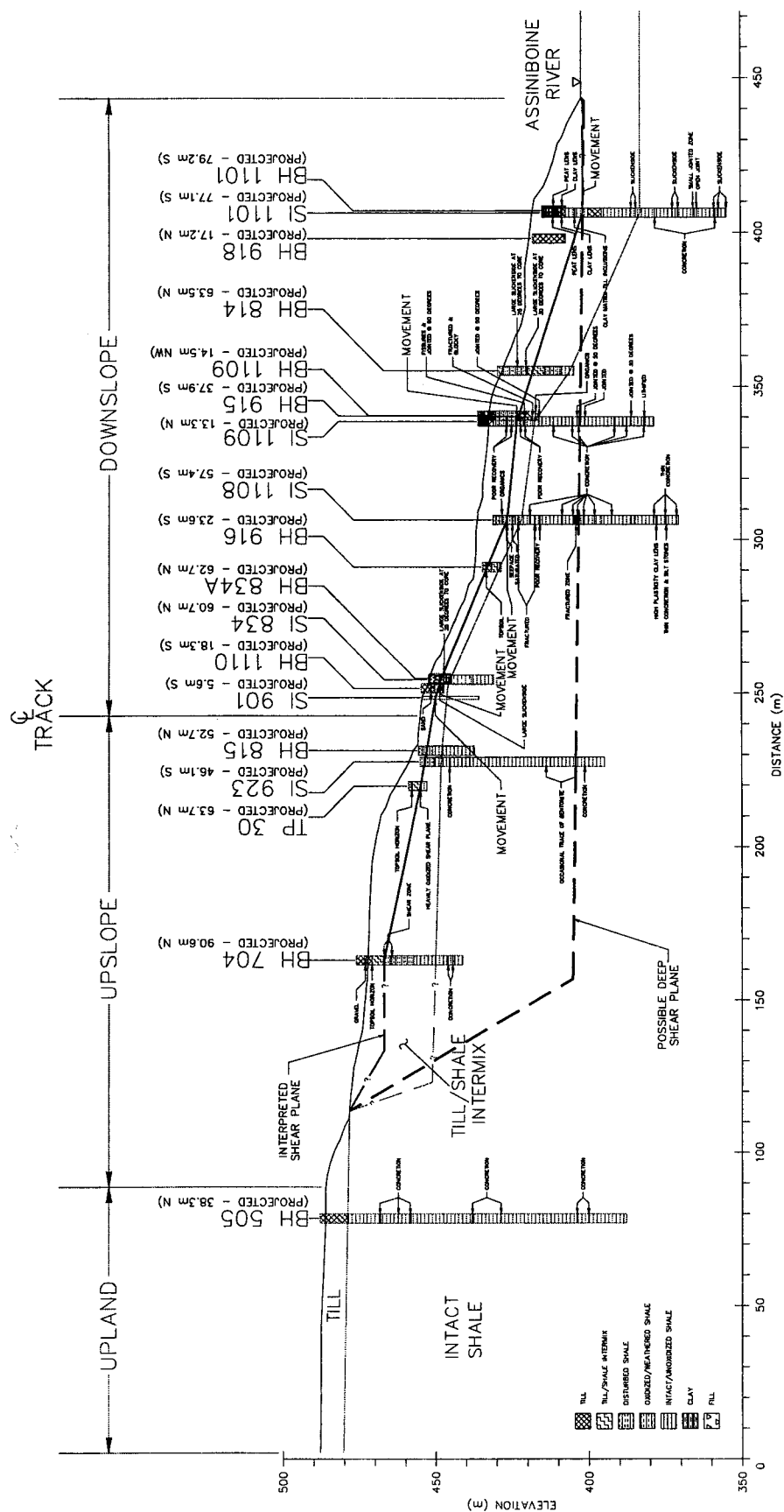
In order to develop mitigative measures to control landslide movements, a thorough understanding of the processes that drive the movements is required. Slope movements in weak rocks such as clay shales are particularly problematic as the failure and triggering mechanisms are complex (Terzaghi, 1936; Hardy, 1957; Peterson et al., 1960; Skempton, 1964; Scott and Brooker, 1966; Brooker and Peck, 1993). The purpose of the following analyses is to deduce the failure mechanism of the slope movements which have occurred along Mile 86.6 and Mile 86.75 via both limit equilibrium and deformation analyses. Limit equilibrium analysis (LEA) was particularly useful in examining the various hypotheses of slope movement mechanisms, while the deformation analysis provided the opportunity to compare the predicted pattern of slope movements with those recorded by the slope inclinometers.

6.1 *LIMIT EQUILIBRIUM ANALYSIS*

Conventional slope stability analysis has focused on the determination of the equilibrium between the imposed loading (i.e. driving forces) and material strength (i.e. resisting forces) via the computation of a factor of safety (FS). Such analyses have been carried out with the use of various limit equilibrium methods, which require information on the topography of the ground surface, failure mode, geometry of the failure surface, shear strength of the material, and pore pressure distribution (Morgenstern, 1992; Duncan, 1996).

Based on the results obtained from the field investigations, a shallow-seated, retrogressive failure mechanism was hypothesized for the slope movements at Miles 86.8 and 86.75. However, the field investigations also alluded to the possibility of a second failure zone as shown in Figure 6-1. The first was shallow-seated, following the movement zones recorded in the inclinometers which paralleled the slope topography within the upper 6 m for the majority of the slope and in the upper 15 m near the toe. The second was deep-seated and coincided horizontally with the elevation of recorded movement in SI 1101. In addition, the possible retrogressive nature of the shallow slope movements was also analyzed due to the plausible concurrence of the base of the movement with the geometry of the intact shale bedrock contact and localized steep faces in the surface topography (Figure 6-1), by which the movement mass could be separated into distinct blocks. Similarly, the deep-seated mechanism could also be separated into distinct blocks with the backslopes coinciding with those inclinometers that recorded movement. As a result, the LEA investigated the possibility of a shallow-seated movement versus a deep-seated one and a retrogressive (multiple block) failure versus a single mass failure.

The feasibility of the failure mechanisms was investigated by a combination of forward-analysis (calculations of factors of safety with differing material properties) and back-analysis (determination of a spectrum of operational strengths). The shear strength properties so determined was also compared with lab-determined values since according to Skempton (1985), a direct comparison can be made between the operational and residual shear strength parameters without any displacement rate corrections due to the slow nature of displacements typical to these slope movements and to conventional laboratory procedures. Therefore, back-analysis of reactivated landslides should yield values which closely match the residual values obtained from laboratory tests at the relevant effective pressure (the values obtained by both methods are unlikely to vary by more than 5%). The inclinometers in



Chapter 4 indicated movement rates ranging from 8 to 1095 mm/yr, which were within the range of typical rates of 20-182 500 mm/yr (Skempton, 1985).

During the course of these analyses, it was also possible to examine the retrogressive mechanism concurrently. The procedure employed in this investigation was one described by Sauer (1983); the lowest block is first analyzed as a single entity followed by analysis of it in combination with the adjacent upslope block until all the blocks have been coalesced into a single mass. Results from an ideal retrogressive failure are shown in Figure 6-2. The following presentation will be categorized according to the depth of failure (i.e. shallow versus deep) while the results from the retrogressive investigation will be incorporated into each of these scenarios.

6.1.1 SHALLOW-SEATED FAILURE

MODEL CONFIGURATION. The interpreted stratigraphic contacts, slip surface location, and piezometric conditions established in Chapter 4 were used in developing the geometry of the model shown in Figure 6-3. It is important to note that the till/shale intermix not only represented the highly disturbed state of colluvium resulting from previous landslide activities, but also included the weathered zone of the intact shale bedrock. The validity of this assumption was justified by the fact that the material in the weathered zone would be expected to have a shear strength lower than the peak due to its softened and jointed condition resulting from exposure and the easy ingress of groundwater and surface runoff; the highly disturbed nature of the colluvium most likely harboured a well-developed joint system by which air and groundwater movement could easily be accommodated. However, the degree to which the weathered zone has reduced in strength, and hence its proximity to the residual state, is unknown at this time. The pore pressure conditions assumed reflected the extremes of the groundwater conditions – at the ground surface (maximum) and at the failure plane (minimum).

From the onset, the geometry of the failure plane appeared to be somewhat shallow, following both the general slope of the ground and to a certain extent, the top of the interpreted intact shale bedrock surface (Figure 6-1). The contact between the intermix and the intact shale appeared as a series of steps following the length of the slope. In the downslope section, the interpolated failure plane appeared to follow this step-like nature

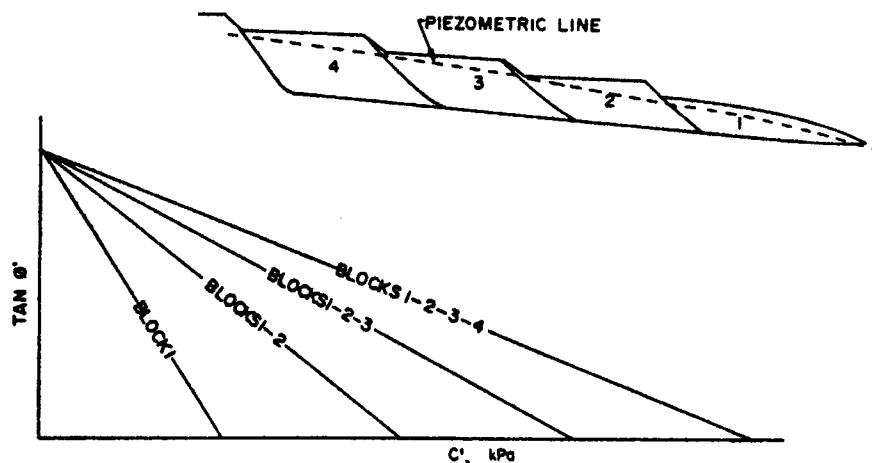


Figure 6-2: An idealized retrogressive failure (modified from Sauer, 1983).

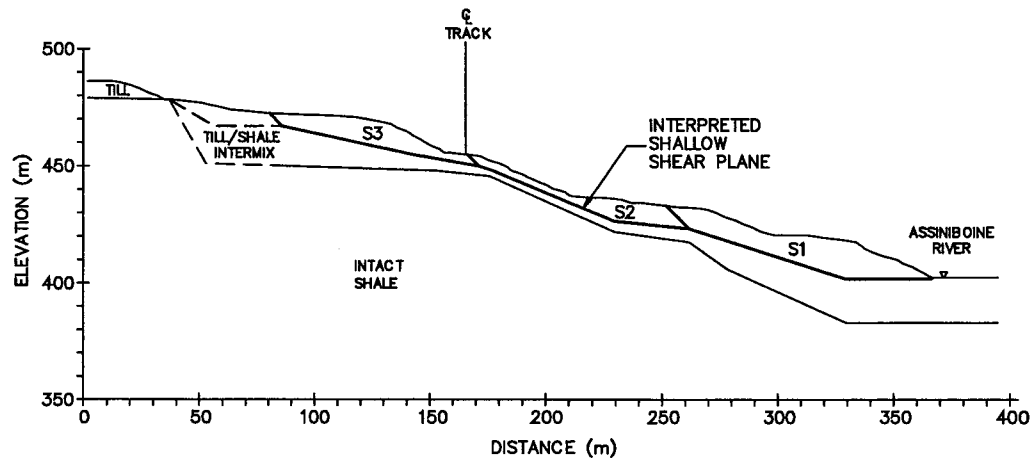


Figure 6-3: Limit equilibrium model of the shallow-seated failure.

quite closely, and continued in this fashion until the toe. Where it deviated from this pattern was in the upslope portion, where it appeared to follow the slope surface. Accordingly, the movement mass was separated into the three blocks shown in Figure 6-3. As noted in Chapter 4, the shear surface upslope of BH 704 was extrapolated horizontally from the uppermost shear zone observed in the borehole log and the corresponding backslope angle assumed the same slope as the crest of the valley wall, where a scarp was somewhat apparent. However, due to the uncertainty presented here and the lack of slope inclinometer installations in the vicinity, this portion of the upslope was not included in the following limit equilibrium analyses. In addition, projection of the shear plane upslope from that observed in SI 901 to the observed uppermost shear zone (i.e. block S3) was also an uncertain process due to the qualitative nature of the information used.

OPERATIONAL STRENGTH. Initially, the shallow-seated failure was analyzed with porewater conditions at ground surface and lab-determined residual values. This was not unreasonable since movements in this slope have been measured since 1986; therefore, either the latest movements have occurred along pre-sheared surfaces or the strength along the shear plane has been sufficiently degraded to such a value. However, under these circumstances, the calculated factor of safety was significantly less than unity (Table 6-1). The model was then analyzed with lab-determined peak values, and as expected, these factors of safety were significantly higher than unity (Table 6-1). Interestingly, the values obtained from the stability analysis of the residual strength values were fairly close to each other for all the different stages; the maximum difference was 4-6%. It appeared that no matter how the blocks were combined with the lower block, the behaviour of the lower block governed the overall behaviour of any subsequent combinations. These shear strength parameters and their corresponding calculated factors of safety are plotted in Figure 6-4. From this plot, it is quite clear that the lab-determined residual strength is too low, yet the lab-determined peak strength is much too high; thus, the mobilized strength must be somewhere in between with greater proximity to the lab-determined residual values.

As a result, the operational residual strength (i.e. $c'=0$ kPa, hence called the $c=0$ operational strength) of the slope was back-calculated. These values, $24.9-26.4^\circ$, were found to be much higher (almost 150%) than the lab-determined residual strength (Table 6-2), which was puzzling since movements have occurred in this slope since 1986. Interestingly, these values

Table 6-1: Summary of stability analysis using lab-determined shear strength parameters (direct shear).

Analysis Stage	Groundwater Conditions	Minimum Factor of Safety ($\phi = 16.7^\circ$, $c' = 0$ kPa)	Minimum Factor of Safety ($\phi = 28.7^\circ$, $c' = 184.7$)
Block S1	at surface	0.61	5.53
	at shear plane	1.27	6.76
Blocks S1-S2	at surface	0.63	6.59
	at shear plane	1.33	7.85
Blocks S1-S2-S3	at surface	0.64	6.85
	at shear plane	1.35	8.15

were much closer (8-13%) to the peak friction angle (28.7°) determined from the direct shear tests, but differed by 27-31% from the triaxial peak friction angle (36.1°). In this case, it appeared that mobilization of the shallow-seated movement also required a strength somewhere between the peak and the residual, but with a greater proximity to the peak.

In order to establish a reasonable operational strength and since back-analysis can yield an infinite number of combinations between the two shear strength parameters, the cohesion value required to satisfy a condition of limiting equilibrium with the lab-determined residual friction angle was back-calculated. From Figure 6-4, the shear strength parameters of the operational strength (i.e. c-17 operational strength) thus ascertained was $c'=17$ kPa corresponding to $\phi'=16.6^\circ$.

RETROGRESSIVE NATURE. The retrogressive nature of the staged analysis is shown in Figure 6-5, and it can be seen that it did not correspond with the ideal retrogressive failure mechanism. In fact, the stages were in reverse order of the idealized failure shown in Figure 6-2. The last two stages (combination of the Blocks S1-S2 and Blocks S1-S2-S3) were very close to each other with a separation of 1% in friction angle and 4% in cohesion. In addition, the analysis implied possible deviant behaviour of the lower block from its combination with the other blocks due to its relatively large separation from the subsequent stages in Figure 6-5. Again this analysis also implied that once the lower block was combined with its adjacent upslope block, its overall behaviour would be substantially altered.

SENSITIVITY ANALYSIS. Sensitivity analyses were carried out to ascertain the sensitivity of factors such as the location of the specified slip axis, the various limit equilibrium methods (only methods which satisfy both force and moment equilibrium were employed), the location of the slip surface, and the location of the groundwater table.

The limit equilibrium analyses were carried out with the use of the program SLOPE/W and the methods utilized were the Spencer, Morgenstern-Price (at half-sine function), and General Limit Equilibrium (at constant and half-sine functions) methods. The difference in the factors of safety calculated from these methods ranged from 1-2%. The analyses were carried out under the condition of a specified slip surface with specified slip axis locations and the maximum difference in the factors of safety calculated from the different axis locations was 2%. Similarly, sensitivity to the location of the failure plane (Figure 6-6) was minimal with a difference in the calculated factor of safety ranging from 0.3-7.4% (Figure 6-7).

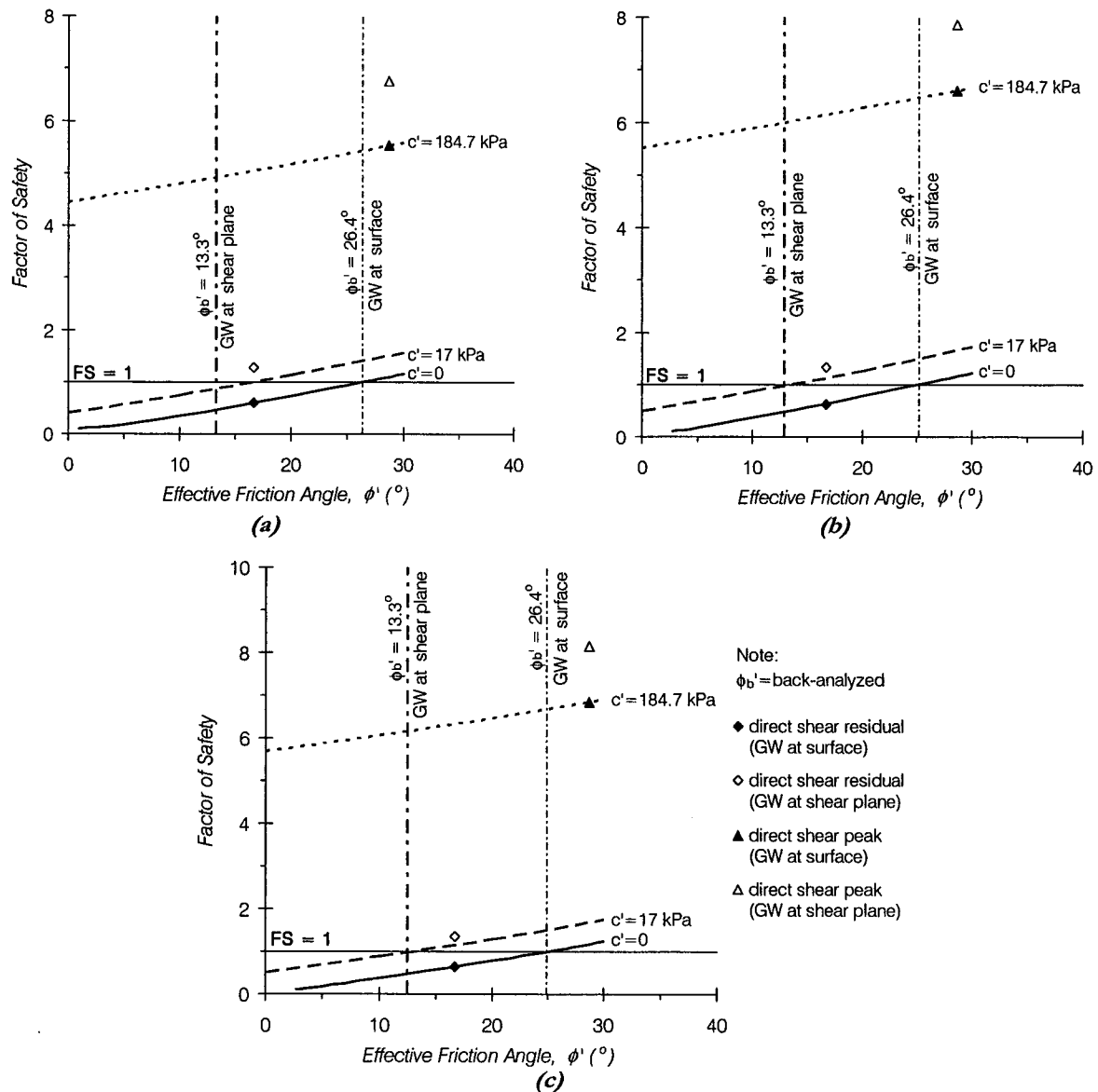


Figure 6-4: Shear strength parameters for the shallow-seated, retrogressive failure mechanism (groundwater at surface).

The greatest sensitivity in the LEA resulted from the location of the groundwater table (Figure 6-6) as illustrated in Figures 6-7 and 6-8. In the shallow mechanism, the difference in the calculated factors of safety between its location at the ground surface and at the piezometric level ranged from 17-23%, and that between the location at the ground surface and at the failure surface ranged from 52-53%. If the piezometric level represented the minimum groundwater conditions in the study area, then the sensitivity analysis implied that this, like the original assumption of pore pressure conditions at the ground surface, was also conservative. However, neither extreme groundwater conditions satisfied the condition of limiting equilibrium or FS=1 (Figure 6-8); groundwater at the surface was conservative in yielding factors of safety less than one, but quite naturally, the case where the groundwater is located at the shear plane resulted in factors of safety which exceeded unity. Since use of the residual shear strength under both groundwater conditions produced factors of safety which

Table 6-2: Summary of shallow-seated back-analysis (direct shear peak at $\phi' = 28.7^\circ$ and $c' = 184.7$ kPa; direct shear residual at $\phi' = 16.7^\circ$ and $c' = 0$ kPa).

Analysis Stage	Groundwater Conditions	Effective Friction Angle, ϕ' ($^\circ$)	Effective Cohesion, c' (kPa)
Block S1	at surface	26.4	0
		0	41.9
	at shear plane	13.3	0
		0	41.5
Blocks S1-S2	at surface	25.2	0
		0	33.9
	at shear plane	12.8	0
		0	33.9
Blocks S1-S2-S3	at surface	24.9	0
		0	32.7
	at shear plane	12.5	0
		0	32.7

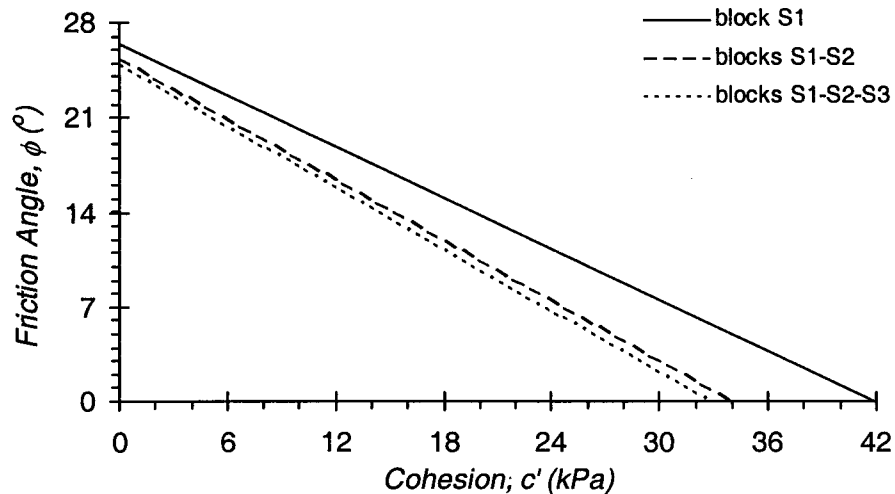


Figure 6-5: Analysis for a retrogressive mechanism in the shallow-seated failure.

fell on either side of the limiting equilibrium condition, it appeared use of the residual values would be realistic only if the groundwater conditions were refined. In such a case, the groundwater would have to be reduced to depths ranging from 8.5 to 4.5 m (block S1 required a drop of 8.5 m, blocks S1-S2 required a 5 m drop, and blocks S1-S2-S3 required a drop of 4.5 m) in order to achieve shear strength parameters equal to the lab-determined residual values ($\phi' = 16.7^\circ$ and $c' = 0$ kPa).

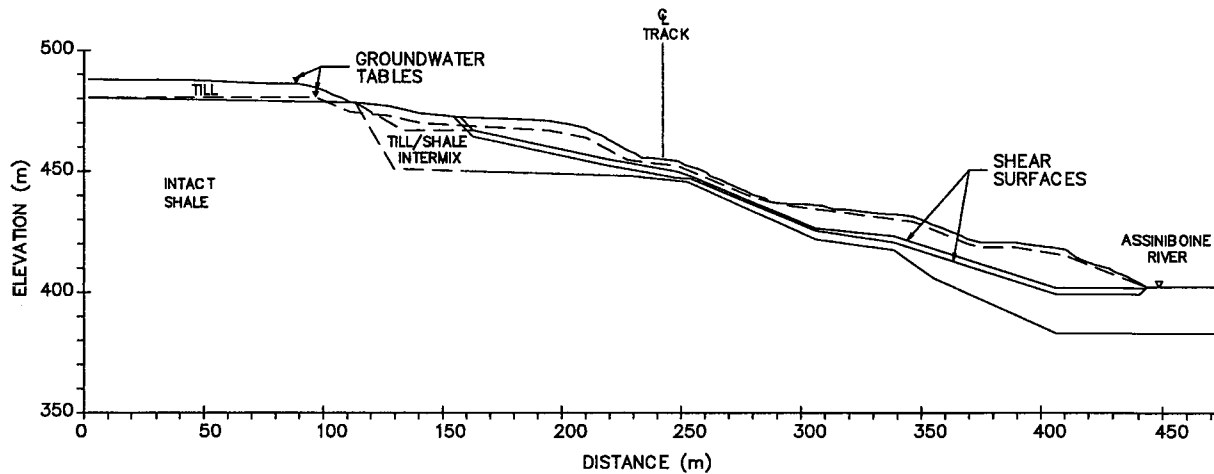


Figure 6-6: Location of the shear surfaces and groundwater conditions used in the sensitivity analysis.

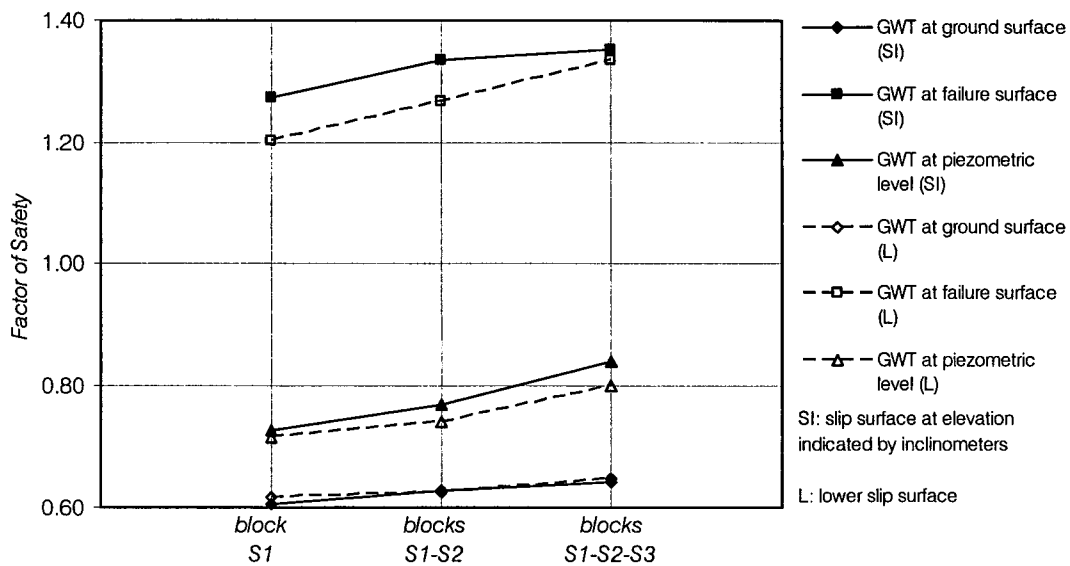


Figure 6-7: Sensitivity analysis of the location of the shear surfaces and groundwater conditions.

6.1.2 DEEP-SEATED FAILURE

MODEL CONFIGURATION. The stratigraphic boundaries used in the deep-seated failure were unchanged from those of the shallow-seated failure. However, the shear plane was simplified to a single nearly horizontal plane (Figure 6-9), (at a slope of 1.4% or 0.8°) with a maximum elevation of 405.4 m near the backslope and 401.3 m at the toe. In this case, the backslope angle was approximated at an angle corresponding to that observed in the failure of the triaxial tests carried out in Chapter 5. Since SI 1101 was the only slope inclinometer that recorded movement at this shear plane elevation, it was assumed that the movements recorded in the other inclinometers were coincident with movement of the backslopes of deep-seated blocks. In this manner, the slope was divided into the four blocks shown in

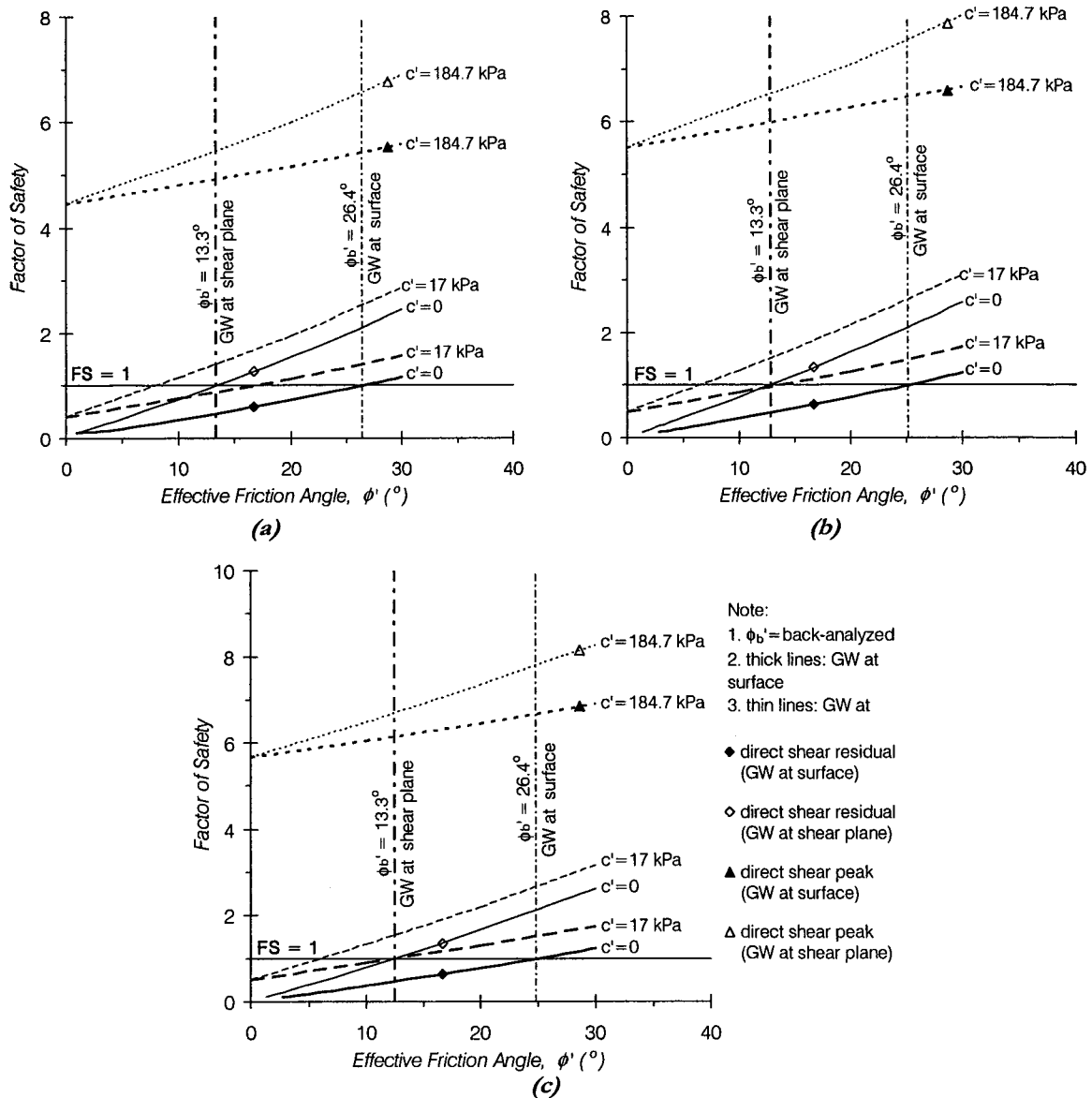


Figure 6-8: Sensitivity analysis of the groundwater conditions in the shallow-seated failure.

Figure 6-9 for the retrogressive analysis. The same groundwater conditions were also maintained in the analysis of the deep-seated mechanism.

OPERATIONAL STRENGTH. Despite the possibility of a retrogressive mechanism, only the lower block (Block D1) was analyzed with material properties based on the lab-determined residual shear strength parameters since it was the only block explicitly defined by movements recorded in the inclinometers. The resulting factor of safety for porewater conditions at ground surface was 0.8 (Table 6-3), which was closer than the shallow-seated mechanism to, but still considerably lower than unity. Analysis of the remaining upslope blocks required material properties defined by a combination of residual and peak shear strengths. Residual strength was justified in the upper portion of the backslopes since inclinometers had recorded movements and because the disturbed colluvium and weathered

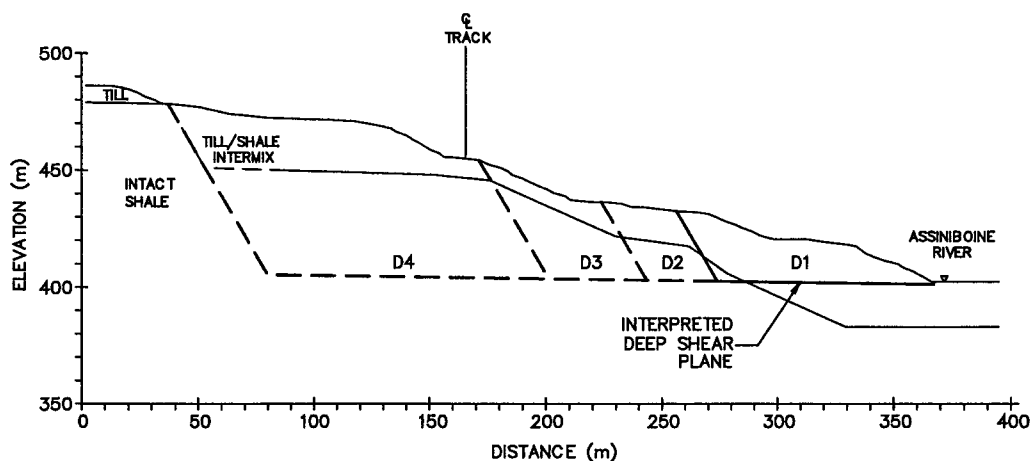


Figure 6-9: Geometry of the possible retrogressive nature of the deep-seated slope movement.

Table 6-3: Summary of stability analysis of deep-seated failure (direct shear peak at $\phi' = 28.7^\circ$ and $c' = 184.7$ kPa; direct shear residual at $\phi' = 16.7^\circ$ and $c' = 0$ kPa).

Analysis Stage	Groundwater Conditions	Minimum Factor of Safety
Block D1	at surface no groundwater	0.8 1.7
Blocks D1-D2	at surface no groundwater	3.1 4.7
Blocks D1-D2-D3	at surface no groundwater	3.2 4.9
Blocks D1-D2-D3-D4	at surface no groundwater	2.9 4.7

bedrock were intersected. The remaining portions of the blocks which lay within the intact shale zone were analyzed with peak shear strength parameters ($\phi' = 28.7^\circ$ and $c' = 184.7$ kPa). Results from this stability analysis are tabulated in Table 6-3. The small differences (4.1-9.4%) in the factors of safety of the combined mass movements in Table 6-3 also implied that once the lower block was combined with adjacent blocks, the collective mass moved independently of any influence from the single lower block. Again, this alluded to the possibility that the lower block may exhibit behaviour which deviates from the mechanism of deep-seated slope movement of the overall slope.

Since the residual shear strength parameters determined from the direct shear tests in Chapter 5 resulted in a stability condition which exceeded limiting equilibrium, the c-17 operational shear strength determined in the shallow-seated mechanism was used to analyze the deep-seated failure of the lower block (Table 6-4). Unexpectedly, the resulting factors of safety resulted in a value 11% greater than unity (Table 6-4). This was unusual since the operational strength determined in the shallow-seated failure should have resulted in a

condition of limiting equilibrium when applied to the deep-seated movement if the mode of failure for both mechanisms was the same.

The residual operational strength ($c=0$) of the lower block was also calculated and compared to the $c=17$ values in Table 6-4. Like the shallow-seated failure, the $c=0$ operational strength for the deep-seated failure was lower (26.8-41.8%) than the peak strength determined from both the direct shear and triaxial tests, but higher than the residual lab values (Figure 6-10). Unlike the shallow-seated failure, it was much closer to the residual lab values; the difference in this case was 20.5% compared to a difference of 32.9-36.7% in the shallow-seated scenario.

RETROGRESSIVE NATURE. Results from the retrogressive analysis are tabulated in Table 6-5 and illustrated in Figure 6-11. Unlike the shallow-seated failure, the feasibility of a retrogressive mechanism was more apparent and realistic in the deep-seated mechanism as shown in Figure 6-11; the plotted results of the back-analysis revealed a relationship not far from the expected ideal retrogressive mechanism of Figure 6-2. An exception to this was the behaviour of the lower block as a single entity as it had a much larger friction angle, but not a

Table 6-4: Summary of the operational shear strengths determined for the deep-seated failure of the lower block (groundwater conditions at surface).

Operational Shear Strength	Effective Friction Angle, ϕ' ($^\circ$)	Effective Cohesion, c' (kPa)	Minimum Factor of Safety
$c=0$	21.0	0	1.00
$c=17$	16.6	17	1.11

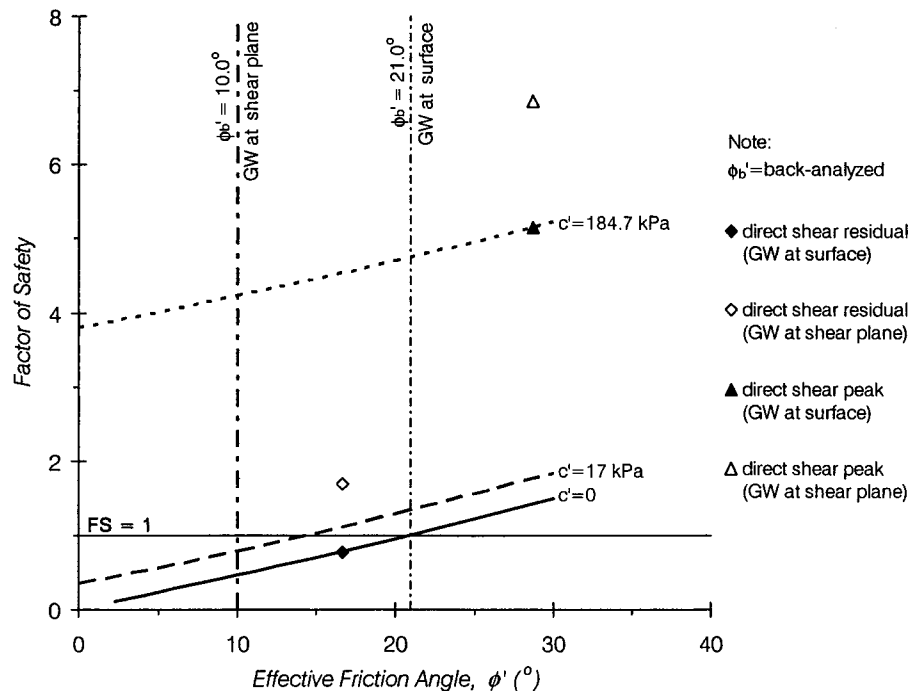


Figure 6-10: Shear strength parameters for the deep-seated failure of the lower block (groundwater at surface).

Table 6-5: Summary of the deep-seated back-analysis (direct shear peak at $\phi' = 28.7^\circ$ and $c' = 184.7$ kPa; direct shear residual at $\phi' = 16.7^\circ$ and $c' = 0$ kPa).

Analysis Stage	Groundwater Conditions	Effective Friction Angle, ϕ' ($^\circ$)	Effective Cohesion, c' (kPa)
Block D1	at	21.0	0
	surface	0	48.9
	no	10.0	0
	groundwater	0	48.9
Blocks D1-D2	at	17.6	0
	surface	0	50.5
	no	8.5	0
	groundwater	0	50.5
Blocks D1-D2-D3	at	19.3	0
	surface	0	66.1
	no	9.3	0
	groundwater	0	66.1
Blocks D1-D2-D3-D4	at	17.8	0
	surface	0	106.0
	no	8.7	0
	groundwater	0	106.0

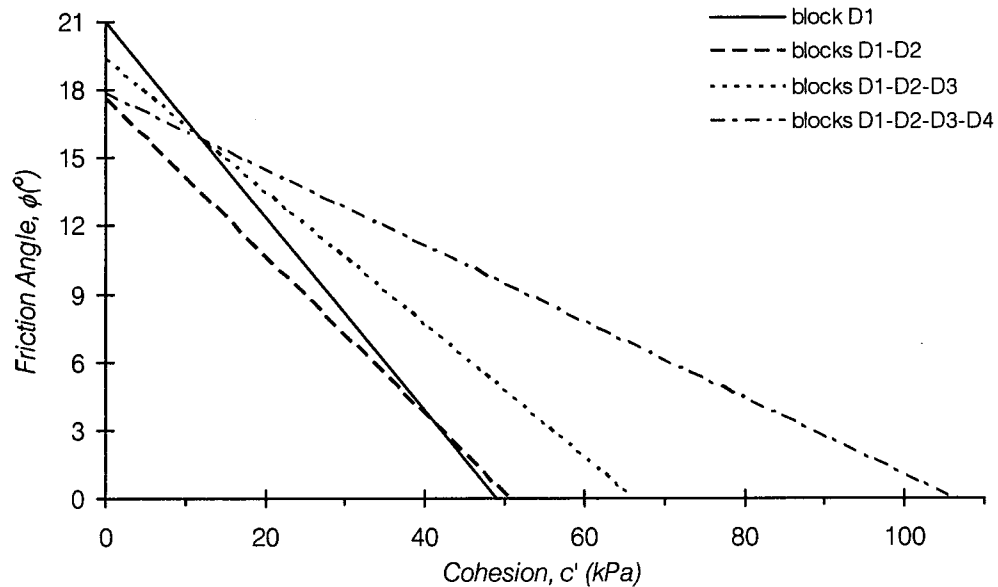


Figure 6-11: Analysis for a retrogressive failure in the deep-seated mechanism.

markedly smaller cohesion than the subsequent stage (Figure 6-11). Mobilization of the combined blocks resulted in a strength near the lab-determined residual (5.1 to 13.5%), while that of the lower block lay farthest away from the residual (20.5%). Again the anomalous behaviour of the lower block as a single entity was evident in the deep-seated failure. Similar to the case of the shallow-seated failure, once the lower block was combined with the adjacent upslope block, its unique behaviour disappeared, becoming more typical of a retrogressive mechanism.

SENSITIVITY ANALYSIS. Results from the sensitivity analysis of the deep-seated mechanism echoed those of the shallow-seated mechanism, and alluded to the necessary refinement of the groundwater conditions in order to produce more plausible results under lab-determined residual shear strength parameters (Figure 6-12). As expected, analysis of the lower block again indicated that location of the groundwater condition at both the surface (FS=0.8) and piezometric level (FS=0.9) was conservative, yet more closely represented the field condition than the condition with no groundwater (FS=1.7) permeating the movement mass. For a condition of limiting equilibrium in the lower block, the groundwater must be lowered by 4 m in order to achieve mobilized shear strength parameters ($\phi'=17^\circ$ and $c'=0$ kPa) close to the lab-determined residual values ($\phi'=16.7^\circ$ and $c'=0$ kPa).

6.1.3 PROPOSED FAILURE MECHANISMS

The results from the LEA have implicated a complex mechanism, which may not be confined to a singular failure mechanism, but strongly allude to the possibility of a dual mechanism.

Both the shallow- and deep-seated mechanisms revealed that the stability of the slope under lab-determined residual shear strength parameters was severely undermined, and yet

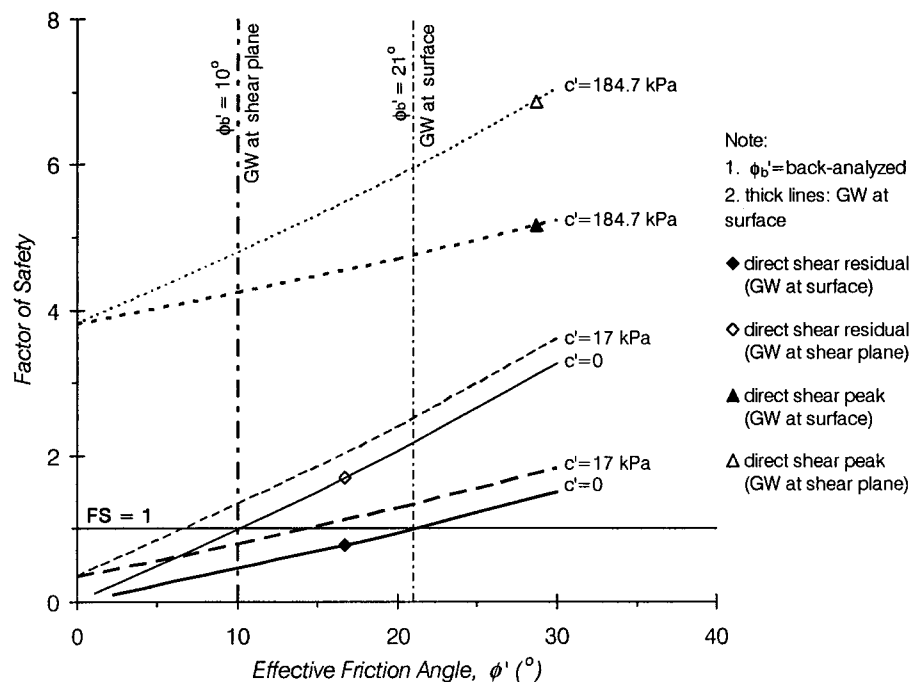


Figure 6-12: Sensitivity analysis of the groundwater conditions in the deep-seated failure.

excessively conservative under lab-determined peak values. Both also illustrated a closer proximity to the residual lab values; the factors of safety calculated for the shallow-seated failure was about 36-39% below a condition of limiting equilibrium for the lab residual parameters, but 553-685% above it for peak values. However, when the operational residual strength (c-0) was determined, the shallow-seated mechanism indicated a friction angle much closer (8% from peak compared to 36.7% from residual) to the peak lab value while the friction angle from the deep-seated mechanism was closer (20.5% from residual compared to 26.8% from peak) to the residual lab value. In addition, when the c-17 operational strength determined in the shallow-seated mechanism was applied to the deep-seated mechanism, the resulting factor of safety was not close to unity as it would be expected of identical failure modes between the shallow and deep movements. Also, refinement of the groundwater conditions seems an unrealistic alternative to achieving results near the lab-determined residual values since the field investigation clearly indicated that groundwater conditions were quite near the surface (owing to the frequent occurrence of ponded areas and the shallow nature of the surface drainage courses). The LEA also implied that a retrogressive mechanism was not at work in the shallow-seated failure, but is a strong possibility in the deep-seated failure. Finally, analyses of both scenarios indicated that the lower block as an individual behaved in a manner substantially different than when it was coalesced with adjacent block(s).

Consequently, both the geometry of the shear plane and slope inclinometer data were revisited. Thomson and Hayley (1975) have indicated that the deformational pattern distinctive of a retrogressive mechanism was one in which the shortest displacement vectors were found closest to the scarp while the maximum vectors were found at the toe. However, the pattern of movement from slope inclinometer data indicated a reverse trend from the typical retrogressive deformational pattern with the maximum displacements and displacement rates occurring closest to the scarp (SI 834, SI 1002, and SI 1108 with displacements ranging from 111.4-173.3 mm and rates ranging from 17.8-645.6 mm/yr). With the exception of SI 834 and 1002, the least amount of movement was recorded by the slope inclinometers located above the latest scarp. As the toe of the slide was approached, the displacements and rates decreased from those closest to the scarp (SI 1109 and 1101 with displacements ranging from 50.6-56.2 mm and rates ranging from 202.9-476.7 mm/yr). In addition, the vectors of SI 834, 1002, and 1108 pointed in the same direction towards the northeast, while SI 1109 and 1101 pointed toward the southeast (Figure 3-19). Hence, it appeared that the lower block (defined by SI 1109 and 1101) was indeed moving in a different manner and direction from the upslope mass.

These facts substantiate the following revision to the original hypothesis of the mechanism by which the slope at Miles 86.8 and 86.75 has moved. A dual mechanism is proposed (Figure 6-13); the lower block (defined by SI 1109 and 1101) is deep-seated and moves along a discrete plane independent of the upslope mass which consists of shallow-seated mass wastage as an effect of weathering and in response to removal of its toe support by the encroaching Assiniboine River (i.e. the two failures occur along different planes of weakness). In the shallow-seated failure, the slip plane occurred parallel to the topography of the valley wall and involved a mixture of till and shale. As a result, slippage would most likely involve quasi cross-bedding movement within each bed and between the two materials and the strength of the stronger till would also lend itself to a greater overall mobilized strength. In addition, if intact blocks of the unweathered shale bedrock were encountered in the mass of the colluvium, movements parallel to the bedding planes would be synonymous with mobilizing peak strength. Shallow-seated failure in the upper portion of the slope is further justified by the lower factors of safety (about 22%) calculated under residual lab values relative to the deep-seated failure. However, any effects of retrogressive movements

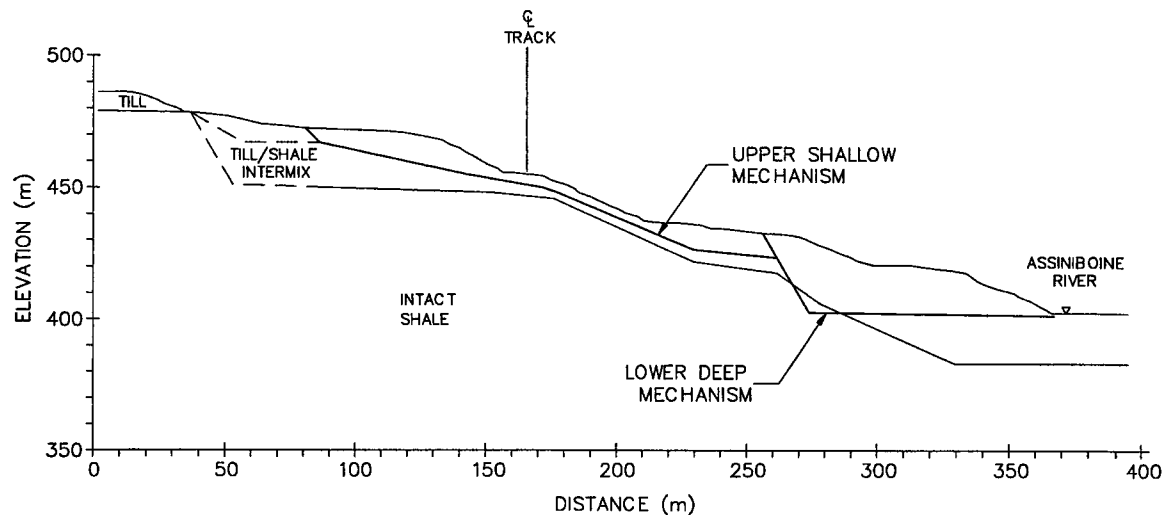


Figure 6-13: Proposed failure mechanism.

seem to elude the shallow-seated failure, but impart a strong presence in the deep-seated failure. This implies that if the lower block moved to an extent that resulted in the propagation of its plane of weakness into the adjacent mass, retrogressive failure is a very likely occurrence. And as the LEA illustrated, once this transpires, the independent behaviour of the lower block disappears and becomes amalgamated with any combination of the upslope blocks. In this case, the operational strength required for mobilization of the blocks is considerably lower than the peak strength and closely concurs with the lab-determined residual values. The previous analysis implies that stability of the lower block would have a significant influence on the overall performance of the slope.

6.1.4 FEASIBILITY OF THE PROPOSED FAILURE MECHANISMS

In order to justify the proposed dual failure mechanism, the means by which they contribute to the corresponding slope movements must be examined. Back-analysis of the shallow-seated failure of the portion of the slope above the lower deep-seated block indicated mobilization of a strength near the peak friction angle at a value of zero cohesion. However, back-analysis of the lower deep-seated block indicated that mobilization would occur at a value somewhere between the peak and the residual strengths with a slight preference towards the residual friction angle. The following discussion will focus on the various methods by which the two mechanisms impose slope instability.

SHALLOW-SEATED MECHANISM. According to Hvorslev (Wong, 1998), the shear strength parameters can be separated into two components with one relying on stress (i.e. friction) and the other on void ratio (i.e. cohesion). Schmertmann and Osterberg (1960) have shown that measured cohesion and friction in many cohesive soils act independently of each other due to the 'fundamental difference between the mechanical behaviour of cohesion & friction' (p. 672) exhibited by the clay materials they tested. They found that the cohesion component reached a maximum value generally at an axial compressive strain of less than 1% and then 'measurably decreases at a decreasing rate' (p. 672) thereafter resulting in a 'peaking effect' while the friction component reached its maximum at much larger strains. They speculated that this peaking effect may be more pronounced as the coarse fraction increases and also reasoned

that such a fundamental difference in the behaviour of the two shear strength parameters should be expected since,

'... cohesion is generally thought to be based on electrical attractive forces between clay particles and large strains should not be required to activate these forces. On the other hand, friction is thought to depend on the interference between particles and it is easier to imagine that considerable strain is required to achieve maximum interference and therefore maximum friction.' (p. 672)

In addition, Hvorslev (Wood, 1990) has demonstrated that the cohesion parameter of the Mohr-Coulomb criterion depends linearly on the equivalent consolidation pressure and thus cohesion decreases exponentially with increasing water content if a linear relationship is assumed between water content and the logarithm of consolidation pressure (Figure 6-14(a)).

The degradation of cohesion has been attributed to unloading (i.e. swelling) and weathering (i.e. equalization of negative pore pressures due to desiccation, softening due to hydration, and similar effects suffered from freeze-thaw cycles), both of which result in an increased water content and the common presence of joint discontinuities. Scarpelli and Calabresi (1984) have shown that the internal friction angle is preserved while the cohesion component is reduced during the swelling process when they compared samples of swelled-reconsolidated clay to remoulded ones. Petley (1984) noted that some loss of strength results from the softening along discontinuities which may open due to small movements following removal of any lateral support. Softening leads to an increased water content (void ratio) and a disturbed (and even remoulded) fabric subsequent to local, non-uniform swelling along open fissures and the breakage of diagenetic bonds (Chandler, 1984b). This destruction of diagenetic bonds was alluded to in the water deterioration test of Chapter 5 where the shale instantly disintegrated after a period of air-drying versus its in-situ counterpart which showed no reaction to water. In addition, the water content profiles of the borehole logs in Chapter 4 showed an increasing trend as the surface was approached, indicating that the shallow surficial zone is most likely where the softening processes would have the greatest impact. Chandler (1984b) has also noted that if softening is taken to the limit, the resulting soil fabric when subsequently sheared will render the existence of any past cohesion insignificant as illustrated in Figure 6-14(b). Figures 6-4 and 6-10 also illustrate this with the factor of safety decreasing as the cohesion is reduced at the same friction angle.

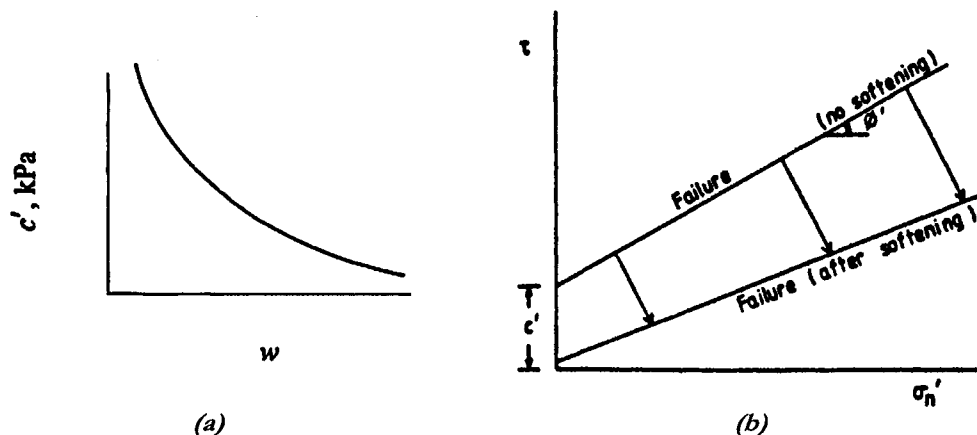


Figure 6-14: Reduction in cohesion: (a) relationship between effective cohesion and water content (modified from Wood, 1990) and (b) reduction of the cohesion component (modified from Chandler, 1984b).

The processes of weathering have been attributed to two mechanisms: disintegration (first phase) leading to the gradual destruction of diagenetic bonds (results in the tendency of the material to expand laterally) and the occurrence of chemical changes and decomposition of the minerals (second phase). The former occurs relatively rapidly and is most prevalent just beneath the surface due to the frequency with which it is subjected to freezing, temperature changes, and repeated wet-dry cycles in addition to the chemical processes of oxidation and decomposition of the mineral constituents. This zone overlies a zone of lesser disintegration attributed to the cyclic variation of effective stresses from seasonal changes in groundwater conditions and freezing of the overlying soil. Where the effects of the near-surface conditions is absent is in the underlying lowest zone, and it is in this zone that the shear plane most commonly occurs since it is where the shear stresses due to gravitational loading and internal lateral stresses exceeds the cohesion component of the shear strength. The former increases proportionally with depth, however, the latter only slightly increases with depth. Following weathering, the shear strength is reduced due to an increase in water content and fissuring. (Bjerrum, 1967)

With a back-analyzed friction angle so close to the peak value, it was quite possible that the shallow-seated failure of the upper slope occurred as a result of the weathering phenomenon in which the cohesion component of shear strength was sufficiently degraded due to exposure consistent with the increased water content of the failed material. From the field investigation of Chapter 4, the water content profiles of the borehole logs indicated a general increasing trend from the ground surface (due to surficial drying) followed by a decreasing trend as the intact shale bedrock was approached. This implied the likelihood that the cohesion in the weathered zone was indeed reduced, however the amount to which it was reduced is unknown at this time.

DEEP-SEATED MECHANISM. The back-calculated friction angle for the lower block implies a mobilized strength between the peak and residual values, which was unexpected of movement along a pre-sheared surface or the assumption that the strength of the material had somehow sufficiently been degraded to a residual value. Chandler (1984a) has suggested that there are three basic mechanisms by which the discrepancy between the laboratory and field strengths can be explained: softening, time-dependent limit states, and progressive failure. Progressive failure may occur with respect to the bulk strength or due to softening and/or time-dependent limit states, with the mobilized strength lying between peak and residual (Chandler, 1984a; 1984b). The progressive failure mechanism entails the progressive reduction of the material from a peak strength to a residual value as it develops a continuous sliding surface along which failure eventually occurs (Bjerrum, 1967). The three conditions which must be satisfied prior to the development of progressive failure are a source which can impose stress concentrations in front of the advancing sliding surface, a material with sufficient amounts of recoverable strain energy to produce the necessary expansion of the material in the direction of sliding, and a brittle nature where the residual value is significantly less than the peak (Bjerrum, 1967). The first condition is easily supplied by the presence of any joint discontinuities where stresses can be concentrated and cause localized failure which then propagates along what will eventually become the slip surface as the peak strength of the material is exceeded at every step (Petley, 1984). The second condition depends on the overconsolidation ratio of the material and the degree to which it has been unloaded. The third condition is easily accommodated by any overconsolidated clay shale. The greatest hurdle with the concept of progressive failure is the number of different mobilized strengths which can exist along the slip surface at any one time owing to the fact that at no two points along the slip surface will the movements be equal. Botts (1986) has claimed that first-time slides in clay shales which occur at strengths significantly greater than residual (but rather mobilize a softened strength) is not an uncommon occurrence. Hence, it

is quite possible that movement of the lower block represents a first-time slide where either the back-analyzed strength represented an average of the bulk strength along the slip surface or a softened strength significantly greater than residual.

Mesri and Shahien (2003) have indicated that softening leads to a lowering of the peak strength envelope towards a fully softened strength (Figure 6-14 (b)), which represents a more random arrangement of particles with predominant edge to face interaction and interference. They have also found that the degradation in strength from a fully softened condition to a residual one depends on the plasticity of an arenaceous material, and have developed an empirical correlation between the fully softened and residual friction angles and the plasticity index for materials consisting of plate-shaped minerals. Such a relationship between these friction angles and the liquid limit or plasticity index should be expected since they are '*directly or indirectly related to ... the fundamental factors of particle size and plateyness*' (Mesri and Shahien, 2003 p. 14). According to these correlations and with a plasticity index of 30-35%, the fully softened friction angle is 30-31° for a normal stress of 50 kPa and 25-26° for 400 kPa; at the maximum depth, the deep-seated plane of the lower block (D1) is located about 30 m below surface (or a normal stress of 600 kPa). However, further testing would be required in order to confirm if the back-calculated shear strength values are indeed those of a fully softened condition.

ALTERNATIVE MECHANISM. An alternative explanation of the slope instability at Miles 86.8 and 86.75 involve the concept of abandoned cliffs (Figure 6-15), similar to those documented in the London Clay in England (Hutchinson, 1995). According to Hutchinson (1995), abandoned cliffs can form at the cessation of a period of erosion where no material is removed from the toe. Subsequent to its formation, surficial degradation occurs thus covering up the abandoned cliff with an accumulation of colluvium (Figure 6-15(a)). With time and further degradation, the surface achieves an "ultimate angle of stability" (approximately 8° for London Clay) at which point the inclination of the degradation and accumulation zones are equal thus also providing an indication of the age of the abandoned cliff (Hutchinson, 1995). Although, the area of greatest instability is typically located at the crest, fresh basal erosion leads to a shift of the greatest landslide hazard to the foot of the slope (due to steepening of the toe) as illustrated in Figure 6-15(b) (Hutchinson, 1995).

6.2 DEFORMATION ANALYSIS

Additional analyses, such as the determination of expected deformations, are useful in supplementing conventional stability analysis in order to assess the tolerance of movements within the scope of project constraints. Advances in the last two decades have focused on the use of stress-deformation studies (based on finite element methods) to complement conventional analysis (Propescu, 1997). Duncan (1996) has noted that they are particularly practical when performed in conjunction with field instrumentation studies; they can be a valuable tool in planning instrumentation and in the interpretation of instrumentation data. In this way, if the data matches predicted values from the deformation analysis, such analytical methods may be a viable application at other locations given that similar field conditions exist (Duncan, 1996).

The intent of this section was to examine the pattern of deformation given the geometry previously established and for clarification of the failure mechanism. The movement trends obtained from the deformation analysis was compared to those measured by the slope inclinometers data with respect to the shape, location, and relative magnitudes of movement

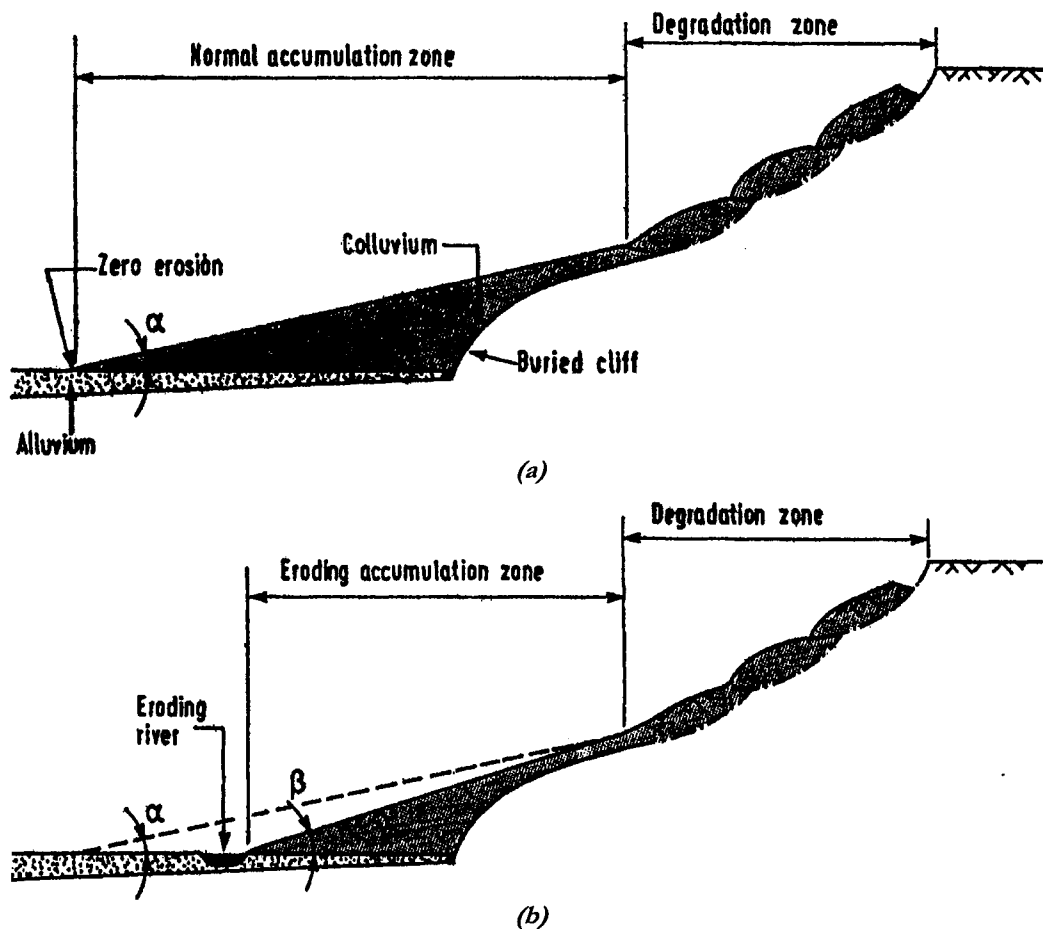


Figure 6-15: Abandoned cliff concept: (a) Hadleigh type with zero erosion and a normal accumulation zone (b) degrading cliff with an eroding accumulation zone (modified from Hutchinson, 1995).

in order to assess the accuracy and feasibility with which this kind of analysis is capable of attaining. The failure mechanism deduced from the deformational pattern was also used to assess the validity of the previously hypothesized mode of slope failure. This analysis was accomplished via the use of the program, FLAC (Fast Lagrangian Analysis of Continua), developed and supplied by Itasca (Coetzee et al., 1998).

FLAC, based on a Lagrangian calculation scheme that is appropriate for modeling large distortions and material collapse, is a two-dimensional, explicit finite difference program. It uses an explicit, time-marching method in order to solve the set of algebraic equations written in terms of field variables (e.g. stress, displacement) at discrete points in space, which are derived from the governing equations. The advantage of an explicit methodology lies in its ability to compute stresses from strains in an element in the absence of the need for iteration even under circumstances of wildly non-linear constitutive laws. However, its disadvantage lies in the small time-steps necessary to accomplish this, thereby requiring a large number of steps to complete analysis. As a result, explicit methods are least suited for modeling linear, small-strain problems, and best suited for ill-behaved systems such as those that experience non-linear, large strain, or physical instability. (Coetzee et al., 1998)

The problem is modeled as a mesh of elements, which can be manipulated by the user to fit the grid to the shape of the object to be modeled. Material properties are assigned to the elemental mesh, and each element behaves according to the prescribed linear or non-linear stress-strain constitutive law in response to applied forces and/or boundary restraints. The grid is capable of deforming (in large strain mode) and moving with the material that it represents since the material is able to yield and flow. (Coetzee et al., 1998)

In the application of FLAC, the analysis can be simple or complex with the level of complexity defined by the user in the choice of the mesh configuration, constitutive law, and physical processes to be modeled. Its strength lies in its ability to simulate the wide range of physical processes encountered in geotechnical engineering problems either individually or in combination; mechanical, fluid flow, and thermal analyses can be performed as separate or coupled calculations. The spectrum of its application is represented by the two extremes of full prediction and as a numerical laboratory to test ideas; the former applies to well-defined problems (i.e. complete and accurate set of data) while the latter applies to poorly-defined problems with limited geological information. (Coetzee et al., 1998)

6.2.1 MODEL CONFIGURATION

The geometry of the model used in the following FLAC analysis was based on a simplified version of cross-section Z3 (Figure 6-16); both the surface topography and contact between the softened and shale zones were smoothed out. Building of the model began as a rectangular mesh divided into two sections – upper and lower portions. It was then compressed and shaped to match the surface topography, and the contact between the intact and softened shale zones was modelled as a discrete plane. For increased computational accuracy, the upper portion of the mesh included twice the number of elements of the lower portion. In total the mesh contained 6640 elements of varying triangular and quadrilateral shapes and sizes; 1200 in the lower portion and 5440 in the upper portion with 1763 of these latter elements contained in the softened shale zone. In addition, two groundwater conditions were imposed on the model – groundwater at the surface and no groundwater.

The properties of the shale zones assigned to the model shown in Figure 6-16(b) were determined from the results of the direct shear and triaxial tests in Chapter 5 (Table 6-6), and groundwater was given a density of 1000 kg/m³. The lowest elastic modulus determined from lab testing was used in the calculation of the shear and bulk moduli of the softened zone while the highest elastic modulus was used for the intact zone according to the following formulations:

$$G = \frac{E}{2(1 + \nu)} \quad (5-1)$$

$$K = \frac{E}{3(1 - 2\nu)} \quad (5-2)$$

Under each groundwater condition, equilibrium of the model was first established with all materials bearing the characteristics of the intact shale under the load of gravity and elastic material behaviour. Subsequently, the softened zone was introduced with its own set of properties (Table 6-6) and assigned as a plastic, Mohr-Coulomb material ($\phi' = 16.6^\circ$, $c' = 17$ kPa, and tensile strength set to zero), while the properties and elastic behaviour of the intact

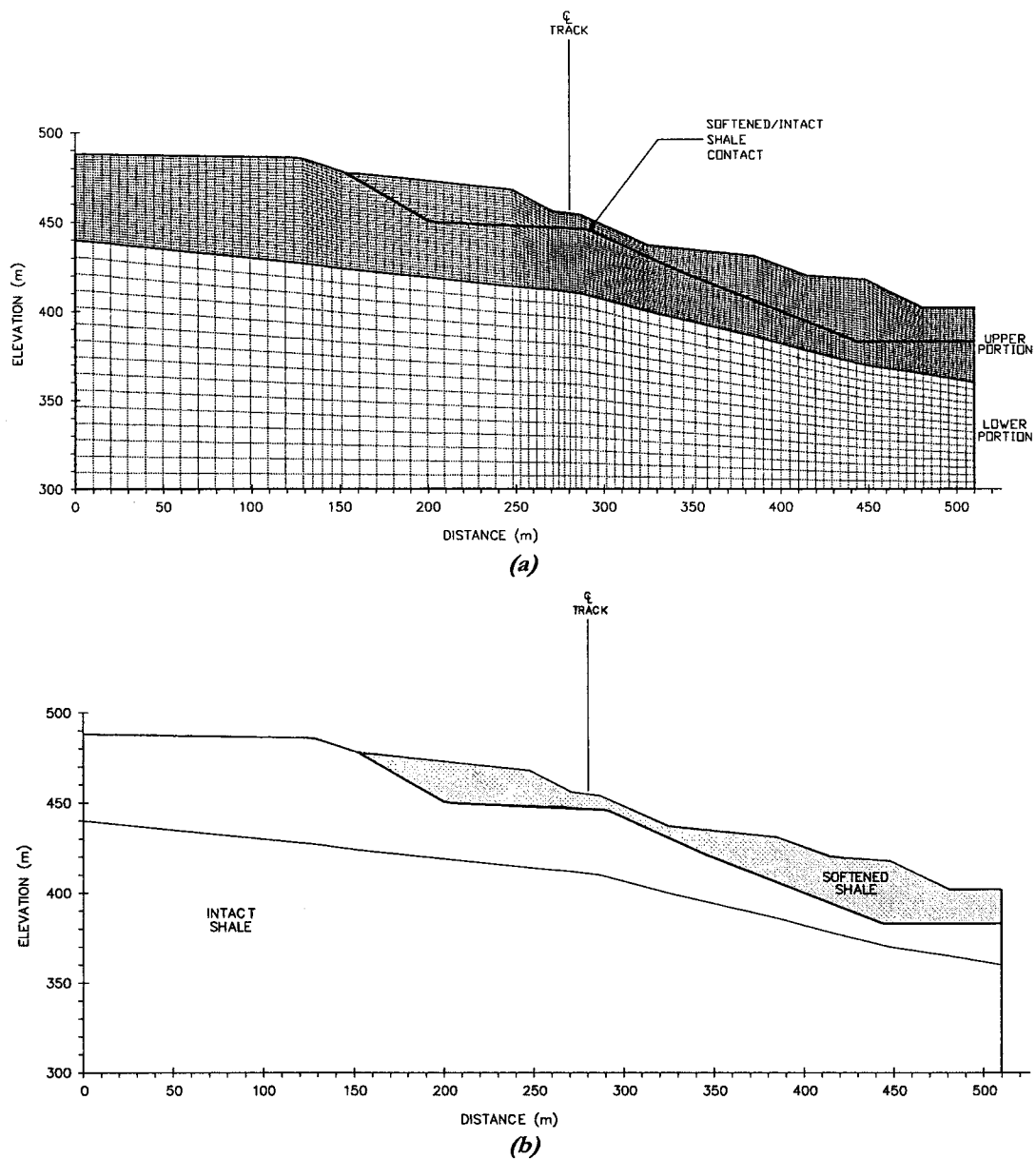


Figure 6-16: Configuration of the model used in the FLAC analysis. An enlarged section of the mesh is included in Appendix C (Figure C-2).

Table 6-6: Summary of the material properties used in the FLAC analysis.

Material	Dry Density (kg/m ³)	Poisson's Ratio, ν^{20}	Elastic Modulus, E (MPa)	Shear Modulus, G (MPa)	Bulk Modulus, K (MPa)
Softened shale	1591.6	0.29	32	12.4	25.4
Intact shale	1719	0.29	73.2	28.4	58.1

²⁰ from the FLAC (Version 4.0) User's Guide (2000), Table 3.3, of laboratory-scale elastic constants for rocks, which was adapted from Goodman

shale remained unchanged. The model was allowed to cycle 425 time-steps prior to stoppage and data was then extracted for the following discussion.

6.2.2 SLOPE MOVEMENT TRENDS

Data extraction from the FLAC analysis was based on the actual field locations of the relevant inclinometers, while the depths of each corresponded to the depth of each field installation (Figure 6-17). However, it should be noted that the top of each inclinometer of actual field locations did not always correspond with the top of the ground surface. Correspondingly, the bottom of each field installation does not necessarily coincide with the depth of the data extraction from the model. As a result, the comparison between the model and the field installations are expected to reflect these inconsistencies. The validity of the FLAC analysis will be determined by considering three factors: the shape of the movement profile, the location of the slip plane, and the relative magnitudes of movement.

On the whole, results from the FLAC model indicated shapes more or less similar to those obtained from the field inclinometers (Figure 6-18). Of the six inclinometers, three gave fairly encouraging results with respect to the expected shape; results from SI 923, 901, and 1108 were quite different. The FLAC shapes of SI 923 and 901 indicated movement along a discrete plane, whereas little movement and certainly not along a discrete plane was detected in the field installations. Conversely, SI 1108 did not indicate the existence of such a discrete plane in the model unlike that measured in the field installation. Results from the analysis revealed a rather odd shape for SI 1101, which was initiated as a unified mass moving discretely (similar to the movements recorded in the inclinometer) but became more gradual past this depth until the material contact was reached. In general, the FLAC shapes did not have the sharp changes in path indicated by the discrete-plane movements of the field installations, but they did indicate that movement was most unlikely of a gradual nature.

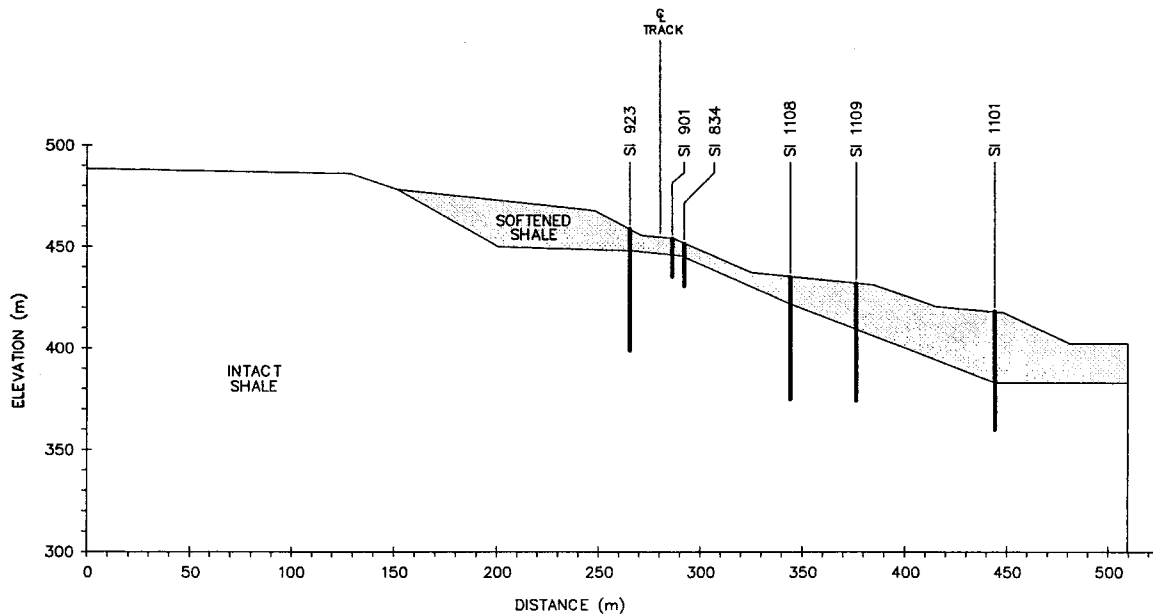


Figure 6-17: Location and depth of the SI data extraction from the FLAC analysis.

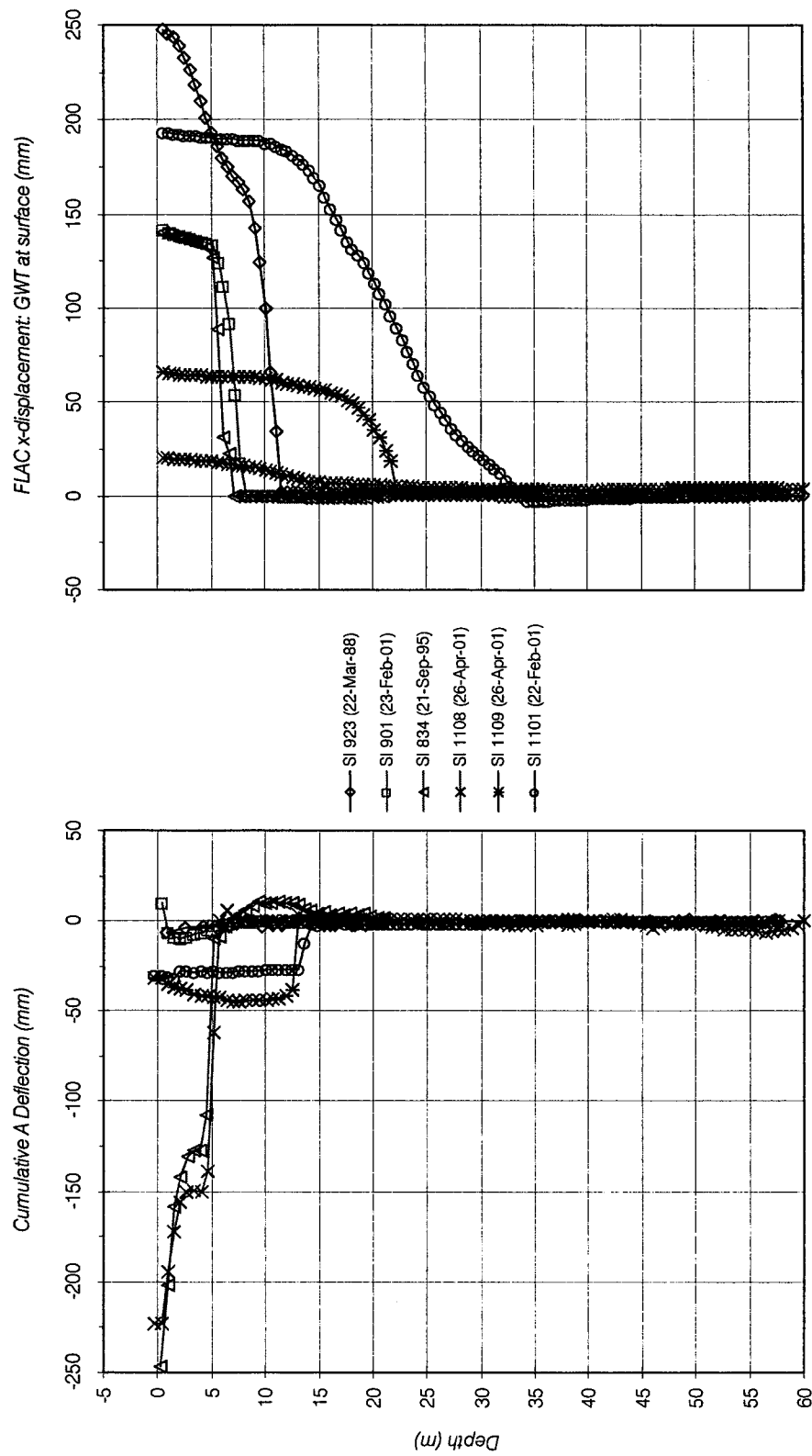


Figure 6-18: Comparison of slope movements between field installations and FLAC trends (inclinometer data assumed negative values for downslope movement, but the opposite was true for the FLAC results).

In all cases, the location of the slip plane was lower (1.3 to 1.5 times) in the model than in the field installations with the exception of SI 1101 (Figure 6-18). The thickness of the slip zone ranged from 0.6 to 1.8 m in the field installations, whereas it ranged from 5 to 10 m in all the FLAC inclinometers with the exception of SI 1109 where it was found to be about 17 m. The movement in SI 1101 is somewhat unique in that only the upper 10-11 m of mass appeared to move in a discrete manner as a cohesive unit.

When comparing the magnitudes of movement between the FLAC model and the field installations, it was soon realized that the model had to be fine-tuned with respect to the number of time-steps analyzed in order to produce the same order of magnitude of displacements between these two methods. As a result, only the relative magnitudes of maximum movement can be rightly compared (Figure 6-18). The order of the field inclinometers from those that experienced the most movements at their slip surfaces to those that experienced the least was SI 1108, 834, 1109, 1101, 901, and 923, whereas in the FLAC model, the order was SI 1101, 923, 901, 834, 1109, and 1108 (Table 6-7). The range of measured movements differed by 99.4%, with a maximum of 150.2 mm (SI 1108 at the slip surface zone) to a minimum of 0.9 mm (SI 923 at the surface since no slip plane could be discerned). In the FLAC model, the difference in the range was about 90% with a maximum of 188 mm (SI 1101 at the slip surface zone) to a minimum of 19 mm (SI 1108 the upper 5 m). The largest discrepancy between the FLAC model and the field data can be seen in this comparison of the relative magnitudes since those inclinometers which recorded the smallest movements were considerable in the model (Table 6-7).

The two inclinometers which resulted in encouraging behaviour in terms of all three aspects were SI 834 and 1109. SI 834 most closely matched the field conditions with respect to shape, location of slippage, and overall magnitude of movement; the slippage zone was measured between 3.9-5.8 m depth with a maximum displacement of 127.6 mm in the field installation, but it was found to be between the depths of 4.6-7.7m with a maximum displacement of 132.6 mm in the FLAC model. However, the results of SI 1109 were not as encouraging with the largest discrepancy occurring in the location of the slip plane; actual plane was recorded at a depth of 11.9-13.7 m compared to 17 m in the model.

The most likely explanation for these discrepancies lie in the model configuration and the required simplifications made for analysis. It was found that fine-tuning of the model from the initial period of analysis, which sought a simple geometry and typical material properties in order to examine the feasibility of this analysis, resulted in movement trends which matched the shape, slippage location, and relative magnitudes more closely. Fine-tuning consisted of using lab-determined properties, the back-calculated operational strength determined in the LEA, and the exact location of the slope inclinometers within the FLAC

Table 6-7: Comparison of the magnitudes of the measured and FLAC movements (values below are at the location of the slip plane where apparent and at surface where indicated by *).

Inclinometer	Measured Movement (mm)	FLAC Movement (mm)
923	0.9*	157
901	10*	134
834	127.6	133
1108	150.2	19
1109	44.0	63
1101	26.8	188

model configuration. Further fine-tuning would be required to the overall geometry of the mesh in terms of closer matching of the intact-softened shale contact. In addition, the pore pressure condition was found to be a significant factor in all three aspects of shape, slippage location, and relative magnitudes (Figure 6-19). This demonstrated the importance of accuracy in the placement and modelling of the pore pressure conditions, material properties (i.e. a proper constitutive model), and slope geometry in order to use such analysis in a predictive mode.

As Figure 6-19 indicated, the absence of groundwater presented a more stable condition, which would experience very little movement with the exception of SI 1101. However, the model estimated as much as 62 mm of movement at the surface in SI 1101 even in the absence of groundwater. This has implications on the overall stability of the slope being governed by the toe region, which appears to be the weakest point in the model.

Results from the FLAC analysis with respect to the deformational pattern are shown in Figure 6-20 (groundwater conditions at surface). The x-displacement contours shown in Figure 6-20 indicate two zones where movements are concentrated with the greatest movements occurring in the lower zone. These two zones are separated by a zone which experiences comparatively smaller movements, thereby rendering the indication of any retrogressive failure to be inconclusive. Furthermore, the previous hypothesis of the locations of the upper and middle blocks appears to have been inaccurately defined according to Figure 6-20. The more accurate representation would be the combination of the upper block with the upper half of the middle block, the lower half of the middle block on its own, and no change to the lower block.

6.3 SUMMARY

The objective of this chapter was to ascertain the mode of failure of the study site – the depth of failure and the geometry of the movement mass. This was accomplished by the conventional LEA and the more contemporary deformation analysis (FLAC) of cross-section Z3 from Chapter 4.

Both the shallow- and deep-seated mechanisms from LEA revealed that the stability of the slope under lab-determined residual shear strength parameters was severely undermined, and yet excessively conservative under lab-determined peak values. Both also illustrated a closer proximity to the residual lab values; the factors of safety calculated for the shallow-seated failure was about 36-39% below a condition of limiting equilibrium for the lab residual parameters, but 553-685% above it for peak values. However, when the operational residual (c-0) strength was determined, the shallow-seated mechanism indicated a friction angle much closer (a difference of 8% from the peak compared to a difference of 37% from the residual) to the peak lab value while the friction angle from the deep-seated mechanism was closer (a difference of 21% from the residual compared to a difference of 27% from the peak) to the residual lab value. In addition, when the c-17 operational strength determined in the shallow-seated mechanism was applied to the deep-seated mechanism, the resulting factor of safety was not close to unity as it would be expected of identical failure modes between the shallow and deep movements.

Anomalous behaviour of the sliding mass was also implied in the limit equilibrium analysis since regardless of the depth of failure; the lower block on its own appeared to behave in a manner different from the upper portions of the slope. This was further exemplified by the

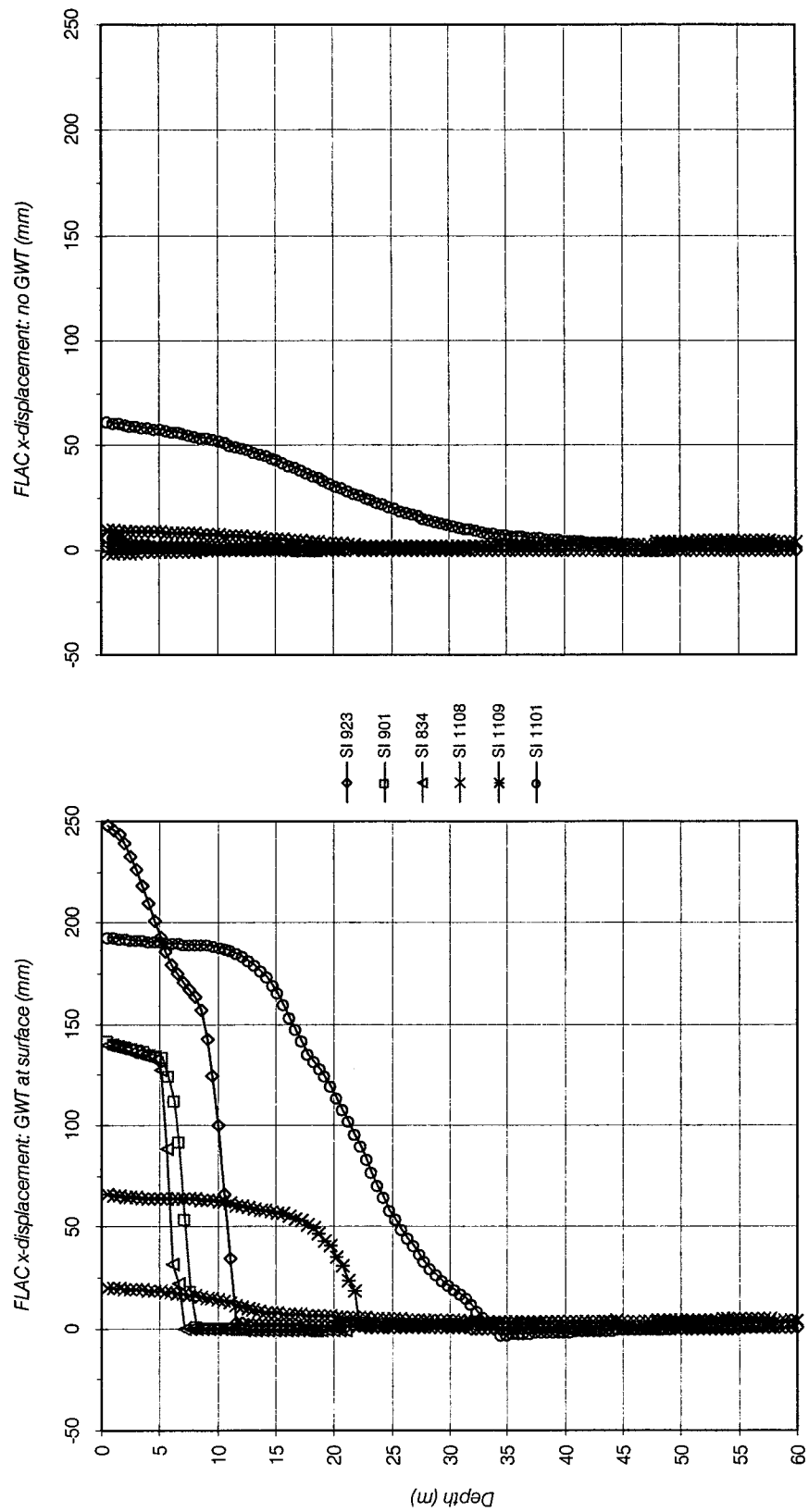


Figure 6-19: Slope movement trends from FLAC at different groundwater conditions.

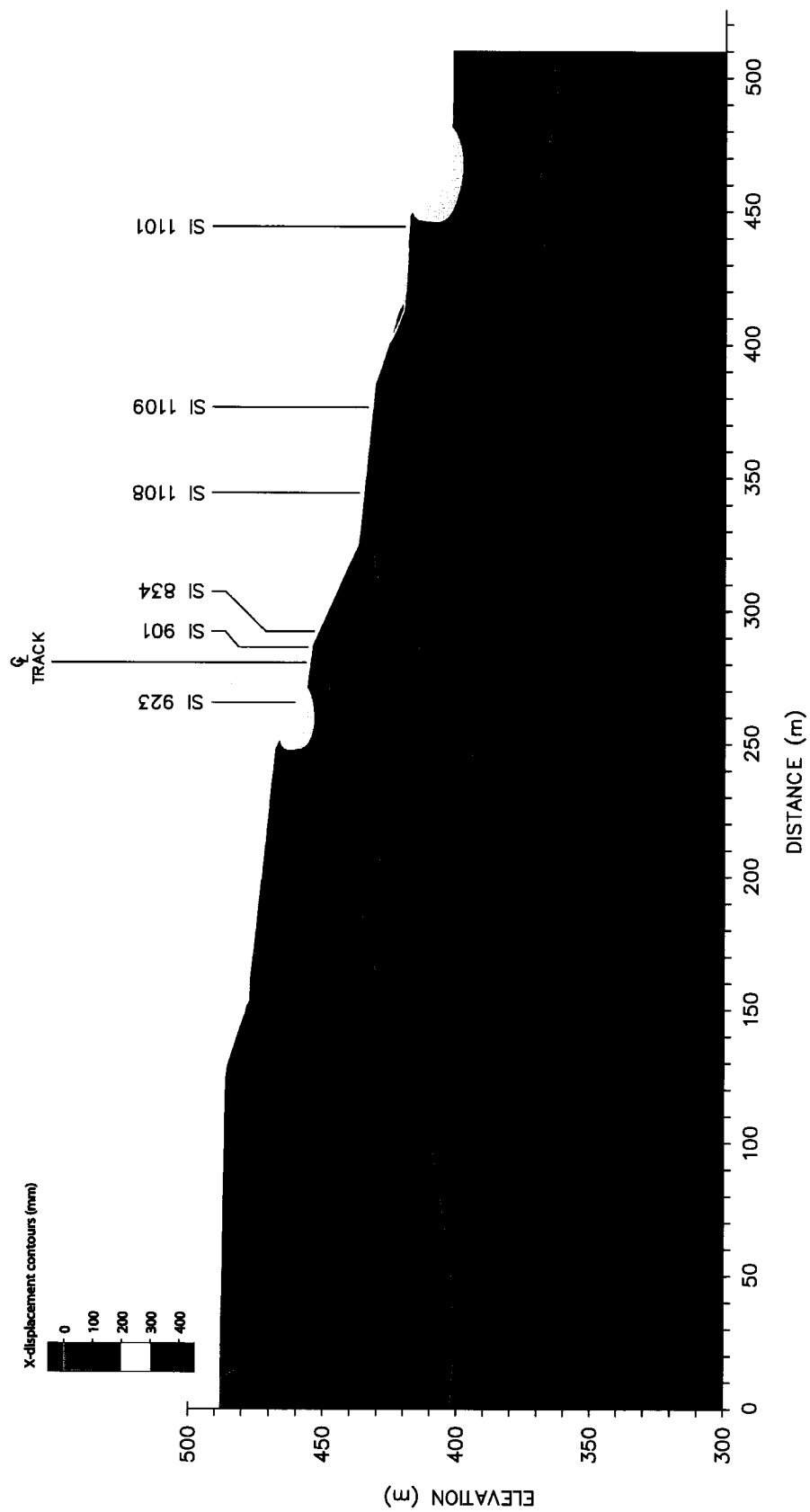


Figure 6-20: *Contours of x-displacements from FLAC analysis with groundwater at surface.*

displacement and displacement rate vectors calculated in Chapter 4, where the lower block was found to move at a faster rate and with higher magnitudes than the upslope mass near the scarp. It was postulated that this inconsistency was the result of a dual failure mechanism, where the lower block moves on a shear plane independent of the upslope portions of the sliding mass. However, the upslope mass may move in a retrogressive manner in response to the movement of the lower block, which releases the toe support of this upslope mass as it moves out along its own shear plane in response to erosion of its toe (most likely by the encroaching Assiniboine River). Loss of cohesion, as indicated by higher water contents most likely due to weathering, has been proposed as the cause of failure in the shallow-seated mechanism, whereas progressive failure appears to be the most likely cause of the deep-seated mechanism. Alternatively, these mechanisms may be attributed to the abandoned cliff concept where instability occurs in the blanketing colluvium due to contemporary basal erosion.

The sensitivity analysis of both the limit equilibrium and FLAC analyses indicated the importance of modeling accuracy of the pore pressure distribution within the movement mass due to the significant influence of the groundwater conditions on both the stability (factors of safety for the condition of zero pore pressure were more than double compared to pore pressure at ground surface) and deformation analyses (displacements under the condition of zero pore pressure were mostly negligible with the exception of the lowest inclinometer which reached a maximum of 62 mm at the surface). This also indicated the significance of seasonal variation on the overall stability of the mass and the high probability with which slope movements can be arrested by remedial actions which focus on drainage of the sliding mass.

Results from the FLAC model on the trend of slope inclinometer data were encouraging, which lead to prospects of extending this analysis to applications such as the study of deformational patterns in response to external loads (e.g. train dynamics, change in slope topography, etc.). If the analysis is capable of predicting instrumentation data with reasonable accuracy, then an extension of the analysis to further study of deformational patterns would be expected to yield realistic results. However, it is important to note that the model depends strongly on the accuracy of the input data to reflect the actual field conditions. With further refinement of the geometry of the cross-section, accurate pore pressure distributions, and constitutive modelling, perhaps the FLAC model would yield movement predictions more reflective of the field instrumentation measurements of Chapter 4.

7 SUMMARY & CONCLUSION

In order to develop mitigative measures to control landslide movements, a thorough understanding is required of the processes that drive the movements. This requires an appreciation of the history of the site with respect to the geological processes which have resulted in its present landscape and geology, in addition to the mechanical behaviour of the materials affected. Both a literature review and the field investigations assisted the former, while the latter was accomplished by laboratory testing of the material which afforded the opportunity to examine the physical aspects of the material and its characterization accordingly. Subsequent to the building of this foundation, the information was used to build models for analysis of the failure mechanism under which the slope at Mile 86.8 and Mile 86.75 has moved. The following summarizes the objectives of this research along with conclusions from interpretation of the field conditions and results from laboratory testing and analyses of the slope failure.

As expected, a few interesting observations and questions arose during the course of this research, which were beyond the scope of this study but are addressed as recommendations for future research in the last section of this chapter.

7.1 SUMMARY

1. Since the construction of the rail line along the west valley wall of the Assiniboine River valley in the late 1800's, an 8 km section of the track between Harrowby and Millwood, Manitoba has suffered from slope movements ranging from shallow-seated sloughing to severe landsliding. This section of track crosses several relict landslides and has experienced movements ranging from slow to sudden displacements, which have led to periodic action ranging from track maintenance (such as track lifting and re-aligning) to more frequent patrols and reductions in train speeds. The study area (Miles 86.8 and 86.75) has been the most recently unstable and was deemed the most critical in 1986. These slopes have been investigated since the early 1980's, and it was concluded that these landslide activities entailed a series of metastable, retrogressive blocks with failure seated in the high-plasticity clay shale bedrock, the Millwood Member of the Pierre Formation.
2. Clay shales are much older sedimentary argillaceous deposits which have been subjected to consolidation from varying depths of overburden pressure in excess of contemporary conditions. They are transitional in nature; exhibit both soil- and rock-like properties, and a tendency to exhibit strength loss with time. Their presence in North America encompass the extensive formations of shale bedrock that extend across the length of the continent and east from the Rocky Mountains for several hundred kilometres, covering an area once occupied by the epicontinental sea of the Late Cretaceous period. Despite their relatively flat-lying to gentle-sloping depositional nature, their presence has become synonymous with challenging performances of foundations as well as naturally-occurring and man-made slopes. They are well-known and well-documented problematic engineering materials.
3. The Cretaceous Period in North America entailed tectonics coupled with volcanism. In the Western Interior Basin, the intense orogenic activities of the western Cordilleran had the greatest impact on the depositional environment while the volcanic activities centred in southwestern Montana and Idaho had a milder impact. Sedimentation during this

period laid down the bedrock formations now found in the Manitoba escarpment (where the study area is located), located at the eastern margin of the basin.

4. Creation of the Assiniboine River valley occurred in the Pleistocene epoch of the Quaternary period as meltwaters from the last deglaciation carved its way through a landscape previously altered by earlier glaciations. The modern Assiniboine River valley is part of an extensive system of meltwater channels that were established mainly within ancestral valleys, which were partly filled and/or re-excavated during the last glaciation. Subsequent to the glacial period, valley evolution has encompassed the continued lateral erosion and deposition of alluvium by the river, as well as, valley widening and slope flattening due to slumping of the oversteepened valley walls.
5. The bedrock stratum, the Millwood member of the Pierre Shale, is an olive-grey, soft, uniform, silty, noncalcareous clay shale with selenite crystals, numerous calcareous concretions, a considerable number of ironstone nodules occurring in bands, and numerous bentonite beds occurring within or close to the top contact. A characteristic feature of the Millwood is the presence of a certain amount of fine sand dispersed throughout the member. In dry conditions, the shale is hard, showing laminations, but not strikingly fissile and tends to break into equidimensional particles. In water, the shale slakes easily, turning into a very tenacious, plastic clay.
6. Correlations of the Millwood member of the Pierre Shale formation (also known as the Riding Mountain formation from Canadian nomenclature) include: the Lea Park, Judith River, and the Bearpaw formations in the Canadian prairies, and the Gregory and DeGrey members of the Pierre Shale in the Dakotas. More specifically, the lower 13 m of the Millwood member correlate with the Lea Park formation of western Saskatchewan and eastern Alberta, while the upper portion correlates with the uppermost Lea Park, Judith River, and the lowermost Bearpaw formations of western Saskatchewan.
7. Surficially, the area has been topographically surveyed on three different occasions since the field investigation began in 1986. The overall nature of the valley wall appeared to be rather gentle sloping and hummocky due to past landsliding activities. Site reconnaissance has identified six drainage courses and four ponded areas immediately affecting the study area. Their sources included not only precipitation and surface runoff, but also drainage from the layers of sand and gravel found at surface and in the blanketing till sheet and two springs located above the track.
8. The subsurface was explored by a combination of 41 boreholes and 23 test pits excavated within the entire slope and the upland plateau. Sampling was also carried out in both boreholes and test pits via grab samples, washed cuttings, Shelby tube, and continuous coring. In addition, block sampling was also carried out in 2002 for the work in this thesis. Almost all boreholes were instrumented with either piezometers or slope inclinometers in order to monitor the groundwater conditions and movement of the slope respectively. On the whole, 33 piezometers and 11 slope inclinometers were installed from 1986 to 2001. However, monitoring has been somewhat sporadic and irregular.

7.2 CONCLUSIONS

1. The stratigraphy was interpreted based on bedrock elevations provided by the consultant, borehole logging, and the use of water content and dry density profiles. Only three strata were identified: till, intermix of till and shale (i.e. colluvium and weathered shale bedrock), and clay shale bedrock. The water contents for the intact shale appeared to be near 20% while the dry densities were in excess of 1700 kg/m^3 . In general, the intact shale appeared to follow the slope topography in a quasi stepwise fashion.
2. Groundwater conditions were simplified to ground surface due to the exclusive use of standpipe piezometers, which have proven to be rather unreliable in clay shale material. Field investigations have indicated that the groundwater conditions are close to the surface due to the frequent occurrence of ponded water the shallow nature of surface drainage courses.
3. Location of the shear plane was based on both borehole logging in the sparsely instrumented upper upslope and slope inclinometer data of the relatively well-instrumented near-track and downslope portions. Generally, the shear plane was found to follow the surface topography for the majority of the slope with the exception of the region closest to the Assiniboine River. This indicated relatively shallow failures within most of the slope with a somewhat deeper-seated failure at the bottom of the slope. Movements recorded near and/or at the shear plane indicated maximum movement of 139.7 mm at a corresponding rate of 520.3 mm/yr (the interval over which this rate was calculated was 98 days), both recorded in SI 1108
4. The last site visit was made during the excavation of the second shear key in late May, 2002. The weathered zone of the shale bedrock was rather blocky and jointed with evidence of orthogonal joint sets and perhaps indicated regional jointing due to a number of parallel, continuous joints apparent in the upslope excavation wall. A shear plane was not clearly identified by the field personnel, but it was speculated to coincide with a rather horizontal iron-stained plane located within the weathered zone of the bedrock. This plane did not appear to follow the slope of the ground surface, but it may have previously projected through the ground surface in a nearly horizontal manner. No seepage was observed from this plane, although it has undoubtedly occurred in the past. The excavation was dry and the walls were maintained at rather steep inclinations without any external support for the duration of the two-day trip.
5. The grain-size distribution of the material tested suggested a primary dominance in silt-sizes with a secondary proportion of clay sizes. However, the material was found to be inorganic clay of high plasticity with a massive fabric displaying no fissility and consisting of a clay matrix in which the coarser fractions existed. This was consistent with the range of hydraulic conductivities determined from consolidation tests ranging from $3.3 \times 10^{-10} \text{ m/s}$ (vertical load of 6.25 kPa) to $6.5 \times 10^{-12} \text{ m/s}$ (vertical load of 798 kPa). These characteristics are consistent with a clay-rich medium which would be expected to exhibit engineering behaviour dominated by this fraction. In addition, the possibility of cementation in the material tested appeared to be very likely. However, due to the persistence of the material in water at its natural water content, but slaking completely after one cycle of air-drying, influence from cementation appeared to be weak.
6. The variability exhibited by the test samples of the Millwood Member as evidenced by the range of stress-strain curves (i.e. brittle, ductile, and by-passed behaviour) can be

indicative of the complexity of the soil/rock mass structure. Samples tested under direct shear and consolidated-drained and consolidated-undrained triaxial conditions indicated a brittle material with an elastic modulus ranging from 32 to 73.2 MPa. The reduction in strength from peak to residual was significant, ranging from 38% to 79%. A remoulded sample tested under direct shear conditions, indicated a loss in strength of roughly 50% from peak to residual due to the destruction of its in-situ structure. Under the low confining pressures of both the direct and triaxial tests, the material exhibited typical overconsolidated behaviour, resulting in brittle stress-strain curves, well-defined failure planes, and a degree of dilatancy.

7. Peak strengths from the direct shear tests indicated a cohesion intercept of 184.7 kPa and a friction angle of 28.7° , while the triaxial tests indicated an effective cohesion of 139.3 kPa and a friction angle of 36.1° . According to the direct shear tests, the residual strength of the material had a cohesion of zero and an angle of friction of 16.7° .
8. Both the shallow- and deep-seated mechanisms from LEA revealed that the stability of the slope using lab-determined residual shear strength parameters was severely undermined, and yet excessively conservative when using lab-determined peak values. However, when the operational residual (c-0) strength was determined, the shallow-seated mechanism indicated a friction angle much closer (8% from peak compared to 37% from residual) to the peak lab value while the friction angle from the deep-seated mechanism was closer (21% from residual compared to 27% from peak) to the residual lab value. In addition, when the c-17 operational strength determined in the shallow-seated mechanism was applied to the deep-seated mechanism, the resulting FS was not close to unity as it would be expected of identical failure modes between the shallow and deep movements.
9. Anomalous behaviour of the sliding mass was also implied in the LEA since regardless of the depth of failure; the lower block on its own appeared to behave in a manner different from its combination with the upslope portions of the slope. This was further exemplified by the displacement and displacement rate vectors calculated in Chapter 4, where the lower block was found to move at a faster rate and with higher magnitudes than the upslope mass near the scarp.
10. These inconsistencies are the result of a dual failure mechanism, where the lower block moves along a deep-seated shear plane independent of the upper shallow-seated portions of the sliding mass. However, the upper mass may move in a retrogressive manner in response to the release of its toe support from the lower block as it moves out along its own shear plane due to toe-erosion (most likely by the encroaching Assiniboine River). The upper slide mass might perhaps be described as a blocky-flow slide.
11. Loss of cohesion, as indicated by higher water contents (most likely due to the softening processes of weathering), has been proposed as the cause of failure in the shallow-seated mechanism, whereas progressive failure appears to be the most likely cause of the deep-seated mechanism. Alternatively, these mechanisms may be attributed to the abandoned cliff concept where instability occurs in the blanketing colluvium due to contemporary basal erosion.
12. The sensitivity analysis of both the limit equilibrium and FLAC analyses indicated the importance of modeling accuracy of the pore pressure distribution within the movement mass due to the significant influence of the groundwater conditions on both the stability

(FS's for the condition of zero pore pressure were more than double compared to pore pressure at ground surface) and deformational analyses (displacements under the condition of zero pore pressure were mostly negligible with the exception of the lowest inclinometer which reached a maximum of 62 mm at the surface). This also indicated the significance of seasonal variation on the overall stability of the mass and the high probability with which slope movements can be arrested by remedial actions which focus on drainage of the sliding mass.

13. Results from the FLAC model on the trends of the slope inclinometer data were encouraging, which lead to prospects of extending this analysis to applications such as the study of deformational patterns in response to external loads (e.g. train dynamics, changed in slope topography, etc). However, caution must be exercised since it has been shown that the model depends strongly on the accuracy of the input data to reflect the actual field conditions. With further refinement of the geometry of the cross-section, accurate pore pressure distributions, and constitutive modeling, perhaps the FLAC model would yield movement profiles more reflective of the field instrumentation measurements of Chapter 4.

7.3 FUTURE RESEARCH PROSPECTS

The peculiar behaviour of the shale when exposed to water in its in-situ water content was atypical of "clay shales." However, its behaviour reverted back to typical when it was exposed to water under its air-dried state. The process by which it retains its "cohesion" at its in-situ content while suffering disintegration under an air-dried state is unknown and is suggested as a topic for further study. Cementation has been suggested as a cause, but due to its disintegration in one cycle of slaking, any possibility of cementation must be weak. As Mitchell (1993) has noted, the possible sources of cementation are: carbonates (which have been ruled out), silica, alumina, iron oxide, and organic compounds. More specifically, Braybrook (SEM Technician) has suggested that there is strong indication of biological cementation in the form of sugars or mucilage. It is suggested that the possibility of cementation in this material be investigated and its influence on the cohesion component of the material strength be clarified. Also, chemical analysis of the deposit left on the samples following evaporation of the water from the beakers should be examined as it may provide further insight into the nature of the material and its interaction with water. In addition, little is known of the interstitial porewater chemistry under which the formation has been created and exists, and knowledge of this may undoubtedly influence the conclusion of this topic. With further study, the deduction of the mechanism by which this material retains its cohesion under its in-situ water content while disintegrating under an air-dried state will identify whether the mechanism is predominantly a chemical or physical one or a combination of both. Conclusions from this investigation have strong implications on weathering and valley-widening processes.

Also in light of its distinctly weakened condition in an air-dried state, causes of slope instability in such material should focus on the climatic condition under which movements occur. More specifically, study of the climatic data should focus on identification of a period of drying immediately preceding an anomalous wet period which may be the final triggering mechanism. Indication of such a possibility has been mentioned by Chandler (1984b). If such a pattern exists or if another emerges, mitigation of slope movements in similar material may be achieved in a more proactive fashion.

BIBLIOGRAPHY

- American Society for Testing and Materials. 2002. *Annual book of standards, Volume 04.08, Soil and Rock; Building Stones*. Hitchin, Herts.
- Bjerrum, L. 1967. Progressive failure in slopes of overconsolidated plastic clay and clay shales. *Journal of Soil Mechanics and Foundations Division, Proceedings of the American Society of Civil Engineers*, **93**: 3-49.
- Botts, M.E. 1986. *The effects of slaking on the engineering behaviour of clay shales*. Doctor of Philosophy Thesis, University of Colorado. 262 p.
- Bowles, J.E. 1992. *Engineering properties of soils and their measurement*. McGraw-Hill, Inc., New York. 241 p.
- Brooker, E.W. and Peck, R.B. 1993. Rational design treatment of slides in overconsolidated clays and clay shales. *Canadian Geotechnical Journal*, **30**: 526-544.
- Bruce, R.L. 1968. Landslides in the Pierre Shale of South Dakota. *Proceedings of the 7th Annual Highway Geology Symposium*, Iowa State University. pp. 66-72.
- Chandler, R.J. 1984a. Recent European experience of landslides in over-consolidated clays and soft rocks. *IV International Symposium on Landslides*, University of Toronto Press, Toronto. **1**: 61-81.
- Chandler, R.J. 1984b. Delayed failure and observed strengths of first-time slides in stiff clays: a review. *IV International Symposium on Landslides*, University of Toronto Press, Toronto. **2**: 19-25.
- Chenevert, M.E. and Sharma, A.K. 1993. Permeability and effective pore pressure of shales. *SPE Drilling & Completion*, **8**: 28-34.
- Clayton, C.R.I. and Serratrice, J.F. 1997. General co-report session 2: The mechanical properties and behaviour of hard soils and soft rocks. *Geotechnical Engineering of Hard Soils – Soft Rocks*, Balkema, Rotterdam. **3**: 1839-1877.
- Clifton Associates Ltd. 1986. *Harrowby Hill grade improvement, Bredenbury Subdivision, final report*. (unpublished) File R573. 73 p.
- Clifton Associates Ltd. 1988. *Harrowby Hill grade improvement, Bredenbury Subdivision, final report*. (unpublished) File R677. 31 p.
- Clifton Associates Ltd. 1996. *Final report of geotechnical investigation of grade instability, Bredenbury Subdivision, Harrowby, Manitoba*. (unpublished) File S884. 25 p.
- Clifton Associates Ltd. 1997. *Construction report, Mile 86.75 and 86.8, Bredenbury Subdivision, Harrowby, Manitoba*. (unpublished) File S884.1. 6 p.
- Clifton Associates Ltd. 2001. *Evaluation of slope hazards, Mile 86.67 to 86.8, Bredenbury Subdivision near Harrowby, Manitoba*. (unpublished) File S884.2. 31 p.

- Coetzee, M.J., Hart, R.D., Varona, P.M., and Cundall, P.A. 1998. *FLAC Basics: An introduction to FLAC and a guide to its practical application in geotechnical engineering*. Itasca Consulting Group, Inc. 68 p.
- Craig, R.F. 1995. *Soil mechanics, fifth edition*. Chapman & Hall, London. 427 p.
- Crandell, D. R. 1952. Landslides and rapid-flowage phenomena near Pierre, South Dakota. *Economic Geology and the Bulletin of the Society of Economic Geologists*. 47:548-568.
- Crandell, D. R. 1958. Geology of the Pierre Area South Dakota. *U.S. Geological Survey Professional Paper 307*. 83 p.
- Cruden, D.M. 1997. General co-report session 4: Slope stability and protection. *Geotechnical Engineering of Hard Soils – Soft Rocks*, Balkema, Rotterdam. 3: 1957-1983.
- Cruden, D.M. and Varnes, D.J. 1996. Landslide types and processes. Chapter 3 in *Landslides Investigation and Mitigation, Transportation Research Board Special Report 247*, National Research Council, Washington. pp. 36-75.
- Douglas, R.J.W., Gabrielse, H., Wheeler, J.O., Stott, D.F., and Belyea, H.R. 1970. Chapter 8 of Geology of Western Canada. *Geology and Economic Minerals of Canada*. Geological Survey of Canada, Ottawa. pp. 366-488.
- Duncan, J.M. 1996. Soil slope stability analysis. Chapter 13 in *Landslides Investigation and Mitigation, Transportation Research Board Special Report 247*, National Research Council, Washington. pp. 337-371.
- Dunnicliff, J. 1988. *Geotechnical instrumentation for monitoring field performance*. John Wiley & Sons, New York City. 577 p.
- Elson, J.A. 1966. Geology of glacial Lake Agassiz. *Life, Land and Water*. University of Manitoba Press, Winnipeg. pp. 36-95.
- Erskine, C.F. 1973. Landslides in the vicinity of the Fort Randall Reservoir, South Dakota. *U.S. Geological Survey Professional Paper 675*. 65 p.
- Fam, M.A. and Dusseault, M.B. 1998. High-frequency complex permittivity of shales (0.02-1.30 GHz). *Canadian Geotechnical Journal* 35: 524-531.
- Fleming, R.W., Spencer, G.S., and Banks, D.C. 1970. Empirical study of behaviour of clay shale slopes. *U.S. Army Engineer Nuclear Cratering Group (NCG) Technical Report No. 15*. 93 p.
- Gage. 1979. [map] *Junior Atlas of Canada*. Gage Educational Publishing Limited, Toronto.
- Georgiannou, V.N., Burland, J.B., and Hight, D.W. 1993. The behaviour of two hard clays in direct shear. *Geotechnical Engineering of Hard Soils – Soft Rocks*, Athens. 1: 501-507.
- Gibson, R.E. and Henkel, E.J. 1954. Influence of duration of tests and constant rate of strain on measured drained strength. *Geotechnique*, 4: 6-15.

- Glass, D.J. (ed.) 1990. *Lexicon of Canadian Stratigraphy, Volume 4*. Canadian Society of Petroleum Geologists, Calgary. 772 p.
- Hancock, J.M. 1975. The sequence of facies in the upper Cretaceous of Northern Europe compared with that in the Western Interior. *The Cretaceous system in the Western Interior of North America*. Geological Association of Canada, Waterloo. pp. 83-118.
- Hardy, R.M. 1957. Engineering problems involving pre-consolidated clay shales. *Engineering Institute of Canada Transactions*, 1: 5-14.
- Head, K.H. 1980. *Manual of soil laboratory testing, Volume 1: Soil classification and compaction tests*. Pentech Press, London. 388 p.
- Head, K.H. 1982. *Manual of soil laboratory testing, Volume 2: Permeability, shear strength and compressibility tests*. John Wiley & Sons, Inc., New York. 747 p.
- Head, K.H. 1986. *Manual of soil laboratory testing, Volume 3: Effective stress tests*. John Wiley & Sons, Inc., New York. 1238 p.
- Hsu, S.C. and Nelson, P.P. 2002. Characterization of Eagle Ford Shale. *Engineering Geology*, 67: 169-183.
- Hutchinson, J.N. 1995. Keynote paper: landslide hazard assessment. *Landslides*, 3: 1805-1841.
- Hvorslev, M.J. 1962. *Subsurface exploration and sampling of soils for Civil Engineering purposes*. Engineering Foundation, New York City. 521 p.
- Itasca Consulting Group Inc. 2000. *FLAC (Version 4.0) User's Guide*. Itasca Consulting Group Inc., Minneapolis. 274 p.
- Jaspar, J.L. and Peters, N. 1979. Foundation performance of Gardiner Dam. *Canadian Geotechnical Journal*, 16: 758-788.
- Johnston, I.W. and Novello, E.A. 1993. Soft rocks in the geotechnical spectrum. *Geotechnical Engineering of Hard Soils – Soft Rocks*, Balkema, Rotterdam. 1: 177-183.
- Kehew, A.E. and Teller, J.T. 1994. History of late glacial runoff along the southwestern margin of the Laurentide ice sheet. *Quaternary Science Reviews*, 13: 859-877.
- Kenney, T.C. 1967. The influence of mineral composition on the residual strength of natural soils. *Proceedings of the Geotechnical Conference on Shear Strength of Cohesive Soils*, Oslo. 1: 123-129.
- Kirk, S.R. 1930. Cretaceous stratigraphy of the Manitoba escarpment. *Geological Survey of Canada Summary Report, 1929, Part B*. pp. 112-135.
- Kjartanson, B.H. 1978. *Delayed failure of a cut slope in stiff clay*. Master of Science Thesis, University of Alberta. 175 p.
- Klassen, R.W. 1969. Quaternary stratigraphy and radiocarbon chronology in southwestern Manitoba. *Geological Survey of Canada Paper 69-27*. 19 p.

- Klassen, R.W. 1972. Wisconsin events and the Assiniboine and Qu'Appelle valleys of Manitoba and Saskatchewan. *Canadian Journal of Earth Sciences*, **9**:544-560.
- Klassen, R.W. 1974. Quaternary geology and geomorphology of Assiniboine and Qu'Appelle valleys of Manitoba and Saskatchewan. *Geological Survey of Canada Bulletin* 228. 61 p.
- Knight, D.K. 1963. Oahe Dam: Geology, embankment, and cut slopes. *Journal of the Soil Mechanics and Foundations Division, Proceedings of the American Society of Civil Engineers*, **89**: 99-167.
- Krahn, J., Johnson, R.F., Fredlund, D.G., and Clifton, A.W. 1979. A highway cut failure in Cretaceous sediments at Maymont, Saskatchewan. *Canadian Geotechnical Journal*, **16**: 703-715.
- Laguros, J.G. and Kumar, S. 1980. Failure of slopes cut into clay shales. 6th Southeast Asian Conference on Soil Engineering, Taipei. pp. 407-413.
- Lambe, T.W. and Whitman, R.V. 1979. *Soil mechanics, SI version*. John Wiley & Sons, New York. 553 p.
- Langmuir, D. 1997. *Aqueous environmental geochemistry*. Prentice-Hall Inc., Upper Saddle River. 600 p.
- Machair Surveys. 1971. Aerial Photo MA 406-643, line 10 643-654 North of McConnell & South of Kelloe. [1:267000].
- Manitoba Trade & Investment Corporation website. www.gov.mb.ca
- McNeil, D.H. and Caldwell, W.G.E. 1981. Cretaceous rocks and their foraminifera in the Manitoba escarpment. *The Geological Association of Canada Special Paper* 21. 439 pp.
- Mesri, G. and Shahien, M. 2003. Residual shear strength mobilized in first-time slope failures. *ASCE Journal of Geotechnical and Geoenvironmental Engineering*, **129**: 12-31.
- Mineral Resources Division, Government of Manitoba website. 2002. *Manitoba geology*. www.gov.mb.ca
- Misfeldt, G.A., Sauer, E.K., and Christiansen, E.A. 1991. The Hepburn landslide: An interactive slope-stability and seepage analysis. *Canadian Geotechnical Journal*, **28**: 556-573.
- Mitchell, J.K. 1993. *Fundamentals of soil behaviour*. John Wiley & Sons, Inc., New York. 437 p.
- Mollard, J.D. 1977. Regional landslide types in Canada. *Geological Society of America, Reviews in Engineering Geology*, **3**: 29-56.
- Morgenstern, N.R. 1977. Slopes and excavations in heavily over-consolidated clays. *Proceedings of the Ninth International Conference on Soil Mechanics and Foundation Engineering*, **2**: 567-581.

- Morgenstern, N.R. 1992. The evaluation of slope stability – A 25 year perspective. *Stability and performance of slopes and embankments II*, Geotechnical Special Publication No. 31. 1: 1-26.
- Morgenstern, N.R. and Eigenbrod, K.D. 1974. Classification of argillaceous soils and rocks. *Journal of the Geotechnical Engineering Division, Proceedings of the American Society of Civil Engineers*. **100**: 1137-1156.
- Nakano, R. 1970. On weathering and change of properties of tertiary sedimentary rocks (mudstone) related to landslide. *Rock Mechanics in Japan*, **1**:71-73.
- Neuzil, C.E. 1986. Groundwater flow in low-permeability environments. *Water Resources Research*, **22**: 1163-1195.
- Neuzil, C.E. 1993. Low fluid pressure within the Pierre Shale: A transient response to erosion. *Water Resources Research*, **29**: 2007-2020.
- Neuzil, C.E. 1994. How permeable are clays and shales? *Water Resources Research*, **30**: 145-150.
- Neuzil, C.E. 1995. Characterization of flow properties, driving forces, and pore-water chemistry in the ultra-low-permeability Pierre Shale, North America. *Proceedings of an International Workshop on Hydraulic and Hydrochemical Characterization of Argillaceous Rocks*, Nottingham, p.65-74.
- Nichols, T.C., Collins, D.S., and Davidson, R.R. 1985. In situ and laboratory geotechnical tests of the Pierre Shale near Hayes, South Dakota – A characterization of engineering behaviour. *Canadian Geotechnical Journal*, **23**: 181-194.
- North, B.R. and Caldwell, W.G.E. 1975. Foraminiferal Faunas in the Cretaceous system of Saskatchewan. *The Cretaceous system in the Western Interior of North America*. Geological Association of Canada, Waterloo. pp. 303-331.
- OCanada.ca website. 2002. www.ocanada.ca
- Pejon, O.J. and Zuquette, L.V. 2002. Analysis of cyclic swelling of mudrocks. *Engineering Geology*, **67**: 97-108.
- Peterson, R. 1958. Rebound in the Bearpaw Shale, western Canada. *Bulletin of the Geological Society of America*, **69**: 1113-1124.
- Peterson, R., Jaspar, J.L., Rivard, P.J., and Iverson, N.L. 1960. Limitations of laboratory shear strength in evaluating stability of highly plastic clays. *American Society of Civil Engineers (Soil Mechanics and Foundation Division) Research Conference on Shear Strength of Cohesive Soils*, Boulder. pp. 765-791.
- Petley, D.J. 1984. Shear strength of over-consolidated fissured clay. *IV International Symposium on Landslides*, Toronto. **2**: 167-172.
- Prest, V.K. 1970. Chapter 8 of Geology of Western Canada. *Geology and Economic Minerals of Canada*. Geological Survey of Canada, Ottawa. pp. 676-764.

- Propescu, M.E. 1997. General co-report session 4: Slope stability and protection. *Geotechnical Engineering of Hard Soils – Soft Rocks*, Balkema, Rotterdam. 3: 1985-2006.
- Reader's Digest Association. 1981. [map] *Atlas of Canada*. The Reader's Digest Association (Canada) Ltd., Montreal.
- Ries, H. and Keele, J. 1912. Preliminary report on the clay and shale deposits of the western Provinces. *Geological Survey of Canada Memoir 24-E*. 231 p.
- Sauer, E.K. 1983. The Denholm landslide, Saskatchewan. Part II: analysis. *Canadian Geotechnical Journal*, **20**: 208-220.
- Scarpelli, G. and Calabresi, G. 1984. A typical earthflow in a weathered clay at Todi. *IV International Symposium on Landslides*, University of Toronto Press, Toronto. 3: 119-121.
- Schaefer, V.R. 2002. Residual strength and back analysis of slopes in Pierre Shale. *The Third International Conference on Landslides, Slope Stability and the Safety of Infrastructures*, Singapore. pp. 87-96.
- Schaefer, V.R. and Lohnes, R.A. 2001. Landslide failure mechanisms in Pierre Shale, South Dakota, U.S.A. *International Conference on Landslides – Causes, Impacts and Countermeasures*, Davos. pp. 87- 96.
- Schmertmann, J.H. and Osterberg, J.O. 1960. An experimental study of the development of cohesion and friction with axial strain in saturated cohesive soils. *ASCE Research Conference on Shear Strength of Cohesive Soils*, Boulder. pp. 643-692.
- Scott, J.S. and Brooker, E.W. 1966. Geological and engineering aspects of upper Cretaceous shales in western Canada. *Geological Survey of Canada Paper 66-37*. 75 p.
- Skempton, A.W. 1964. Long-term stability of clay slopes. *Geotechnique*, **14**: 77-101.
- Skempton, A.W. 1985. Residual strength of clays in landslides, folded strata and the laboratory. *Geotechnique*, **35**: 3-18.
- Stott, D.F. and Aitken, J.D. (editors). 1993. *Sedimentary Cover of the Craton in Canada*. Geological Survey of Canada, Ottawa. 863 p.
- Terzaghi, K.V. 1936. Stability of slopes in natural clay. *Proceedings of the First International Conference on Soil Mechanics and Foundation Engineering*, **1**: 161-165.
- Thomson, S. and Hayley, D.W. 1975. The Little Smoky landslide. *Canadian Geotechnical Journal*, **12**: 379-392.
- Thomson, S. and Morgenstern, N.R. 1978. Landslides in argillaceous rock, prairie provinces, Canada. Chapter 14 in *Rockslides and Avalanches, 2: Engineering Sites, Developments in Geotechnical Engineering*, **14B**: 515-540.
- Travel Manitoba website. www.travelmanitoba.com

- Tweedie, R.W. 1976. *An investigation of the Edgerton landslide, Wainright, Alberta*. Master of Science Thesis, University of Alberta. 139 p.
- Tyrell, J.B. 1890. Cretaceous of Manitoba. *American Journal of Science*, **140**: 227-232.
- Tyrell, J.B. 1892. North-western Manitoba with portions of the districts of Assiniboia and Saskatchewan. *Geological Survey of Canada Annual Report 5, part E*. pp. 5-235.
- Wallace, R.C. 1925. *The geological formations of Manitoba*. The Natural History Society of Manitoba. 58 p.
- Wolfe, B. and Teller, J.T. 1995. Sedimentation in ice-dammed glacial Lake Assiniboine, Saskatchewan, and catastrophic drainage down the Assiniboine valley. *Geographie Physique et Quaternaire*, **49**: 251-263.
- Wickenden, R.T.D. 1945. Mesozoic stratigraphy of the eastern plains, Manitoba and Saskatchewan. *Geological Survey of Canada Memoir 239*. 87 p.
- Wong, R.C.K. 1998. Swelling and softening behaviour of La Biche shale. *Canadian Geotechnical Journal*, **35**: 206-221.
- Wood, D.M. 1990. *Soil behaviour and critical state soil mechanics*. Cambridge University Press, Cambridge. 462 p.
- Wu, T.H. 1996. Soil strength properties and their measurement. Chapter 12 in *Landslides Investigation and Mitigation, Transportation Research Board Special Report 247*, National Research Council, Washington. pp. 319-336.

Appendix A

Field Investigation

borehole profiles
slope inclinometer profiles
enlarged sections

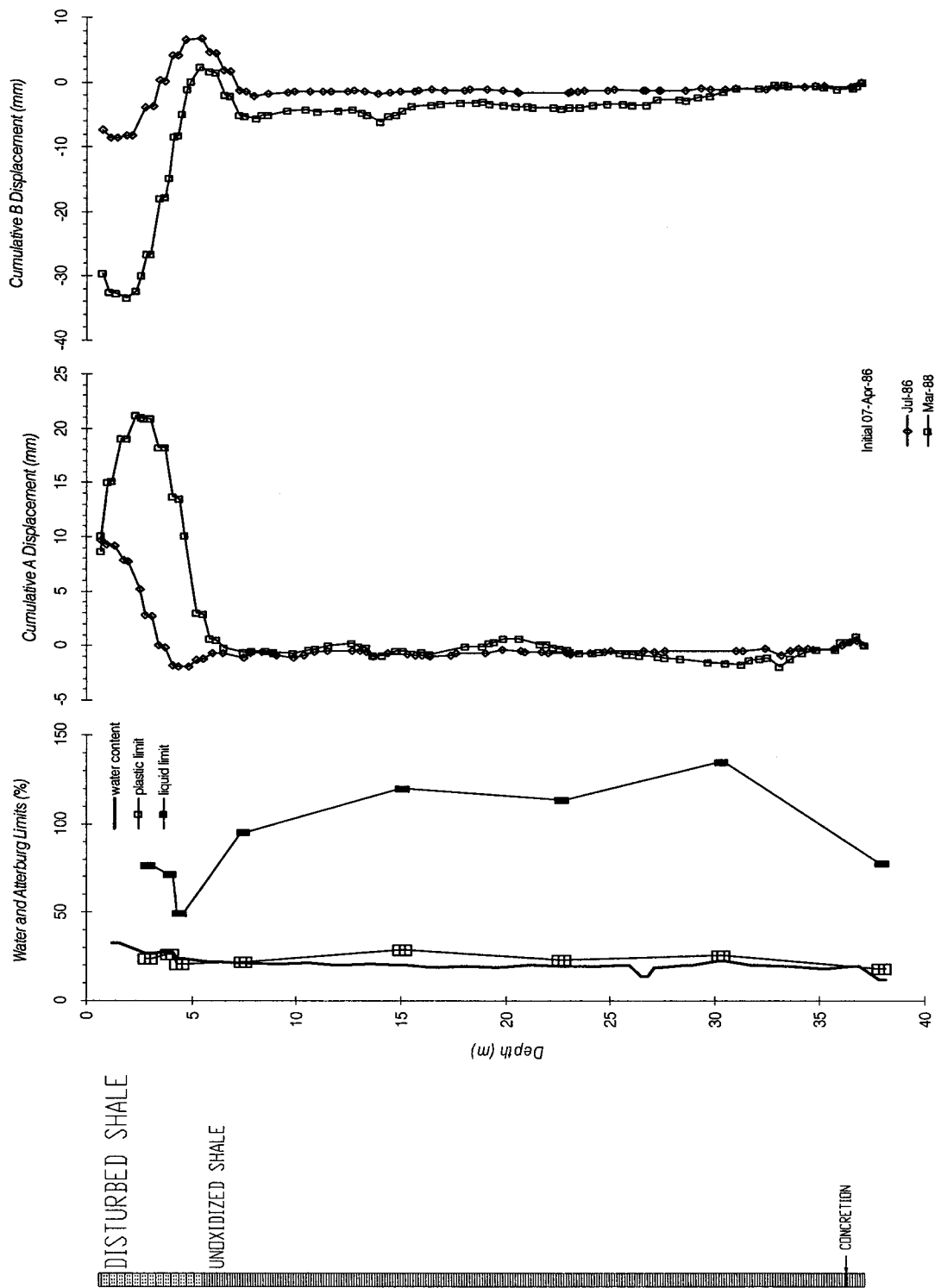


Figure A-1: Profile of BH302.

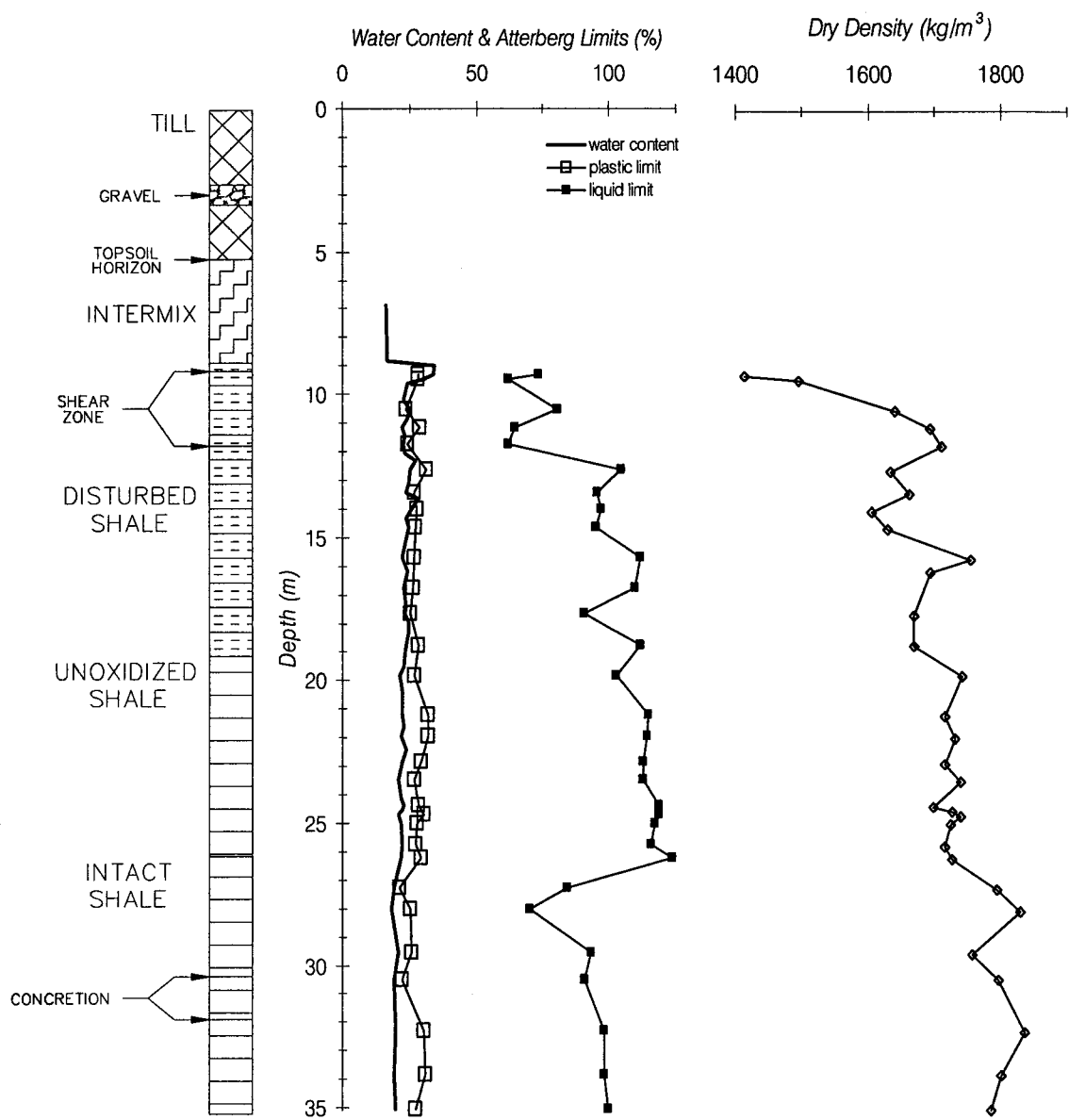


Figure A-2: Profile of BH704.

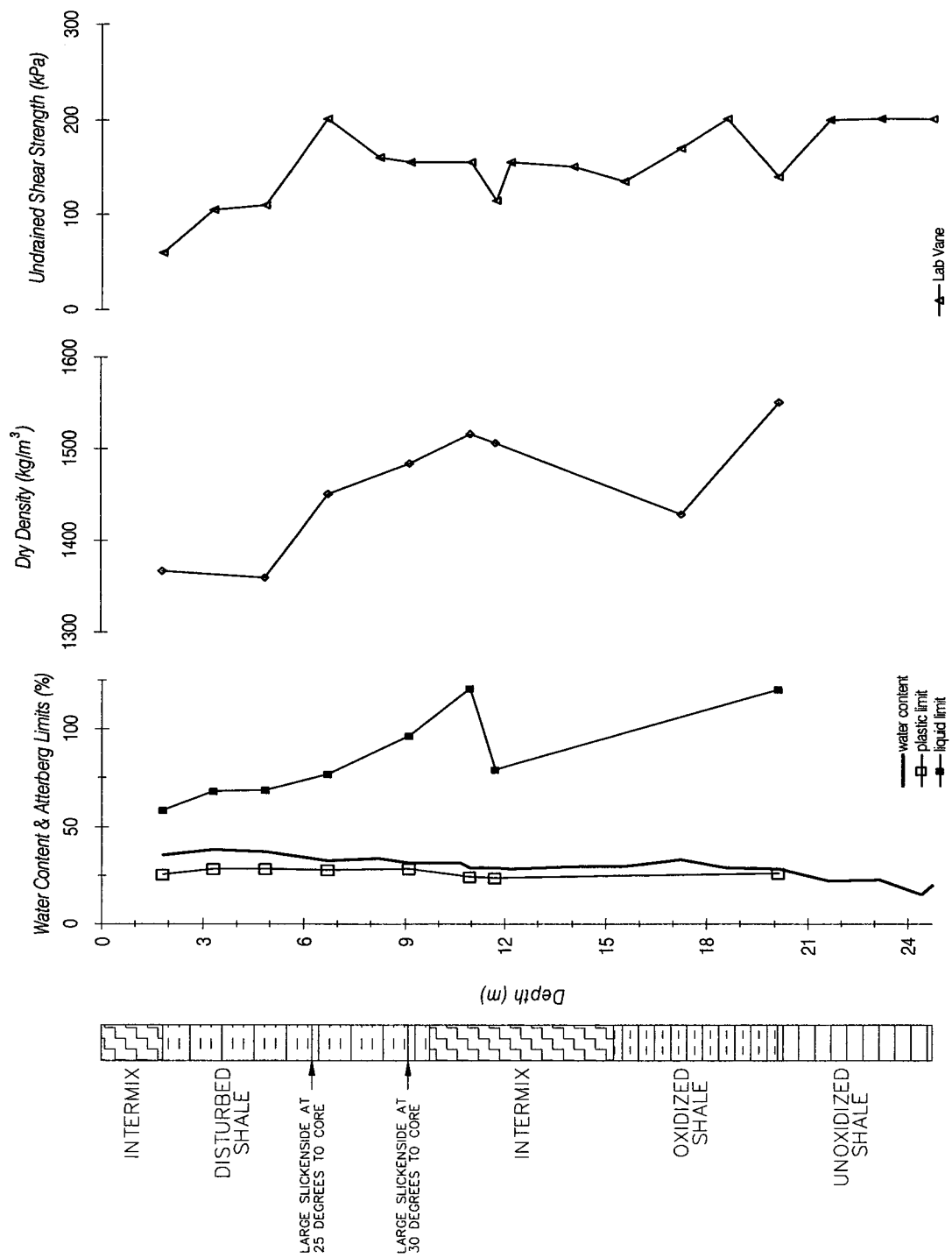


Figure A-3: Profile of BH814.

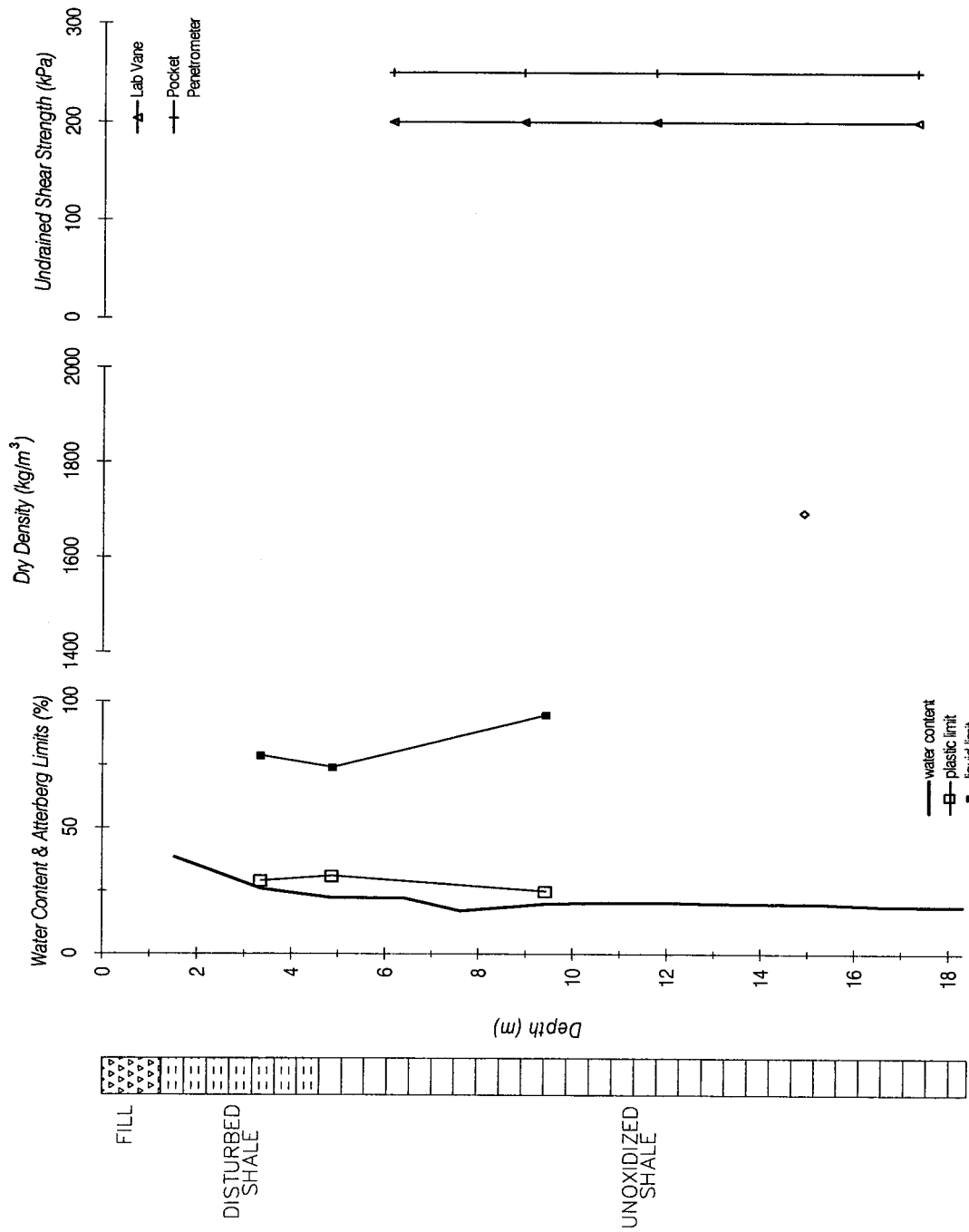


Figure A-4: Profile of BH815.

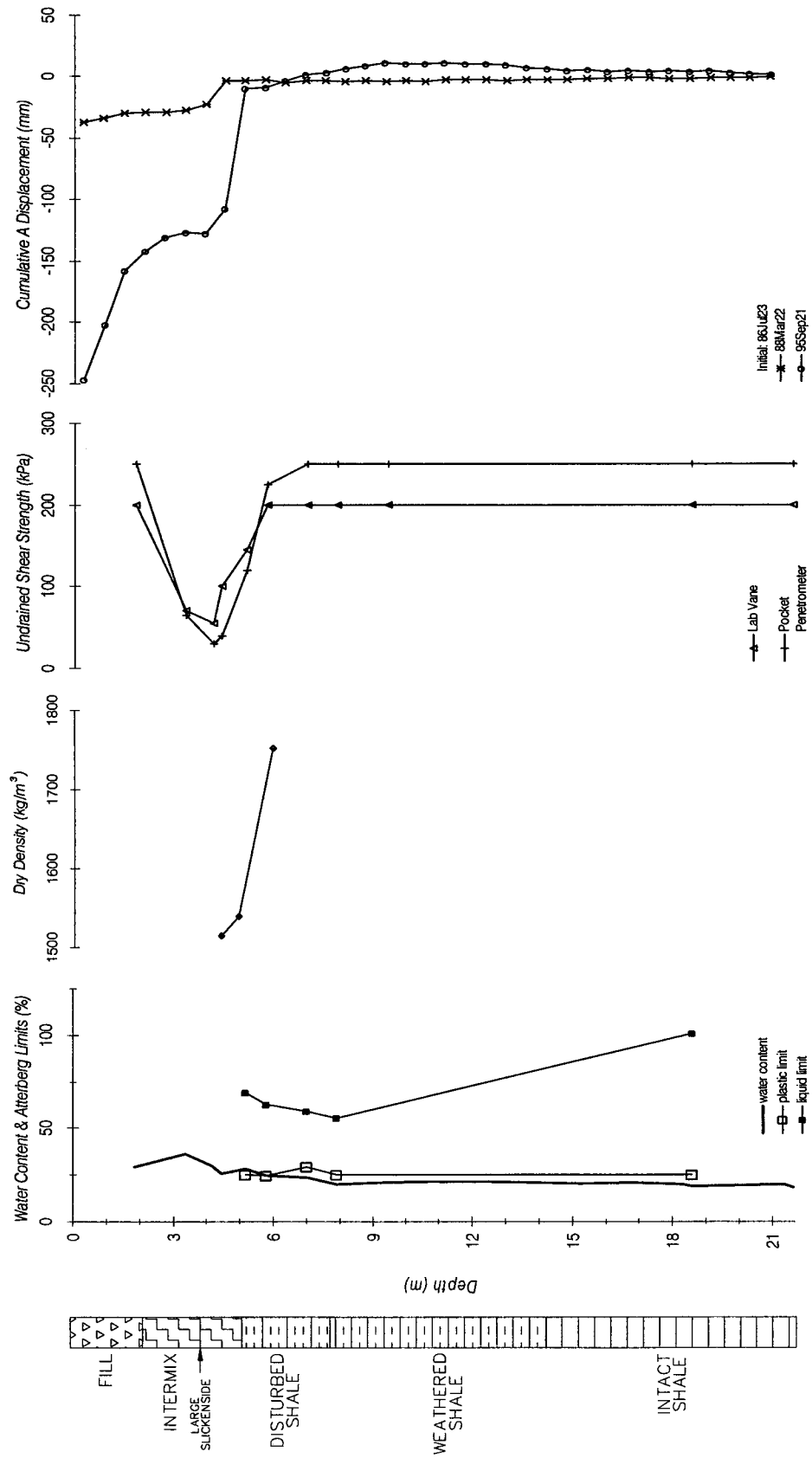


Figure A-5: Profile of BH834.

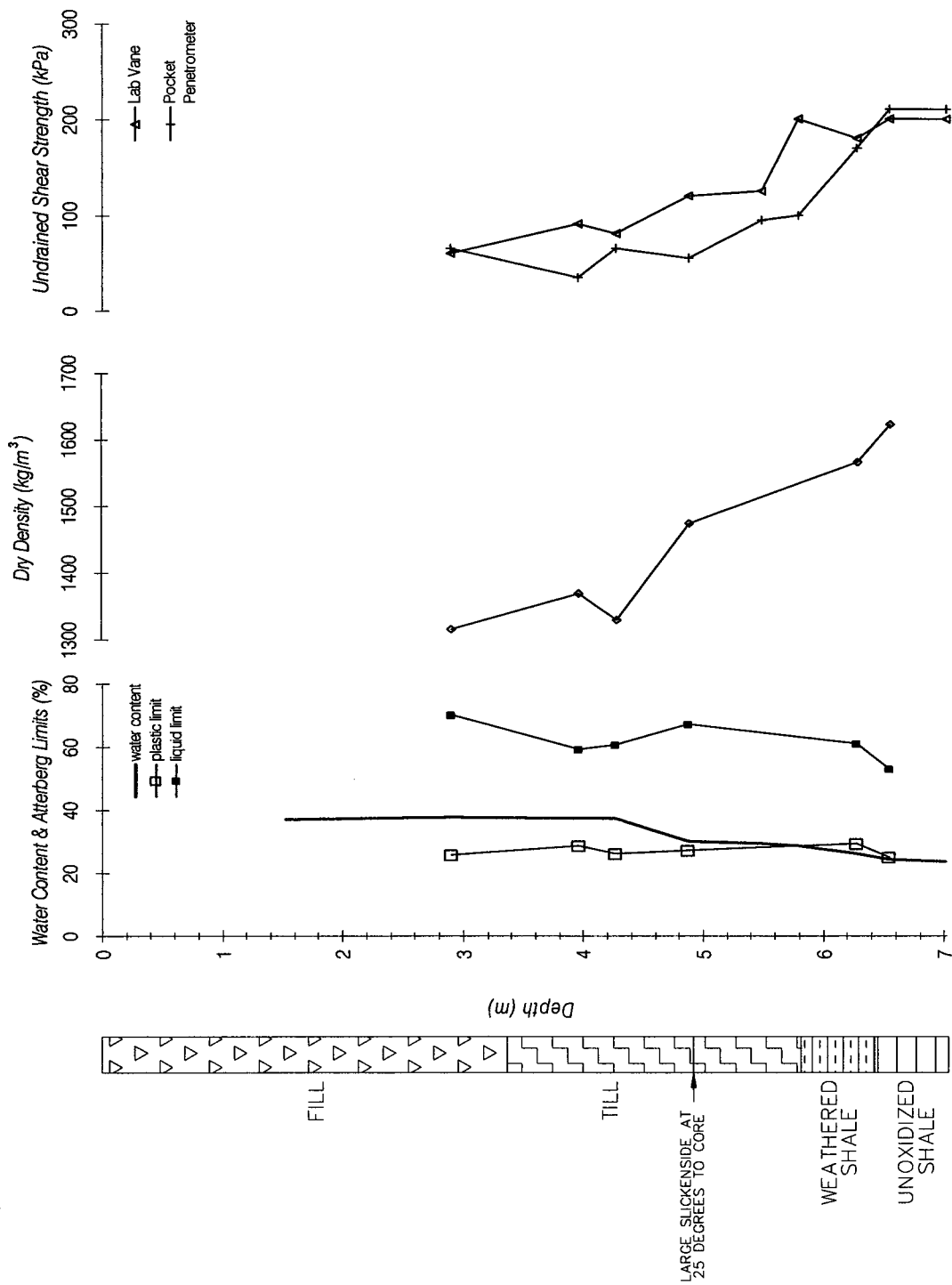


Figure A-6: Profile of BH834A.

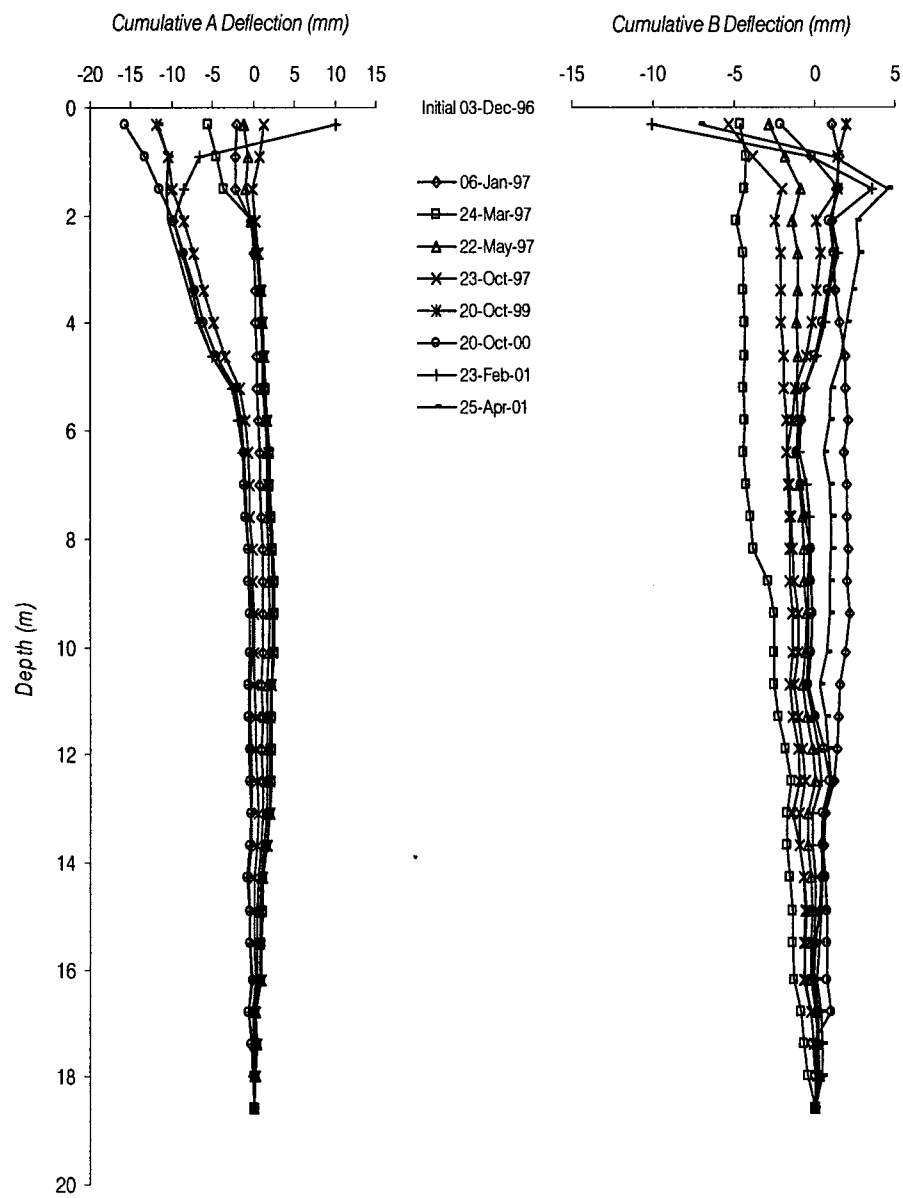


Figure A-7: Profile of BH901.

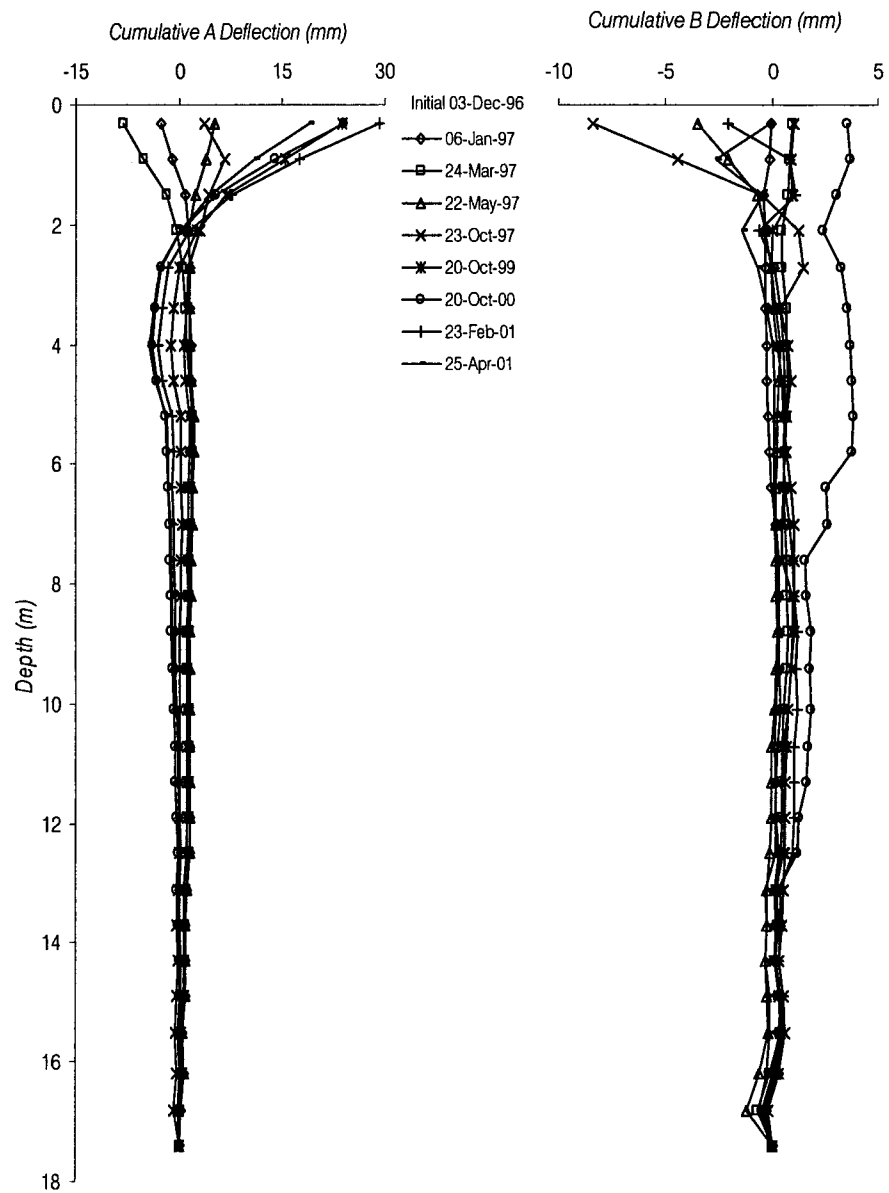


Figure A-8: Profile of BH902.

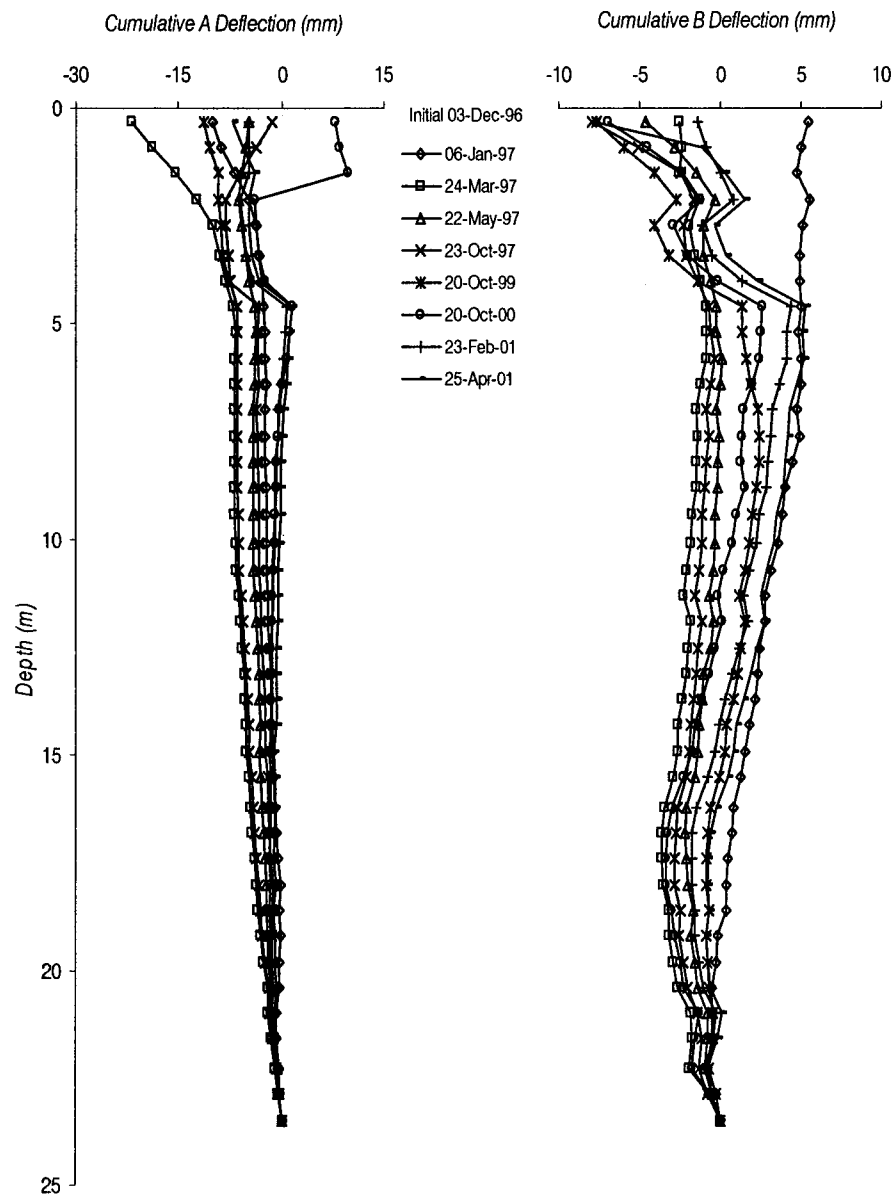


Figure A-9: Profile of BH903.

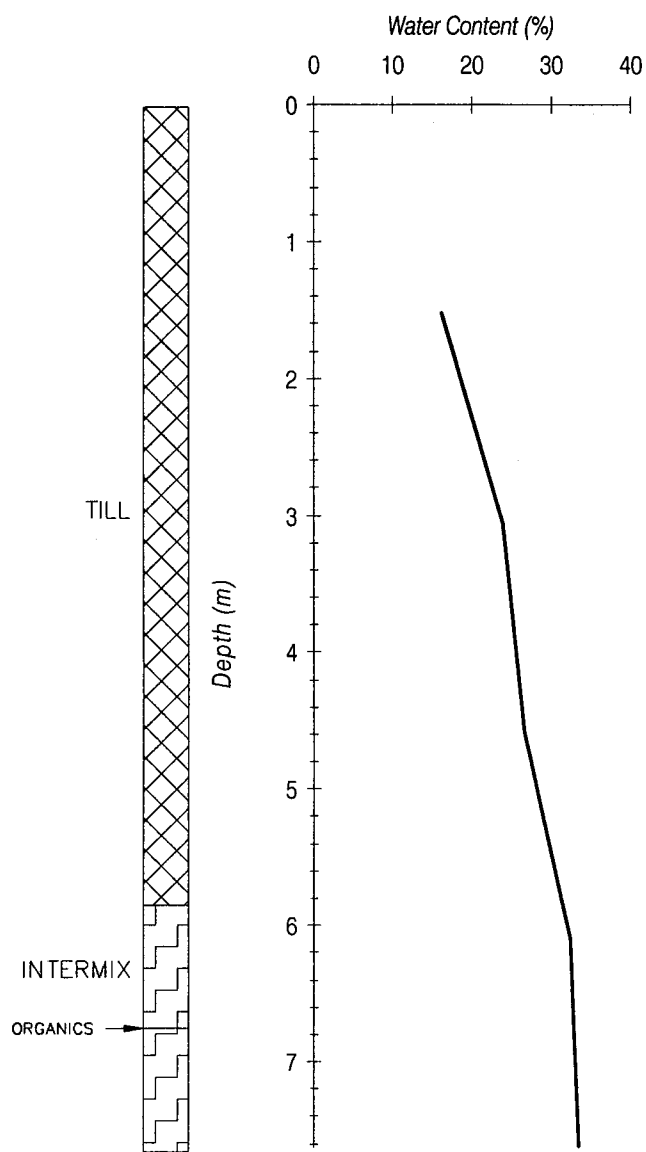


Figure A-10: Profile of BH915.

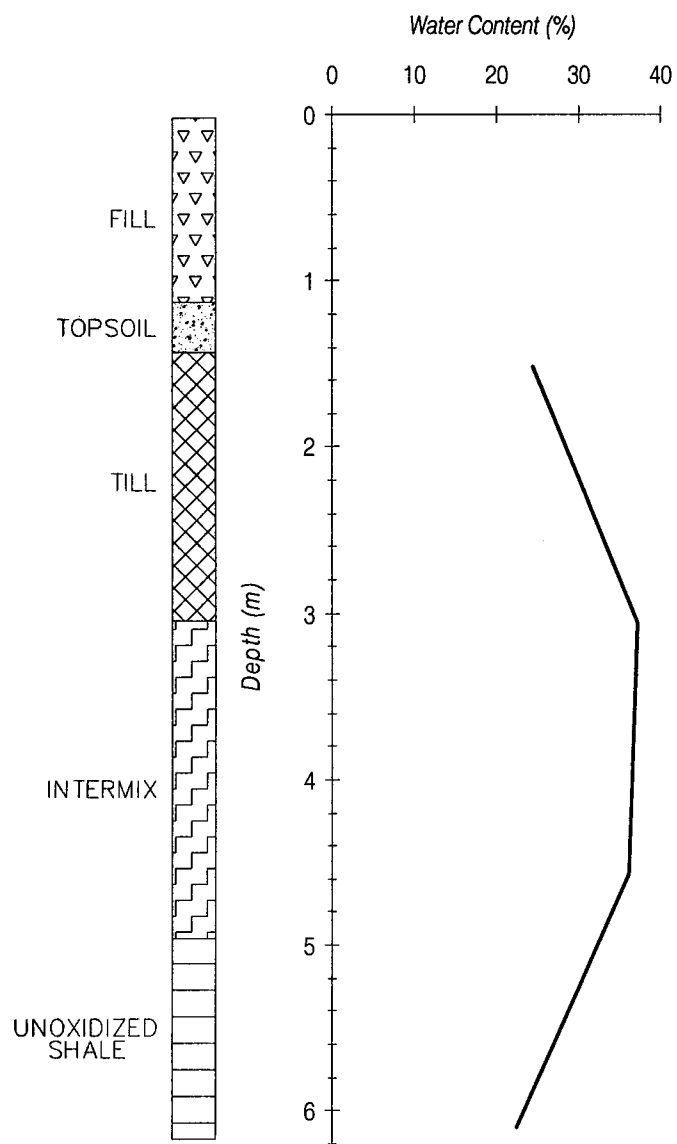


Figure A-11: Profile of BH916.

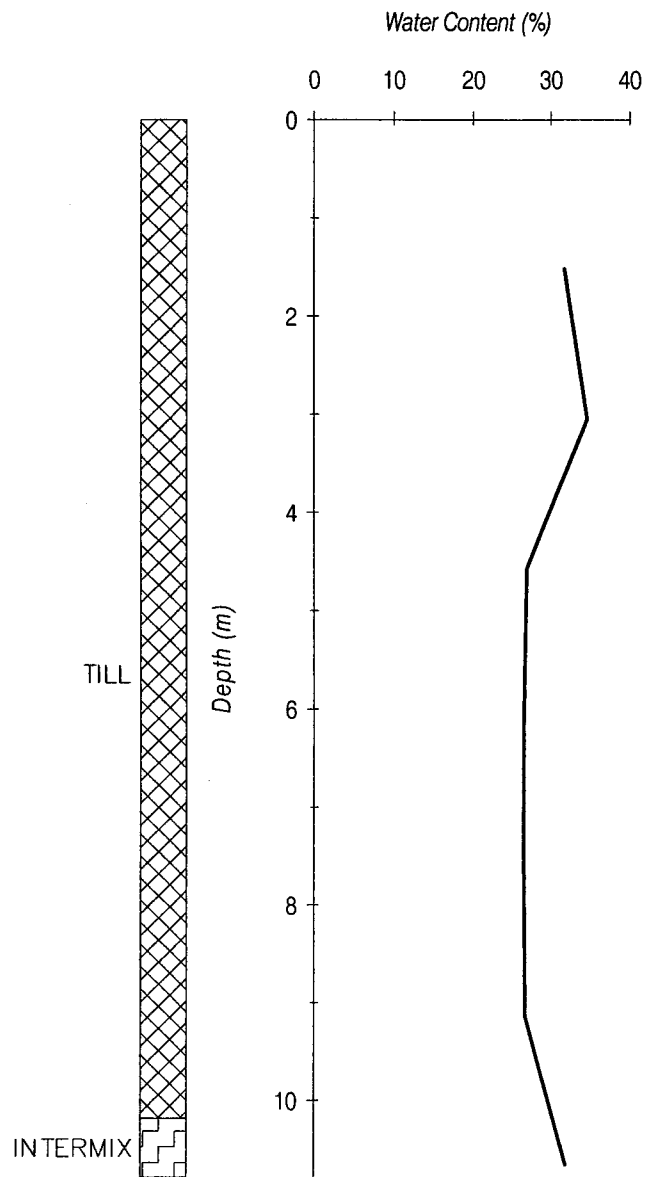


Figure A-12: Profile of BH918.

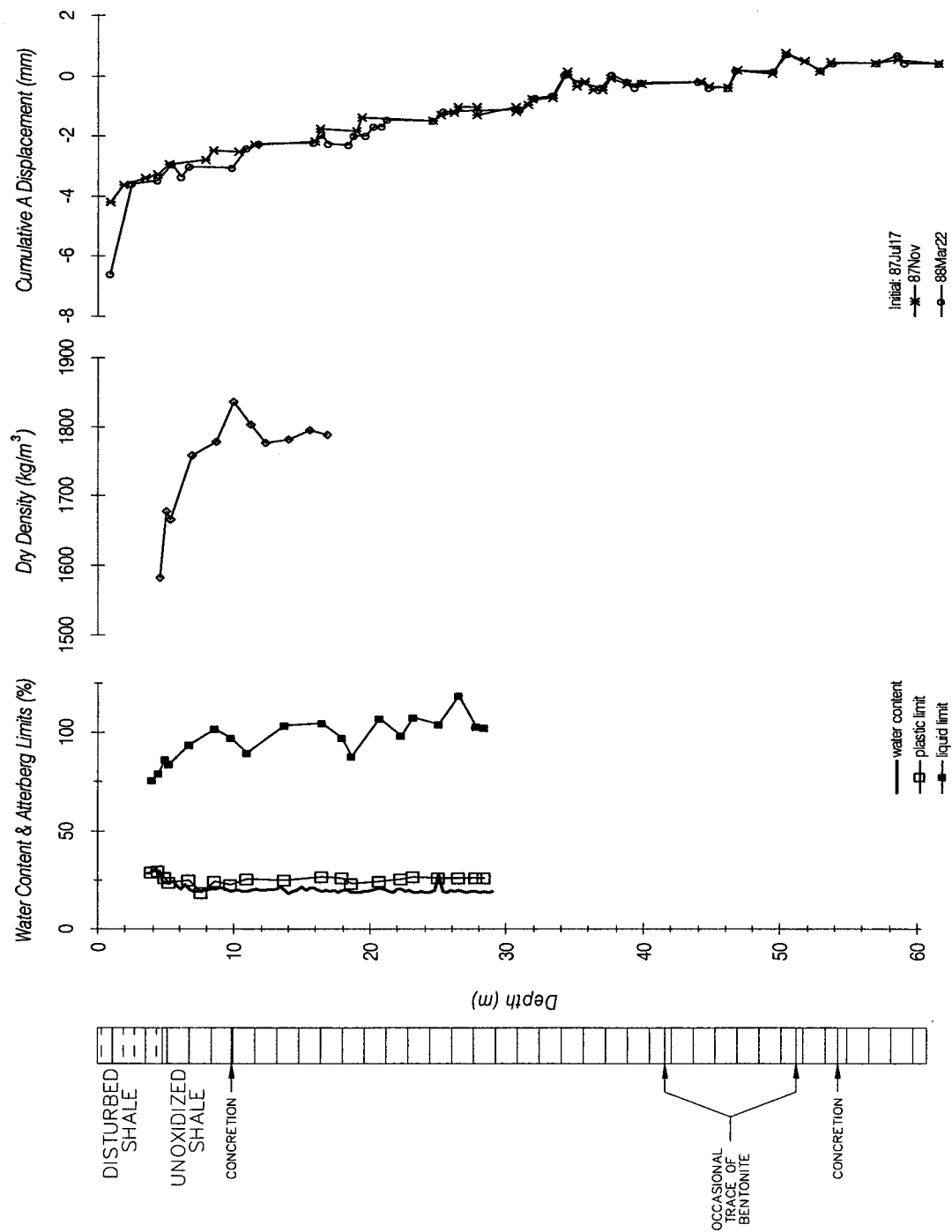


Figure A-13: Profile of BH923.

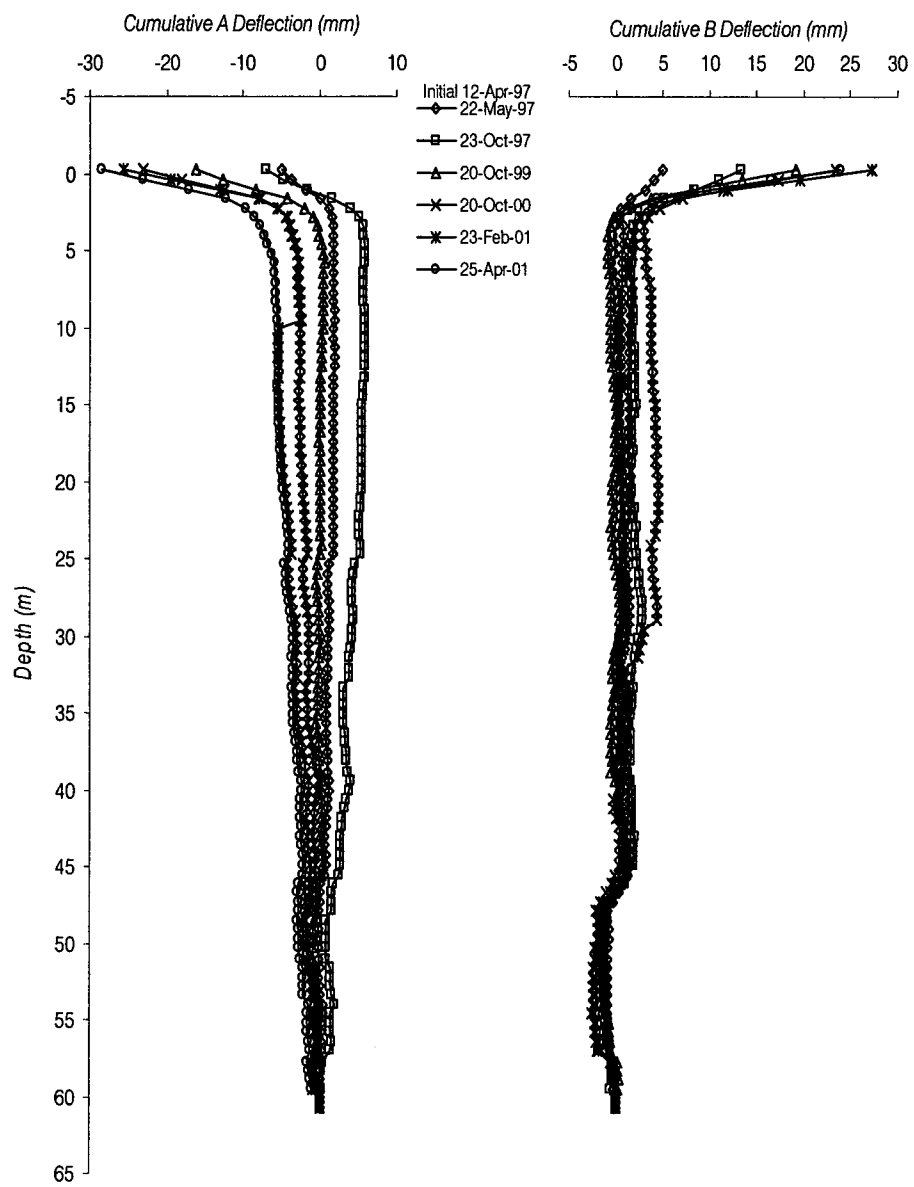


Figure A-14: Profile of BH1001.

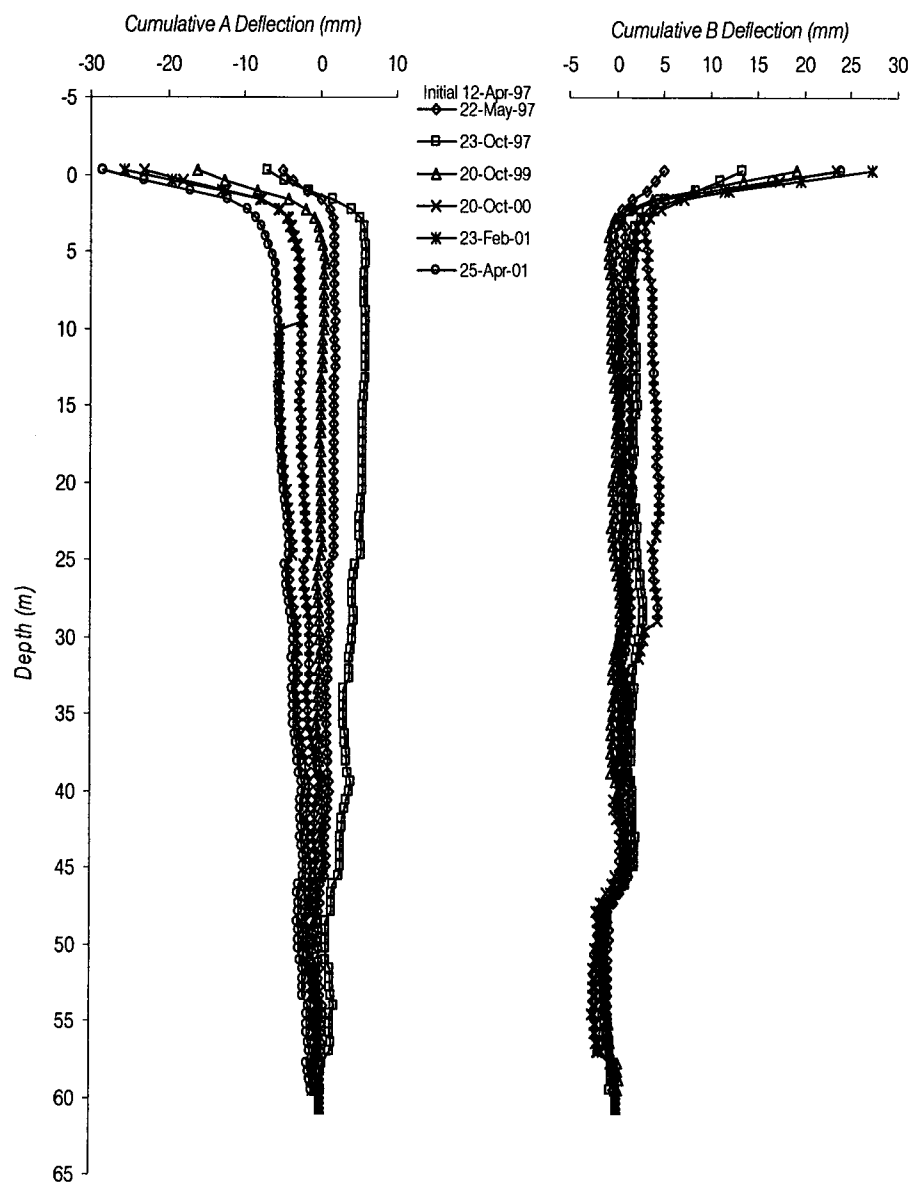


Figure A-15: Profile of BH1002.

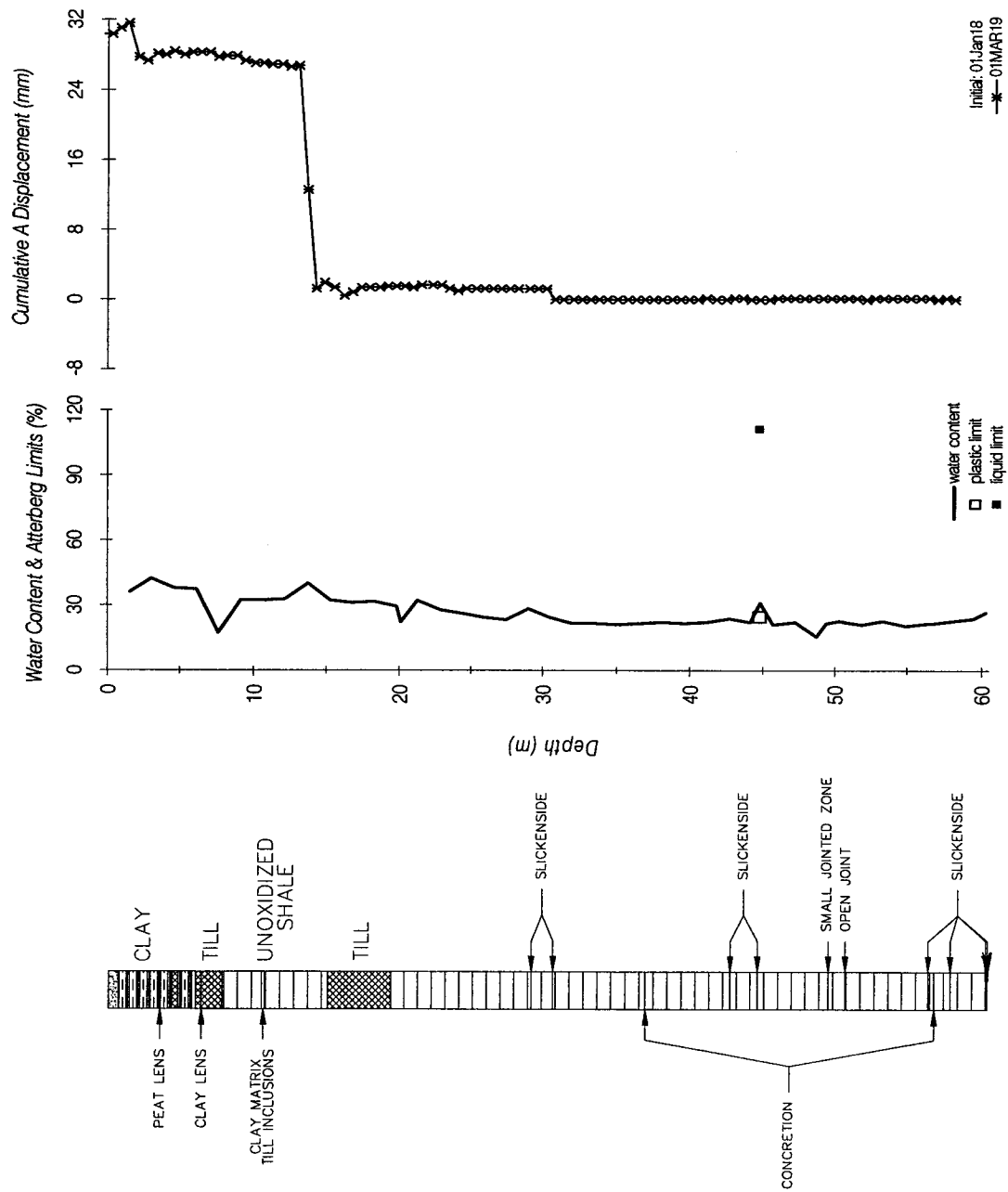


Figure A-16: Profile of SI1101.

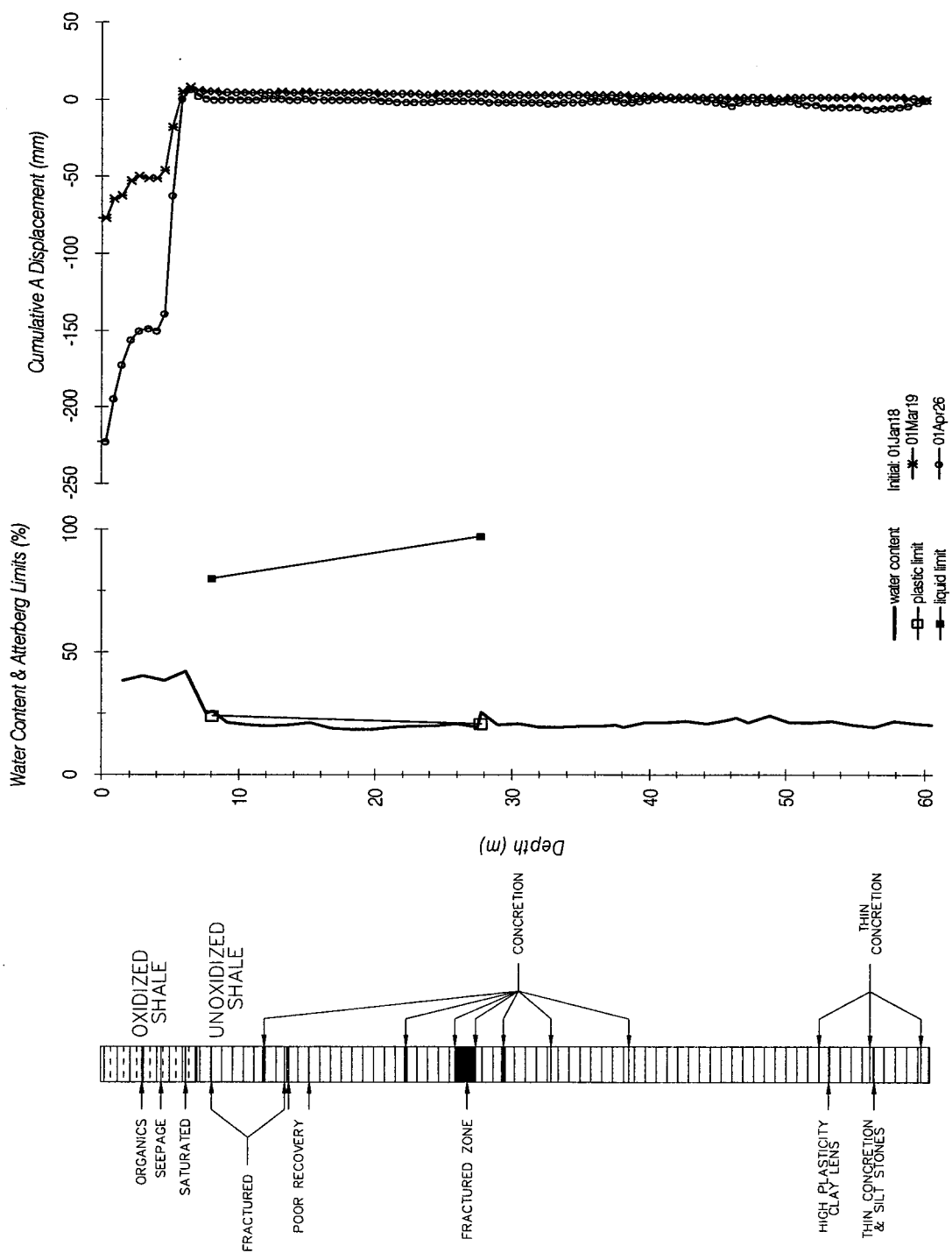


Figure A-17: Profile of S11108.

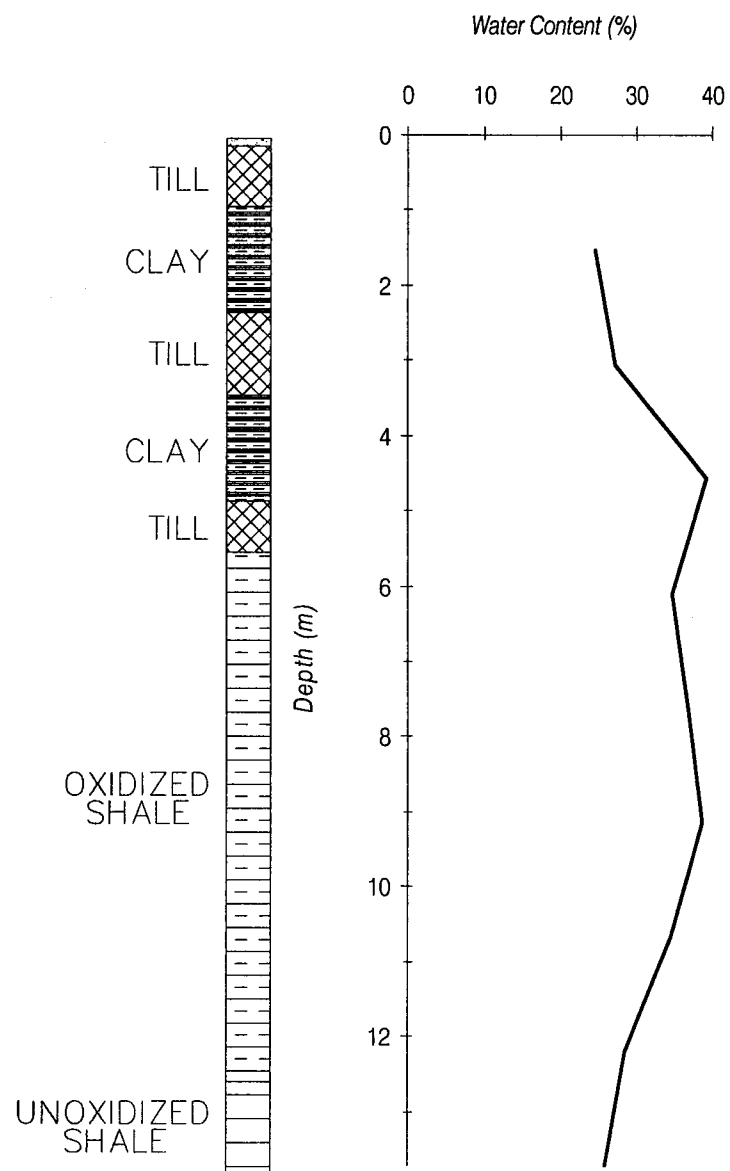


Figure A-18: Profile of BH1109.

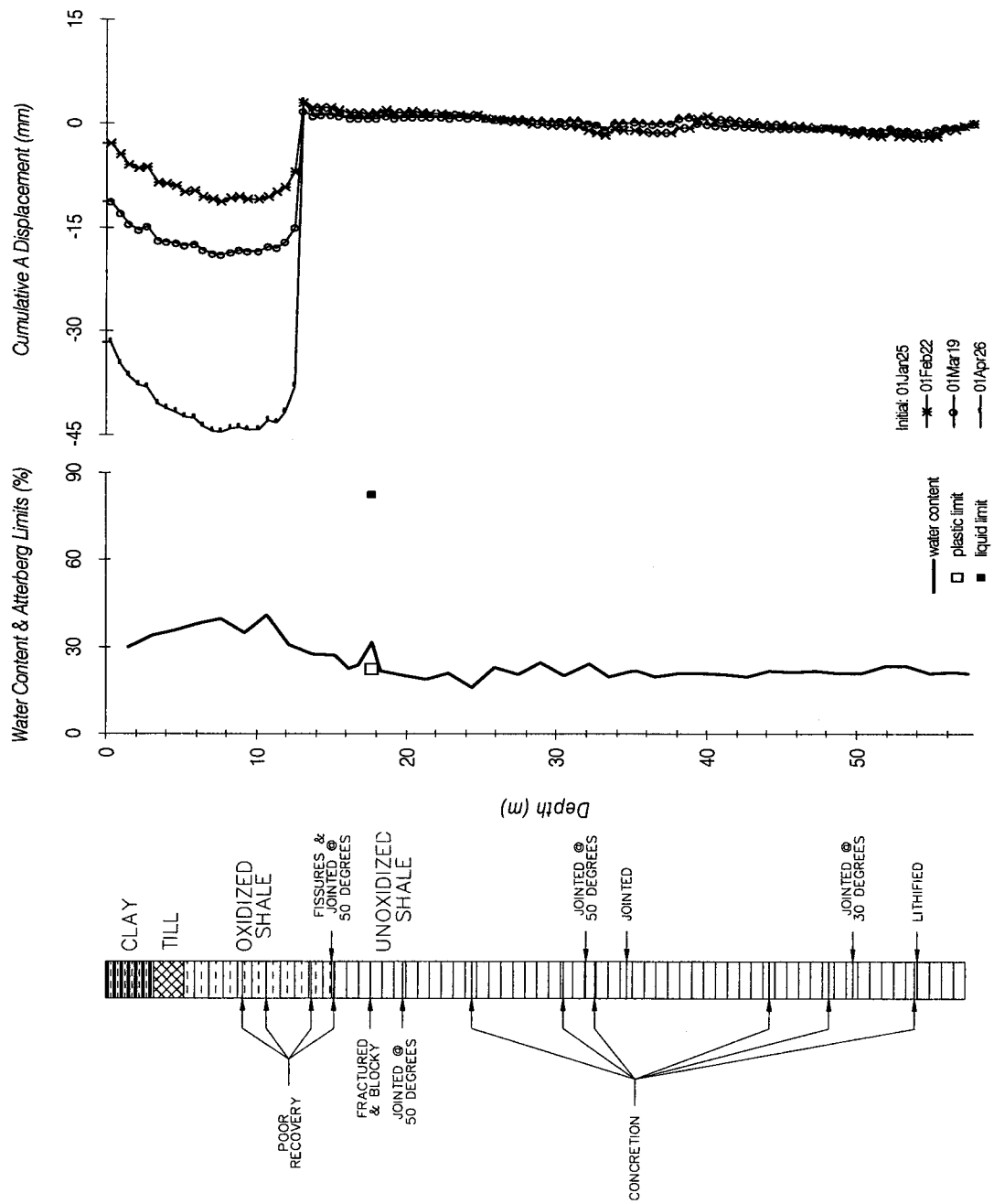


Figure A-19: Profile of S11109.

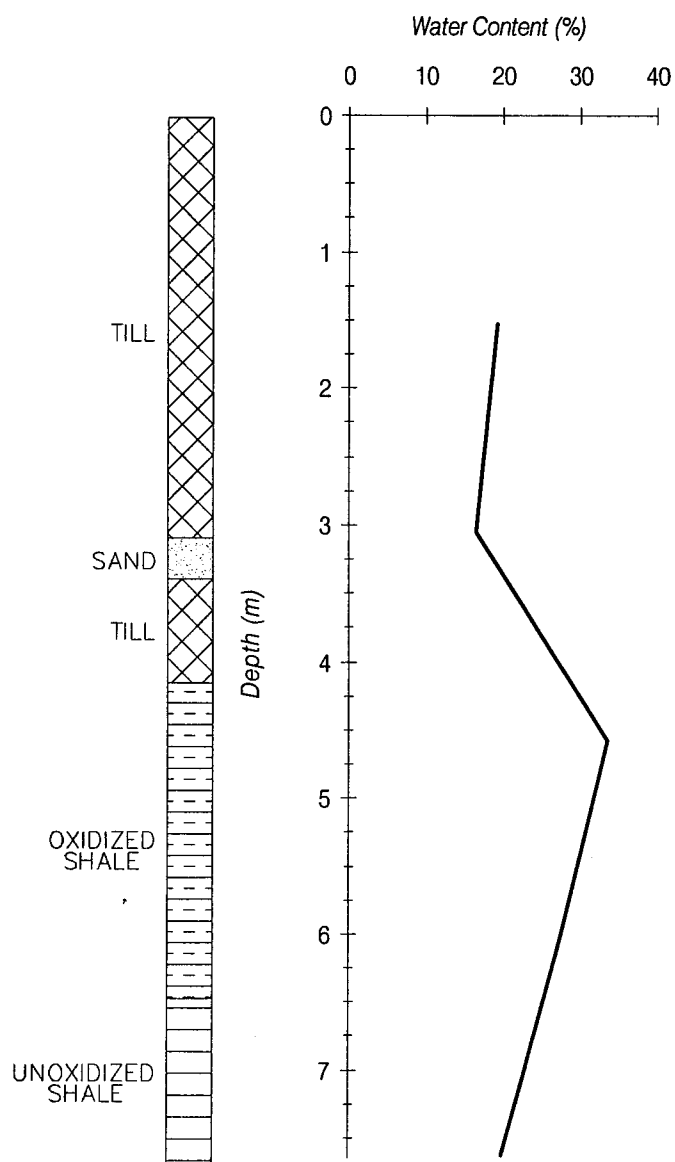


Figure A-20: Profile of BH1110.

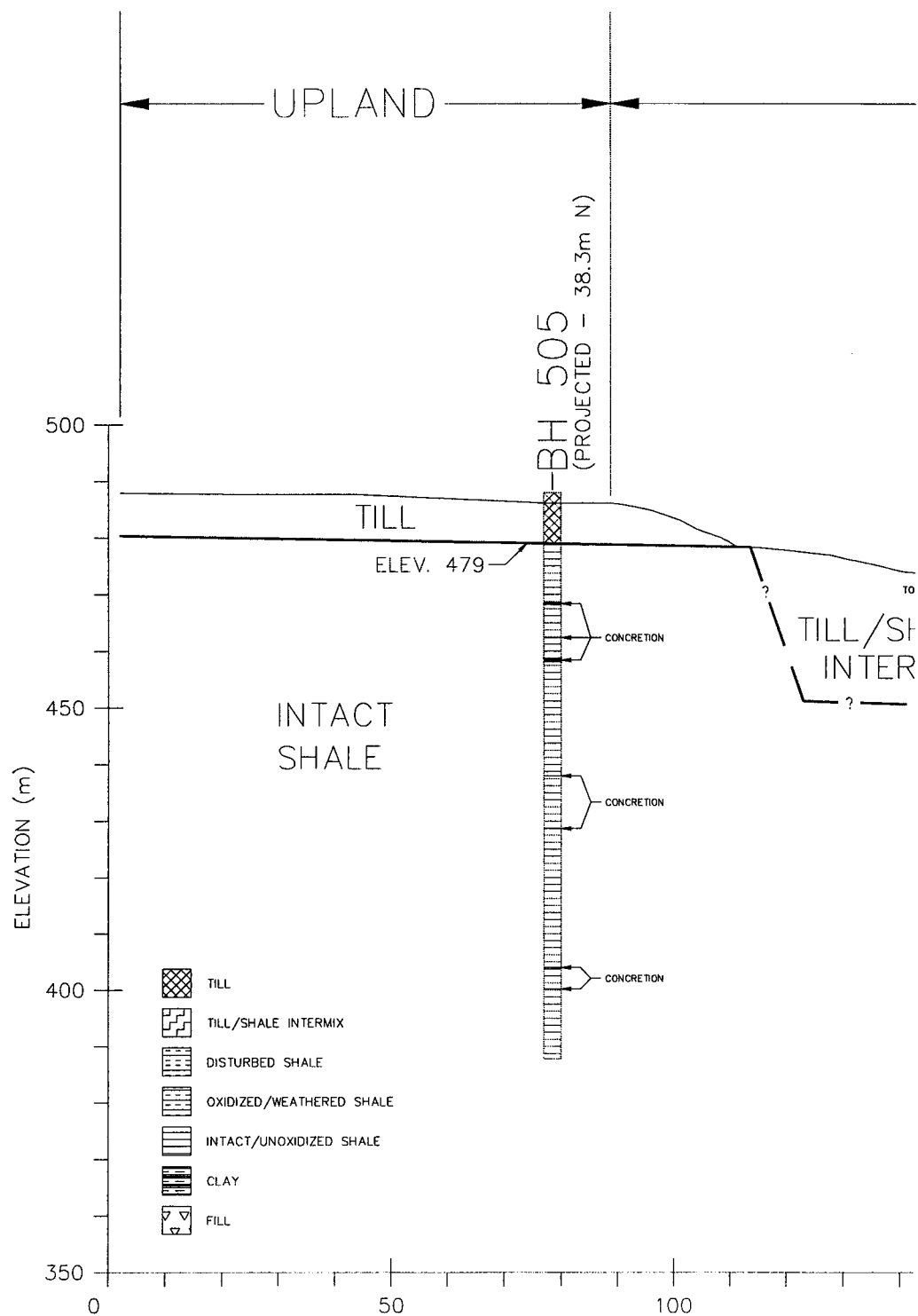


Figure A-21a: Enlarged section of the stratigraphic interpretation of Figure 4-11.

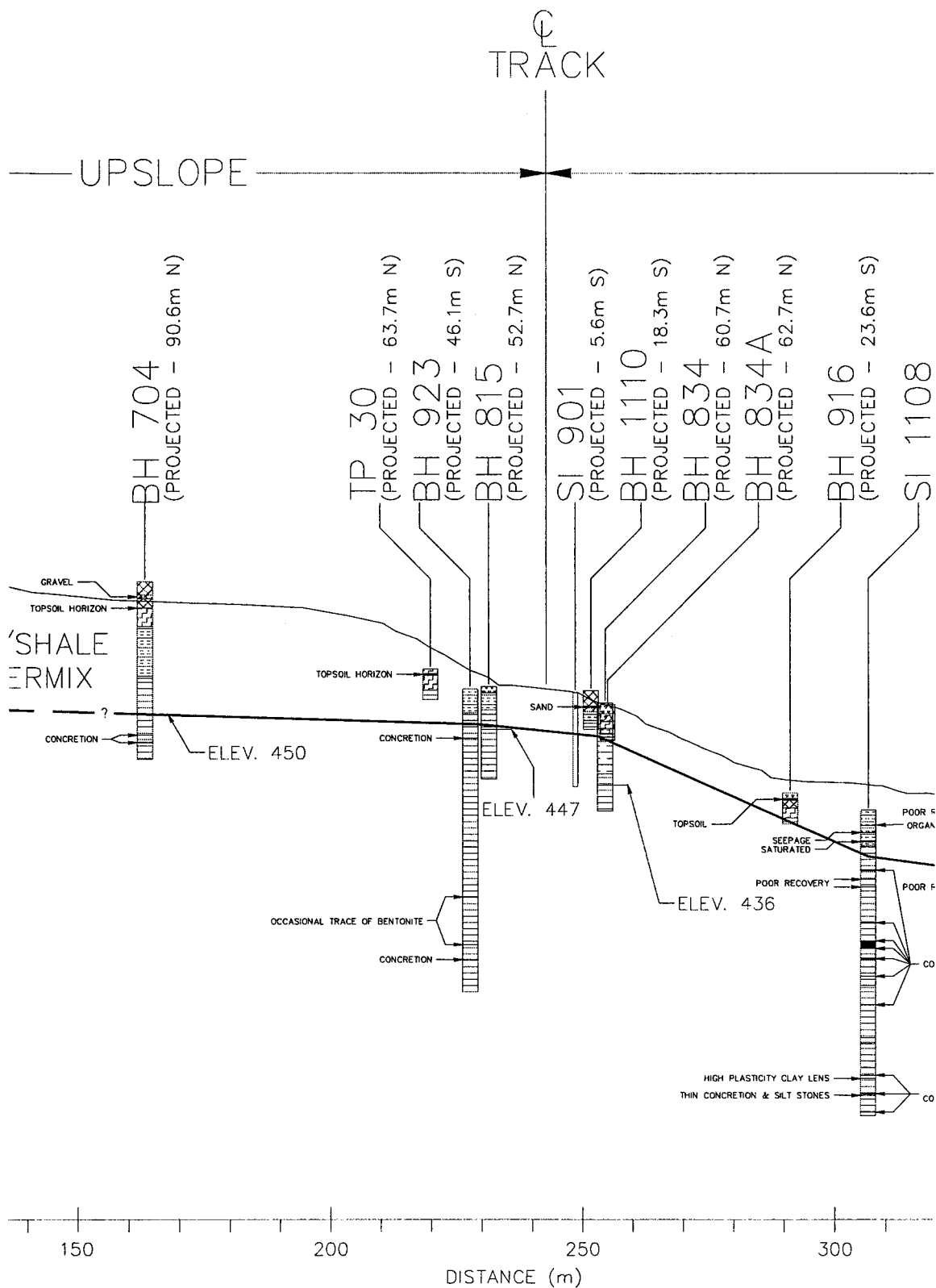


Figure A-21b: Enlarged section of the stratigraphic interpretation Figure 4-11 (cont.).

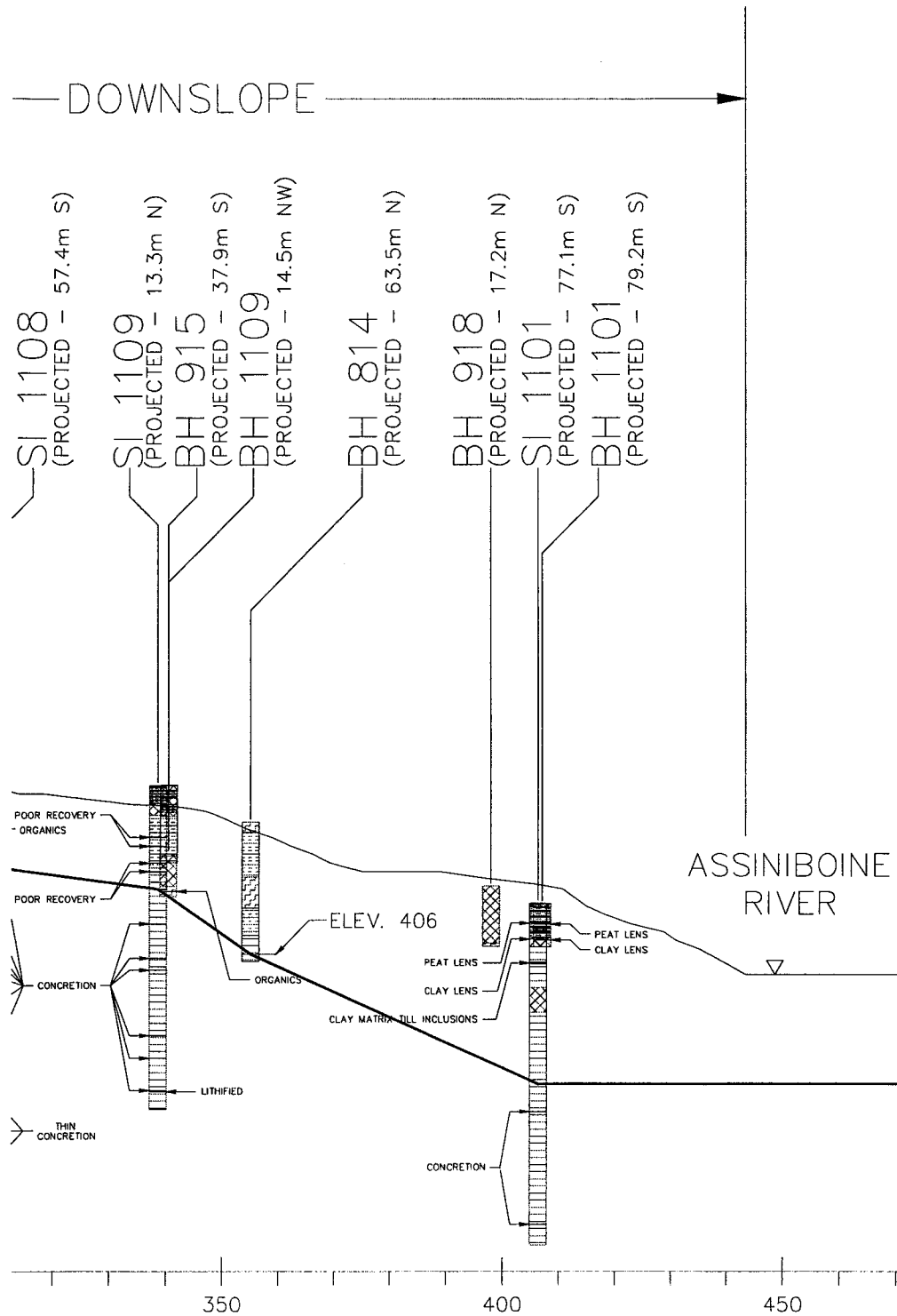


Figure A-21c: Enlarged section of the stratigraphic interpretation Figure 4-11 (cont.).

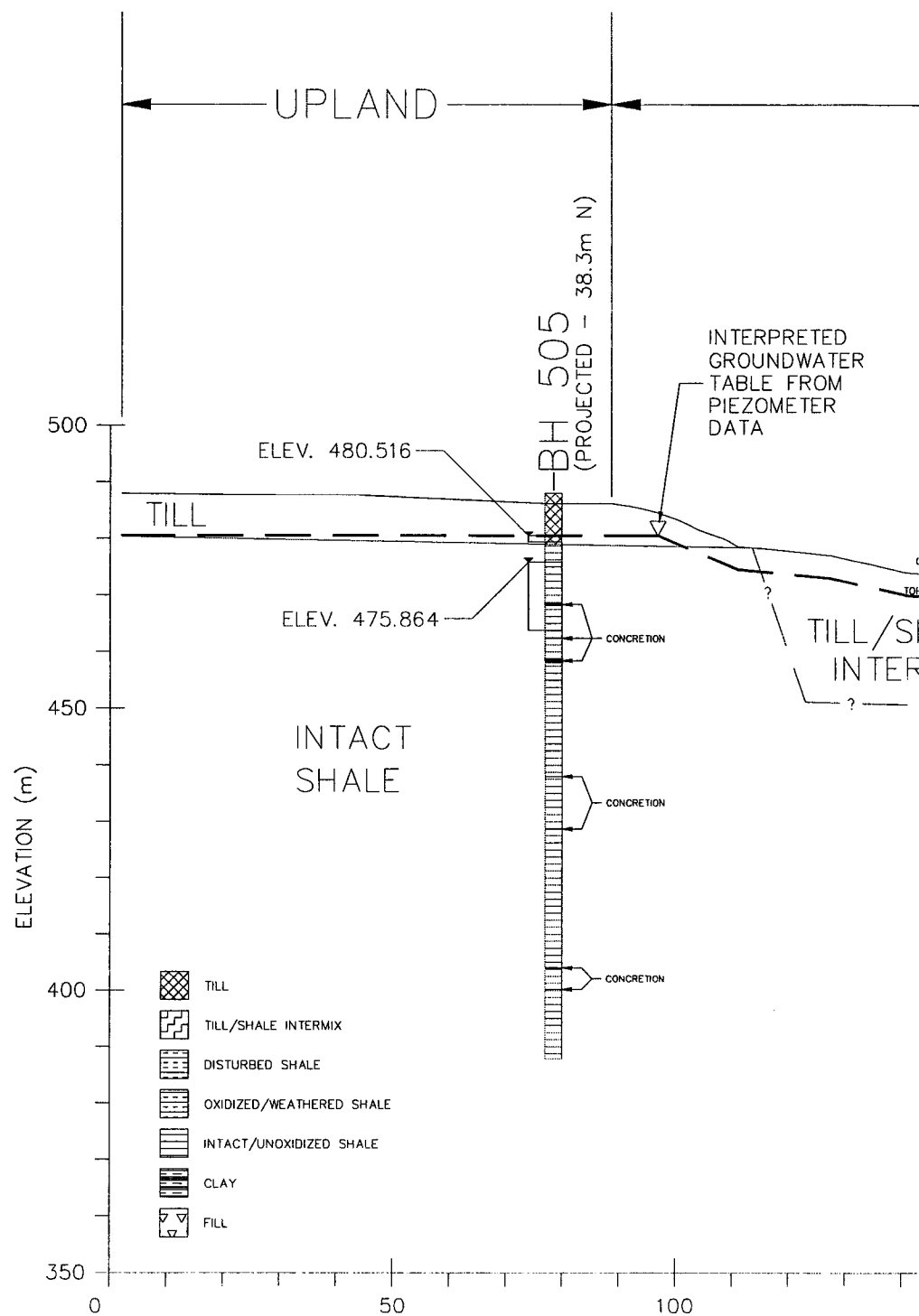


Figure A-22a: Enlarged section of the groundwater conditions of Figure 4-15.

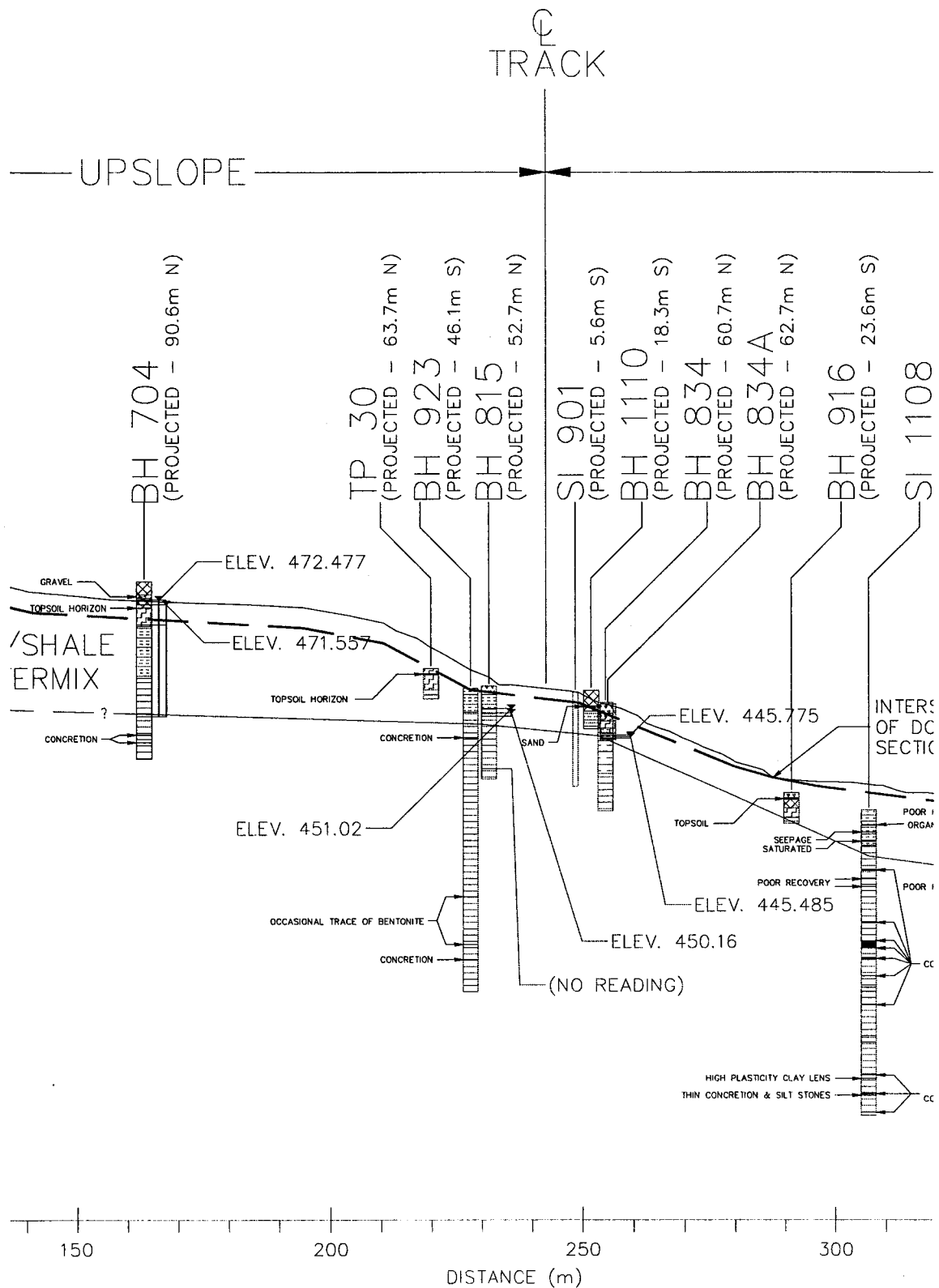


Figure A-22b: Enlarged section of the groundwater conditions of Figure 4-15 (cont.).

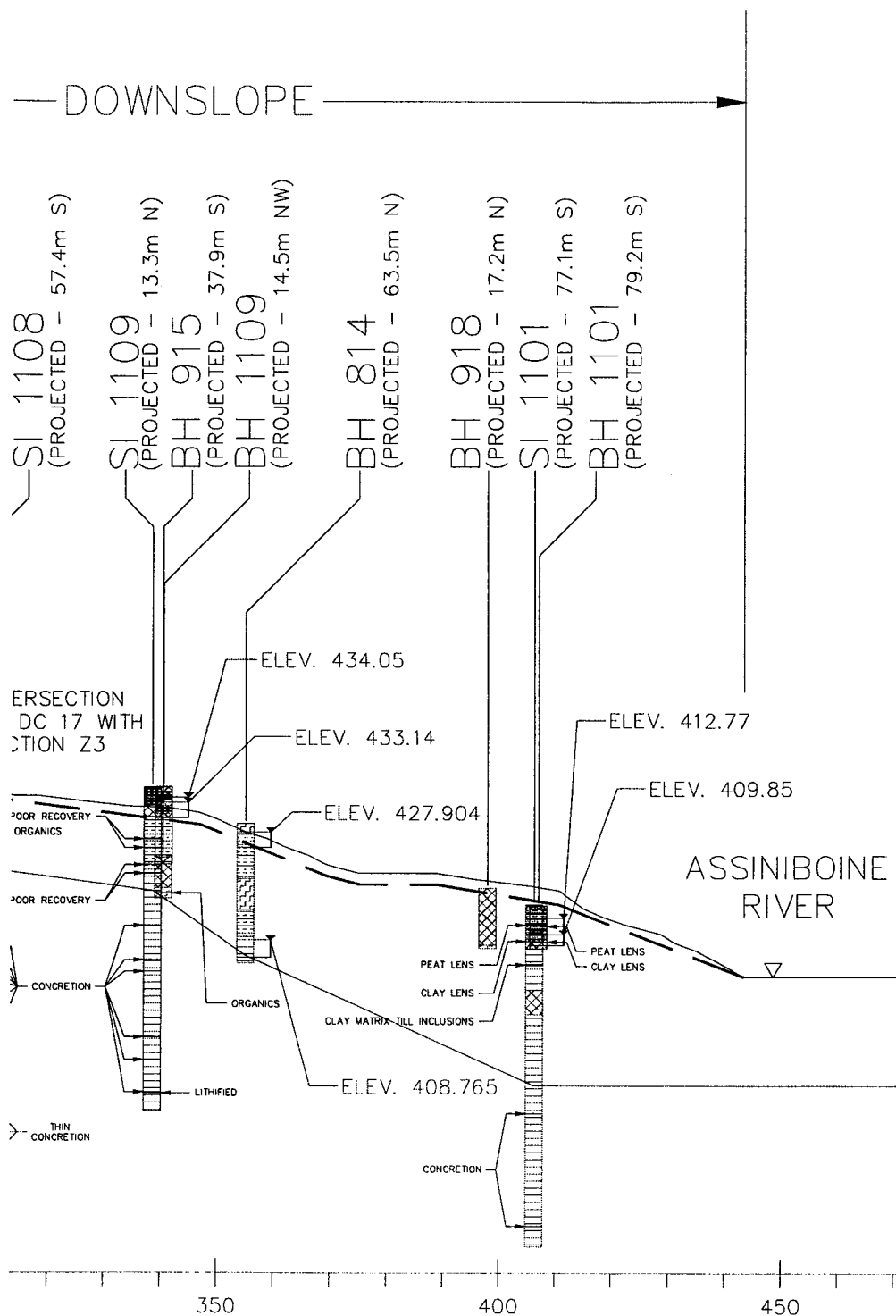


Figure A-22c: Enlarged section of the groundwater conditions of Figure 4-15 (cont.).

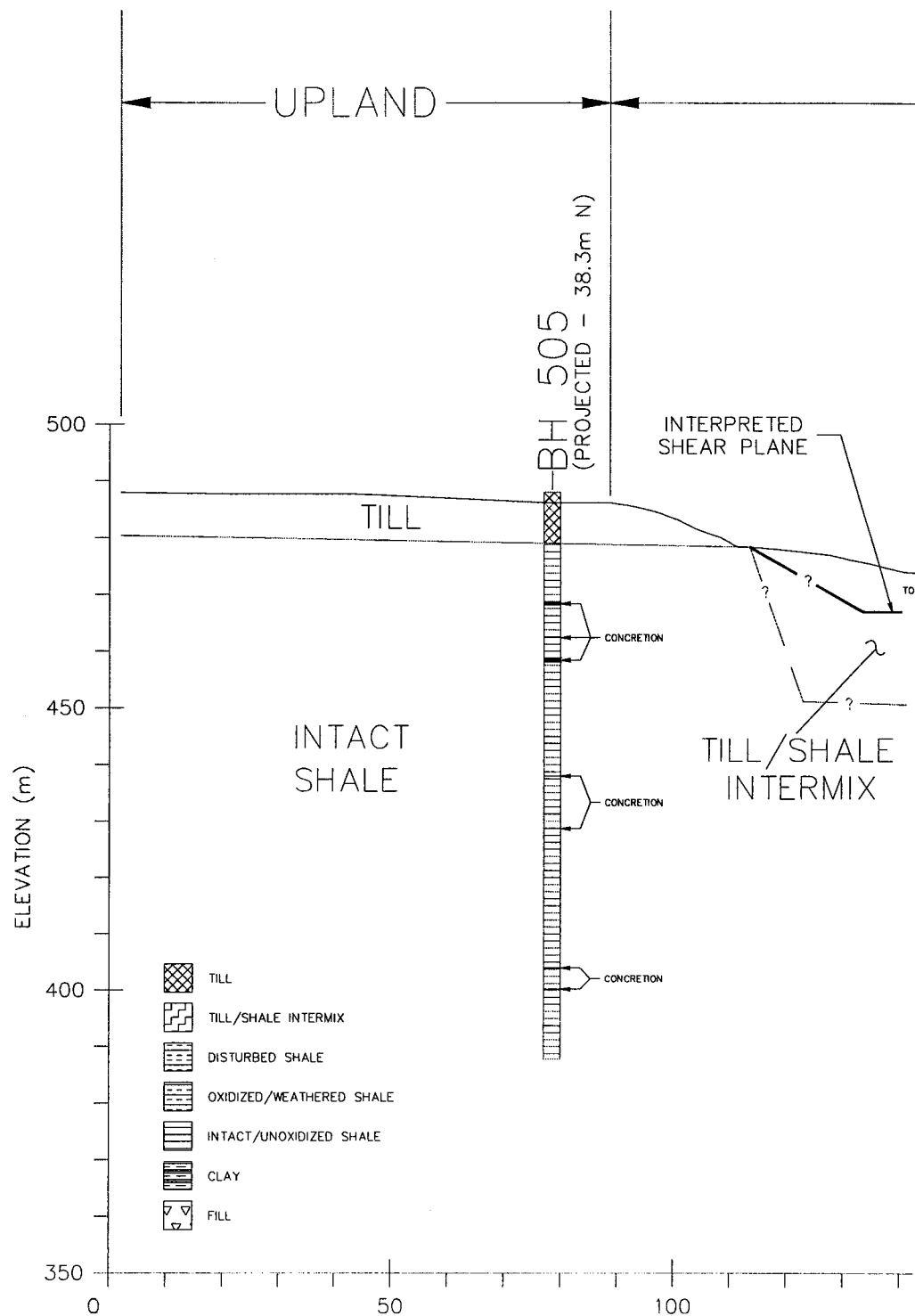


Figure A-23a: Enlarged section of the shear plane location of Figure 4-16.

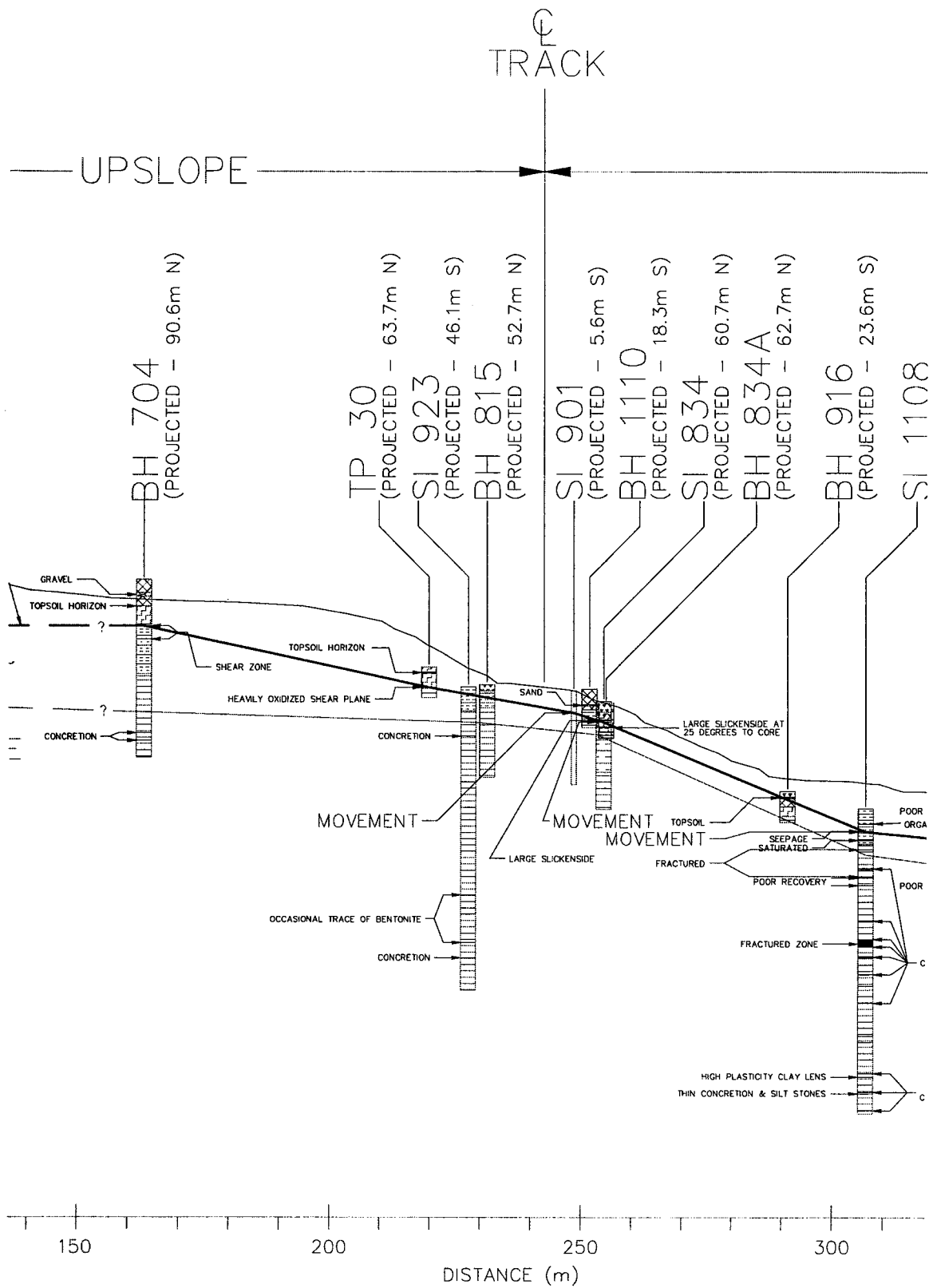


Figure A-23b: Enlarged section of the shear plane location of Figure 4-16 (cont.).

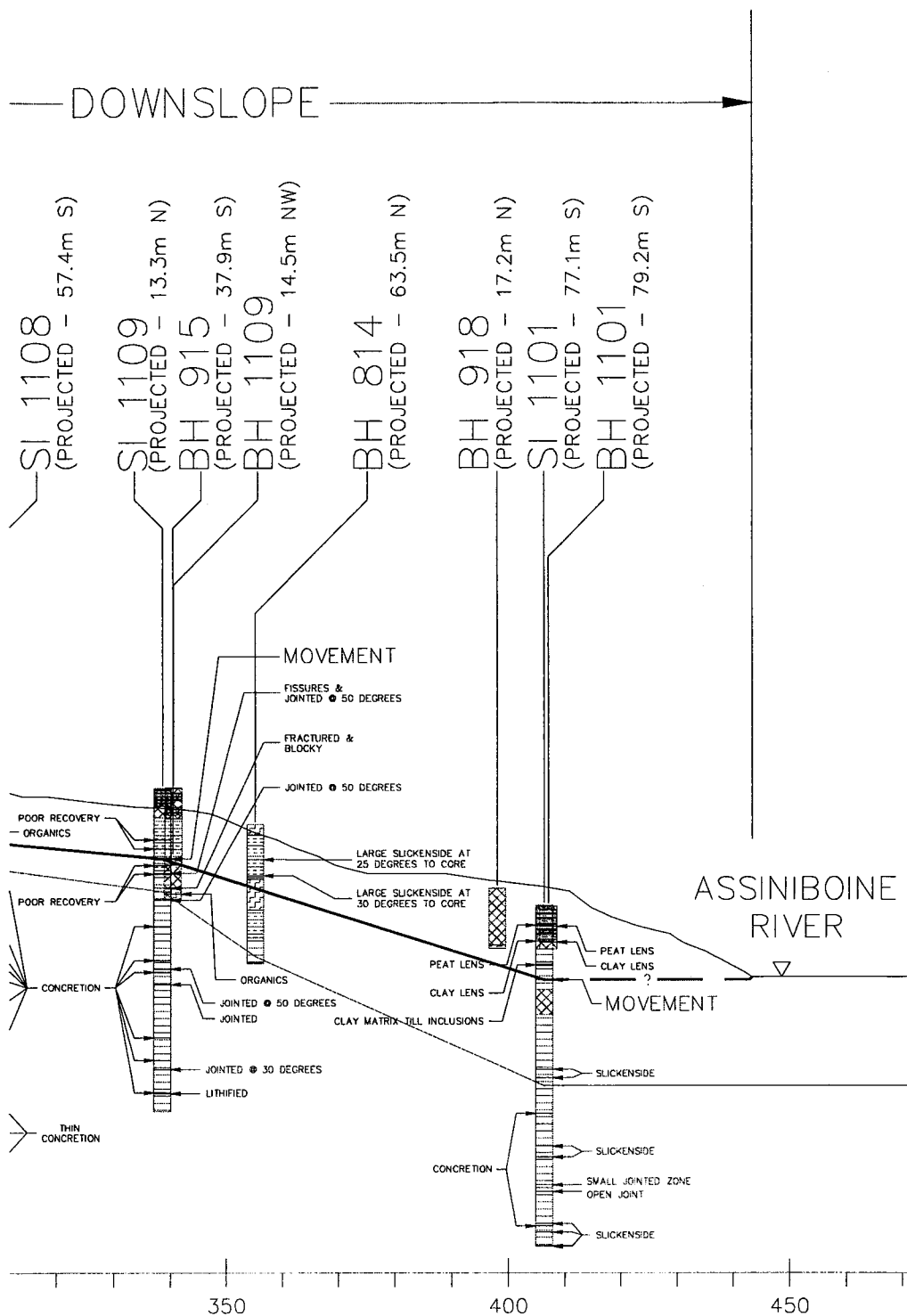


Figure A-23c: Enlarged section of the shear plane location of Figure 4-16 (cont.).

Appendix B

Laboratory Testing

grain size analyses
water deterioration test
consolidation test

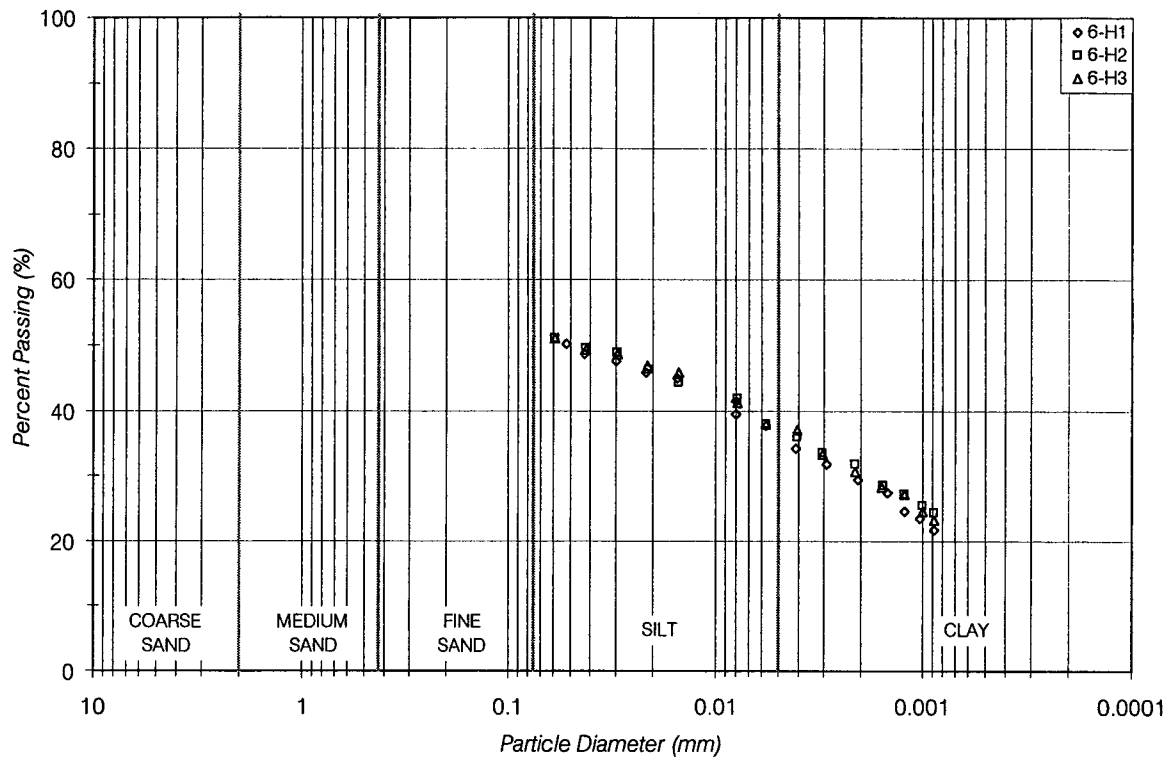


Figure B-1: Grain size distribution of Block 6.

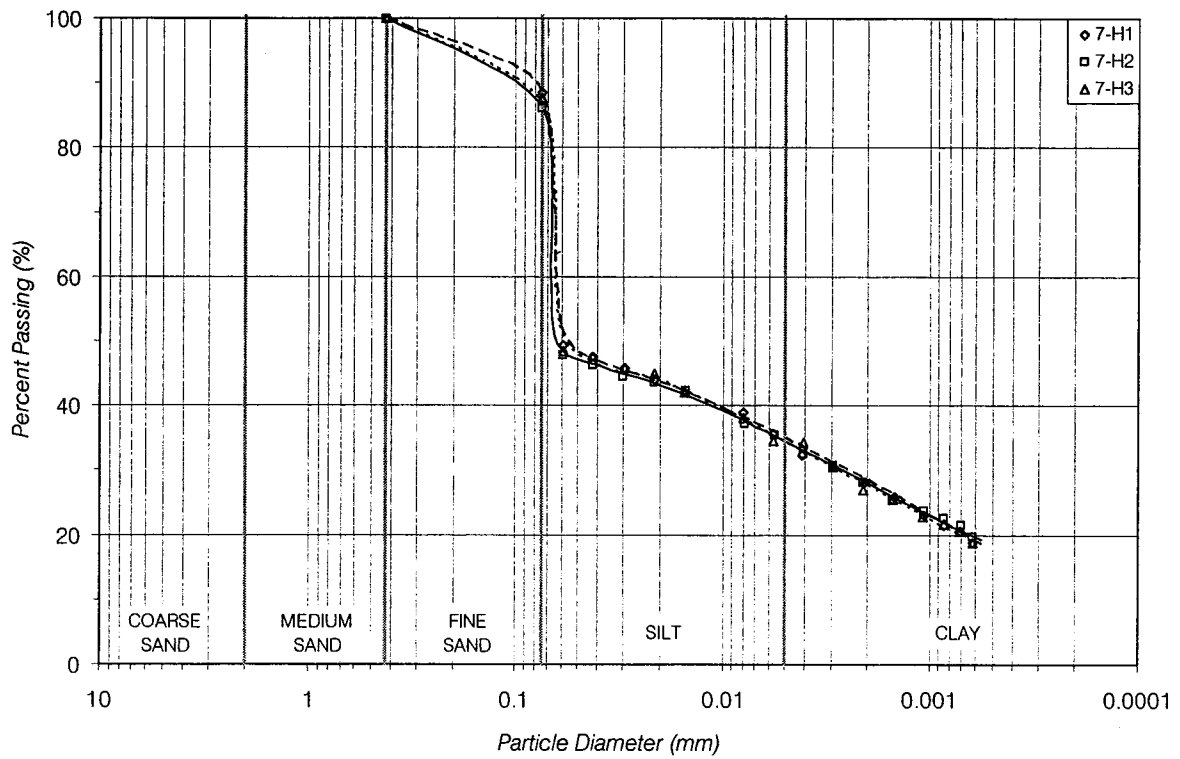
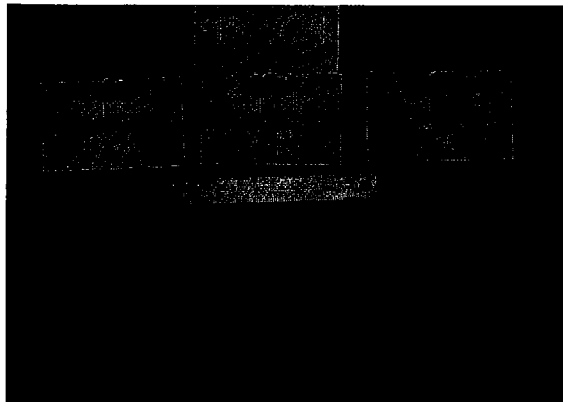
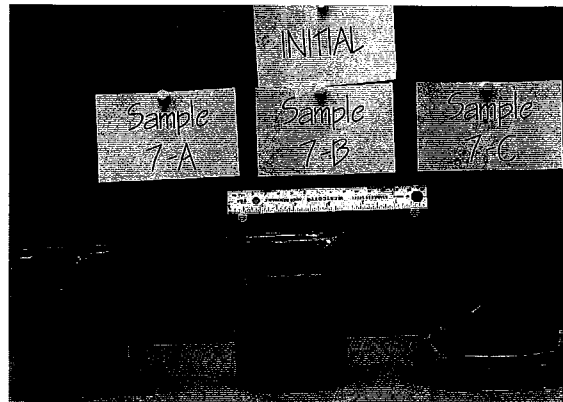


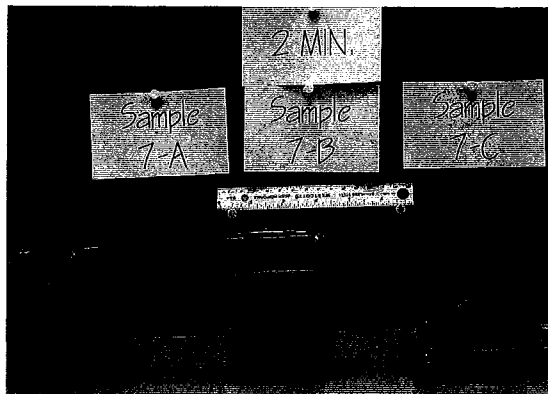
Figure B-2: Grain size distribution of Block 7 (first trial).



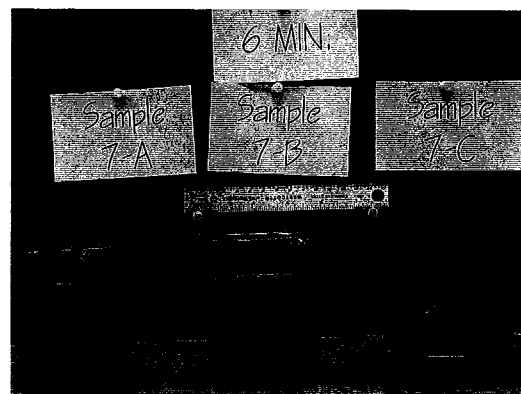
(a)



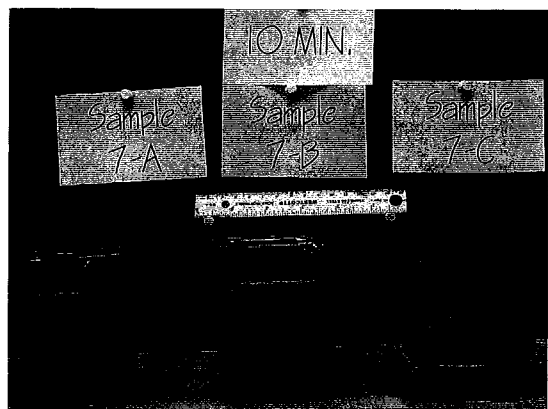
(b)



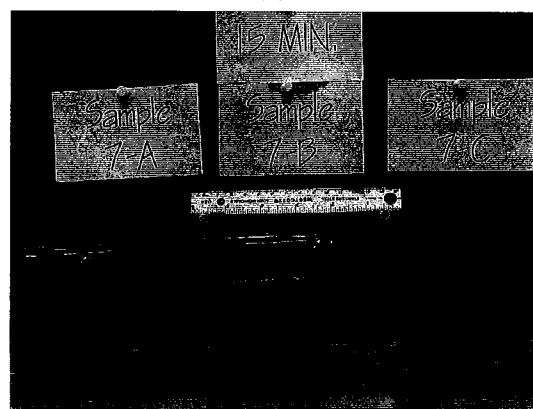
(c)



(d)



(e)

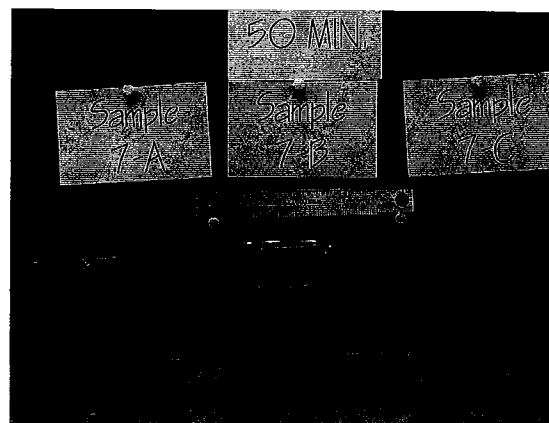


(f)

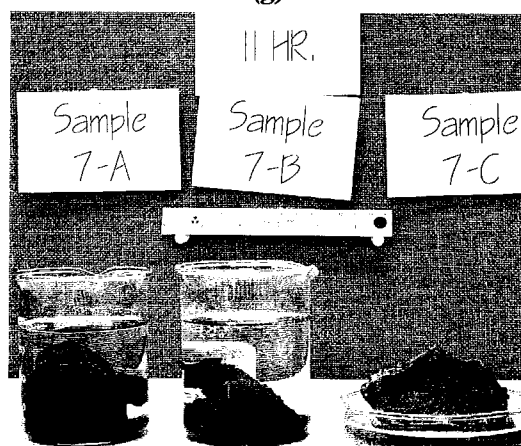
Figure B-3: Documentation of the water deterioration test.



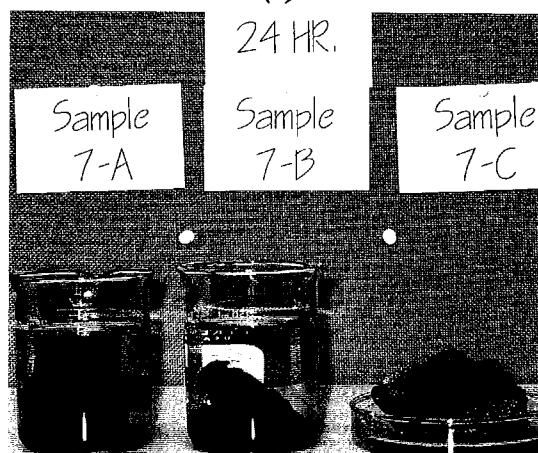
(g)



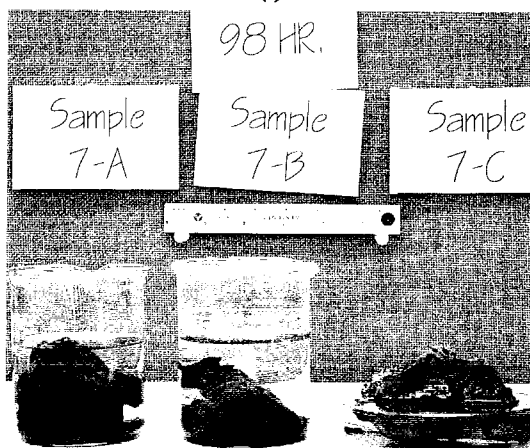
(h)



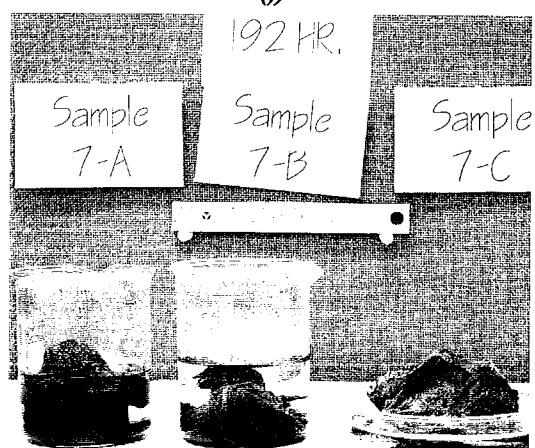
(i)



(j)



(k)

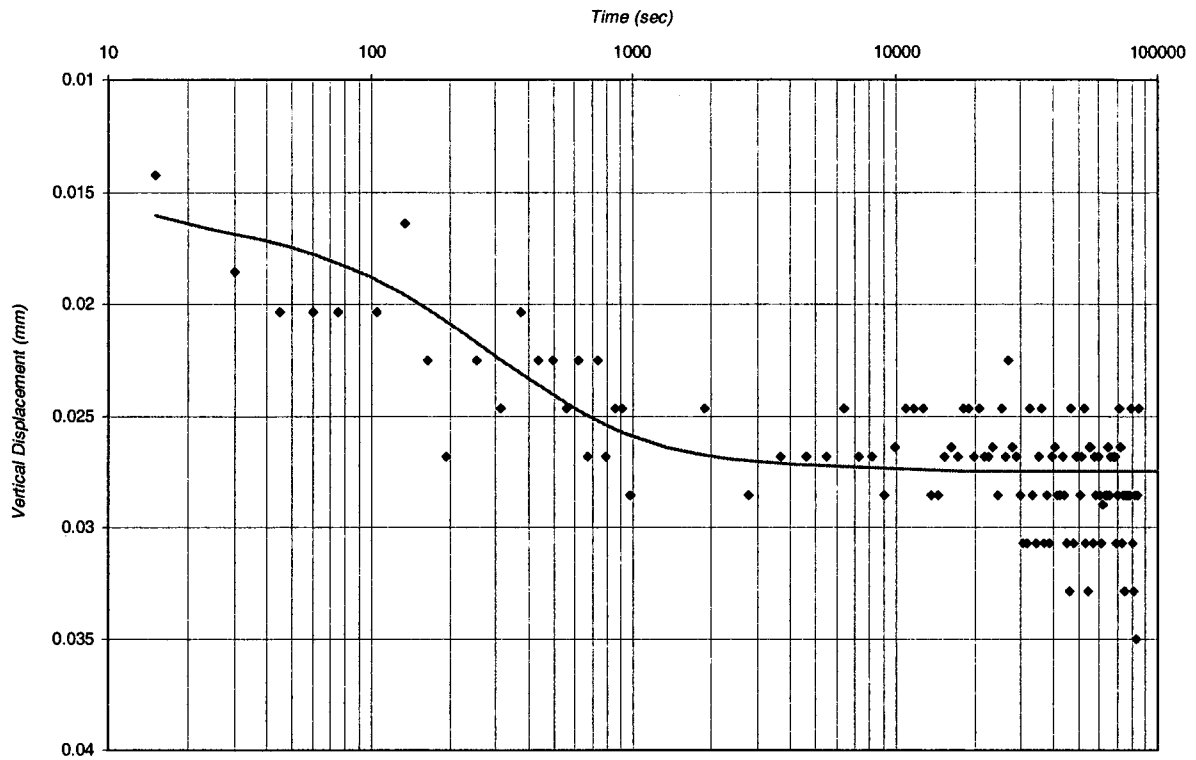


(l)

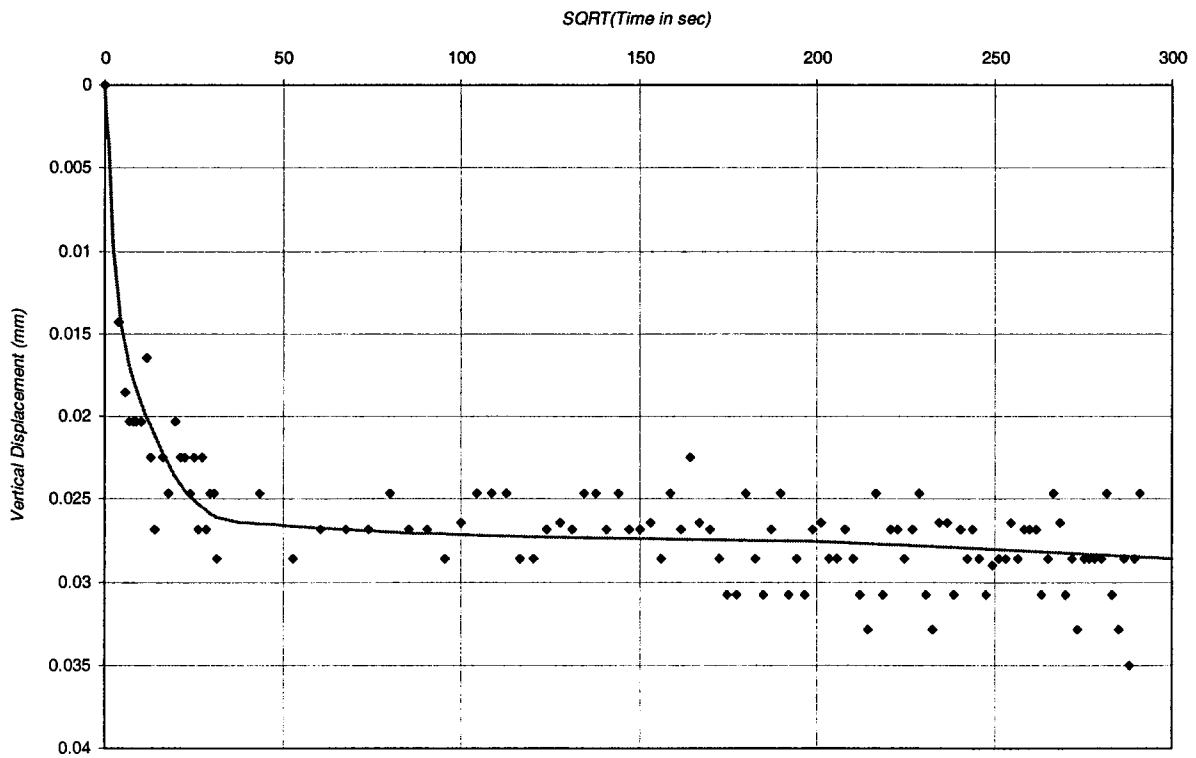
Figure B-3a: Documentation of the water deterioration test (cont.).

Table B-1: Summary of consolidation loading stages.

Load Stage (kPa)	Change in Height (mm)	Void Ratio, e	Porosity, n	Coefficient of Volume Compressibility, m_v (m ² /MN)	Coefficient of Consolidation, c_v (m ² /yr)	Coefficient of Permeability, k (m/s)
Sample 6-2						
6.25	0.037	0.627	0.385	0.312	3.41	3.3x10 ⁻¹⁰
12.6	0.031	0.625	0.385	0.259	4.33	3.5x10 ⁻¹⁰
24.9	0.045	0.621	0.383	0.196	0.59	3.6x10 ⁻¹¹
50.0	0.070	0.615	0.381	0.150	0.70	3.3x10 ⁻¹¹
99.8	0.095	0.607	0.378	0.102	0.90	2.9x10 ⁻¹¹
199.7	0.117	0.596	0.373	0.064	1.00	2.0x10 ⁻¹¹
392.9	0.154	0.583	0.368	0.043	0.72	9.7x10 ⁻¹²
798.0	0.252	0.561	0.359	0.034	0.61	6.5x10 ⁻¹²
392.9	-0.097	0.570	0.363			
199.7	-0.117	0.580	0.367			
99.8	-0.093	0.588	0.370			
50.0	-0.070	0.594	0.373			
24.9	-0.052	0.598	0.374			
12.6	-0.031	0.601	0.375			
6.25	-0.025	0.603	0.376			
Sample 7-1						
24.8	0.013	0.619	0.382	0.027	-	-
49.9	0.023	0.617	0.382	0.047	1.72	2.5x10 ⁻¹¹
100.1	0.078	0.610	0.379	0.083	1.46	3.8x10 ⁻¹¹
200.0	0.138	0.599	0.375	0.074	1.52	3.5x10 ⁻¹¹
400.2	-	-		-	1.20	-
800.0	-	-		-	-	-
400.2	-	-				
200.0	-	-				
100.1	-	-				
49.9	-	-				
24.8	-	-				

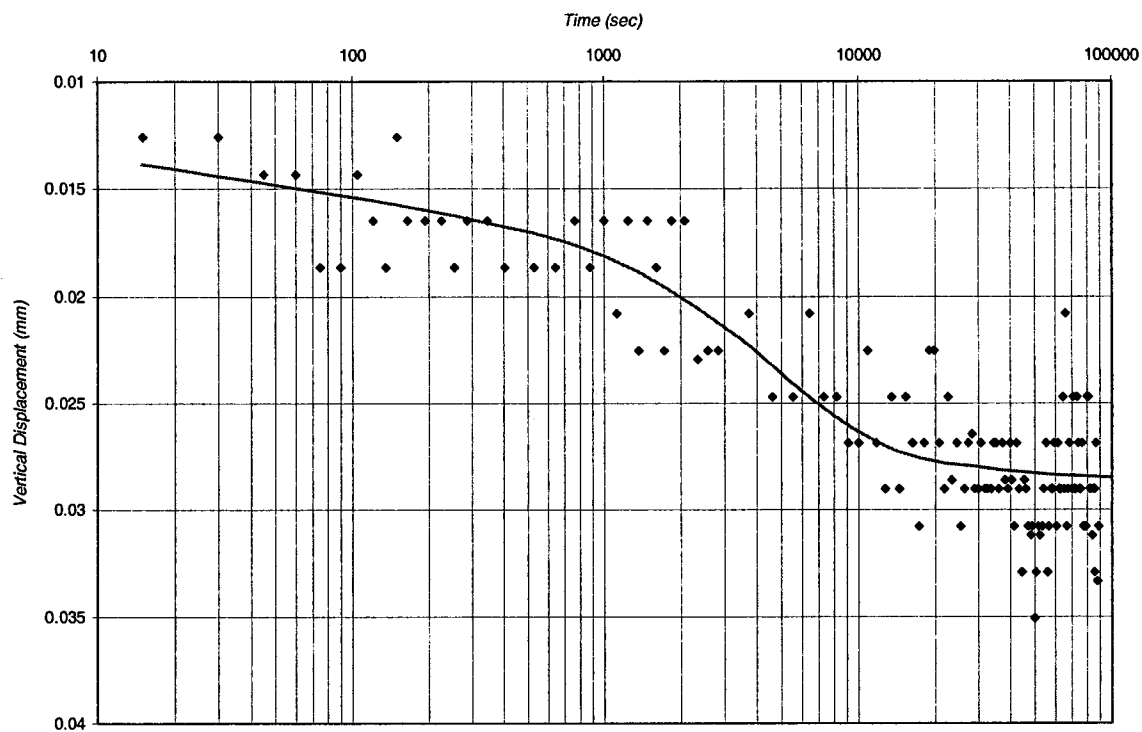


(a)

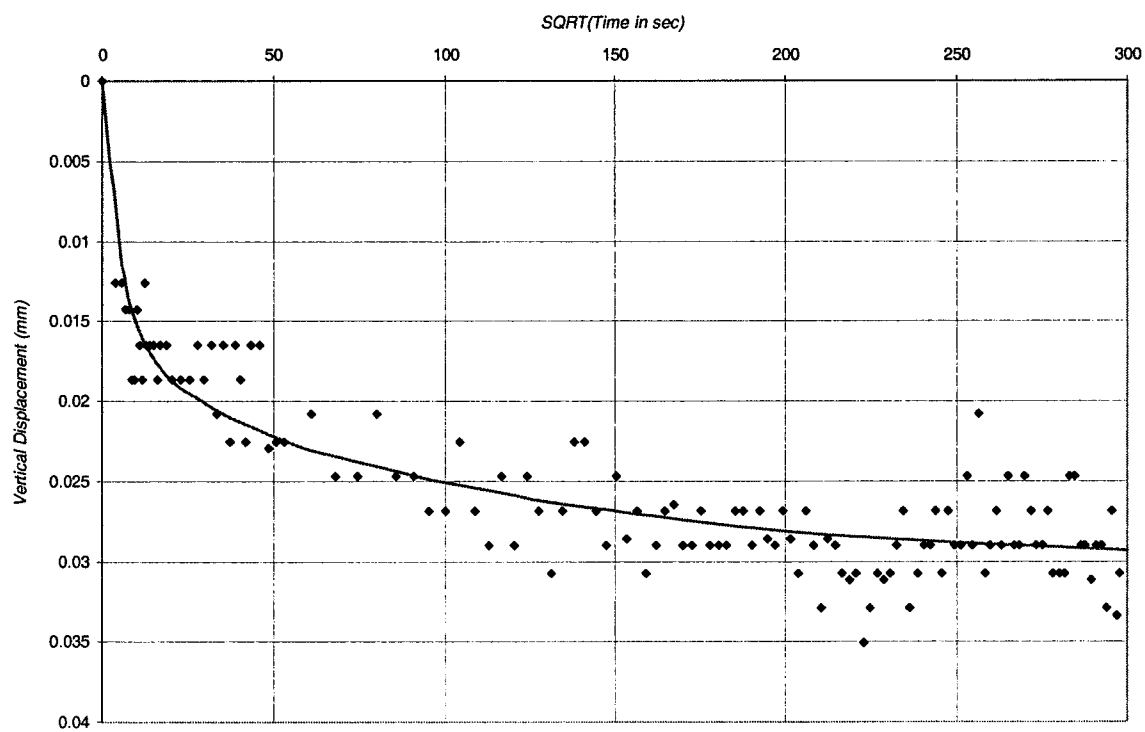


(b)

Figure B-4: Consolidation of Sample 6-2 at 6.25 kPa (a) log time method (b) square root time method.

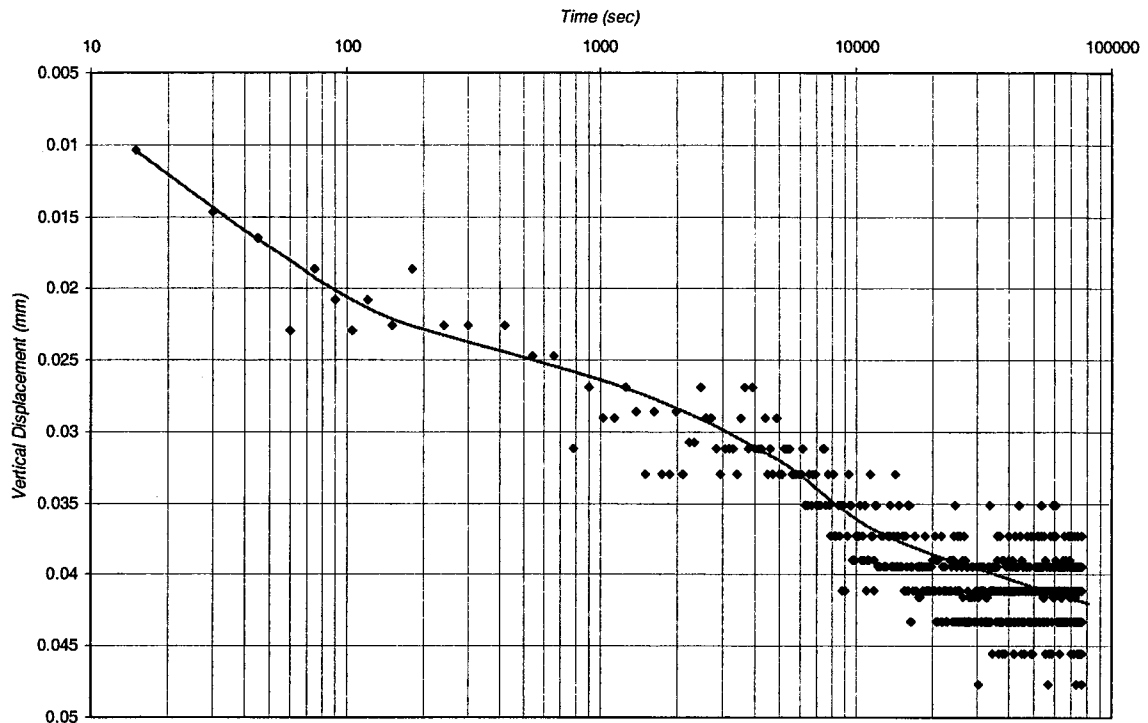


(a)

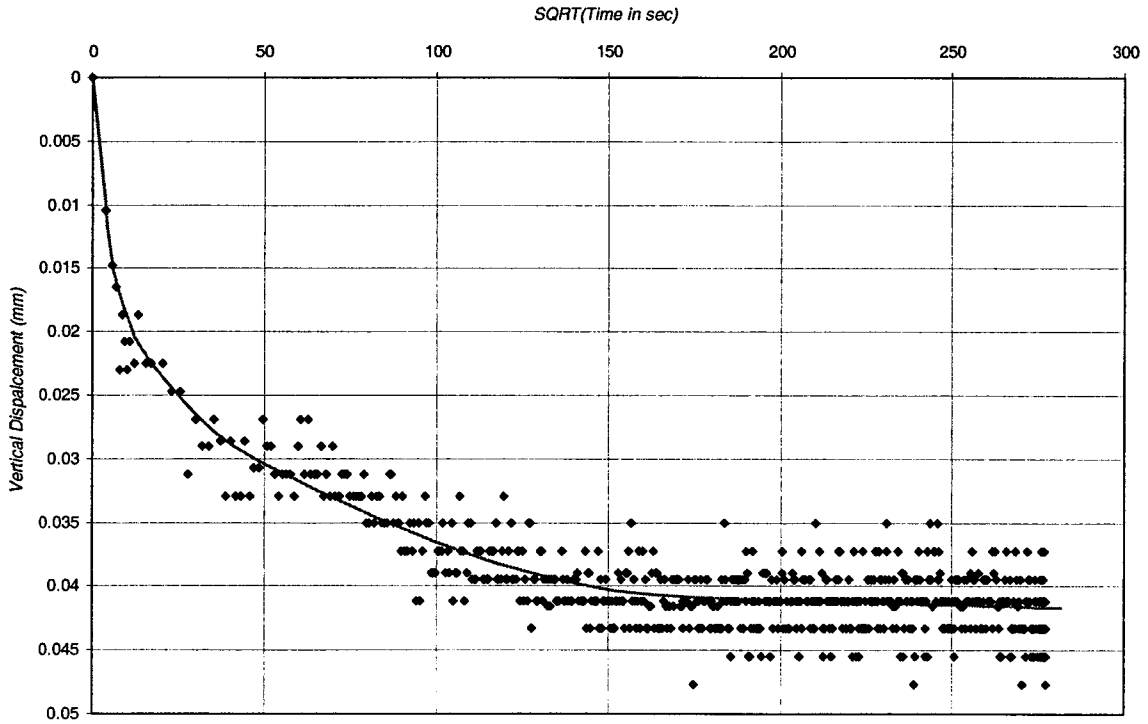


(b)

Figure B-5: Consolidation of Sample 6-2 at 12.5 kPa (a) log time method (b) square root time method.

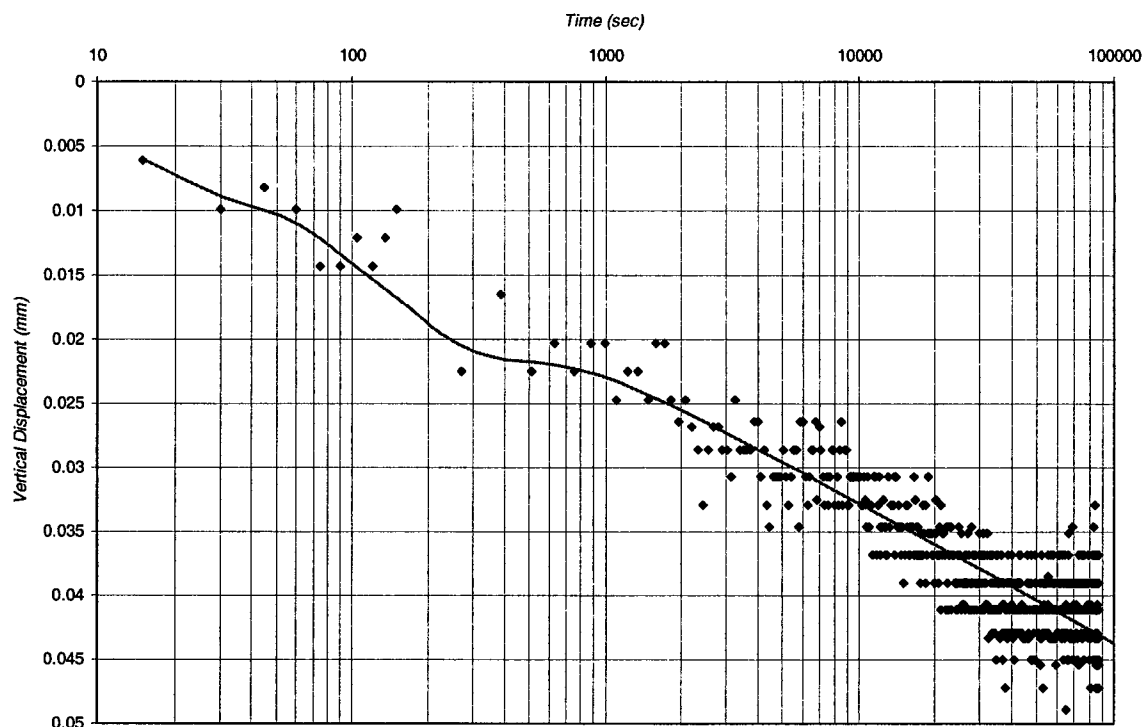


(a)

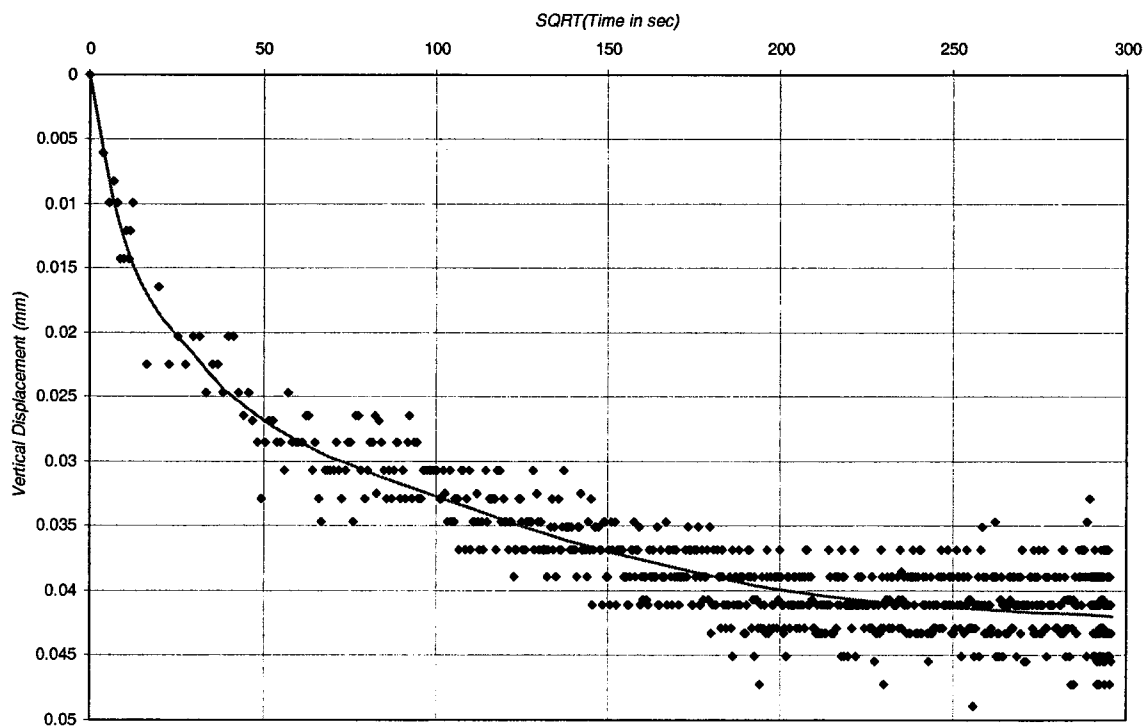


(b)

Figure B-6: Consolidation of Sample 6-2 at 25 kPa (a) log time method (b) square root time method.

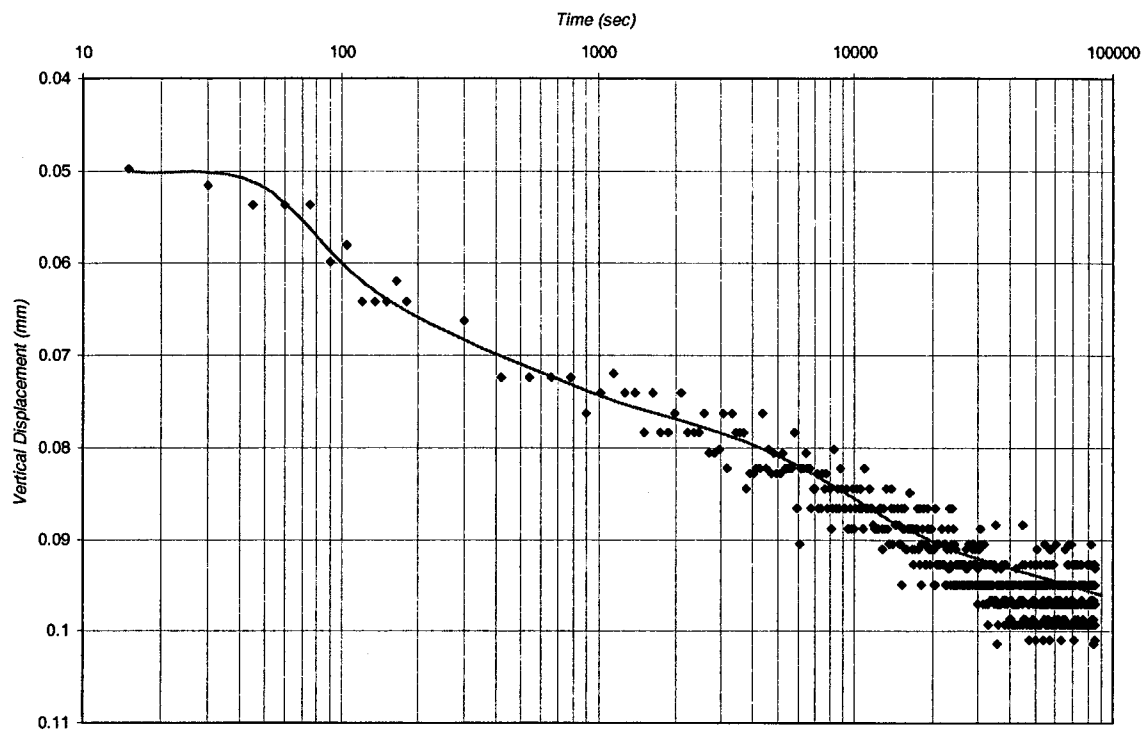


(a)

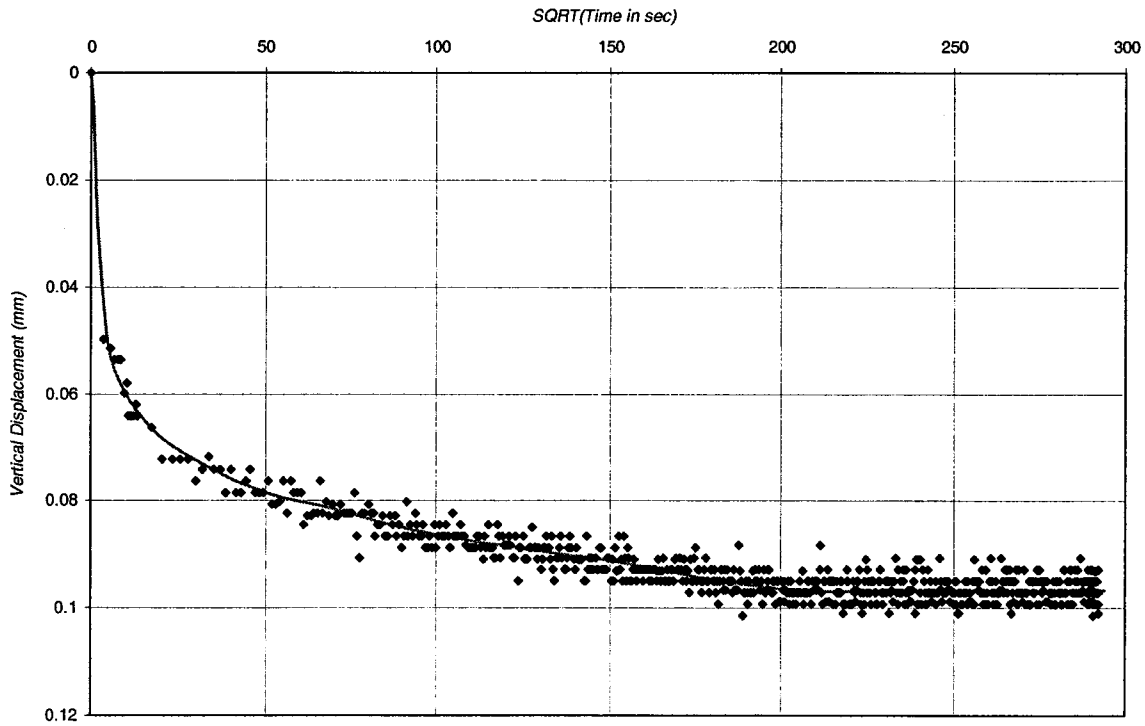


(b)

Figure B-7: Consolidation of Sample 6-2 at 50 kPa (a) log time method (b) square root time method.

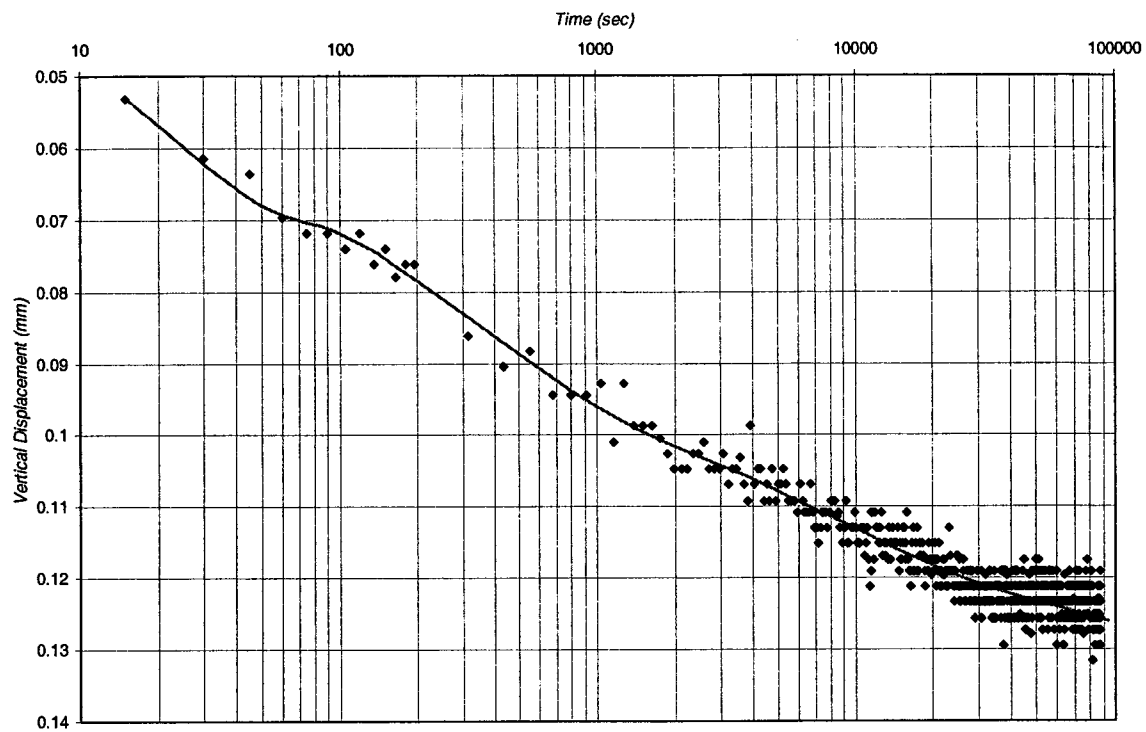


(a)

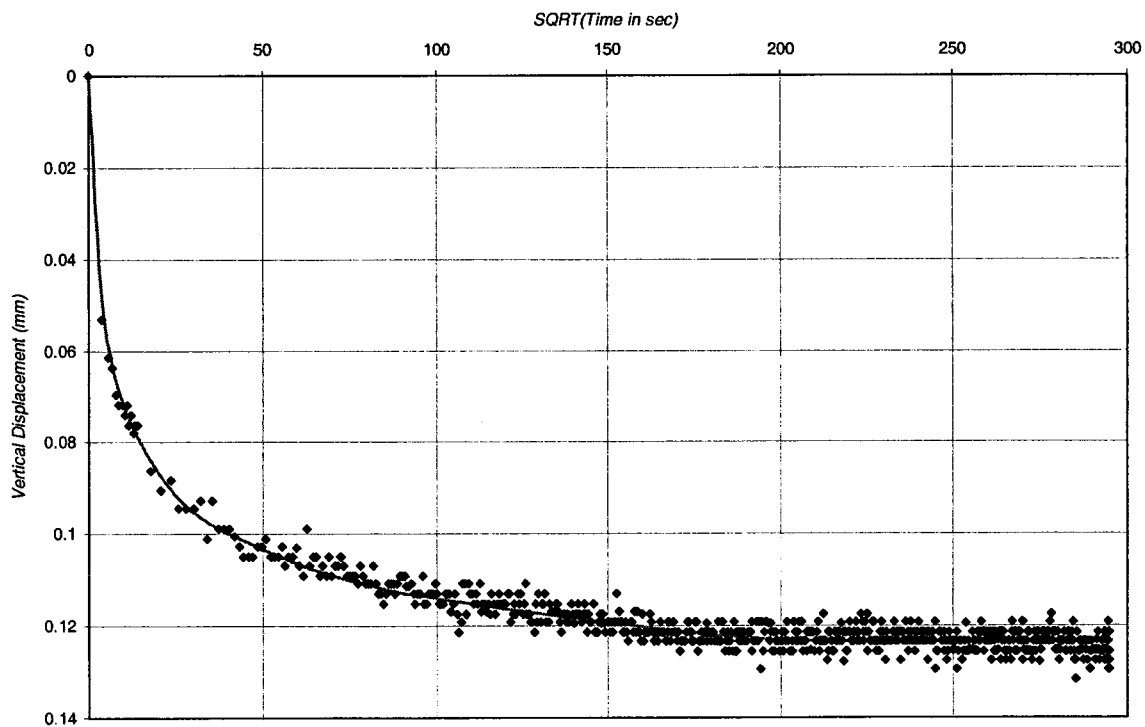


(b)

Figure B-8: Consolidation of Sample 6-2 at 100 kPa (a) log time method (b) square root time method.

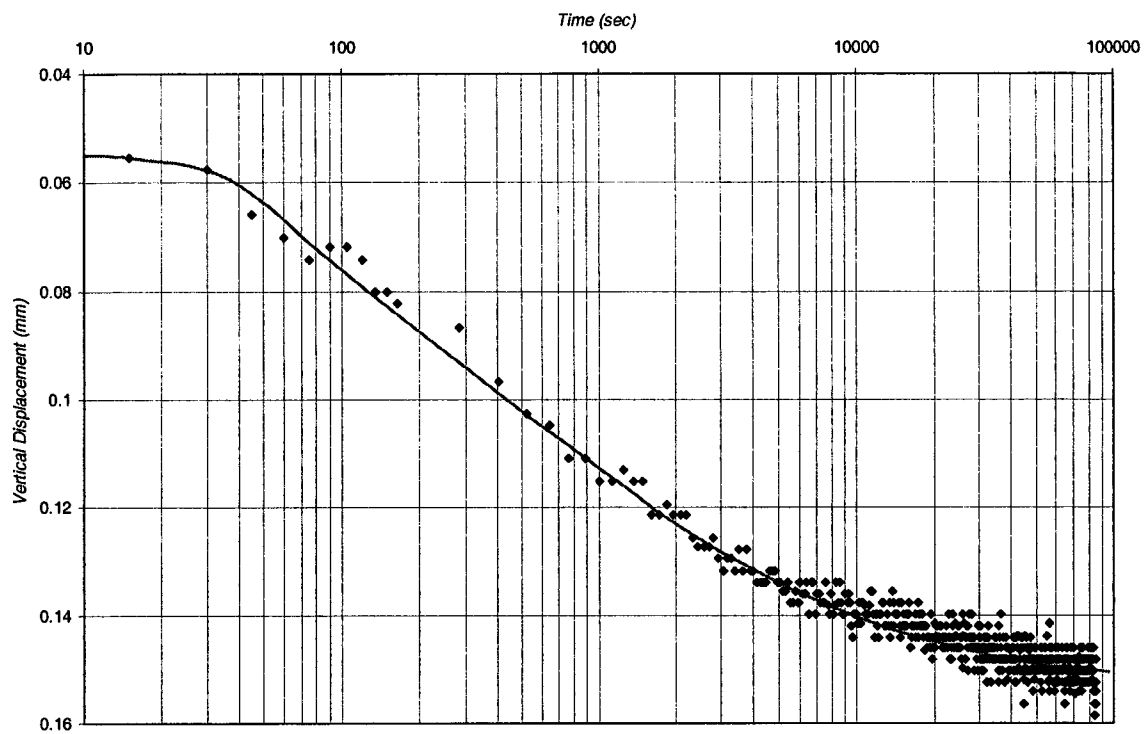


(a)

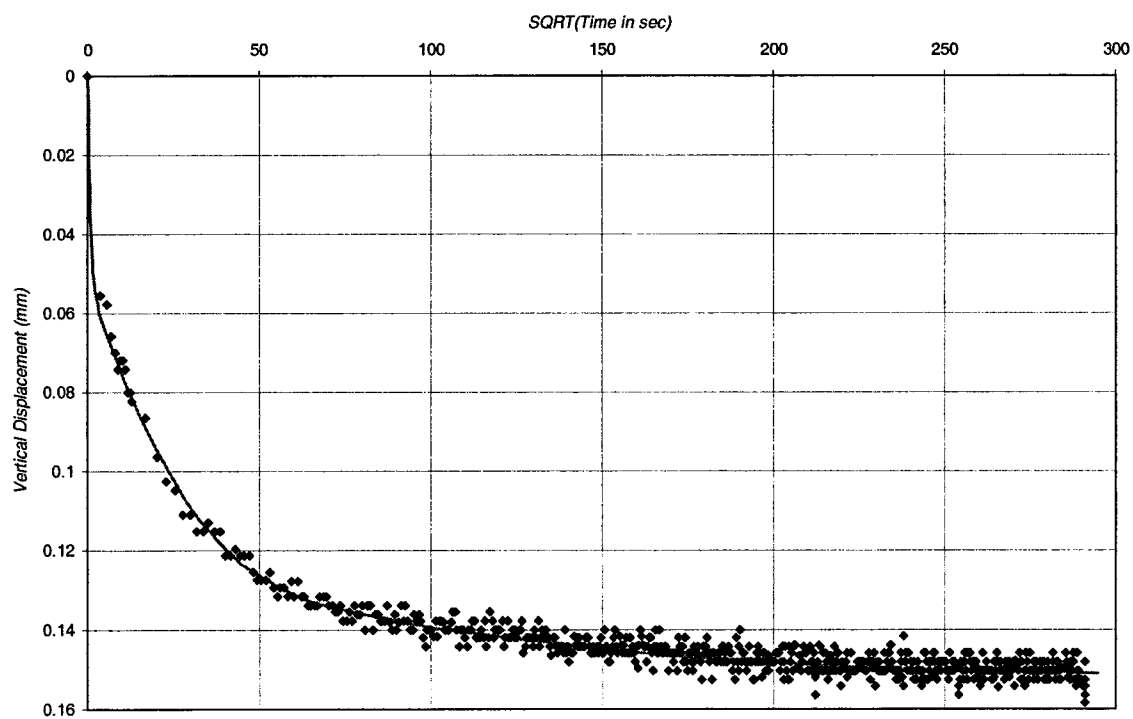


(b)

Figure B-9: Consolidation of Sample 6-2 at 200 kPa (a) log time method (b) square root time method.

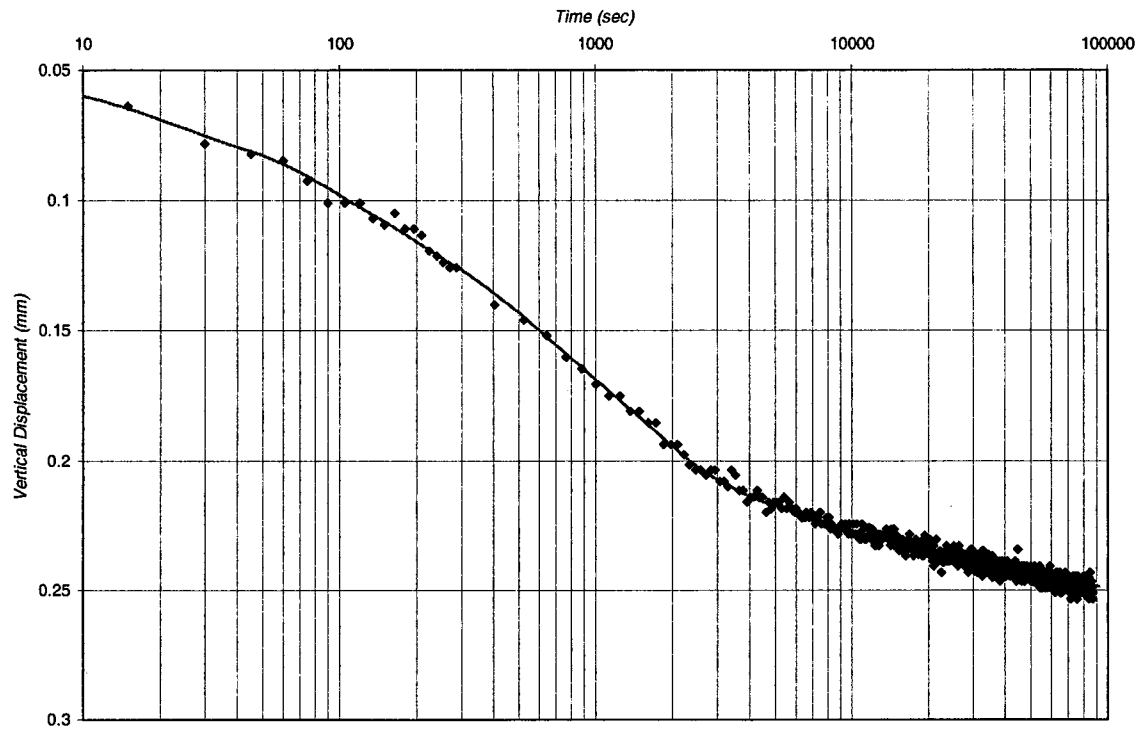


(a)

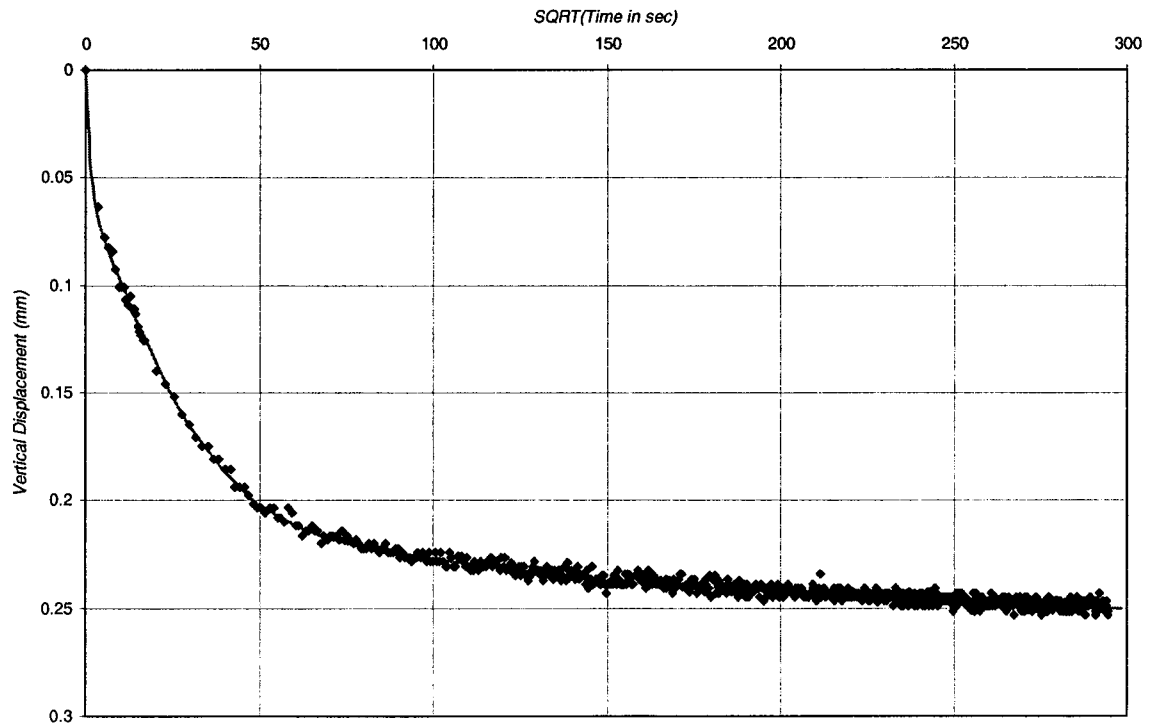


(b)

Figure B-10: Consolidation of Sample 6-2 at 400 kPa (a) log time method (b) square root time method.

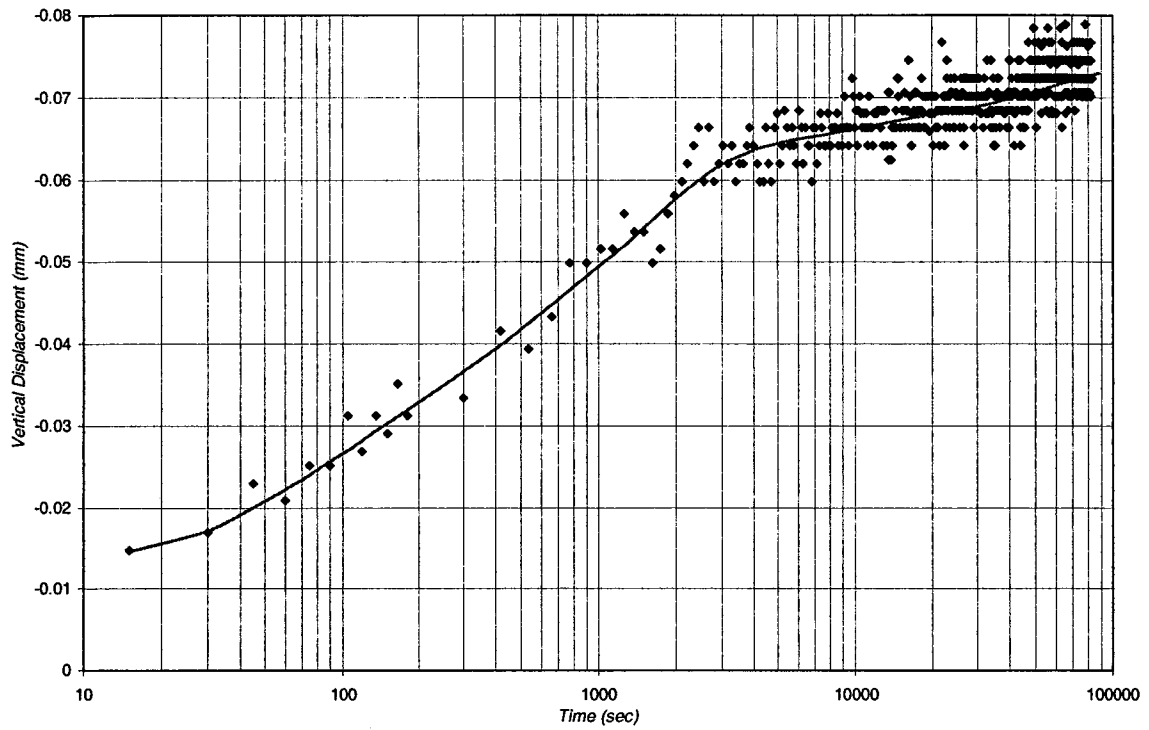


(a)

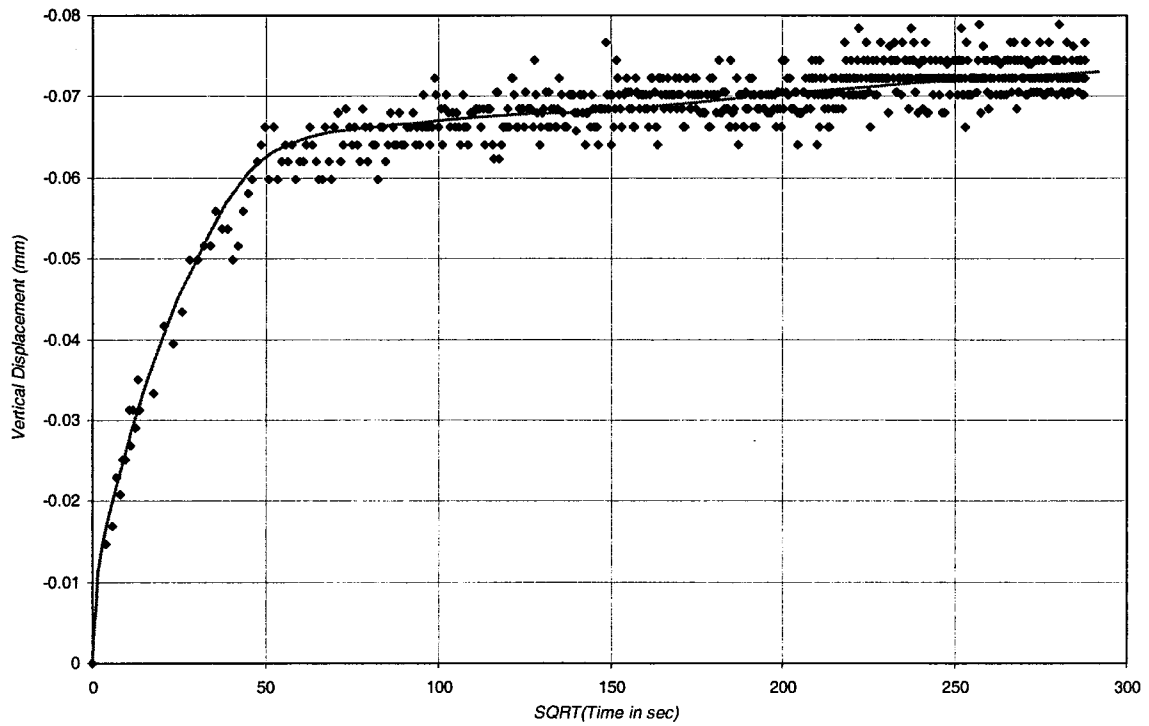


(b)

Figure B-11: Consolidation of Sample 6-2 at 800 kPa (a) log time method (b) square root time method.

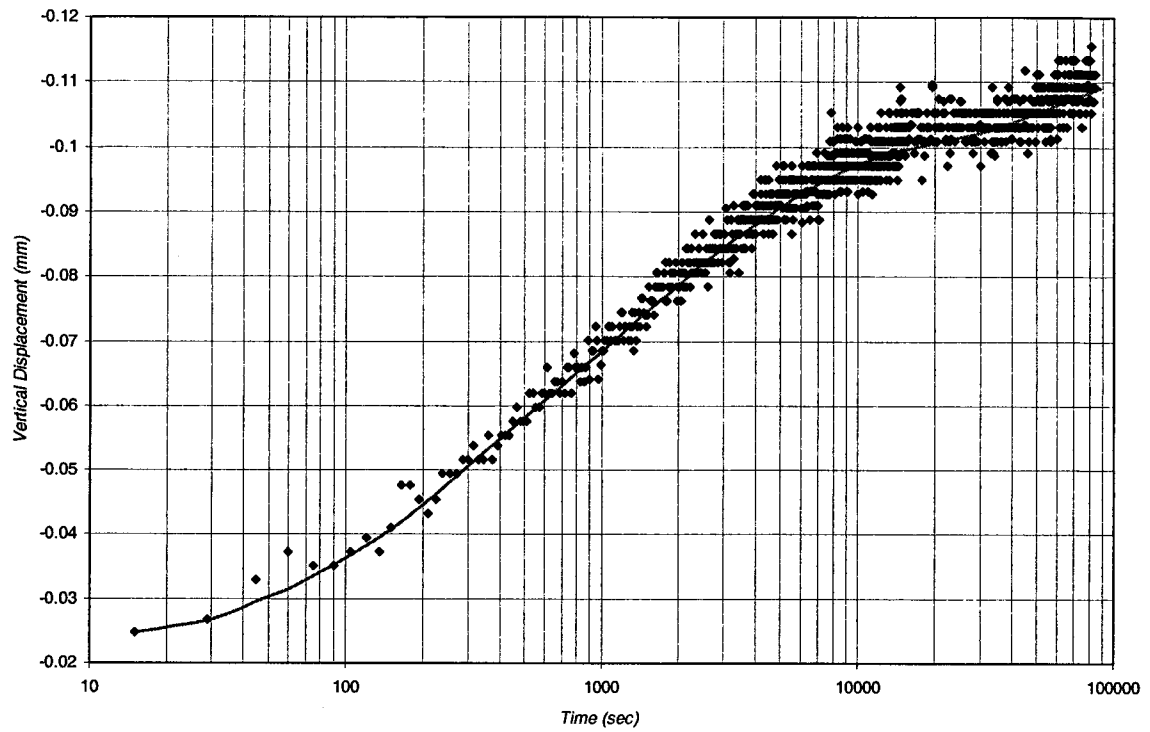


(a)

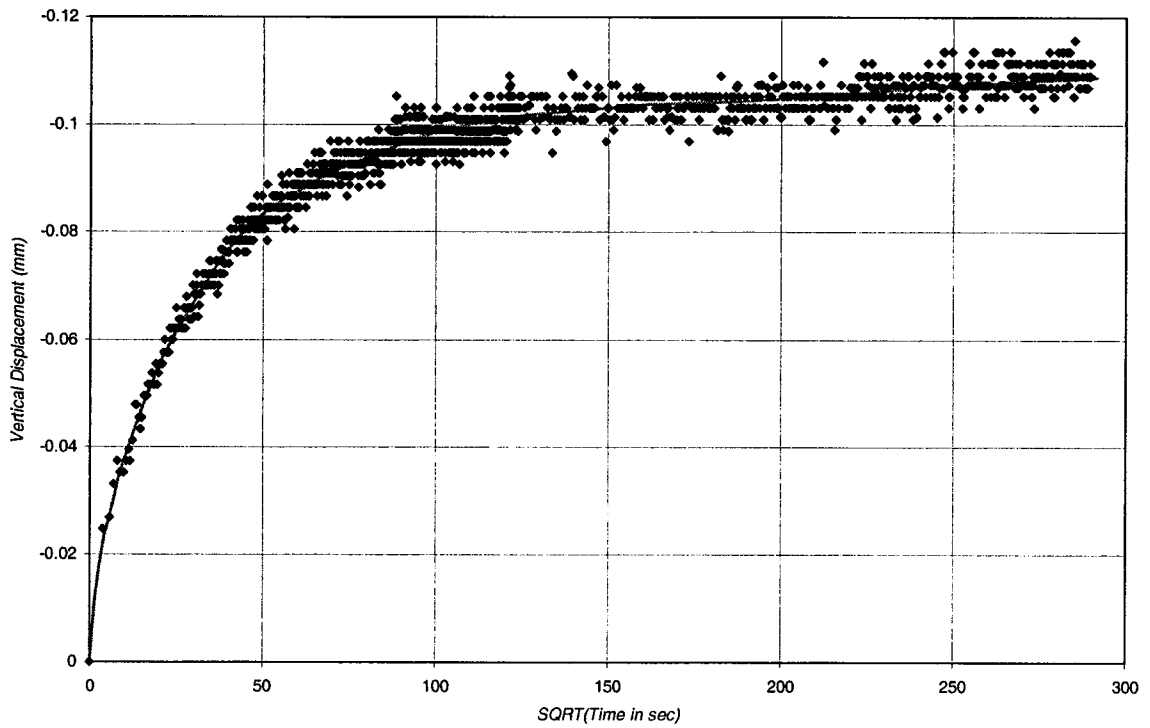


(b)

Figure B-12: Unloading of Sample 6-2 at 400 kPa (a) log time method (b) square root time method.

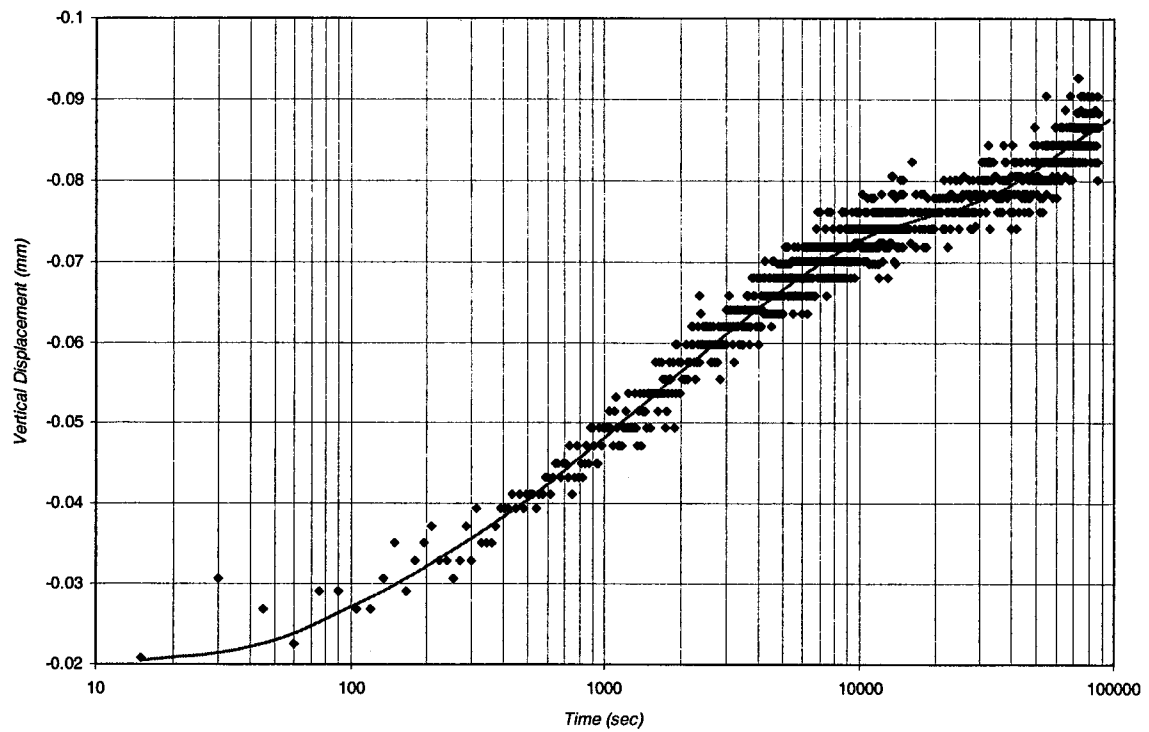


(a)

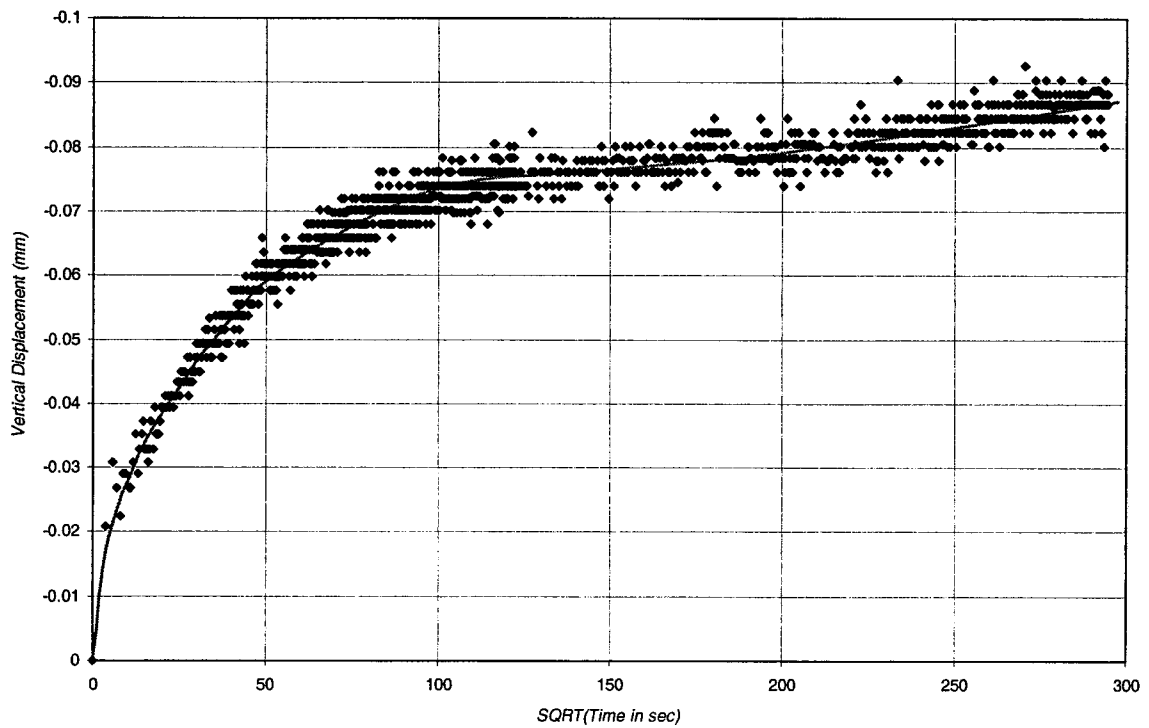


(b)

Figure B-13: Unloading of Sample 6-2 at 200 kPa (a) log time method (b) square root time method.

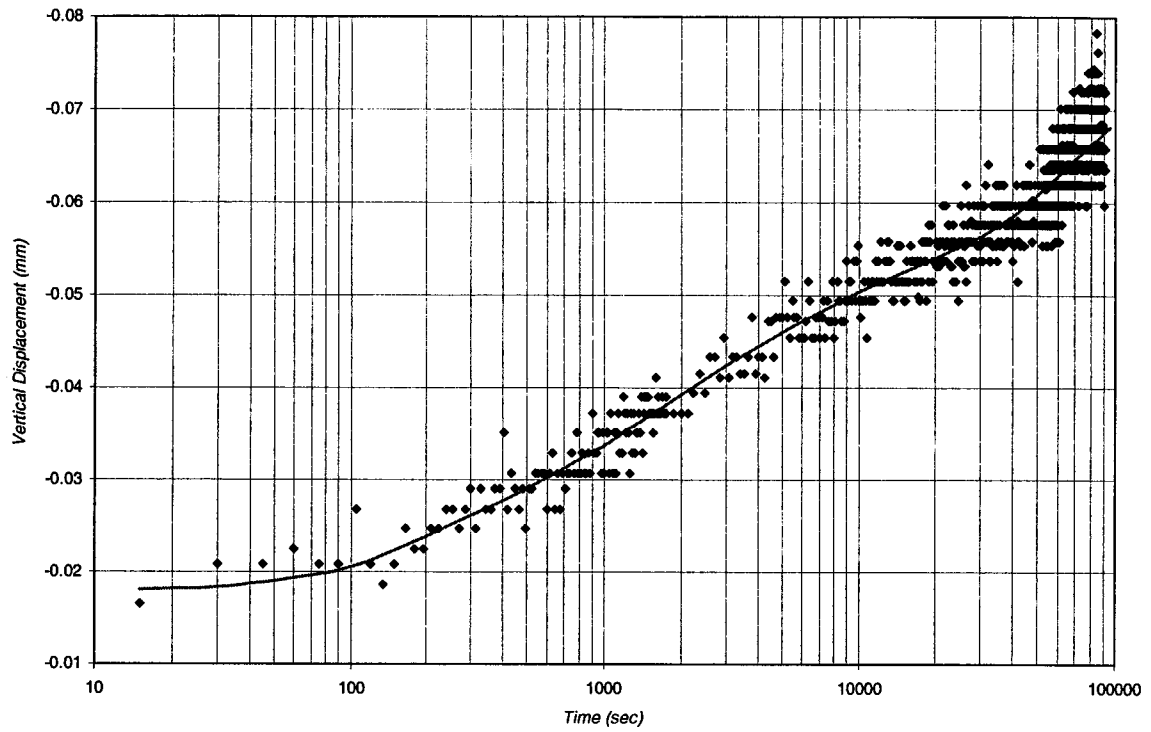


(a)

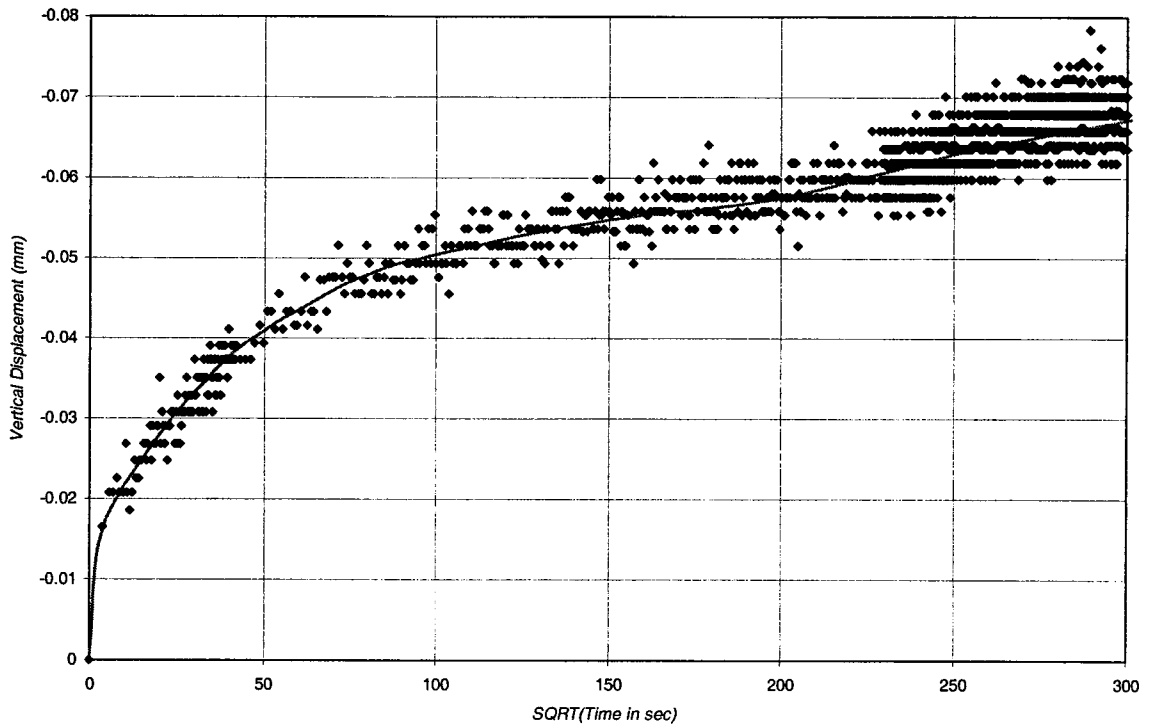


(b)

Figure B-14: Unloading of Sample 6-2 at 100 kPa (a) log time method (b) square root time method.

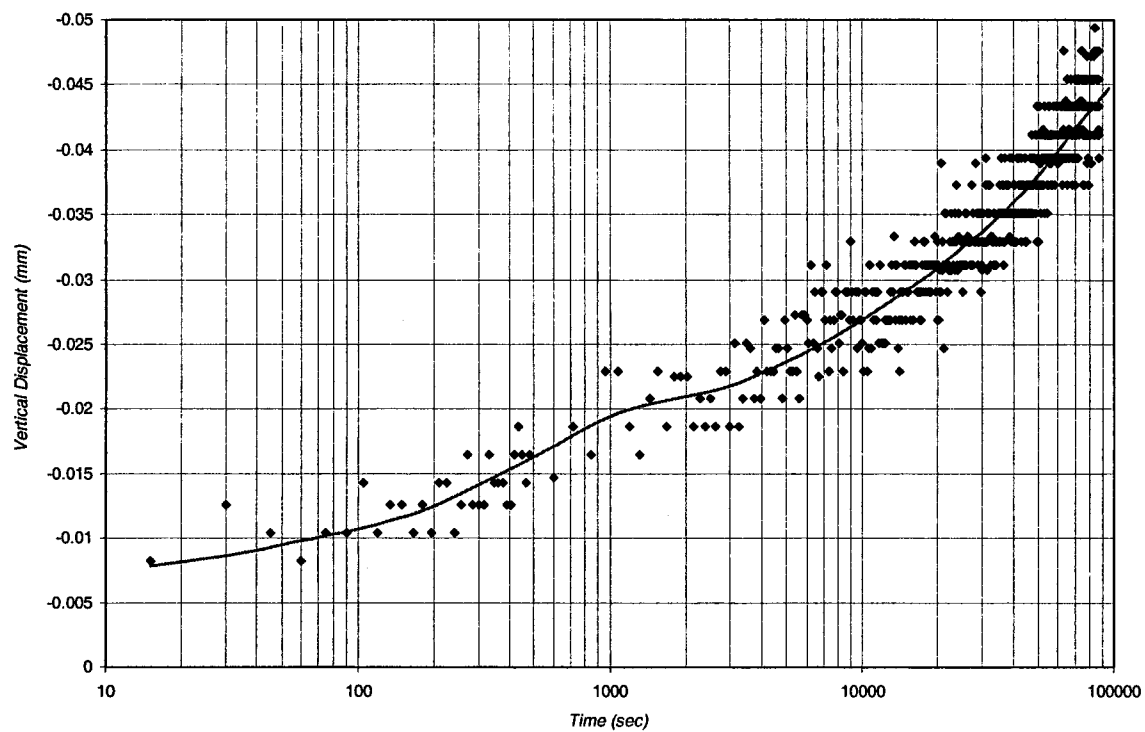


(a)

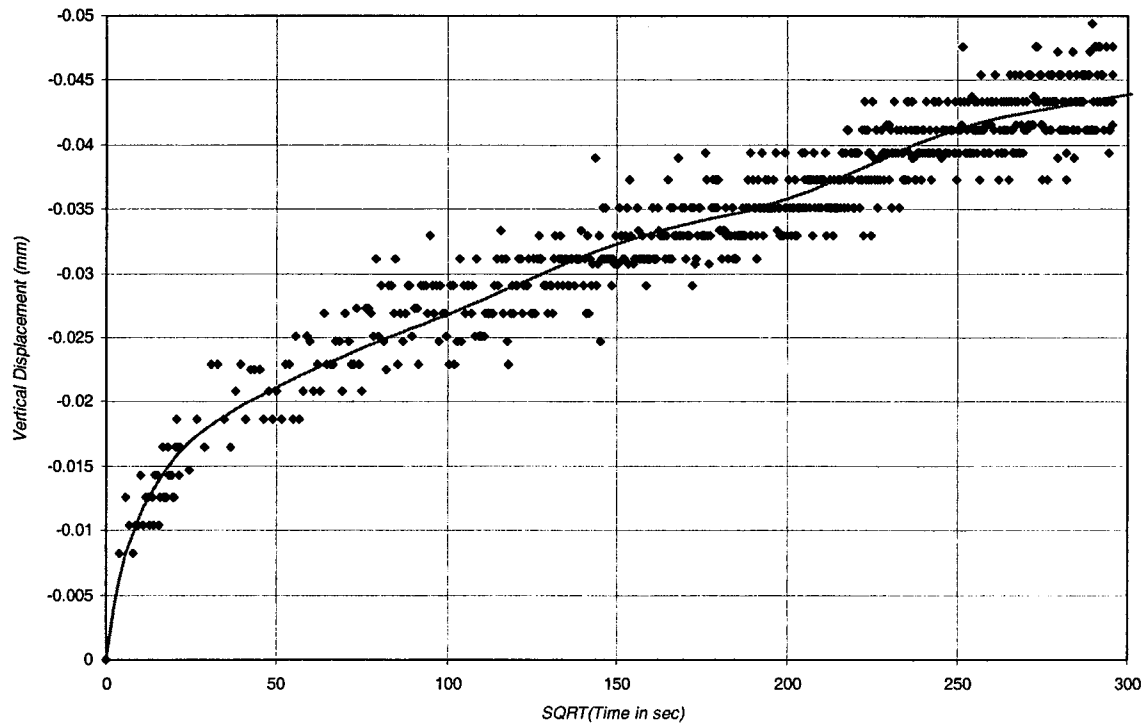


(b)

Figure B-15: Unloading of Sample 6-2 at 50 kPa (a) log time method (b) square root time method.

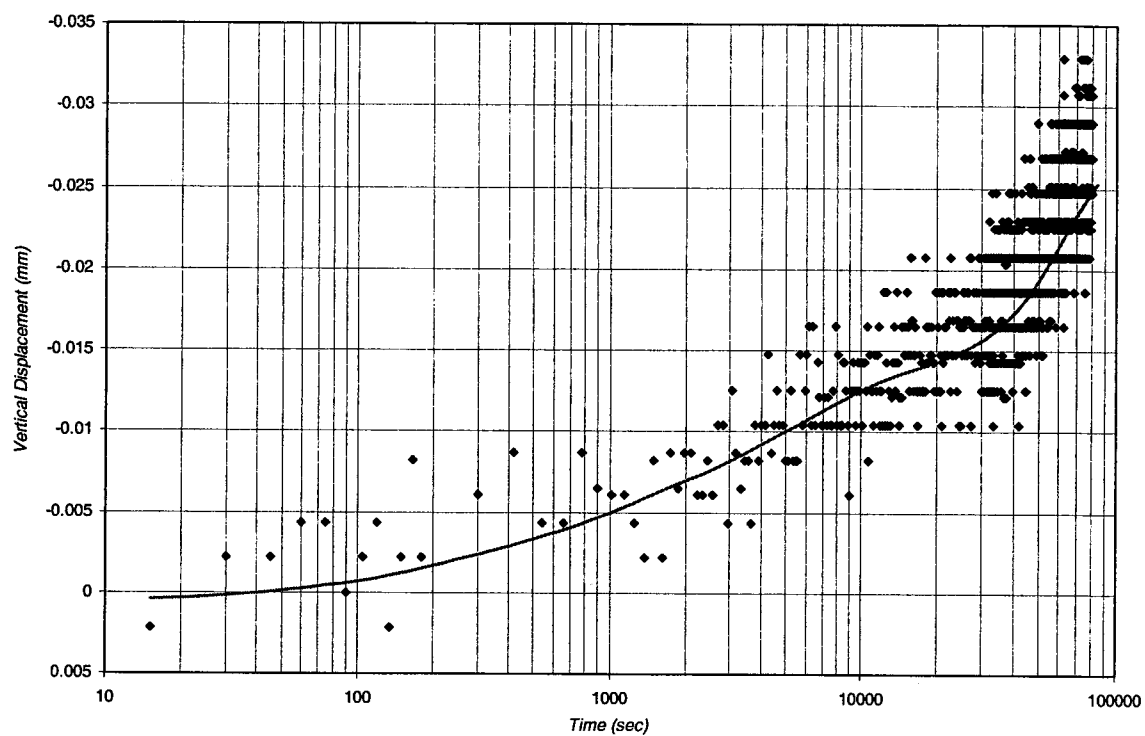


(a)

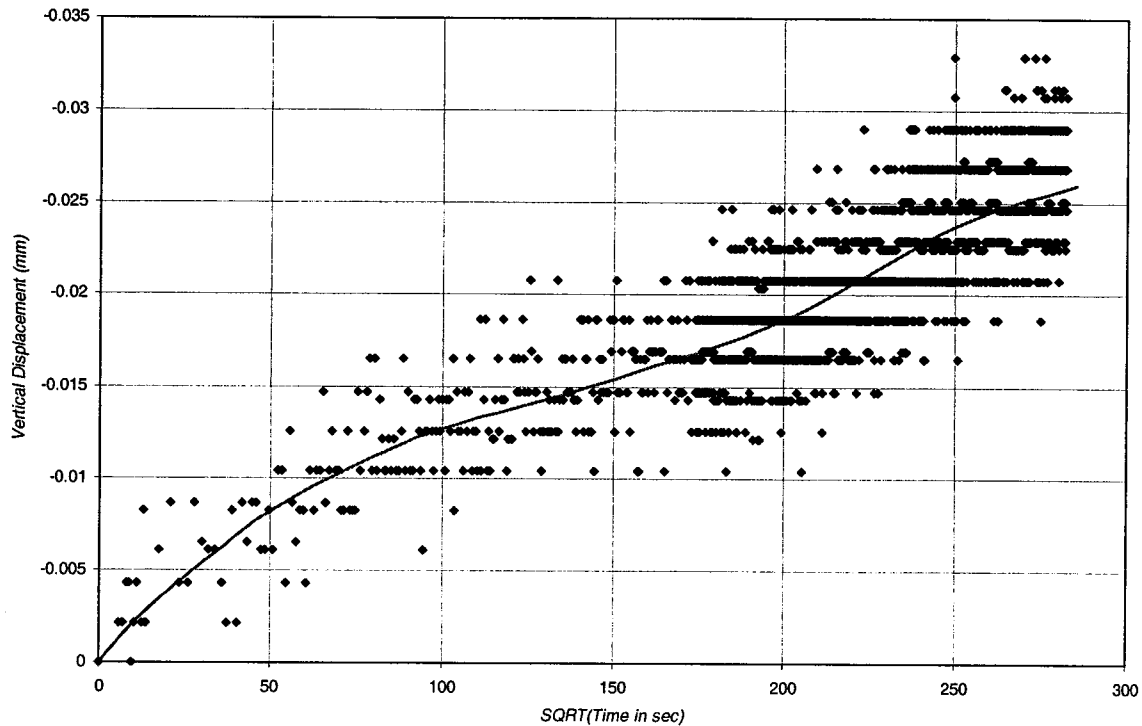


(b)

Figure B-16: Unloading of Sample 6-2 at 25 kPa (a) log time method (b) square root time method.

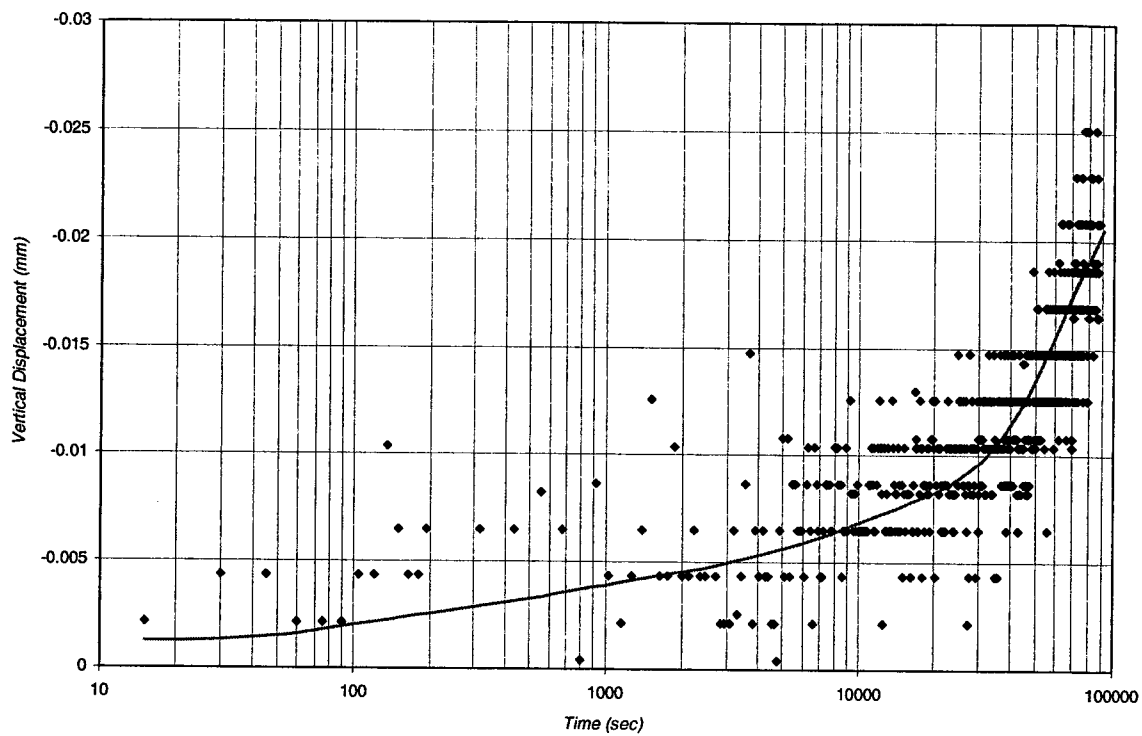


(a)

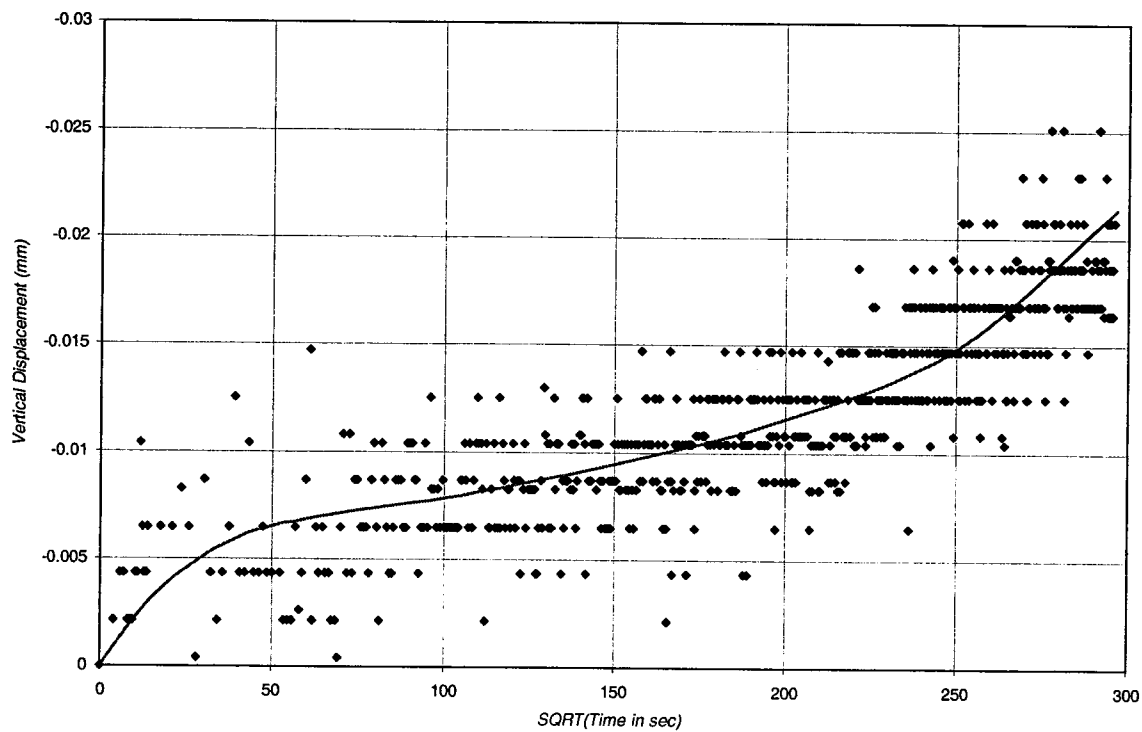


(b)

Figure B-17: Unloading of Sample 6-2 at 12.5 kPa (a) log time method (b) square root time method.

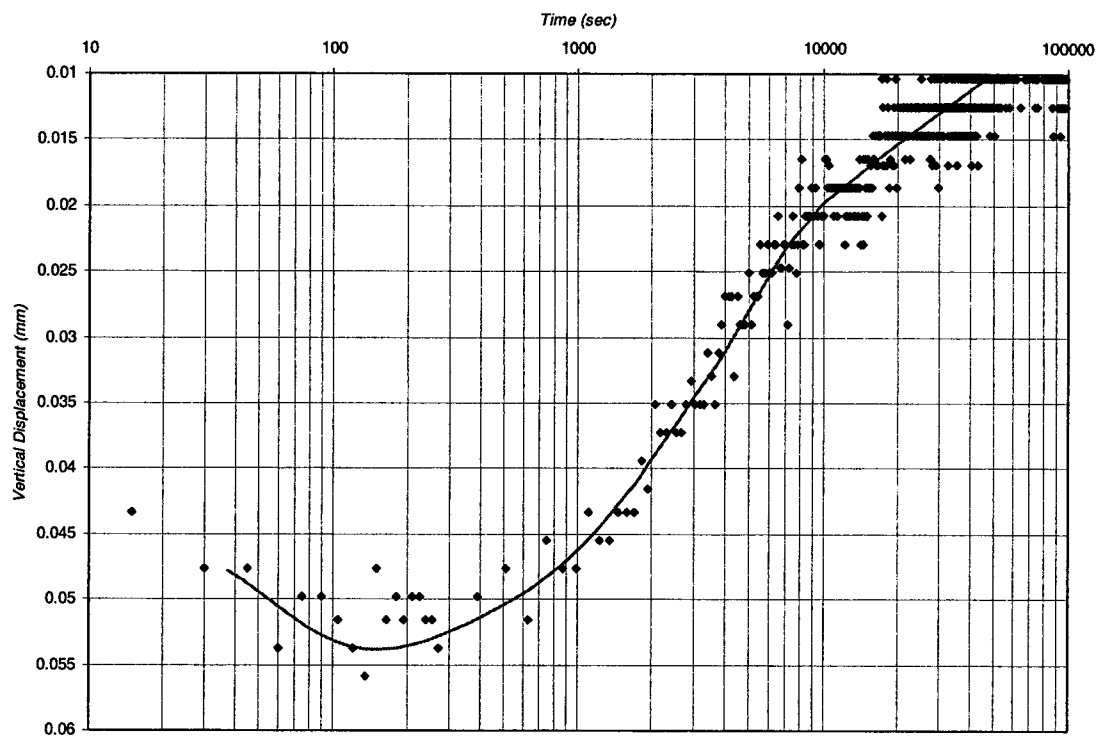


(a)

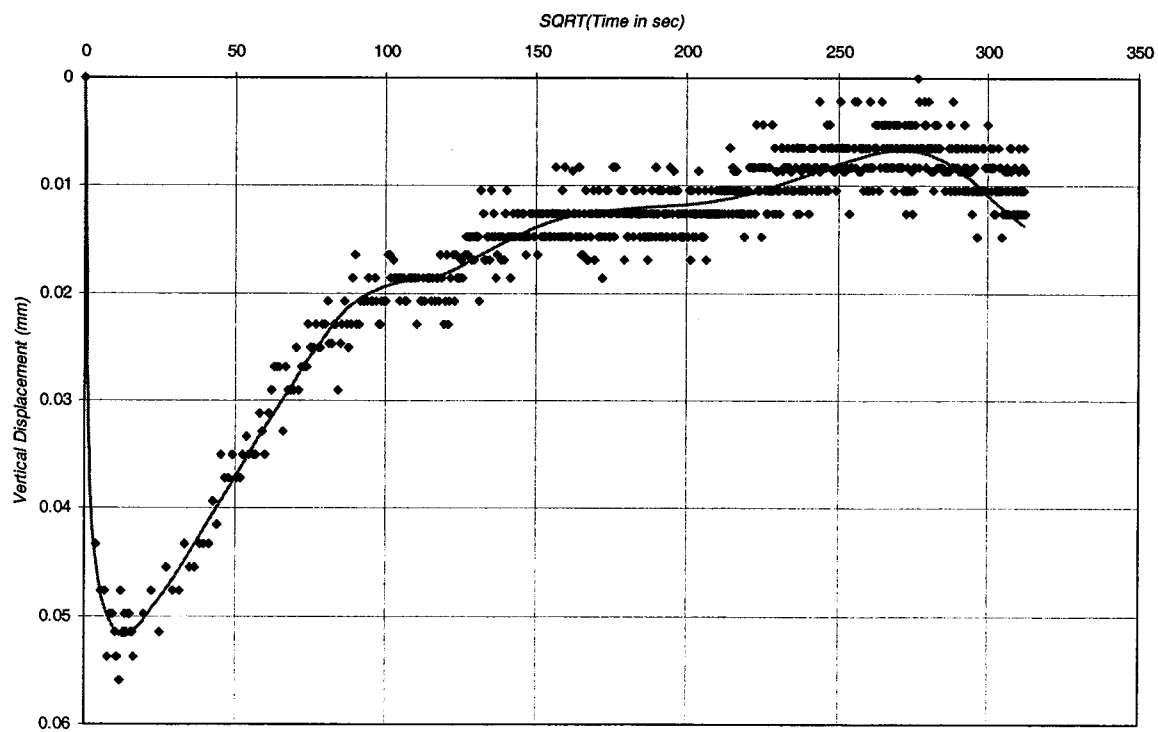


(b)

Figure B-18: Unloading of Sample 6-2 at 6.25 kPa (a) log time method (b) square root time method.

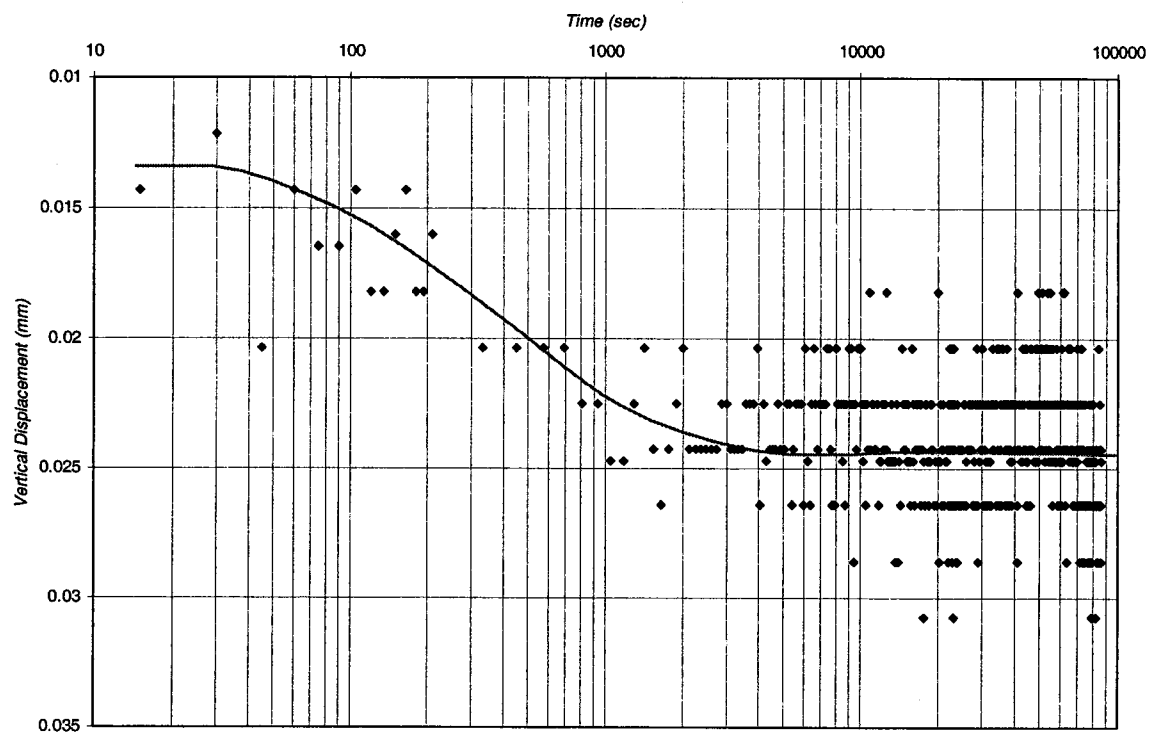


(a)

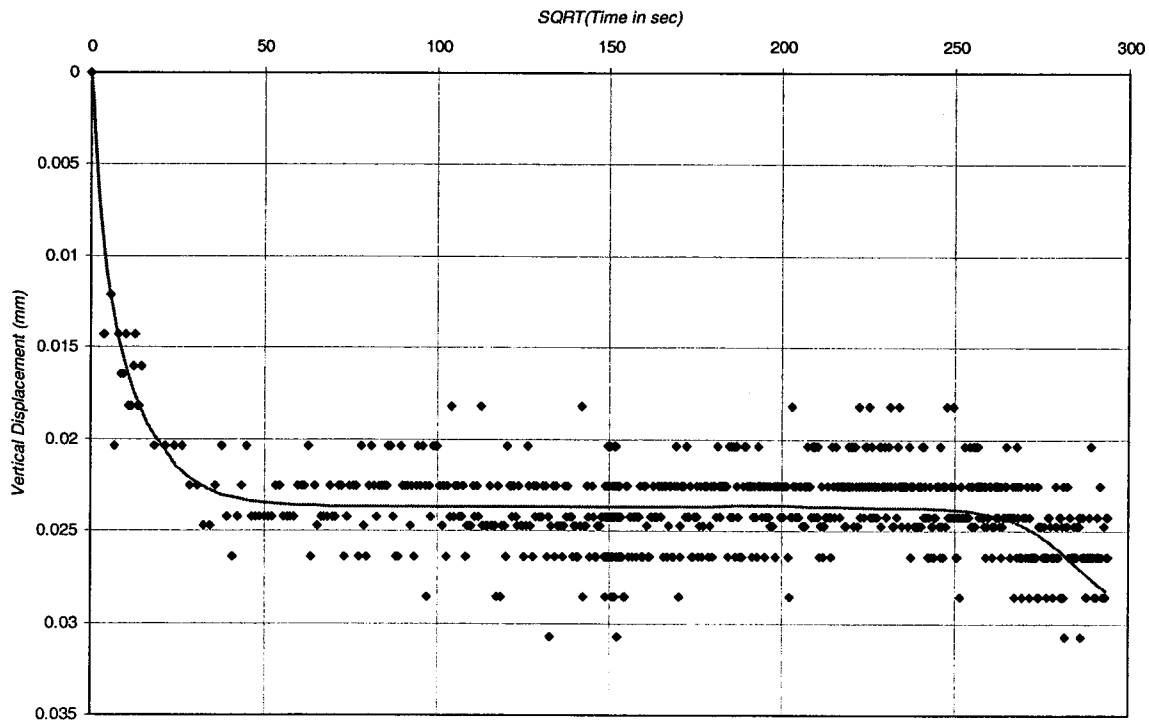


(b)

Figure B-19: Consolidation of Sample 7-1 at 25 kPa (a) log time method (b) square root time method.

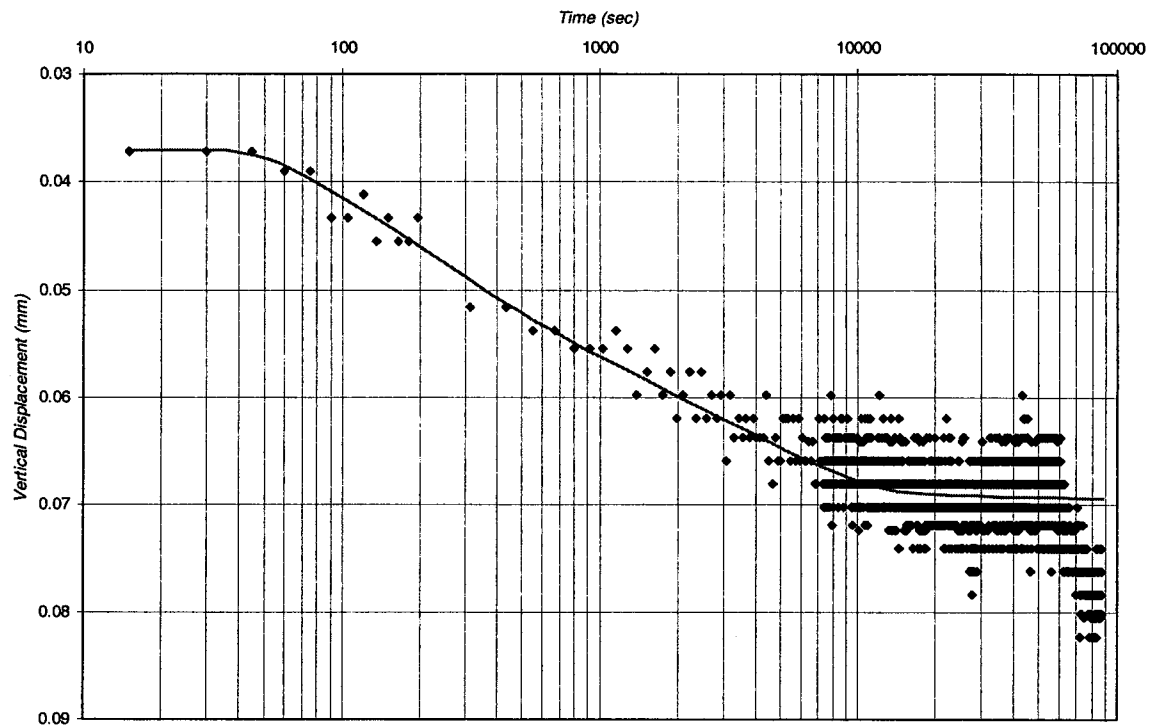


(a)

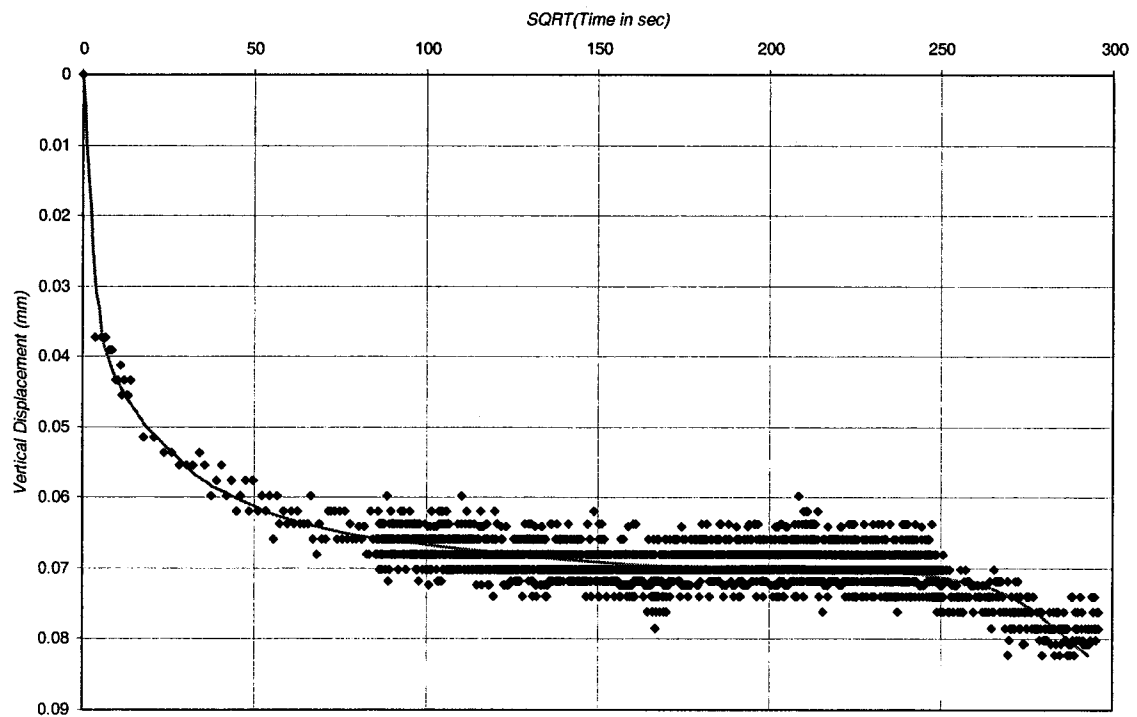


(b)

Figure B-20: Consolidation of Sample 7-1 at 50 kPa (a) log time method (b) square root time method.

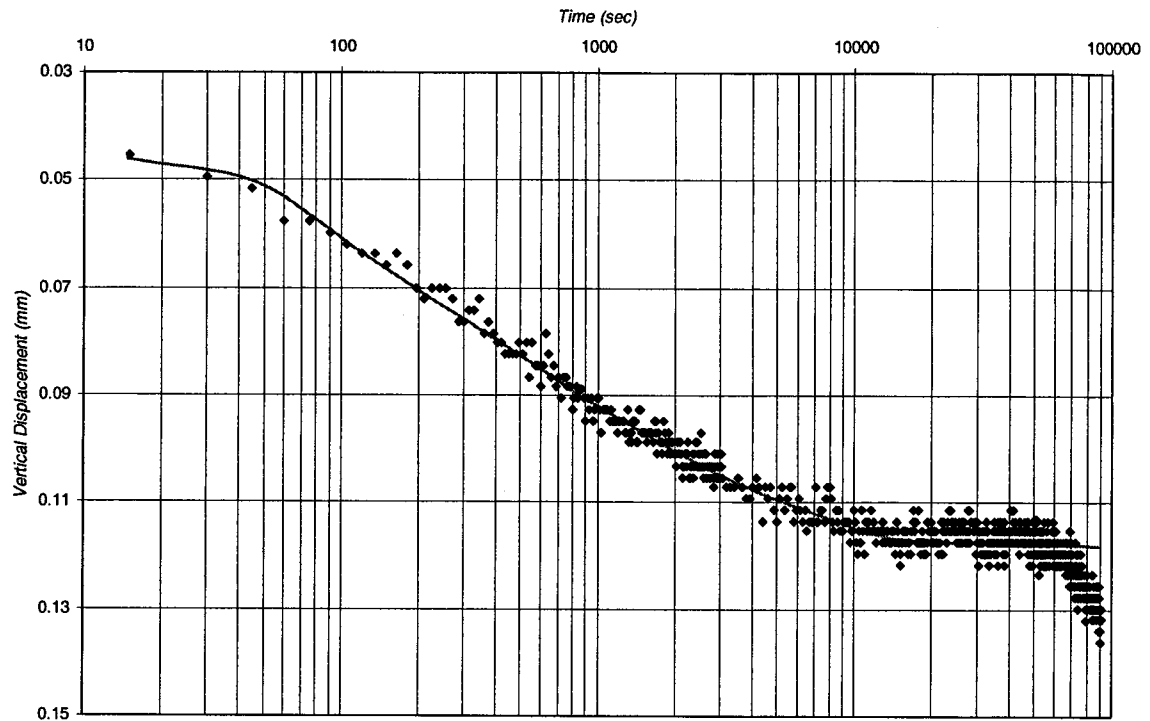


(a)

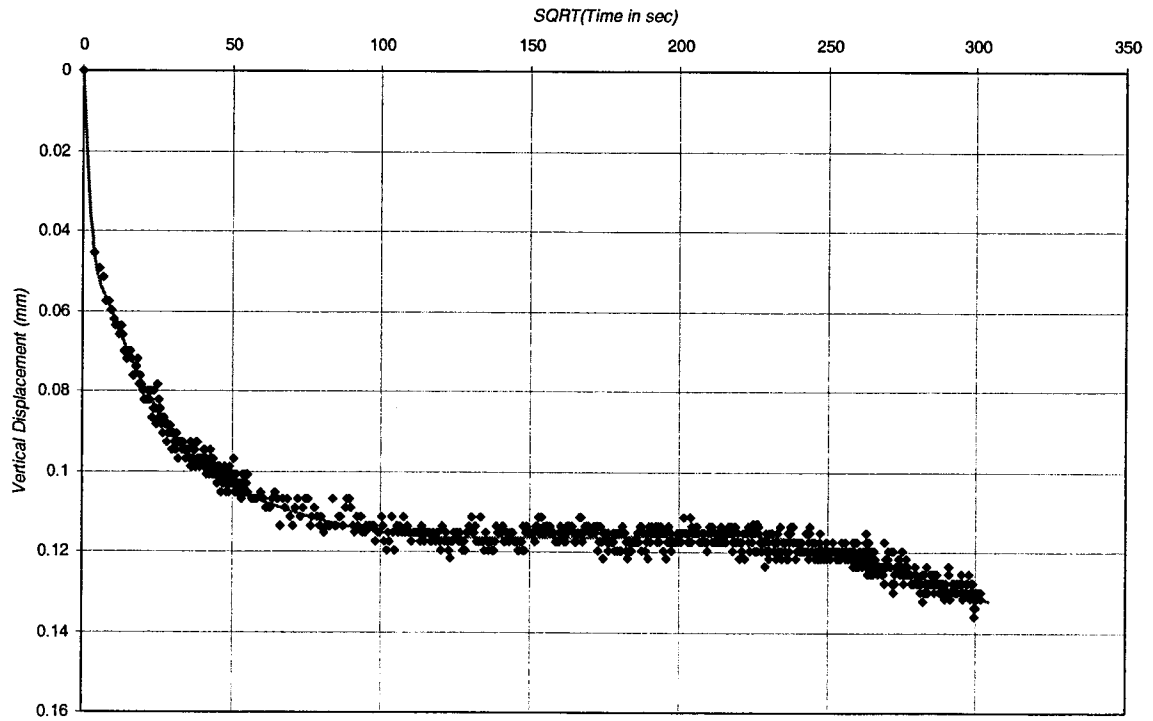


(b)

Figure B-21: Consolidation of Sample 7-1 at 100 kPa (a) log time method (b) square root time method.

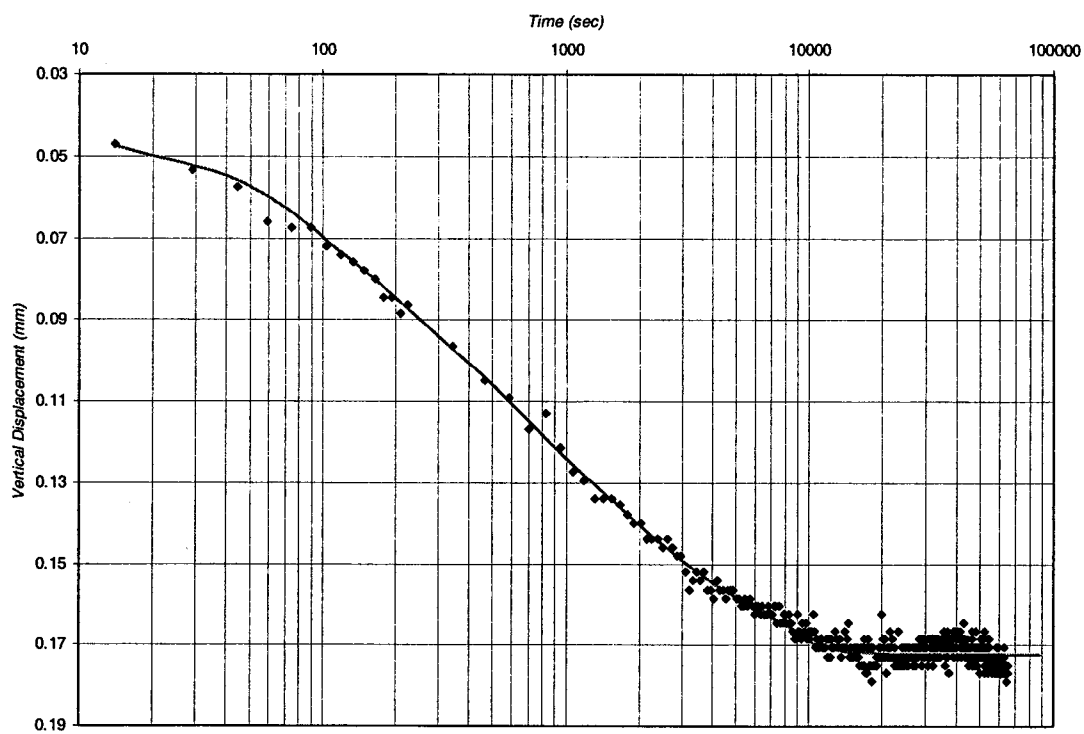


(a)

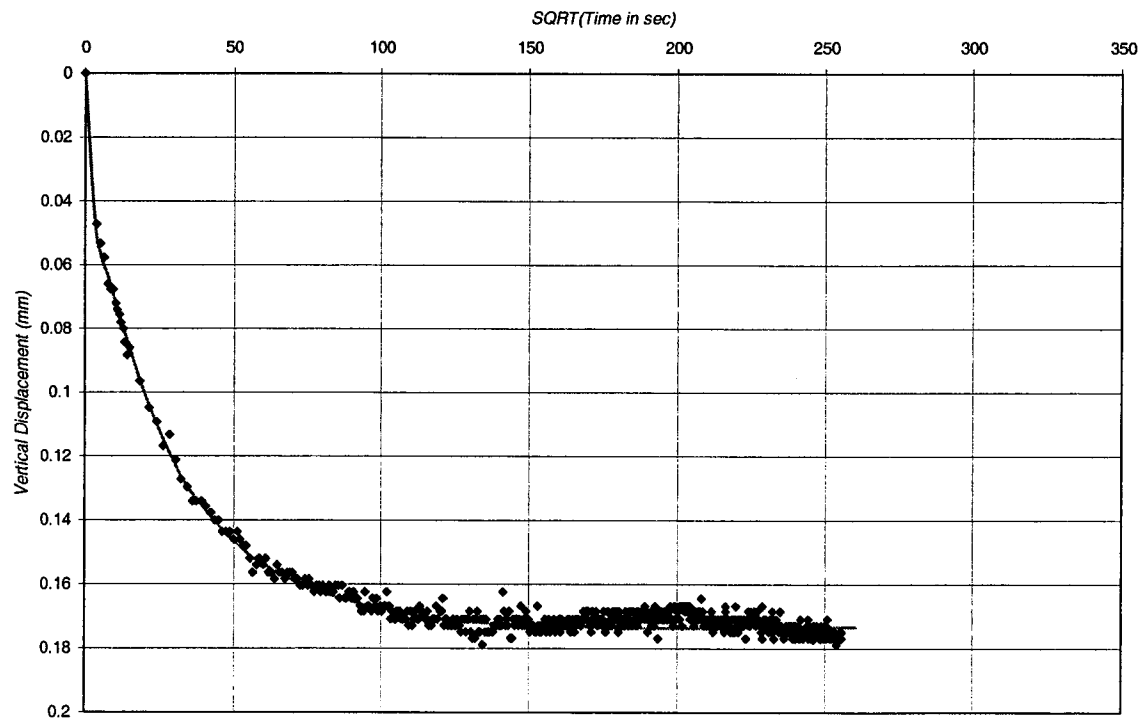


(b)

Figure B-22: Consolidation of Sample 7-1 at 200 kPa (a) log time method (b) square root time method.



(a)



(b)

Figure B-23: Consolidation of Sample 7-1 at 400 kPa (a) log time method (b) square root time method.

Appendix C

Stability and Deformation Analyses

enlarged section
FLAC mesh

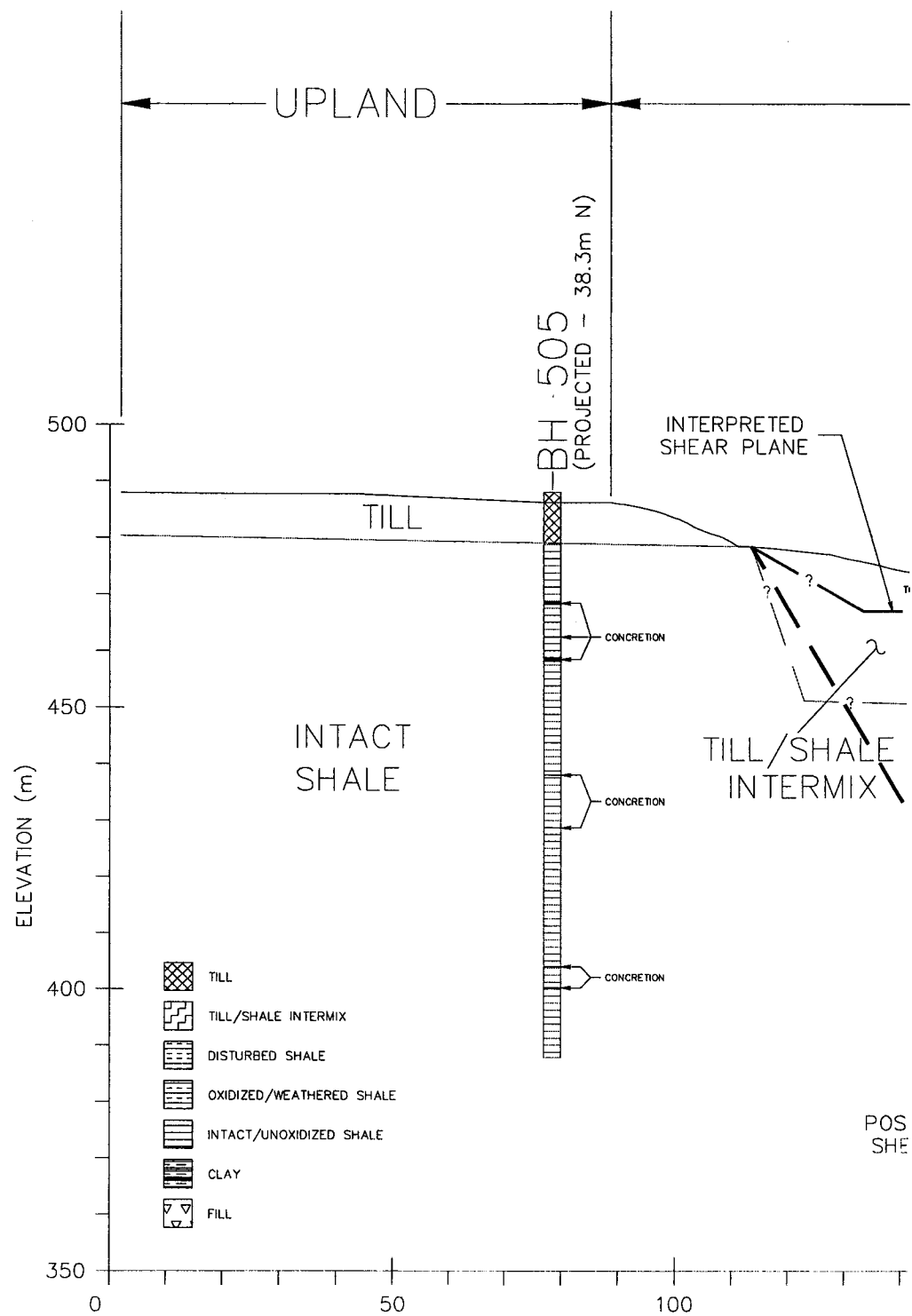


Figure C-1: Enlarged section locating possible shear surfaces.

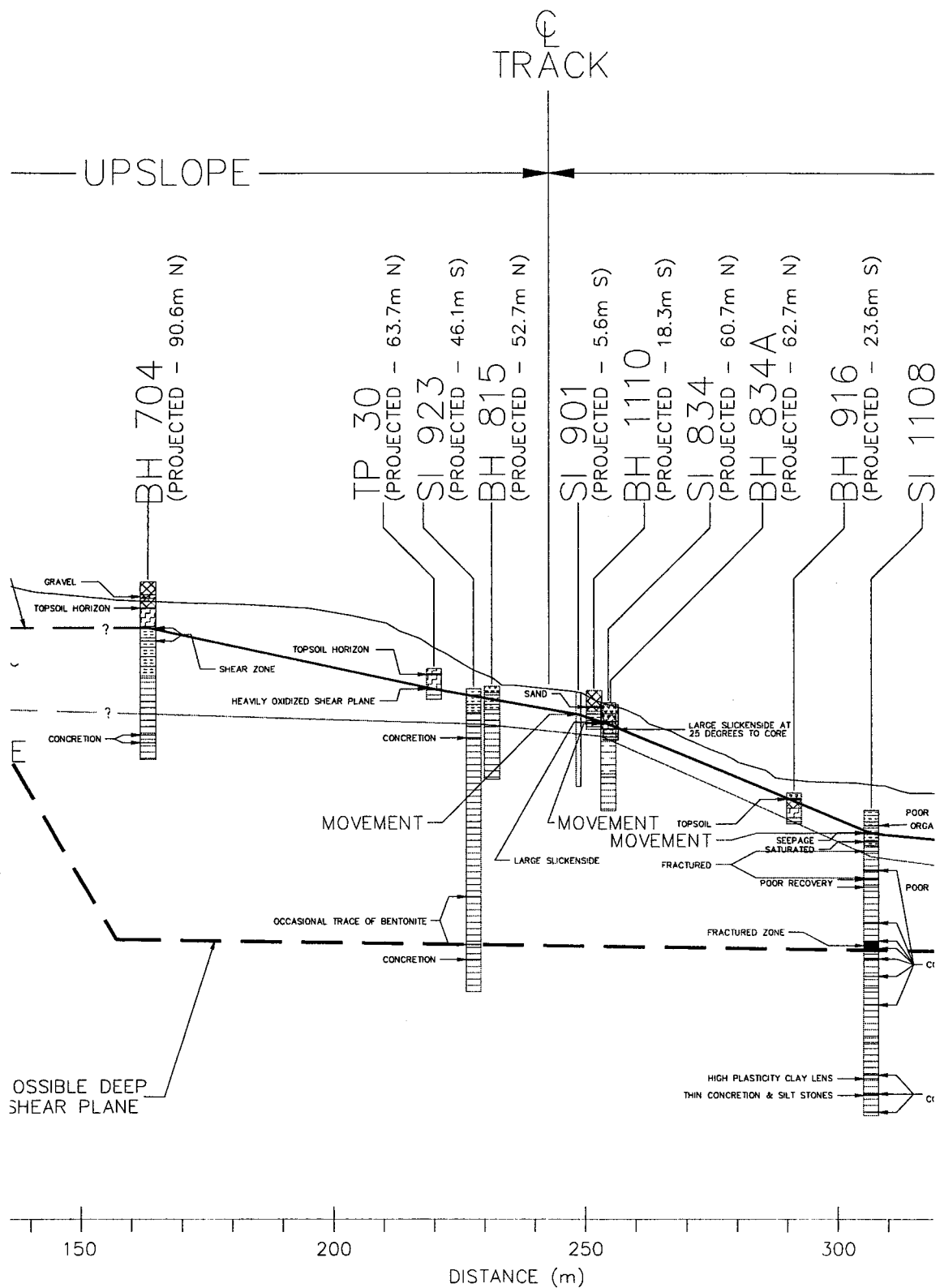


Figure C-1: Enlarged section locating possible shear surfaces (cont.).

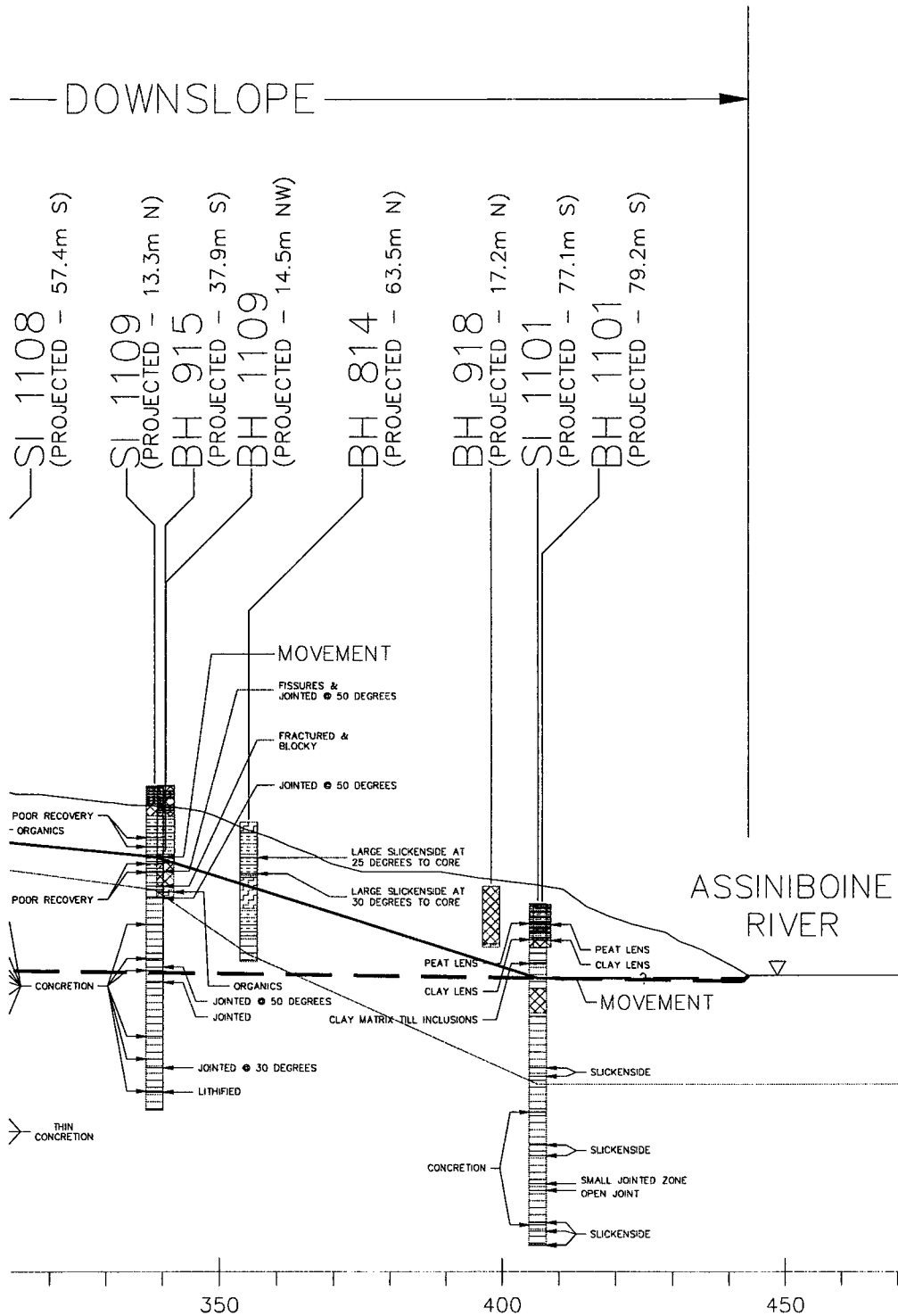


Figure C-1: Enlarged section locating possible shear surfaces (cont.).

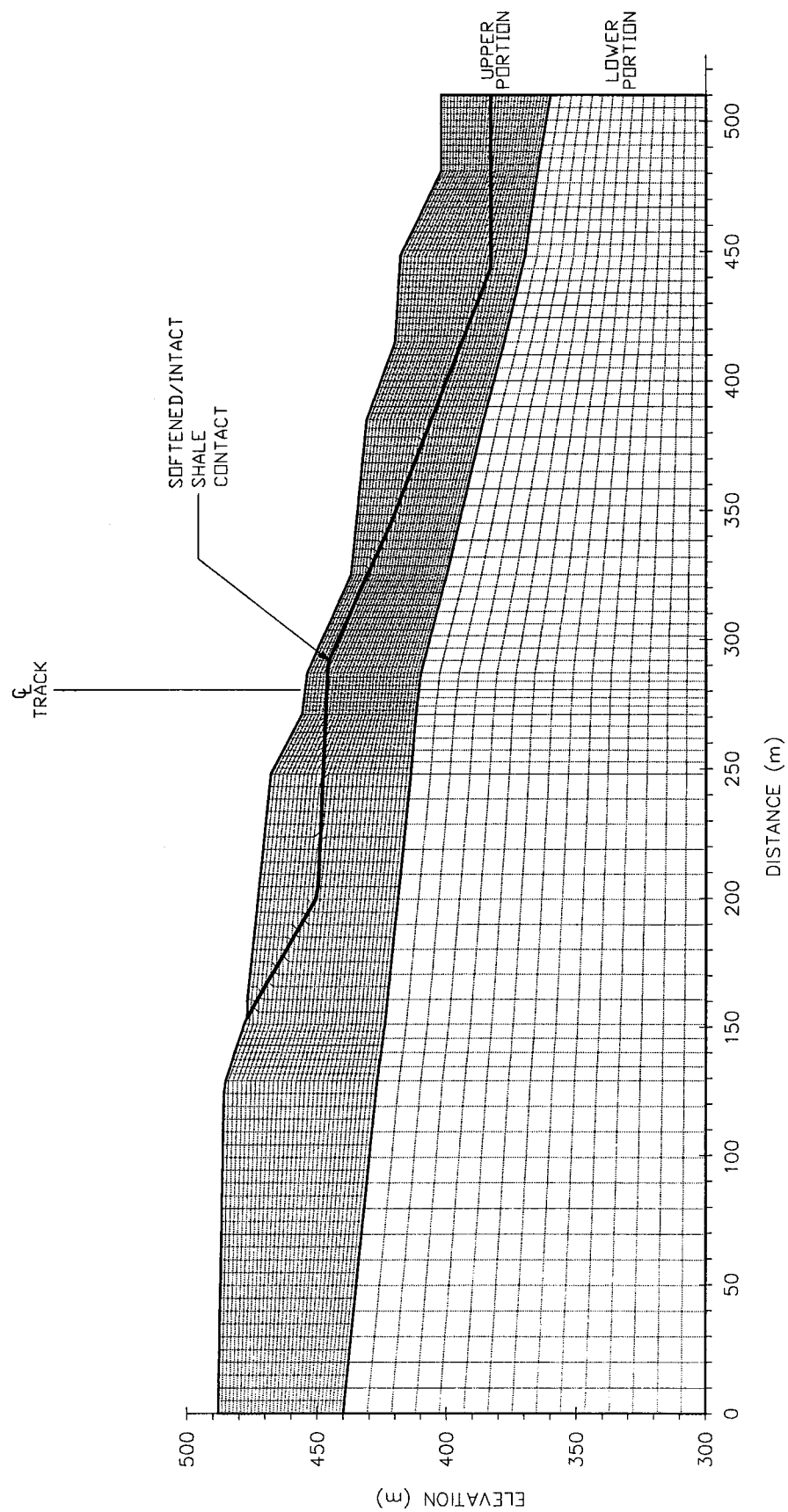


Figure C-2: Enlarged FLAC mesh